

**STUDY OF NEW  
CHITOSAN BASED DERIVATIVES FOR  
REMOVAL OF HEAVY METALS FROM  
WASTEWATER**

Thesis

Submitted in partial fulfilment of the requirement for the degree  
of

DOCTOR OF PHILOSOPHY

By

BALAKRISHNA PRABHU K.



DEPARTMENT OF CHEMICAL ENGINEERING  
NATIONAL INSTITUTE OF TECHNOLOGY KARNATAKA  
SURATHKAL, MANGALURU – 575025. INDIA.  
OCTOBER, 2017.



## DECLARATION

I hereby *declare* that the Research Thesis entitled “**Study of new chitosan based derivatives for removal of heavy metals from wastewater**” which is being submitted to the **National Institute of Technology Karnataka, Surathkal** in partial fulfillment of the requirements for award of the Degree of *Doctor of Philosophy* is a *bonafide report of the research work carried out by me*. The material contained in this Research Thesis has not been submitted to any University or Institution for the award of any degree.

BALAKRISHNA PRABHU K,

Reg. No. 121158CH12P01,

Department of Chemical Engineering.

NITK, Surathkal.

Place: NITK, Surathkal

Date:



## CERTIFICATE

This is to *certify* that the Research Thesis entitled “**Study of new chitosan based derivatives for removal of heavy metals from wastewater**” submitted by **Balakrishna Prabhu K (Reg. No. 121158CH12P01)** as the record of the research work carried out by him is accepted as the *Research Thesis* submission in partial fulfillment of the requirements for the award of degree of **Doctor of Philosophy**.

### Research Guides

**Dr. M. B. Saidutta,**  
Professor,  
Dept. of Chemical Engineering,  
NITK, Surathkal,  
Mangaluru, India.

**Dr. Arun M. Isloor,**  
Associate Professor,  
Dept. of Chemistry,  
NITK, Surathkal,  
Mangaluru, India.

Chairman- DRPC



## ACKNOWLEDGEMENTS

This journey on the way of Doctoral studies has been one of the most demanding and challenging times of my life. This momentous phase has indeed been a very satisfying and rewarding experience. Progress on this path wouldn't have been possible without the support, encouragement and best wishes from many people to whom I owe a deep sense of gratitude and thankfulness.

First and foremost, I would like to express my deepest gratitude towards my research guide **Dr. M. B. Saidutta**. His guidance, support and critical inputs have been very vital in keeping the flame of this research work burning constantly. His deep and insightful suggestions during the course of this work have helped me immensely on the professional front. I am especially thankful to him for generously agreeing to my multiple requests for meetings at a very short notice. I would like to thank him for his inexhaustible patience, friendly demeanor, and for his belief in me.

Words fail to adequately express my gratitude towards **Dr. Arun M. Isloor**, my research co-guide. A dynamic and multifaceted personality that he is, he was always kind to me with his valuable time. His guidance and suggestions have been priceless in shaping this thesis. I specially value the countless meetings I had with him, all at a short notice, that were highly inspirational and motivating.

I would like to extend my deep appreciation towards the RPAC committee members, **Dr. Vidya Shetty K.** and **Dr. S. Shrihari** for their invaluable suggestions and constructive comments during the review meetings which helped me fine-tune this research work.

I offer my humble gratitude to the **Director, NITK**; the former and present Academic Deans **Dr. Suman David**, **Dr. Katta Venkataramana** and **Dr. M. B. Saidutta**; the former and present Heads of Chemical Engineering Department, **Dr. M. B. Saidutta**, **Dr. Vidya Shetty K.**, **Dr. Raj Mohan B.** and **Dr. Hari Mahalingam**; the former and present Heads of Chemistry Department, **Dr. Ramachandra Bhat B.** and **Dr. Krishna Bhat D.** for providing the facilities required for carrying out this research.

I extend my sincere gratitude towards all the faculty members of Chemical Engineering Department and Chemistry Department, NITK Surathkal, for their help and support. In particular, I express my humblest regards for **Dr. D.V.R. Murthy** for providing constant inspiration, encouragement and motivation during the course of this research. I would like to thank **Dr. G. Sriniketan, Dr. A. Nithyananda Shetty, Dr. A. Vasudeva Adhikari** and **Dr. Krishna Bhat D.** for sharing their valuable time for technical discussions.

My humble gratitude and appreciation goes out to the former and present Directors of MIT Manipal, **Dr. Vinod Thomas** and **Dr. G. K. Prabhu**; Joint Director of MIT Manipal, **Dr. B.H.V. Pai**; Associate Director of MIT Manipal, **Dr. Narayana Shenoy**, for their support and encouragement.

My sincere thanks are due to the former and present Heads of Chemical Engineering Department of MIT Manipal, **Dr. Harish Kumar** and **Dr. Krishna Bandaru** for providing the infrastructure and facilities for conducting this research work.

Thanks are due to my close colleagues and fellow faculty members at MIT Manipal. In particular I would like to thank **Prof. S. Sivasankaran, Dr. Srinivas Kini M., Dr. V. R. C. Murty** and **Dr. S. Nethaji** for their constant support and best wishes.

My special thanks are due to **Dr. Rajesha Kumar**, my senior research colleague, for helping out with all the syntheses works related to this research. My thanks are due to **Dr. Garudachari B. and Dr. K. K. Srinivasan** for technical discussions; research colleague **Dr. Raghavendra Hebbar** for his invaluable help during the execution of the membrane studies; **Dr. Kunal Kumar, Dr. S. Rajasekhara** and **Mr. Syed** for their help during the final stages of completion of this work.

I would like to thank **Mr. Sadananda Tendulkar** for helping with the analysis of samples by AAS; **Mr. S. Adiga** and **Mr. Ganesh Prabhu** for helping with laboratory maintenance.



I owe a debt of gratitude to **Mr. Girish Kamath** for helping with FTIR and XRD analyses. I would like to thank all my friends and well-wishers at NITK Surathkal and MIT Manipal who contributed directly or indirectly in bringing this work to fruition.

My humble gratitude goes out to my mother **Smt. Radhabai Prabhu** and to the memory of my father **Late Damodara Prabhu**; parents-in-law **Smt. Anuradha N. Nayak and Shri N.A.Nayak** ; and all my family members for their love and silent prayers.

Saving the best for the last, I am truly at a loss of words to adequately express my appreciation and gratitude towards my pillars of strength- my wife **Kalpana** and my son **Milind**. I owe it to my wife for her absolute and unflinching love, help and understanding during the entire phase of this research. Words also fail me to thank her enough for her support throughout some uncertain and challenging times during this journey. I would like to thank my son **Milind** for sharing his computer skills and for his affection and understanding through the course of this research work. I also thank him for sparing his study table for me during the writing of this thesis.

Most of all, my humble obeisance to **Almighty God** whose perpetual grace and blessings were instrumental in granting me health, patience, perseverance and wisdom while carrying out this research work.

**Balakrishna Prabhu K.**



***DEDICATED TO MY  
FAMILY***



## ABSTRACT

Heavy metals (such as Cu, Pb and Cr) are harmful contributors to pollution of fresh and marine aquatic bodies. Adsorption is a very efficient and popular technique used in wastewater treatment. Chitosan is a biopolymer derived from chitin, an abundantly occurring natural polymer in nature. As an adsorbent, use of chitosan in natural form is constrained by its inferior mechanical, chemical and swelling properties. In this study, four new chitosan derivatives were synthesized by grafting four ligands on chitosan with a view of improving its characteristics. Each ligand had a single pyrazole ring with two additional nitrogen atoms which are potential binding sites for heavy metal sequestration. Batch studies were carried out to determine the optimum pH for adsorption, the most fitting isotherm, the most fitting kinetic model and the relevant thermodynamic parameters. The maximum monolayer adsorption capacities obtained were 63.5 mg/g for Cr (VI), 91.7 mg/g for Pb (II) and 45.6 mg/g for Cu (II). The probable mode of adsorption was chemisorption. The pseudo-second order model fitted experimental kinetic data very well. The FTIR study revealed that amine, imine and hydroxyl groups participated in metal sequestration. The major decrease in the swelling property of the prepared derivatives makes them a promising choice for applications in practical water treatment contacting equipment. Polysulfone membranes blended with the new chitosan derivative CTSL-2 were prepared. The hydroxyl, amine and the imine functional groups present in the additive evidently increased the hydrophilicity of the surface of the blended membranes as confirmed by contact angle measurements. The contact angle of the blended membrane having 2 wt % additive was  $62.55 \pm 1$  as compared to  $70.01 \pm 1$  for neat polysulfone membrane. The blended membranes also showed a significant improvement in maximum pure water flux ( $351 \text{ Lm}^{-2}\text{h}^{-1}$  against  $24 \text{ Lm}^{-2}\text{h}^{-1}$  of neat membrane). The BSA anti-fouling test exhibited improved anti-fouling characteristic of blended membrane (FRR of 56%). In the metal rejection study, the maximum rejections observed were 36%, 29% and 61% respectively for the three metals Pb (II), Cu (II) and Cr (VI). Overall, the incorporation of additive in polysulfone membranes demonstrated significant improvement in the permeation properties investigated.

**Keywords: Chitosan, chitosan derivative, adsorption, heavy metal, polysulfone, membrane**



## TABLE OF CONTENTS

	<b>ABSTRACT</b>	i
	<b>TABLE OF CONTENTS</b>	iii-ix
	<b>LIST OF FIGURES</b>	xi-xviii
	<b>LIST OF TABLES</b>	xix-xx
	<b>LIST OF ABBREVIATIONS</b>	xxi-xxiv
	<b>NOMENCLATURE</b>	xxv
<b>CHAPTER</b>		<b>PAGE NO</b>
<b>1</b>	<b>INTRODUCTION</b>	1-18
1.1	Water pollution by heavy metals	3
1.1.1	Classification of elements as “heavy metals”	3
1.1.2	Dose-response relationship	4
1.1.3	Sources and toxic effects of heavy metals	5
1.1.4	Heavy metals: A persistent and problematic polluter	6
1.2	Methods of heavy metal removal	7
1.2.1	Chemical precipitation	7
1.2.1.1	Hydroxide precipitation	7
1.2.1.2	Sulphide precipitation	8
1.2.1.3	Xanthate process	8
1.2.2	Solvent extraction	8
1.2.3	Membrane process	9
1.2.3.1	Ultrafiltration (UF)	9
1.2.3.2	Reverse Osmosis (RO)	9
1.2.3.3	Nano filtration	10
1.2.3.4	Electrodialysis	10
1.2.4	Ion exchange	10
1.2.5	Electrochemical method	10
1.2.6	Adsorption	11
1.3	Scope of the study	11

1.4	Objectives of the research work	16
1.5	Organization of the thesis	17
<b>2</b>	<b>LITERATURE REVIEW</b>	<b>19-56</b>
2.1	Chitosan	21
2.1.1	Molecular structure of chitin and chitosan	21
2.2	Chemical structure and properties of chitosan	22
2.3	Uses of chitosan	23
2.4	Chitosan as an adsorbent material in pollution treatment	24
2.5	Modifications of chitosan	26
2.5.1	Physical modifications	26
2.5.2	Chemical modifications	26
2.5.2.1	Schiff base derivatives of chitosan	31
2.5.2.2	Composite materials with chitosan	33
2.5.2.3	Miscellaneous derivatives of chitosan	36
2.6	Adsorption studies	37
2.6.1	Adsorption isotherms	37
2.6.2	Adsorption kinetics	40
2.6.3	Adsorption thermodynamics	41
2.7	Polysulphone membranes	42
2.7.1	Mechanism of electrolyte separation by membranes	45
<b>3</b>	<b>MATERIALS AND METHODS</b>	<b>57-82</b>
3.1	Materials	59
3.1.1	Chitosan	59
3.1.2	Chemicals used	61
3.1.3	Instruments used	62
3.2	Syntheses of chitosan derivatives	63
3.2.1	Synthesis of CTSL-1	63



3.2.1.1	Synthesis of semicarbazone-1	63
3.2.1.2	Synthesis of Ligand (L-1)	64
3.2.1.3	Grafting of L-1 on chitosan to form CTSL-1	66
3.2.2	Synthesis of CTSL-2	68
3.2.3	Synthesis of CTSL-3	69
3.2.3.1	Synthesis of semicarbazone-3	69
3.2.3.2	Synthesis of the ligand-L-3: 3-p-tolyl-1H-pyrazole-4-carbaldehyde	70
3.2.3.3	Grafting of L-3 on chitosan to form chitosan derivative CTSL-3	71
3.2.4	Synthesis of the chitosan derivative CTSL-4	71
3.2.4.1	Synthesis of Semicarbazone-4: ((E)-1-(1-(4-chlorophenyl) ethylidene) semicarbazide)	72
3.2.4.2	Synthesis of L-4 (3-(4-chlorophenyl)-1H-pyrazole-4-carbaldehyde)	72
3.2.4.3	Reaction of ligand L-4 with chitosan to form CTSL-4	73
3.3	Adsorption studies	74
3.3.1	Preparation of stock solutions of metal ions	74
3.3.1.1	Preparation of 1000 mg/L stock solution of Cr (VI)	74
3.3.1.2	Preparation of 1000 mg/L stock solution of Cu (II)	74
3.3.1.3	Preparation of 1000 mg/L stock solution of Pb (II)	75
3.3.2	Characterization and analysis	75
3.3.2.1	Fourier transformed infrared (FTIR) spectroscopic studies	75
3.3.2.2	Proton Nuclear Magnetic Resonance ( <sup>1</sup> H NMR) studies	75
3.3.2.3	Solid state <sup>13</sup> C NMR studies	75

3.3.2.4	Scanning electron microscopy (SEM) studies	75
3.3.2.5	Powder X-ray diffraction (XRD) studies	76
3.3.2.6	Differential scanning calorimetry (DSC) studies	76
3.3.3	Effect of initial pH on adsorption	76
3.3.4	Adsorption equilibrium studies	76
3.3.5	Adsorption kinetic studies	77
3.3.6	Adsorption thermodynamic studies	77
3.4	Membrane Studies	77
3.4.1	Preparation of neat polysulfone membrane (P-0)	77
3.4.2	Preparation of PSf :CTSL-2 blend membranes	78
3.4.3	Membrane characterization	79
3.4.3.1	Scanning Electron Microscopy (SEM) studies	79
3.4.3.2	Contact angle measurement	79
3.4.3.3	Powder XRD analysis	79
3.4.4	Membrane experiments	80
3.4.4.1	Pure water flux study	80
3.4.4.2	Membrane hydraulic resistance	81
3.4.4.3	Anti-fouling studies	81
<b>4</b>	<b>RESULTS AND DISCUSSION</b>	<b>83-180</b>
	<b>PART A Adsorption Studies</b>	<b>85-162</b>
4.1	Studies using chitosan derivative CTSL-1	87
4.1.1	Characterization of Ligand L-1	87
4.1.2	Characterization of the chitosan derivative CTSL-1	88
4.1.2.1	Solid state <sup>13</sup> C NMR analysis of CTSL-1	88
4.1.2.2	FTIR analysis of CTSL-1	89
4.1.2.3	Scanning electron microscope analysis of CTSL-1	91

4.1.2.4	XRD analysis of CTSL-1	92
4.1.2.5	DSC analysis of CTS and CTSL-1	92
4.1.3	Adsorption studies with CTSL-1	94
4.1.3.1	Effect of pH	94
4.1.3.2	Adsorption equilibrium	96
4.1.3.3	Adsorption kinetics	100
4.1.3.4	Adsorption thermodynamics	104
4.1.3.5	Proposed mechanism of metal removal	106
4.1.3.6	Post adsorption XRD analysis of CTSL-1- Metal complexes	110
4.2	Studies using chitosan derivative CTSL-2	112
4.2.1	Characterization of ligand L-2	112
4.2.2	Characterization of the chitosan derivative CTSL-2	113
4.2.2.1	Solid state <sup>13</sup> C NMR analysis of CTSL-2	113
4.2.2.2	FTIR analysis of CTSL-2	113
4.2.2.3	XRD analysis	116
4.2.2.4	DSC thermogram studies of CTSL-2	117
4.2.3	Adsorption studies with CTSL-2	118
4.2.3.1	Effect of pH	118
4.2.3.2	Adsorption equilibrium	118
4.2.3.3	Adsorption kinetics	121
4.2.3.4	Adsorption thermodynamics	124
4.2.3.5	Post-adsorption CTSL-2 characterization	126
4.3	Studies using chitosan derivative CTSL-3	128
4.3.1	Characterization of ligand L-3	128
4.3.2	Characterization of the chitosan derivative CTSL-3	129
4.3.2.1	Solid state <sup>13</sup> C NMR analysis of CTSL-3	129
4.3.2.2	FTIR analysis	129
4.3.2.3	XRD analysis	132

4.3.2.4	DSC Thermogram of CTSL-3	132
4.3.3	Adsorption studies with CTSL-3	133
4.3.3.1	Effect of pH	133
4.3.3.2	Adsorption equilibrium	134
4.3.3.3	Adsorption kinetics	137
4.3.3.4	Adsorption thermodynamics	140
4.3.3.5	Post-adsorption CTSL-3 characterization	141
4.4	Studies using chitosan derivative CTSL-4	143
4.4.1	Characterization of ligand L-4	143
4.4.2	Characterization of the chitosan derivative CTSL-4	144
4.4.2.1	Solid state <sup>13</sup> C NMR analysis of CTSL-4	144
4.4.2.2	FTIR analysis	145
4.4.2.3	XRD analysis	147
4.4.2.4	DSC Thermogram of CTSL-4	147
4.4.3	Adsorption studies using CTSL-4	148
4.4.3.1	Effect of pH	148
4.4.3.2	Adsorption equilibrium	149
4.4.3.3	Adsorption kinetics	151
4.4.3.4	Adsorption thermodynamics	155
4.4.3.5	Post-adsorption CTSL-4 characterization	156
4.5	Summary of adsorption studies carried out	158
4.6	Swelling studies and bulk density measurement	161
<b>PART B</b>	<b>Membrane Studies</b>	<b>163-180</b>
4.7	Studies using polysulfone membranes blended with CTSL-2	165
4.7.1	Study of membrane morphology	165
4.7.2	Contact angle	168
4.7.3	XRD analysis	169

4.7.4	Permeation studies	170
4.7.5	Membrane hydraulic resistance	171
4.7.6	Anti-fouling studies	172
4.7.7	Heavy metal rejection studies	174
4.7.7.1	Pb (II) rejection study	174
4.7.7.2	Cu (II) rejection study	175
4.7.7.3	Cr (VI) rejection study	176
4.7.7.4	Mechanism of metal rejection by membranes	177
<b>5</b>	<b>SUMMARY AND CONCLUSIONS</b>	<b>179-186</b>
	<b>APPENDICES</b>	<b>187-192</b>
	APPENDIX I	189
	APPENDIX II	190
	APPENDIX III	191
	<b>REFERENCES</b>	<b>193-218</b>
	<b>LIST OF RESEARCH PUBLICATIONS</b>	<b>219</b>
	<b>BIODATA</b>	<b>221</b>



## LIST OF FIGURES

FIGURE NO	FIGURE CAPTIONS	PAGE NUMBER
1.1	Association between dose and response for essential and toxic elements	4
2.1	Structure of a) chitin b) chitosan with complete deacetylation c) chitosan with partial deacetylation	21-22
2.2	Functional group positions in chitosan	23
2.3	Schematic representation of the chitosan and cross-linked chitosan beads: (a) chitosan, (b) chitosan-glutaraldehyde (c) chitosan-epichlorohydrin (d) chitosan-ethylene glycol diglycidyl ether	27-28
3.1	Structure of chitosan a) with complete deacetylation and b) with partial deacetylation	59
3.2	Photograph of chitosan powder	60
3.3	Synthesis of semicarbazone-1 from 4-methoxyacetophenone	64
3.4	Experimental setup for the synthesis of semicarbazone intermediate	64
3.5	Synthesis of ligand (L-1) from semicarbazone-1	65
3.6	Experimental setup for the synthesis of the ligand (L-1) under nitrogen atmosphere	66
3.7	Synthesis of chitosan derivative CTSL-1	67
3.8	CTSL-1 a) in wet form before drying, b) after drying	67
3.9	Reaction scheme for the synthesis of CTSL-2	68
3.10	Reaction scheme for the synthesis of semicarbazone-3	69
3.11	Reaction scheme for the synthesis of the ligand (L-3)	70
3.12	Reaction scheme for grafting L-3 on chitosan to form CTSL-3	71
3.13	Reaction scheme for the synthesis of semicarbazone-4	72

	intermediate	
3.14	Reaction scheme for the synthesis of the ligand (L-4)	73
3.15	Reaction scheme for synthesis of CTSL-4	74
3.16	Chemical structure of polysulfone and CTSL-2	79
3.17	Schematic view of the filtration cell.	80
3.18	Illustration of flux before fouling ( $J_{w1}$ ), after fouling ( $J_p$ ) and after the post-fouling wash ( $J_{w2}$ )	82
4.1	$^1\text{H}$ NMR spectrum of the ligand (L-1)	88
4.2	Solid state $^{13}\text{C}$ NMR spectra of a) Chitosan and b) CTSL-1	89
4.3	FTIR spectra of a) Chitosan b) CTSL-1 c) CTSL-1-Pb d) CTSL-1-Cu e) CTSL-1-Cr	90
4.4	Scanning electron micrographs of a) CTS b) CTSL-1	92
4.5	a) XRD spectrum of chitosan b) XRD spectrum of CTSL-1	92
4.6	DSC thermograms of a) Chitosan and b) CTSL-1	93-94
4.7	Effect of pH on % removal (Initial concentration=100 mg/L; Temperature=303K; Ads. Dose=4g/L; Agitation speed=150 rpm; Contact time 24h	95
4.8	Plot of various adsorption isotherms to CTSL-1-Cu (II) adsorption data (Initial conc.=100 mg/L; T=303 K; pH 7; Ads. Dose=2g/L; Stirring speed=150 rpm; t=24 h)	98
4.9	Plot of various adsorption isotherms to CTSL-1-Pb (II) adsorption data (Initial conc. =100 mg/L; T =303 K; pH 4; Ads. Dose=2 g/L; Stirring speed=150 rpm, t =24 h)	98
4.10	Fit of various isotherms to CTSL-1-Cr (VI) adsorption data (Initial conc. =100 mg/L; T=303 K; pH 3; Ads. Dose=2g/L; Agitation speed=150 rpm; Contact time=24 h)	99
4.11	Photographic images of CTSL-1 (before adsorption) and CTSL-1-Metal complexes (after adsorption)	100



4.12	Plot of CTSL-1-Cr (VI) kinetic study data [a) Quantity adsorbed v/s time b) Pseudo-first order c) Pseudo-second order d) Intra particle diffusion] (Initial concentration=100mg/L; Temperature=303K; pH=3; Ads. Dose=2g/L; Agitation speed=150rpm)	102
4.13	Plot of CTSL-1-Cu (II) kinetic study data [a) Quantity adsorbed v/s time b) Pseudo-first order c) Pseudo-second order d) Intra particle diffusion] (Initial concentration=100mg/L; Temperature=303K; pH=7; Ads. Dose=2g/L; Agitation speed=150rpm)	102-103
4.14	Plot of CTSL-1-Pb (II) kinetic study data [a) Quantity adsorbed v/s time b) Pseudo-first order c) Pseudo-second order d) Intra particle diffusion] (Initial concentration=100mg/L; Temperature=303K; pH=4; Ads. Dose=2g/L; Agitation speed=150rpm)]	103-104
4.15	Proposed mechanisms of adsorbate uptake. (M <sup>2+</sup> =Pb (II) or Cu (II))	107-108
4.16	Proposed mechanism of adsorption for Cr (VI) removal	109
4.17	XRD spectra of a) CTSL-1 b) CTSL-1-Cr c) CTSL-1-Cu d) CTSL-1-Pb	111
4.18	<sup>1</sup> H NMR spectrum of the ligand (L-2)	112
4.19	<sup>13</sup> C NMR of CTSL-2	113
4.20	FTIR spectra of a) Chitosan b) CTSL-2 c) CTSL-2-Pb d) CTSL-2-Cu e) CTSL-2-Cr	115
4.21	XRD spectrum of CTSL-2	116
4.22	DSC thermogram of CTSL-2	117
4.23	Effect of pH on % removal (Initial concentration=100mg/L; Temperature=303K; Ads. Dose=4 g/L; Agitation speed=150rpm; Contact time=24h)	118
4.24	Plot of various adsorption isotherms to CTSL-2-Cr (VI)	120

	adsorption data (Initial concentration=100 mg/L; Temperature=303K; pH=3; Ads. Dose=2g/L; Agitation speed=150 rpm; Contact time=24 h)	
4.25	Plot of various adsorption isotherms to CTSL-2-Cu (II) adsorption data (Initial concentration=100 mg/L; Temperature=303K; pH=6; Ads. Dose=2g/L; Agitation speed=150 rpm; Contact time=24 h)	120
4.26	Plot of various adsorption isotherms to CTSL-2-Pb (II) adsorption data (Initial concentration=100 mg/L; Temperature=303K; pH=6; Ads. Dose=2g/L; Agitation speed=150 rpm, Contact time=24 h)	121
4.27	Plot of CTSL-2-Cr (VI) kinetic study data [a) Quantity adsorbed v/s time b) Pseudo-first order c) Pseudo-second order d) Intra particle diffusion] (Initial concentration=100mg/L; Temperature=303K; pH=3; Ads. Dose=2g/L; Agitation speed=150rpm)	122
4.28	Plot of CTSL-2-Cu (II) kinetic study data [a) Quantity adsorbed v/s time b) Pseudo-first order c) Pseudo-second order d) Intra particle diffusion] (Initial concentration=100mg/L; Temperature=303K; pH=6; Ads. Dose=2g/L; Agitation speed=150rpm)	123
4.29	Plot of CTSL-2-Pb (II) kinetic study data [a) Quantity adsorbed v/s time b) Pseudo-first order c) Pseudo-second order d) Intra particle diffusion] (Initial concentration=100mg/L; Temperature=303K; pH=6; Ads. Dose=2g/L; Agitation speed=150rpm)	123-124
4.30	XRD spectra of a) CTSL-2 b) CTSL-2-Cr c) CTSL-2-Cu d) CTSL-2-Pb	128
4.31	<sup>13</sup> C NMR of CTSL-3	129
4.32	FTIR spectra of a) Chitosan b) CTSL-3 c) CTSL-3-Pb d) CTSL-3-Cu e) CTSL-3-Cr	131

4.33	XRD spectrum of CTSL-3	132
4.34	DSC thermogram of CTSL-3	133
4.35	Effect of pH on % removal (Initial concentration=100 mg/L; Temperature=303K; Ads. Dose=4 g/L; Agitation speed=150rpm; Contact time=24 h)	134
4.36	Plot of various adsorption isotherms to CTSL-3-Cr (VI) adsorption data (Initial concentration=100 mg/L; Temperature=303K; pH=3; Ads. Dose=2g/L; Agitation speed=150rpm; Contact time=24h)	135
4.37	Plot of various adsorption isotherms to CTSL-3-Cu (II) adsorption data (Initial concentration=100 mg/L; Temperature=303K; pH=6; Ads. Dose=2g/L; Agitation speed=150 rpm; Contact time=24 h)	136
4.38	Plot of various adsorption isotherms to CTSL-3-Pb (II) adsorption data (Initial concentration=100 mg/L; Temperature=303K; pH=5; Ads. Dose=2g/L; Agitation speed=150 rpm, Contact time=24 h)	136
4.39	Plot of CTSL-3-Cr (VI) kinetic study data [a) Quantity adsorbed v/s time b) Pseudo-first order c) Pseudo-second order d) Intra particle diffusion] (Initial concentration=100 mg/L; Temperature=303K; pH=3; Ads. Dose=2g/L; Agitation speed=150rpm)	138
4.40	Plot of CTSL-3-Cu (II) kinetic study data [a) Quantity adsorbed v/s time b) Pseudo-first order c) Pseudo-second order d) Intra particle diffusion] (Initial concentration=100 mg/L; Temperature=303K; pH=6; Ads. Dose=2g/L; Agitation speed=150rpm)	138-139
4.41	Plot of CTSL-3-Pb (II) kinetic study data [a) Quantity adsorbed v/s time b) Pseudo-first order c) Pseudo-second order d) Intra particle diffusion] (Initial concentration=100 mg/L; Temperature=303K; pH=5;	139

	Ads. Dose=2g/L; Agitation speed=150rpm)	
4.42	XRD spectra of a) CTSL-3 b) CTSL-3-Cr c) CTSL-3-Cu d) CTSL-3-Pb	143
4.43	<sup>1</sup> H NMR spectrum of the ligand (L-4)	144
4.44	<sup>13</sup> C NMR of CTSL-4	145
4.45	FTIR spectra of a) Chitosan b) CTSL-4 c) CTSL-4-Pb d) CTSL-4-Cu e) CTSL-4-Cr	146
4.46	XRD spectrum of CTSL-4	147
4.47	DSC thermogram of CTSL-4	148
4.48	Effect of pH on % removal (Initial concentration=100 mg/L; Temperature=303K; Ads. Dose=4 g/L; Agitation speed=150 rpm; Contact time=24h)	149
4.49	Plot of various adsorption isotherms to CTSL-4-Cr (VI) adsorption data (Initial concentration=100 mg/L; Temperature=303K; pH=3; Ads. Dose=2g/L; Agitation speed=150 rpm; Contact time=24 h)	150
4.50	Plot of various adsorption isotherms to CTSL-4-Cu (II) adsorption data (Initial concentration=100mg/L; Temperature=303K; pH=6; Ads. Dose=2g/L; Agitation speed=150rpm; Contact time=24h)	151
4.51	Plot of various adsorption isotherms to CTSL-4-Pb (II) adsorption data (Initial concentration=100mg/L; Temperature=303K; pH=5; Ads. Dose=2g/L; Agitation speed=150rpm, Contact time=24h)	151
4.52	Plot of CTSL-4-Cr (VI) kinetic study data [a) Quantity adsorbed v/s time b) Pseudo-first order c) Pseudo-second order d) Intra particle diffusion] (Initial concentration=100mg/L; Temperature=303K; pH=3; Ads. Dose=2g/L; Agitation speed=150rpm)	153
4.53	Plot of CTSL-4-Cu (II) kinetic study data [a) Quantity adsorbed v/s time b) Pseudo-first order c) Pseudo-second	153-154

	order d) Intra particle diffusion] (Initial concentration=100 mg/L; Temperature=303K; pH=6; Ads. Dose=2g/L; Agitation speed=150 rpm)	
4.54	Plot of CTSL-4-Pb (II) kinetic study data [a) Quantity adsorbed v/s time b) Pseudo-first order c) Pseudo-second order d) Intra particle diffusion] (Initial concentration=100 mg/L; Temperature=303K; pH=5; Ads. Dose=2g/L; Agitation speed=150rpm)	154
4.55	XRD spectra of a) CTSL-4 b) CTSL-4-Cr c) CTSL-4-Cu d) CTSL-4-Pb	158
4.56	SEM micrographs of membranes: (a) surface of P-0 membrane (b) cross-section of P-0 membrane (c) surface of a PSf : CTSL-2, 99.0:1.0% membrane d) cross-section of a PSf : CTSL-2, 99.0:1.0% membrane (e) surface of a PSf : CTSL-2, 98.0:2.0% membrane (f) cross-section of a PSf : CTSL-2, 98.0:2.0% membrane , (g) cross section of PSf :CTSL-2, 98:2% membrane showing macro voids (h) cross section of PSf : CTSL-2, 98: 2% membrane showing microporous structure on the walls of macro voids	167-168
4.57	Reconstructed three dimensional view of a) Neat polysulfone membrane (P-0), and b) Polysulfone membrane blended with 2% CTSL-2 (P-2)	168
4.58	Contact angle of the (a) neat polysulfone membrane (b) PSf:CTSL-2, 99.0 : 1.0% membrane(c) PSf : CTSL-2, 98.0 : 2.0%, membrane	169
4.59	X-ray diffraction patterns of chitosan derivative (CTSL-2), PSf-CTSL-2 blend membrane with 2% CTSL-2 (P-2), and neat PSf (P-0) membrane	170
4.60	Variation of pure water flux of the membranes at 0.4 Mpa TMP and 27°C	171

4.61	Pure water flux of the membranes as a function of TMP at 27°C	171
4.62	Time dependent flux of PSf-CTSL-2 membranes at 0.8 Mpa TMP during three different conditions. PWF for 60 min, BSA flux (pH =7 ± 0.2) for 60 min and water flux for 60 min after 15 min of washing with distilled water.	173
4.63	Pb (II) metal rejection of membranes	175
4.64	Cu (II) metal rejection of membranes	176
4.65	Cr (VI) metal rejection of membranes	177
4.66	The proposed mechanisms of heavy metal rejection by membranes (a) Pb (II) and Cu (II), and b) Cr (VI)	178
5.1	Structure of novel chitosan derivatives	181

## LIST OF TABLES

<b>TABLE NO</b>	<b>TABLE CAPTION</b>	<b>PAGE NUMBER</b>
1.1	Industrial sources and toxic effects of a few heavy metals	5-6
2.1	Main characteristics and adsorption capacities of chitosan/ chitosan based derivatives for the removal of Cu (II), Pb (II), Cr (VI)	47-55
3.1	Properties and characteristics of chitosan (Data provided by the supplier)	60
3.2	Chemicals used and their suppliers	61-62
3.3	List of instruments used	62-63
4.1	Equilibrium model parameters for adsorption of Cu (II), Pb (II) and Cr (VI) on CTSL-1	97
4.2	Comparison of kinetic model parameters for Cr (VI), Cu (II) and Pb (II) on to CTSL-1	101
4.3	Results of thermodynamic study for the adsorption of Cr (VI), Cu (II) and Pb (II) on to CTSL-1	104-105
4.4	FTIR peak vibrations before and after adsorption on to CTSL-1	110
4.5	Equilibrium model parameters for adsorption of Cr (VI), Cu (II) and Pb (II) on CTSL-2	119
4.6	Kinetic model parameters for adsorption of Cr (VI), Cu (II) and Pb (II) onto CTSL-2	122
4.7	Thermodynamic parameters for the adsorption of Cr (VI), Cu (II) and Pb (II) onto CTSL-2	125
4.8	FTIR peak vibrations before and after adsorption on to CTSL-2	127
4.9	Equilibrium model parameters for adsorption of Cr (VI), Cu (II) and Pb (II) on CTSL-3	135
4.10	Kinetic model parameters for adsorption of Cr (VI),	137

	Cu (II) and Pb (II) onto CTSL-3	
4.11	Thermodynamic parameters for the adsorption of Cr (VI), Cu (II) and Pb (II) onto CTSL-3	140
4.12	FTIR peak vibrations before and after adsorption on to CTSL-3	142
4.13	Equilibrium model parameters for adsorption of Cr (VI), Cu (II) and Pb (II) on CTSL-4	150
4.14	Kinetic model parameters for adsorption of Cr (VI), Cu (II) and Pb (II) onto CTSL-4	152
4.15	Thermodynamic parameters for the adsorption of Cr (VI), Cu (II) and Pb (II) onto CTSL-4	155
4.16	FTIR peak vibrations before and after adsorption on to CTSL-4	156-157
4.17	Summary of results of adsorption studies	160
4.18	Regression coefficient values obtained for various adsorbents for the fitment of adsorption isotherms to experimental data	161
4.19	Percentage of swelling and bulk density of chitosan and chitosan derivatives	162
4.20	Filtration and antifouling performances of the membranes	173



## LIST OF ABBREVIATIONS

$\Delta G^\circ$ (kJ.mol <sup>-1</sup> )	- Change in standard Gibb's free energy
$\Delta H^\circ$ (kJ.mol <sup>-1</sup> )	- Change in standard enthalpy
$\Delta S^\circ$ (J.mol <sup>-1</sup> K <sup>-1</sup> )	- Change in standard entropy
<sup>13</sup> C NMR	- Carbon-13 nuclear magnetic resonance
<sup>1</sup> H NMR	- Hydrogen proton nuclear magnetic resonance
A (m <sup>2</sup> )	- Effective area of the membrane
a.u.	- Absorbance units
AAS	- Atomic adsorption spectrometer
a <sub>e</sub>	- Activity of the metal ion in the solution at equilibrium
AFM	- Atomic force microscopy
a <sub>R</sub> (L mg <sup>-1</sup> )	- Parameter in Redlich-Peterson isotherm
a <sub>s</sub>	- Activity of the adsorbed metal ion on the surface of the adsorbent
ATR	- Attenuated total reflectance
b (L/mg)	- Langmuir constant
BET	- Brunauer–Emmett–Teller
b <sub>R</sub>	- Dimensionless parameter in Redlich-Peterson isotherm
BSA	- Bovine serum albumin
C (mg g <sup>-1</sup> )	- Intercept
C <sub>e</sub> (mg/L)	- Concentration of the solute in solution at equilibrium
CHN analyzer	- Carbon-hydrogen-nitrogen analyzer
CNT	- Carbon nanotube
C <sub>o</sub> (mg/L)	- Initial concentration of solute in solution
Conc.	- Concentration
CS	- Chitosan
CTS	- Chitosan
CTSL-1	- Chitosan derivative no.1
CTSL-1-Cr	- Complex of Chitosan derivative -1 with chromium
CTSL-1-Cu	- Complex of Chitosan derivative -1 with copper
CTSL-1-Pb	- Complex of Chitosan derivative -1 with lead
CTSL-2	- Chitosan derivative no.2
CTSL-2-Cr	- Complex of Chitosan derivative -2 with chromium
CTSL-2-Cu	- Complex of Chitosan derivative -2 with copper
CTSL-2-Pb	- Complex of Chitosan derivative -2 with lead
CTSL-3	- Chitosan derivative no.3
CTSL-3-Cr	- Complex of Chitosan derivative -3 with chromium
CTSL-3-Cu	- Complex of Chitosan derivative -3 with copper
CTSL-3-Pb	- Complex of Chitosan derivative -3 with lead
CTSL-4	- Chitosan derivative no.4
CTSL-4-Cr	- Complex of Chitosan derivative -4 with chromium
CTSL-4-Cu	- Complex of Chitosan derivative -4 with copper
CTSL-4-Pb	- Complex of Chitosan derivative -4 with lead
CuSO <sub>4</sub> .5H <sub>2</sub> O	- Copper sulfate pentahydrate

<b>DCL</b>	- Degree of cross linking
<b>DMF</b>	- Dimethyl formamide
<b>DSC</b>	- Differential scanning calorimetry
<b>DTA</b>	- Differential thermal analysis
<b>dz (g/L)</b>	- Adsorbent dose
<b>E</b>	- Elovich
<b>EA</b>	- Elemental analysis
<b>ED</b>	- Electrodialysis
<b>EDTA</b>	- Ethylene-diamine-tetra-acetic-acid
<b>EDXRF</b>	- Energy dispersive X-ray fluorescence
<b>EPR</b>	- Electron paramagnetic resonance
<b>ESR</b>	- Electron spin resonance
<b>EtOH</b>	- Ethyl alcohol
<b>F</b>	- Freundlich
<b>Fe<sub>2</sub>O<sub>3</sub></b>	- Ferric oxide
<b>FeS</b>	- Ferrous sulfide
<b>FESEM</b>	- Field emission scanning electron microscopy
<b>FRR</b>	- Flux recovery ratio
<b>FTIR</b>	- Fourier transform infrared spectroscopy
<b>H<sup>+</sup></b>	- Hydrogen ion
<b>H<sub>2</sub>S</b>	- Hydrogen sulfide
<b>HCl</b>	- Hydro chloric acid
<b>HCrO<sub>4</sub><sup>-</sup></b>	- Hydrogen chromate ion
<b>ICP-OES</b>	- Inductively coupled plasma optical emission spectroscopy
<b>J<sub>p</sub> (Lm<sup>-2</sup> h<sup>-1</sup>)</b>	- Flux after fouling of the membrane
<b>J<sub>w</sub> (L m<sup>-2</sup> h<sup>-1</sup>)</b>	- Pure water flux
<b>J<sub>w1</sub> (Lm<sup>-2</sup> h<sup>-1</sup>)</b>	- Initial flux
<b>J<sub>w2</sub> (Lm<sup>-2</sup> h<sup>-1</sup>)</b>	- Flux of the membrane after washing
<b>k<sub>1</sub>(min<sup>-1</sup>)</b>	- pseudo-first order adsorption rate constant
<b>k<sub>2</sub> (g mg<sup>-1</sup>min<sup>-1</sup>)</b>	- Second order adsorption rate constant
<b>K<sub>2</sub>Cr<sub>2</sub>O<sub>7</sub></b>	- Potassium dichromate
<b>K<sub>f</sub> (mg/g)</b>	- Freundlich adsorbent constant
<b>K<sub>id</sub> (mg g<sup>-1</sup>min<sup>-1/2</sup>)</b>	- Intra-particle diffusion rate constant
<b>K<sub>o</sub></b>	- Equilibrium constant, dimensionless
<b>K<sub>R</sub> (L g<sup>-1</sup>),</b>	- Parameter in Redlich-Peterson isotherm
<b>L</b>	- Langmuir
<b>L-1</b>	- Ligand-1
<b>L-2</b>	- Ligand-2
<b>L-3</b>	- Ligand-3
<b>L-4</b>	- Ligand-4
<b>L-F</b>	- Langmuir-Freundlich
<b>M<sup>2+</sup></b>	- Divalent metal ion
<b>MEUF</b>	- Micellar enhanced ultrafiltration
<b>MS</b>	- Metal sulfide
<b>MW</b>	- Molecular weight
<b>MWCNT</b>	- Multi walled carbon nanotubes

<b>MWCO</b>	- Molecular weight cut-off
<b>n</b>	- Dimensionless Freundlich exponent
<b>NA</b>	- Not available/ not applicable
<b>Na<sub>2</sub>S<sub>2</sub>O<sub>3</sub></b>	- Sodium thiosulfate
<b>NaAc</b>	- Sodium acetate
<b>NaOH</b>	- Sodium hydroxide
<b>NMP</b>	- N-Methyl-2-Pyrrolidone
<b>NMR</b>	- Nuclear magnetic resonance
<b>OH<sup>-</sup></b>	- Hydroxyl ions
<b>P-0</b>	- Neat membrane with 100% PSf and 0% CTSL-2
<b>P-1</b>	- PSf: CTSL-2 blend membrane with 99% PSf and 1% CTSL-2
<b>P-2</b>	- PSf: CTSL-2 blend membrane with 98% PSf and 2% CTSL-2
<b>Pb(NO<sub>3</sub>)<sub>2</sub></b>	- Lead nitrate
<b>PEG</b>	- Poly ethylene glycol
<b>PEG-1000</b>	- Polyethylene glycol with average molecular weight of 1000
<b>PEI</b>	- Polyethelyneimine
<b>PEUF</b>	- Polymer enhanced ultrafiltration
<b>PFO</b>	- Pseudo first order
<b>POCl<sub>3</sub></b>	- Phosphorus oxychloride
<b>PSf</b>	- Polysulfone
<b>PSO</b>	- Pseudo second order
<b>PVP</b>	- Polyvinylpyrrolidone
<b>PUF (Lm<sup>-2</sup> h<sup>-1</sup>)</b>	- Pure water flux
<b>Q (L)</b>	- Volume of water collected
<b>Q<sub>e</sub> (mg g<sup>-1</sup>)</b>	- Quantity adsorbed at equilibrium
<b>Q<sub>e calc</sub> (mg g<sup>-1</sup>)</b>	- Adsorption capacity at equilibrium (calculated)
<b>Q<sub>e expt.</sub> (mg g<sup>-1</sup>)</b>	- Adsorption capacity at equilibrium (experimental)
<b>Q<sub>o</sub> (mg g<sup>-1</sup>)</b>	- Maximum monolayer adsorption capacity
<b>Q<sub>t</sub> (mg g<sup>-1</sup>)</b>	- Quantity adsorbed at time t
<b>R<sub>h</sub> (MPa. L<sup>-1</sup> m<sup>2</sup> h)</b>	- Hydraulic resistance
<b>R<sub>m</sub> (L<sup>-1</sup> m<sup>2</sup>)</b>	- Hydraulic resistance
<b>R<sub>ir</sub></b>	- Irreversible loss in flux due to fouling as a percentage of initial flux
<b>R<sub>L</sub></b>	- Dimensionless separation factor of Langmuir isotherm
<b>RO</b>	- Reverse osmosis
<b>RP</b>	- Redlich-Peterson
<b>R<sub>r</sub></b>	- Flux recovery as a percentage of initial flux
<b>RT</b>	- Room temperature
<b>R<sub>t</sub></b>	- Total loss of flux due to membrane fouling as a percentage of initial flux
<b>SEM</b>	- Scanning electron microscopy
<b>SSE</b>	- Sum of squared error
<b>TEM</b>	- Transmission electron microscopy

<b>TG/DTG</b>	- Thermogravimetry/ Differential thermogravimetry
<b>TGA</b>	- Thermo gravimetric analysis
<b>TMP</b>	- Trans membrane pressure
<b>UF</b>	- Ultrafiltration
<b>USEPA</b>	- United States environmental protection agency
<b>V(L)</b>	- Volume of the solution
<b><math>v_e</math></b>	- Activity coefficient of the adsorbate in the equilibrated solution.
<b><math>v_s</math></b>	- Activity coefficient of the adsorbate on the adsorbent surface
<b>VSM</b>	- Vibrating sample magnetometer
<b>W (g)</b>	- Mass of the adsorbent taken
<b>WAXRD</b>	- Wide angle X-ray diffraction
<b>WHO</b>	- World health organization
<b>XPS</b>	- X-ray photoelectron spectroscopy
<b>XRD</b>	- X-ray diffraction
<b>XRPD</b>	- X-ray powder diffraction
<b>ZnCl<sub>2</sub></b>	- Zinc chloride
<b><math>\Delta G</math> (kJ.mol<sup>-1</sup>)</b>	- Change in Gibb's free energy
<b><math>\Delta P</math> (Pa)</b>	- Difference in trans-membrane pressure
<b><math>\Delta t</math> (h)</b>	- Time interval of water collection

## NOMENCLATURE

<b>%</b>	- percentage
<b>~</b>	- approximately
<b>2<math>\theta</math></b>	- Bragg's angle
<b><math>\mu</math></b>	- Viscosity (Pa.sec)
<b>cm</b>	- centimeter
<b>d</b>	- day
<b>g</b>	- gram
<b>g/L</b>	- gram per liter
<b>h</b>	- hour
<b>J</b>	- Joule
<b>K</b>	- Kelvin
<b>kJ</b>	- Kilo Joule
<b>L</b>	- liter
<b>mg</b>	- milligram
<b>mg/L</b>	- milligram/liter
<b>min</b>	- minute
<b>mL</b>	- milliliter
<b>mm</b>	- millimeter
<b>mmol g<sup>-1</sup></b>	- millimol per gram
<b>MPa</b>	- Mega Pascal
<b>nm</b>	- nanometer
<b>°C</b>	- degree Celsius
<b>Pa</b>	- Pascal
<b>ppm</b>	- parts per million
<b>psi</b>	- pounds per square inch
<b>R</b>	- universal gas constant
<b>r<sup>2</sup></b>	- coefficient of determination
<b>rpm / RPM</b>	- rotations per minute
<b>s</b>	- sec
<b>t</b>	- time
<b>T</b>	- temperature
<b>V</b>	- volume
<b>v/v</b>	- volume/volume
<b>w/v</b>	- weight/volume
<b><math>\mu</math></b>	- micron



# **CHAPTER 1**

## **INTRODUCTION**





## **1.1 WATER POLLUTION BY HEAVY METALS**

Covering in excess of 70% of the surface of planet earth, water is indisputably among the most valued natural assets. Life on earth, as we know it, would be impossible without this prized resource. Availability of uncontaminated water is central to the survival of all forms of flora and fauna. Ever increasing growth in human population coupled with industrialization is leading to escalating levels of industrial pollution. Pollution attributable to industrial wastewater is turning out to be a grave concern facing humanity. Hence, the remediation of polluted waters presents a worldwide challenge as these waters have to be finally restored and returned to environmental aquatic media or to the land.

Heavy metals are key contributors to pollution of fresh and marine aquatic bodies in addition to ground water. The presence of toxic heavy metals in effluents poses a serious challenge to environmental vitality and sustainability. Lead, nickel, cadmium, arsenic and chromium are some of the heavy metals categorized by US Environmental Protection Agency (USEPA) as priority pollutants.

The danger posed by heavy metals to the environment arises from the fact that, apart from being toxic to various life forms, they are also non-biodegradable, stable and possess environmental mobility. World Health Organization has recently recognized the health hazards of toxic metals in food chain even at low concentrations (Srivastava and Goyal 2010).

### **1.1.1 Classification of elements as “heavy metals”.**

According to Duffus (2002), there is no clear basis that may be uniformly applied for the definition of ‘heavy metals.’ The ‘heavy metals’ have been variously classified according to their chemical, physical or biological properties which include atomic weight and number, and density (specific gravity).

Classification based on density describes those having densities less than 5 g/cm<sup>3</sup> as light metals while those having densities more than 5 g/cm<sup>3</sup> as heavy metals (Srivastava and Goyal 2010). Thus metals like Hg, Cd, Cr, Ni, and Pb are generally known as toxic heavy metals by this classification. According to Volesky (2005) toxic

metals are understood to be elements (not only metals) commonly used in industry and generally toxic to living organisms even at low concentrations, including As, Cd, Cr, Cu, Pb, Hg, Ni, Zn and Se. Among these, As and Se are frequently named with a term ‘heavy metal’ although these elements are not metallic. However, based on their toxic properties, they are classified into the same group along with other toxic elements and are named toxic metals (Kabata-Pendias and Pendias 2000).

### 1.1.2 Dose-response relationship.

The favourable and harmful effects of the elements are determined by their dose-response relationship. The Figure 1.1 shows the association between quantity and effect. However, the dosage at which the harmful effects are considered calamitous is a matter of conjecture. The accepted position constantly changes as the sensitivity of measurements rises and very minute effects become known (Srivastava and Goyal 2010).

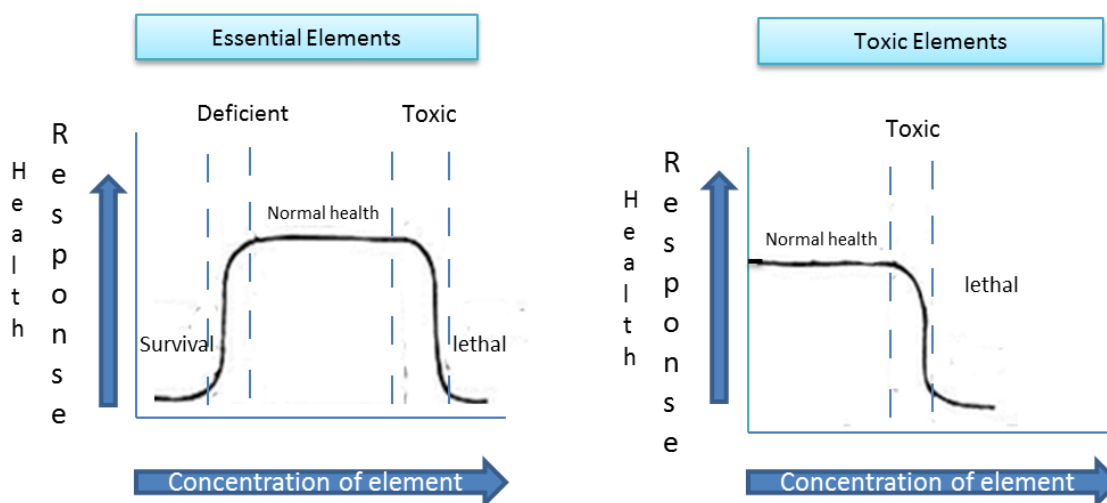


**Figure 1.1 Association between dose and response for essential and toxic elements. (Source: Srivastava and Goyal 2010).**

While lead, mercury, chromium (VI) and cadmium have deleterious effect on living organisms at all levels of concentration, copper (II), chromium (III), and selenium are required in trace amounts. As may be inferred from the preceding discussion, toxicity

is occasionally dependent on the oxidation state: chromium (III) is essential for good health in trace amounts, while chromium (VI) is toxic (oncogenic).

### 1.1.3 Sources and toxic effects of heavy metals

A wide range of human activities produce huge quantities of wastewater containing heavy metals. Potential sources of the heavy metals release into environment are the industries such as mining, electroplating, fabrication, leather tanning, fertilizer, textile dyes, printing, and acid battery manufacturing. Other causes for the metal release include natural weathering processes, waste emissions, atmospheric depositions, landfills, pesticide application to crops and additional anthropogenic activities (Monier et al. 2010; Wang and Chen 2009).

The harmful effect of metals is due to enzyme inhibition or activation, damage of subcellular organelles, carcinogenicity, and effects on kidneys, nervous system, endocrine system, reproduction and respiratory system (Hodgson, 2004).

A selected compilation of industrial sources and their toxic effects is given in Table 1.1.

**Table 1.1 Industrial sources and toxic effects of a few heavy metals.**  
(Source: Maczulak 2010)

	<b>Metals</b>	<b>Sources</b>	<b>Main Toxicity Outcomes</b>
<b>1</b>	Arsenic	Semiconductors, glass, wood preservatives.	Gastro intestinal and lung irritations, decreased red and white blood cells, cancer, death.
<b>2</b>	Cadmium	Electroplating, batteries, nuclear reactor control rods, stabilizers for plastics, tobacco smoke.	Lung damage, bone fracture, Kidney failure, infertility, damage to nervous and immune systems, death.
<b>3</b>	Chromium	Coating on other metals, stainless steel, pigments in cements and plaster, leather tanning, gems,	Allergy, rash, nose irritation, ulcers, respiratory problems, weakened immunity, kidney and liver damage, lung cancer, death.

		recording tapes.	
4.	Cobalt	Alloys, magnets, paints, inks, pottery, stained glass, tile, jewellery	Respiratory, heart, thyroid and vision ailments.
5.	Copper	Electrical equipment, plumbing, heat exchangers, alloys.	Neurological effects, anaemia, liver cirrhosis, brain damage, kidney failure, and copper deposition in cornea.
6.	Lead	Batteries, television and computer screens, pipes, alloys, paint, gasoline, crystals, nuclear reaction shielding, tobacco smoke.	Increased blood pressure, brain and nerve damage, miscarriage, decreased fertility, behavioural disorders, learning disabilities in children.
7.	Mercury	Burning fuels, incinerators, industrial emissions, mining, paper or steel manufacture, electronics.	Weakness, loss of peripheral vision, tremors, behavioural disorders, coma, death.

#### 1.1.4 Heavy metals: A persistent and problematic polluter

Constant release of contaminated waters arising from industrial, agricultural and municipal wastes poses serious threat to the environmental water bodies. Among others, the contaminants include heavy metals, which are non-biodegradable, unlike most of the organic pollutants. The heavy metals accumulate in aquatic fauna like fish, and on consumption by humans, get concentrated in their body (Naimo 1995; Saylor et al. 1975). Hence, it is vitally important to treat the waste waters to remove their metal content before releasing into the environment.

## **1.2 METHODS OF HEAVY METAL REMOVAL**

As discussed in section 1.1.3, a wide range of industrial activities release heavy metals into the environment. Before disposing the effluents, it is obligatory on the industry to remove the metal pollutants. The methods commonly employed for eliminating the metal ions from liquid streams are the following: chemical precipitation, solvent extraction, membrane process, ion exchange, electrochemical method and adsorption (Kanamadi et al. 2006).

### **1.2.1 Chemical precipitation**

Precipitation of heavy metals is accomplished by adding chemical agents to promote coagulation and flocculation. Commonly used agents are lime, trivalent iron or aluminium salts, organic coagulants (cationic polyelectrolytes), inorganic polymers (activated silica) and natural polymers (starches, alginate) (Wang et al. 2009a). The problem of safe disposal of huge amounts of toxic sludge that gets formed during the process is the chief drawback of this method.

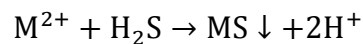
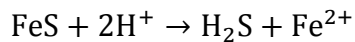
#### **1.2.1.1 Hydroxide precipitation**

The most prevalent method of chemical precipitation is the hydroxide precipitation. Its popularity is due to its ease of operation and cost competitiveness. Removal of metals is achieved by their precipitation as hydroxides using lime or caustic soda. The usual pH required for precipitation is in the range of 8-11. The effectiveness of this method is determined mainly by the readiness of the metal ions to form the hydroxides, oxidation state of the metal ions, formation of complexation compound with other ions, pH, intensity of mixing, and settling characteristics of the sludge.

There are, however, a few drawbacks of employing hydroxide precipitation. First, the difficulties in handling of the large amounts of metal-bearing sludges that are toxic, and their final disposal which is often troublesome and expensive. Second, non-uniformity in the solubility of the metal ions in different pH, i.e., when one metal precipitates, the other may dissolve. Third, in the presence of complexing agents, the metal hydroxides may not precipitate (Fu and Wang 2011).

### 1.2.1.2 Sulphide precipitation

One of the attractive features of metal sulphide precipitates is that their solubility is greatly lower than metal hydroxides. Therefore excellent metal removal efficiencies can be achieved by sulphide precipitation. The metal precipitation takes place in two steps as given below (Ozverdi and Erdem 2006).



Sulphide precipitation is highly beneficial either as a finishing operation after the hydroxide precipitation process or when very large amount of metal removal is required.

### 1.2.1.3 Xanthate process

A xanthate is an organo-sulfur compound that has the generic chemical formula  $\text{ROCS}_2^- \text{M}^+$ , where R is an alkyl group and  $\text{M}^+$  is  $\text{Na}^+$  or  $\text{K}^+$ . The xanthate functions by the principle of ion-exchange, exchanging the metal ions with  $\text{Na}^+$  or  $\text{K}^+$  forming metal xanthate complex. The advantage of the xanthate process is that it produces less sludge than hydroxide precipitation process (Chang et al. 2002).

### 1.2.2 Solvent extraction

Of late, this method is gaining popularity in effluent treatment due to the availability of many organic reagents that can selectively form complexes with a particular heavy metal which needs to be removed. The feed and the organic reagent are agitated with a water-immiscible organic solvent and the metal is transferred into the organic phase. After separating the organic phase from the aqueous phase, the metal is removed from the organic phase by acid treatment. Thus the metal can be obtained in the final aqueous phase in a highly concentrated form compared to the feed. The organic solvent is then reused.

### **1.2.3 Membrane Process**

Among the key advantages of heavy metal separation using membrane technologies are their efficacy, ease of handling and compactness. Ultrafiltration, reverse osmosis, nanofiltration and electrodialysis are some of the techniques used for removal of heavy metals from aqueous media.

#### **1.2.3.1 Ultrafiltration (UF)**

Ultrafiltration is a membrane process operating at low pressures (0-10 bar) for the removal of dissolved and colloidal material. The metal ion sizes are much smaller than the pore sizes, therefore, an increase in effective dimensions of the ions have to be achieved for their rejection by the membrane. This may be accomplished by the following two techniques: In the first method known as micellar enhanced ultrafiltration (MEUF), an organic surfactant is added to the feed solution to form a micellar layer around the metal ion, and if the size of this formation is more than the pore size, it gets retained by the membrane. In the second method known as Polymer enhanced ultrafiltration (PEUF), a water soluble polymer (e.g. polyetherimine, polyacrylic acid) is added to the feed solution to form a complex with the metal ion. If the size of this metal ion-polymer complex is more than the molecular weight cut-off of the membrane, it gets retained by the membrane (Fu and Wang 2011).

#### **1.2.3.2 Reverse Osmosis (RO)**

In recent years Reverse Osmosis is progressively emerging as a preferred separation technology choice in environmental and chemical engineering. The reverse osmosis technology employs a semi-permeable membrane to split the feed solution into permeate (pure water) and a concentrate (concentrated solutes) (Perez-Gonzalez et al. 2012). It is the most commonly used method to get pure water by desalination of sea water. Reverse osmosis is able to retain a wide ranging array of dissolved chemicals from aqueous solutions.

### **1.2.3.3 Nano filtration**

Nanofiltration membranes utilize pore sizes that are in between reverse osmosis and ultrafiltration. They have a typical operating pressure range of 2-20 bar. Nanofiltration technique has been successfully used for stripping of heavy metals such as nickel, chromium, copper and arsenic from polluted waters.

### **1.2.3.4 Electrodialysis**

Electrodialysis (ED) is a technique which assembles cation-exchange and anion- exchange membranes in alternating positions in a direct current electric field. ED is a promising method that has often been used in an integrated manner with other membrane technologies such as ultrafiltration and reverse osmosis in water treatment and desalination of sea water (Xu and Huang 2008).

### **1.2.4 Ion exchange**

Ion-exchange technology has been extensively adopted to eliminate heavy metals from aqueous solutions. This method enjoys many positives such as large scale operational capability, excellent removal efficacy and superior kinetics of removal (Kang et al. 2004). Synthetic resins are widely chosen for their efficiency in almost completely eliminating the heavy metals from solution. The  $H^+$  or  $Na^+$  of the resin is exchanged for the metal cations in solution. The main drawback is that in the presence of  $Na^+$  and  $Ca^{2+}$  ions this process is very ineffective.

### **1.2.5 Electrochemical method**

Electrocoagulation and electrodeposition are the two important technologies in this category. In the case of electrocoagulation, the coagulants- either aluminium ions or iron ions- are electrically produced from their respective electrodes. The hydrogen gas generated during the process also helps in the flotation of the flocculated particles (Chen 2004).

The electrodeposition (also known as electrowinning or electro refining) works by electrolytically depositing the heavy metal present in solution on the surface



of the cathode. This method has been investigated for the removal of Cu, Ni, and Cd from their near saturated aqueous solutions. Wastewater treatment techniques using electrochemical methods are characterized by high capital and operating costs, so their usage has been limited. However, in the recent past, with strict environmental regulations being implemented, there has been a revival of interest in these technologies (Wang et al. 2007).

### **1.2.6 Adsorption**

Adsorption refers to the accretion of the solute due to the physico-chemical interactions between the surface of the adsorbent material and the solute present in the solution. Adsorption is acknowledged as a very efficient and popular technique used in wastewater treatment owing to its cost effectiveness, simplicity and technical practicability even at low solute concentrations (Shariful et al. 2017). The adsorbents which are in active usage or under development have mineral, organic or biological origins. Among such adsorbents are activated carbons, zeolites, clays, silica beads, low-cost adsorbents, industrial by products, biomass, organic polymeric resins, macro porous hyper crosslinked polymers (Boamah et al. 2015; Crini, 2005). Activated carbon, with its very high specific surface area, often above 1000 m<sup>2</sup>/g, has been greatly utilized, due to its significant adsorptive capacity for heavy metals. However, in spite of wide spread use of activated carbon, its usage is weighed down by considerations of high cost and problems associated with its reusability (Foo and Hameed 2010). A great deal of research has also gone into the use of adsorbents prepared from agricultural wastes, industrial byproducts and wastes, and natural materials (Ngah and Hanafiah 2008; Sud et al. 2008; Fu and Wang 2011; Uddin 2017).

## **1.3 SCOPE OF THE STUDY**

The metal binding capabilities of various biological materials for the removal of toxic metals from wastewaters has generated considerable interest in biosorption as a means to sequester heavy metals (Negm and Ali 2010). Chitosan, a biopolymer, derived from chitin - the second most abundant resource occurring in nature after cellulose, has attracted the attention of many researchers due to the presence of amino

and hydroxyl groups (Lv et al. 2017; Nagireddi et al. 2017). Chitosan has unique characteristics such as high reactivity, chemical stability, excellent chelation behavior and high affinity towards pollutants (Boamah et al. 2015).

In its pure form, chitosan is not suitable for real applications as a biosorbent due to a few limitations: 1) its relatively low mechanical strength; 2) its solubility in acidic media due to protonation of the amine groups in acidic solution (Wang and Chen 2014; Kurita 2006) 3) its swelling nature when immersed in water, which seriously limits the use as an adsorbent in continuous contact columns. When used in waste water treatment, the high swelling quality of chitosan due to water retention may lead to choking of the column and fouling over a period of time. Owing to these factors, till date, chitosan has hardly been used as an adsorbent for industrial uses in water treatment (Kyzas and Bikiaris 2015; Kyzas and Kostoglou 2015).

Due to reasons cited above, chitosan is not preferred in its unmodified form for practical applications in environmental control. Sorption performances of chitosan can be enhanced by various physical and chemical modifications including cross-linking and grafting techniques. The reported literature on such modifications is presented in Chapter 2, from which it is clear that research efforts are being directed towards improving the properties of chitosan such as chemical stability, mass transfer characteristics and/ or hydrodynamics in the contacting equipment by means of physical or chemical modifications.

The presence of amino groups in the chemical structure of chitosan permits reactions with several substituents, with possibility of creating a variety of eclectic modified biopolymers (Guinesi and Cavalheiro 2006). Physical and/or chemical modifications may be employed to favorably tweak the polymer characteristics (improving the sorbent-metal interaction, improvement in metal selectivity, increasing the pH range of polymer stability) or improving adsorption kinetics (controlling diffusion characteristics). Further, the presence of S, O and N atoms in functional groups of cross linking agent or grafted ligand is of prime importance in metal adsorption as they provide active sites for metal binding (Nagireddi et al. 2017).

Modified bio-polymer Schiff bases have an imine group ( $-RC=N-$ ), obtained by reacting the amino groups ( $-NH_2$ ) of chitosan with a carbonyl group ( $>C=O$ ) of an aldehyde or ketone (Kocak et al. 2012). Polymers that possess Schiff bases in their structure make an important group of chelating resins. Schiff bases are well known for their very good selectivity towards complexation of transition metals ions, and low affinity to alkali and alkaline earth metal ions (Ceglowski 2015). Moreover, many Schiff bases contain additional donor groups, which make them very good candidates for metal ion complexation. These Schiff bases can be obtained by simple self-condensation or even multiple self-condensation processes that take place in one synthetic step. Linking Schiff bases to polymers result in chelating resins that show well-defined molecular assemblies (Vigato and Tamburini 2004). All these properties make Schiff base chelating resins very useful to removal of transition metal ions from solutions.

In recent times membranes have played a crucial role in the field of water purification and reuse. Membranes have the ability to allow a selective chemical species in a mixture to pass through, while preventing other species from doing so (Baker 2000). The attractiveness of membrane related processes stem from benefits such as no phase change during separation, low energy expenditure, conceptual simplicity, reduced operating outlays, easy integration and scale up. The capability of the membranes to aid selective permeation is what gives them an important place in this domain (Hebbar et al. 2016; Molinari et al. 2004).

Polysulfone is an important class of polymeric material widely used in ultrafiltration, reverse osmosis and pervaporation membranes (Kumar et al. 2013a). Polysulfone possesses excellent film forming capability, has superior chemical and mechanical properties and is available at competitive prices (Padaki et al. 2012). Further, polysulfone membranes have a wide operating temperature range ( $\sim 75^\circ\text{C}$ ), a broad pH range (3-11) and have excellent resistance to chlorine (up to 200 ppm) (Cho et al. 2011). However polysulfone membranes suffer from poor permeability and inferior anti-fouling behaviour. Low permeability generally, is attributed to small surface pore size and low surface hydrophilic property. Poor anti-fouling performance is attributable to low surface hydrophilicity (Kumar et al. 2013a). Earlier studies have

reported that blending polysulfone with additives like polyvinylpyrrolidone (PVP) or poly(ethylene glycol) (PEG) increases the hydrophilicity and improves anti-fouling characteristics (Kumar et al. 2013b).

The effort to incorporate the property of superior fouling-resistance into membranes is of foremost importance in the preparation of new membranes. Since fouling can be reduced by increasing hydrophilicity, various methods like polymer grafting, custom-made polymers, blending, and doping with oxides have been successfully employed to increase membrane hydrophilicity (Hebbar et al. 2015). Among the aforesaid methods, polymer blending offers a facile way of improving membrane characteristics (Hebbar et al. 2014).

Many earlier studies reporting blending of polysulfone with chitosan or chitosan derivatives to obtain improved permeation performance of membranes have been dealt under Chapter 2. On a similar vein, the presence of hydrophilic groups such as hydroxyl, amine and imine groups in the derivative synthesized in this study was expected to increase hydrophilicity and thereby improve permeation performance and increase the anti-fouling resistance of the membrane (Kumar et al. 2013a; Kumar et al. 2013b). In addition, by incorporating the chitosan derivative, an adsorbent material, into the polymer matrix, it was also expected to enhance the ability of the membrane for heavy metal retention.

Based on the extensive review of literature the following key research questions were raised.

- a) Is it possible to synthesize new Schiff derivatives of chitosan which would have better mechanical, chemical and swelling properties in addition to having a good adsorption capacity?
- b) Since additional N and O atoms are potential sites for heavy metal interactions, is it possible to synthesize novel ligands which have additional N and O atoms to be used as a graft material?
- c) What are the characteristics of such synthesized chitosan derivatives?
- d) Whether the chitosan derivatives with grafted ligands having a pyrazole ring bearing additional N atoms will be effective as adsorbents for the

sequestration of heavy metal ions such as Cu (II), Pb (II), and Cr (VI) in aqueous solutions?

- e) If so, what would be the maximum adsorption capacity of the synthesized derivatives? What are the optimum conditions for conducting the batch adsorption operations?
- f) What are the equilibrium, kinetic and thermodynamic characteristics of the adsorption process?
- g) What is the possible mechanism of heavy metal sequestration by the chitosan derivatives?
- h) Whether the synthesized derivative could be used as an additive to enhance the permeation properties of polysulfone membrane?
- i) Will there be improvement in surface hydrophilicity and anti-fouling properties of membranes so synthesized? Will there be any improvement in heavy metal rejection by such membranes?

## 1.4 OBJECTIVES OF THE RESEARCH WORK

The main objective of this research work was to develop novel and highly efficient chitosan derivatives as adsorbents for the removal of heavy metals from wastewater. It was proposed to investigate the adsorbent behaviour vis-à-vis three heavy metals namely, Cu (II), Pb (II) and Cr (VI), as these were among the most frequently identified contaminant metals.

The second objective was to develop an improved polysulfone-chitosan derivative blend membrane with potentially excellent permeation characteristics and superior heavy metal rejection performance.

The objectives outlined above were achieved through the following steps:

1. Synthesize the ligand molecules required for the modification of chitosan polymer and prepare new derivatives of chitosan by grafting the ligands to the chitosan backbone by Schiff reaction.
2. Characterize the chitosan derivatives prepared by the determination of: molecular structure by NMR, functional groups present by FTIR, crystallinity by XRD, swelling characteristics and other relevant properties.
3. Conduct batch adsorption studies to determine:
  - i. the time required to reach equilibrium,
  - ii. the optimum pH for adsorption,
  - iii. the maximum monolayer adsorption capacity and the best fitting adsorption isotherm,
  - iv. the best fitting kinetic model,
  - v. the spontaneity of the adsorption, and the enthalpy and entropy changes during the adsorption
4. Propose possible mechanism/s of adsorption.
5. Prepare polysulfone membranes blended with the chitosan derivative and to investigate the pore structure, surface hydrophilicity, permeation flux and anti-fouling nature of these membranes.
6. Study the heavy metal rejection behaviour of polysulfone membranes blended with chitosan derivative.

## 1.5 ORGANIZATION OF THE THESIS

This thesis is divided into the following five chapters:

Chapter 1 presents the **Introduction**

This chapter outlines the contextual boundaries of this research, motivation for the study and general problem statement. The objectives of the study are defined at the end of this chapter after careful consideration towards the reported research work and the research questions raised based on research gaps in reported literature.

Chapter 2 presents the detailed **Literature Review**

This chapter presents the relevant literature review that was executed during the study to uncover the research gaps. A summary of the relevant published works is also provided in tabular form in this chapter.

Chapter 3 presents the **Materials and Methods**

This chapter lists the various chemicals, analytical instruments and equipment used in this study. The procedure and the synthesis schemes for four chitosan derivatives are then presented. This is followed by experimental methods employed to achieve the set objectives.

Chapter 4 presents the **Results and Discussions**

This chapter presents the results of the studies carried out as per the methodologies described in Chapter 3. It has two parts, Part A and Part B. In Part A of this chapter, the results of the adsorption studies are presented and in Part B the results of the membrane studies are presented. The results are presented in the form of figures, tables and outputs of the analytical instruments. Detailed discussion and substantiation of the results and findings, along with related research work are also provided in this chapter.

Chapter 5 presents the **Summary and Conclusions**

This chapter enlists the summary and conclusions arrived at the end of this research work along with perspectives for further research.





# **CHAPTER 2**

## **LITERATURE REVIEW**

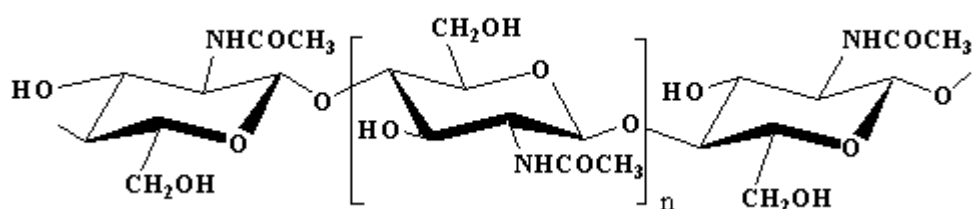


*This chapter presents the details of the reported literature relevant to the present research work. It encompasses the literature on chitosan, its molecular structure, its general uses, its uses as an adsorbent material, its limitations as an adsorbent material when used in the pure form and its physical and chemical modifications. Various derivatives including Schiff base derivatives of chitosan are dealt with here. The different adsorption isotherms, kinetic models and the thermodynamic equations used in the present study are also enumerated. The literature reports about polysulfone and polysulfone-chitosan derivative blend membranes and their characteristics are presented here.*

## **2.1 CHITOSAN**

Chitosan is a natural biopolyaminosaccharide obtained from chitin by the alkaline deacetylation of its acetamide groups (Kocak et al. 2004). Chitin is a natural biopolymer extracted from shells of crustaceans such as prawns, crabs, shrimps; insects, and fungal biomass; it is the most occurring biopolymer in the natural world second only to cellulose (Nadavala et al. 2009). The world availability of chitin is estimated to be around  $10^{10}$  metric tonnes per annum (Prashanth et al. 2007). It was observed by Rouget in 1859 that heating chitin in potassium hydroxide made it dissolve in organic acids. In 1894, Hoppe-Seyler christened it as chitosan and in 1950 its chemical structure was confirmed (Khor 2001).

### **2.1.1 Molecular structure of Chitin and Chitosan**



a)

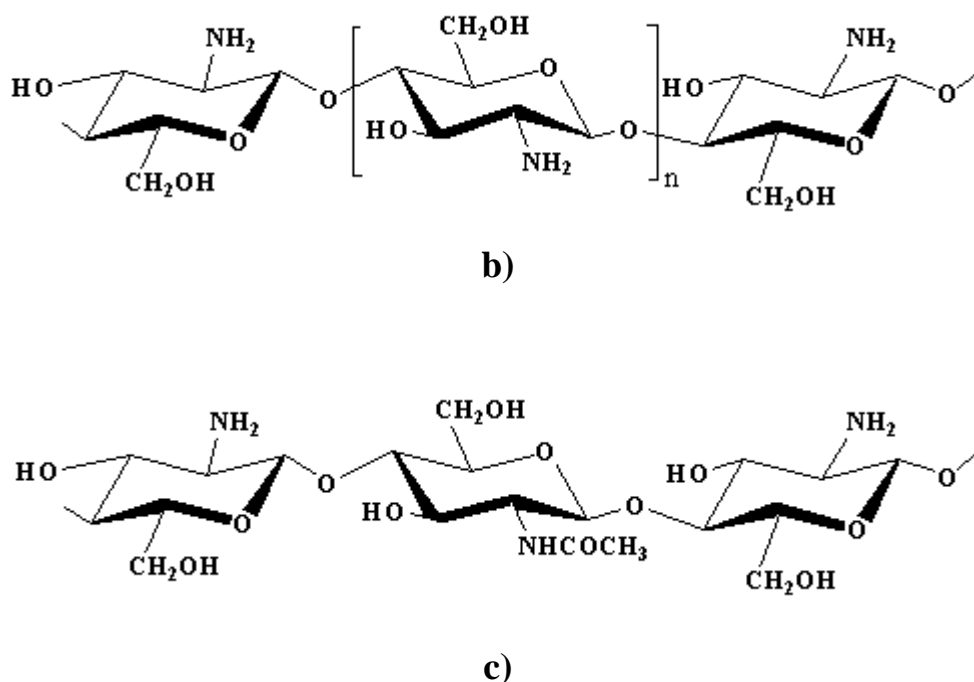


**Figure 2.1 Structure of a) chitin b) chitosan with complete deacetylation c) chitosan with partial deacetylation (Source: Ng et al. 2003).**

## 2.2 CHEMICAL STRUCTURE AND PROPERTIES OF CHITOSAN

The chemical structure of chitosan chain  $(C_6H_{11}NO_4)_n$ , (Figure 2.1 b and c) has a mass of 161 g per unit monomer, with an amino group ( $-NH_2$ ) concentration of 6.21 mmol  $g^{-1}$  under fully deacetylated condition (Wu et al. 2010). Chitosan may have a molecular weight of up to  $10^6$  Da or more (Prashanth et al. 2007). Chitosan is mildly basic and is insoluble in water and organic solvents. However, it is soluble in aqueous acidic solution ( $pH < 6.5$ ) due to protonation of  $R-NH_2$  to  $R-NH_3^+$  (Sinha et al. 2010). Unlike other natural polymers, chitosan has high reactivity and processability for its specific molecular structure and polycationic nature. Chitosan is soluble in dilute acids such as formic acid, acetic acid, lactic acid, pyruvic acid and oxalic acid (Varma et al. 2004).

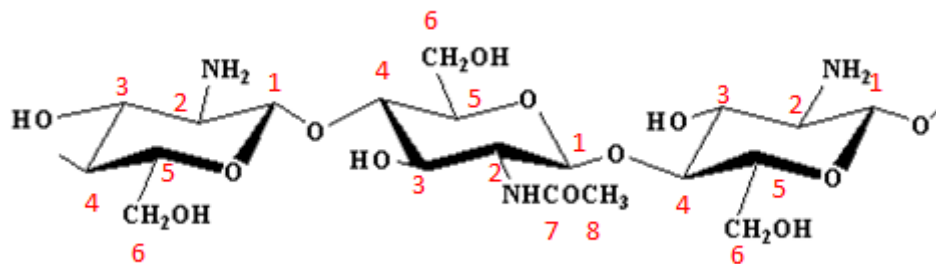


**Figure 2.2 Functional group positions in chitosan**

Chitosan has a number of active groups: one hydroxyl group each in C-3 and C-6 positions, and either an acetamide ( $\text{NHCOCH}_3$ ), if not deacetylated or an amino ( $\text{NH}_2$ ) group, if deacetylated, in the C-2 position (Figure 2.2).

### 2.3 USES OF CHITOSAN

Chitosan has many attractive attributes that are well-recognized viz. biocompatibility, biodegradability, renewability, hydrophilicity, bioactivity, and non-toxicity (Kołodziejka 2012; Varma et al. 2004). The functional groups present in chitosan, especially the amino group at the C-2 position, provides immense possibility for synthesizing a wide variety of derivatives for current or potential specialised applications in varied fields. A sample list of such uses is listed below (Prashanth et al. 2007).

- i. Food and Nutrition:  
Food preservative, anti-oxidant,
- ii. Material Science:  
Cosmetics, packaging, polymeric additive, biosensor.
- iii. Medicine:  
Blood clotting agent, controlled/targeted drug release, quick healing bandages, suture threads, anti-bacterial, anti-fungal, fat reducing agent.
- iv. Environmental:  
Adsorbent, polymeric material, polymeric nanoparticle, flocculating agent

## **2.4 CHITOSAN AS AN ADSORBENT MATERIAL IN POLLUTION TREATMENT**

Even though activated carbon has been extensively employed as an adsorbent for the purpose of water purification, alternatives for the removal of generally encountered pollutants such as heavy metals and dyes are being actively investigated. Biosorbents have secured great interest among researchers, since their precursor raw materials may be available in copious quantities as waste materials and are environmental friendly too. Specifically, biopolymeric materials such as chitin and its derivative chitosan have recently gained traction in active research as adsorbents for eliminating metal ions from aqueous media (Bhatnagar and Sillanpää 2009). Chitosan has been established as an effective agent for the uptake of transition metal ions present in waste water (Guibal 2004; Popuri et al. 2009). The great sorptive affinity of chitosan for heavy metals can be credited to (1) superior hydrophilicity due to an abundance of hydroxyl groups (2) occurrence of a variety of functional groups (hydroxyl, amine or acetamide) for metal binding (3) high chemical reactivity of these groups, and (4) flexible structure of the polymer chain (Crini 2005).

The swelling characteristic of an adsorbent when put into an aqueous media for the sorption of some contaminant is of great consequence. Its importance arises from practical experience that if an adsorbent possesses a high swelling intensity (e.g. >50%), its usage becomes problematic. The reason stems from the final use of every adsorbent material not only in small scale laboratory applications but primarily also in large size columns (i.e., packed-bed). An adsorbent with elevated swelling degree can retain substantial amounts of water, causing a steady buildup in the adsorbent's volume and eventually after a finite time in fouling and choking of the column. The preceding discussion elucidates why swelling is an important factor in adsorption technology and why it merits a closer study. Chitosan presents a high degree of swelling in water, degrees of swelling as high as 2000% have been reported (Kyzas et al. 2008). Particularly in the powdered form, it swells significantly and collapses easily, thus rendering it unsuitable for application in packed-bed adsorption column, ordinarily ending in clogging of the column (Kyzas and Bikiaris 2015).

Elwakeel (2010) reviewed the main advances published in environmental applications of chitosan resins for the treatment of water and wastewater over two decades. They concluded that the use of chitosan resins for removing various pollutants from water and wastewater presents many attractive features such as the outstanding adsorption capacity-especially for metal ions and dyes- and the fact that these materials are low cost, nontoxic and biocompatible.

Ngah et al. (2011) reviewed the relevant literature of the previous ten years on the use of chitosan composites for eliminating dyes and heavy metal ions. A list of chitosan composites with their adsorption capacity and the experimental conditions was recorded. The review also included the mechanisms of the adsorbate uptake. This paper concluded that adsorption using chitosan composites is becoming a promising option to substitute conventional adsorbents in removing dyes and heavy metal ions. Although chitosan may be unstable in acidic medium, using a cross-linking agent such as glutaraldehyde or with some other modification, the stability may be improved, they observed. According to the authors, “this field of research has a great room for improvement in the hope that chitosan composites can be applied commercially instead of only at laboratory scale.”

Fu and Wang (2011) studied a wide range of treatment technologies such as chemical precipitation, coagulation, flocculation, flotation, ion-exchange and membrane filtration which have been developed for heavy metal removal from wastewater. After studying 185 published articles they reported that ion-exchange, adsorption and membrane filtration are the most frequently studied methods for the treatment of heavy metal present in wastewater. They reckoned that “biosorption of heavy metals from aqueous solutions is a relatively new process that has proven very promising for the removal of heavy metal from wastewater.”

Kyzas and Bikiaris (2015) authored an article that reviewed a large volume of work published during the years (2012–2014) regarding the modification reactions of chitosan (grafting, cross-linking, etc.) and their application to adsorption of different environmental pollutants (heavy metals and others). The authors observed that the recent modifications were mainly focused on enhancing the mechanical properties of

chitosan. The authors also highlighted one serious drawback of chitosan which prevented the use of chitosan in continuous columns viz. its swelling nature when immersed in water, which leads to choking of column and high pressure drop. They concluded that the potential for modifications of chitosan was still very high in environment applications.

Zhang et al. (2016) produced a review article which provides in-depth information regarding the published works related to chitosan and modified chitosan derivatives as adsorbents in heavy metal removal from aqueous solutions. The authors examined the effects of all the important variables including pH, temperature, adsorbent dosage, contact time, and co-existing ions. The reported adsorption kinetics and isotherms, proposed adsorption mechanisms, and outcome of adsorption/desorption cycle studies were also discussed. The authors noted that chitosan being both bountiful and inexpensive, the prospects for its commercial-scale uses can only brighten in future.

## **2.5 MODIFICATIONS OF CHITOSAN**

### **2.5.1 Physical modifications**

One of the truly attractive features of chitosan is that it can readily be made into physical forms such as powder, flakes, beads, nano particles, membrane, fibers, hollow fibers and films (Guibal 2004). Physical modification enhances the sorption properties, gel formation and increases the porosity (Nghah and Fatinathan 2006).

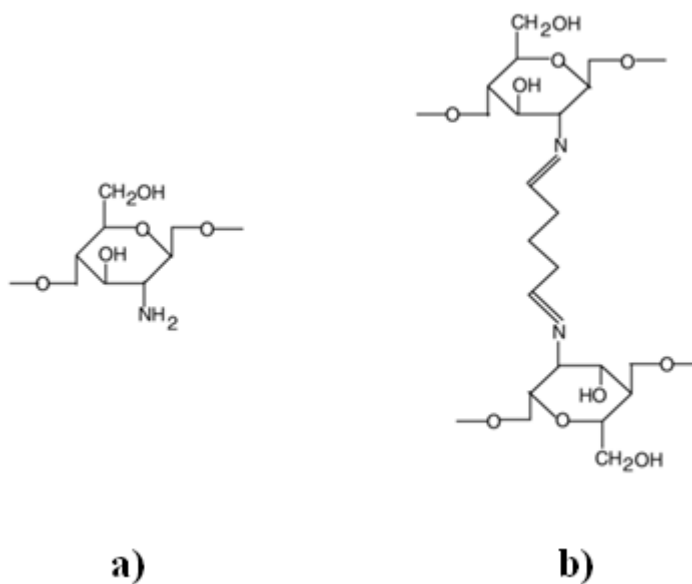
### **2.5.2 Chemical modifications**

Although adsorption operations are usually carried out at or near neutral conditions, the desorption step is generally conducted at a low pH which renders the stability of chitosan at low pH vital. Chitosan is soluble in dilute mineral acids, except for sulfuric acid. Chemical modification increases the sorption properties of chitosan while preventing the dissolution of chitosan in strong acids. It also improves the mechanical strength of chitosan and improves superficial area of the beads (Nghah et al. 2005). Most commonly used chemical modifications are cross-linking, grafting, carboxymethylation and acetylation. A cross-linking step is required to reinforce the



chemical stability of the biosorbents in acidic solutions. Cross-linking can change the crystalline nature of chitosan and enhance the resistance of chitosan against acid, alkali and chemicals and also increase the sorption abilities of chitosan. To make chitosan beads insoluble in acid media, cross linking is often carried out (Nghah and Fatinathan 2006). This technique is used to ensure mechanically and chemically stable beads.

Nghah et al. (2002) used cross linking agents like glutaraldehyde, epichlorohydrin and ethylene glycol diglycidyl ether to introduce new linkages between the chitosan chains (Figure 2.3). The cross linked polymer showed superior resistance to dissolution in highly acidic conditions and also showed lower swelling characteristics. The crosslinked polymer was found to be effective in adsorbing Cu (II), although the adsorption capacity in comparison to chitosan beads without cross linking was found to be lower. The decrease in adsorption capacity was attributed to reduced number of NH<sub>2</sub> sites after cross-linking.



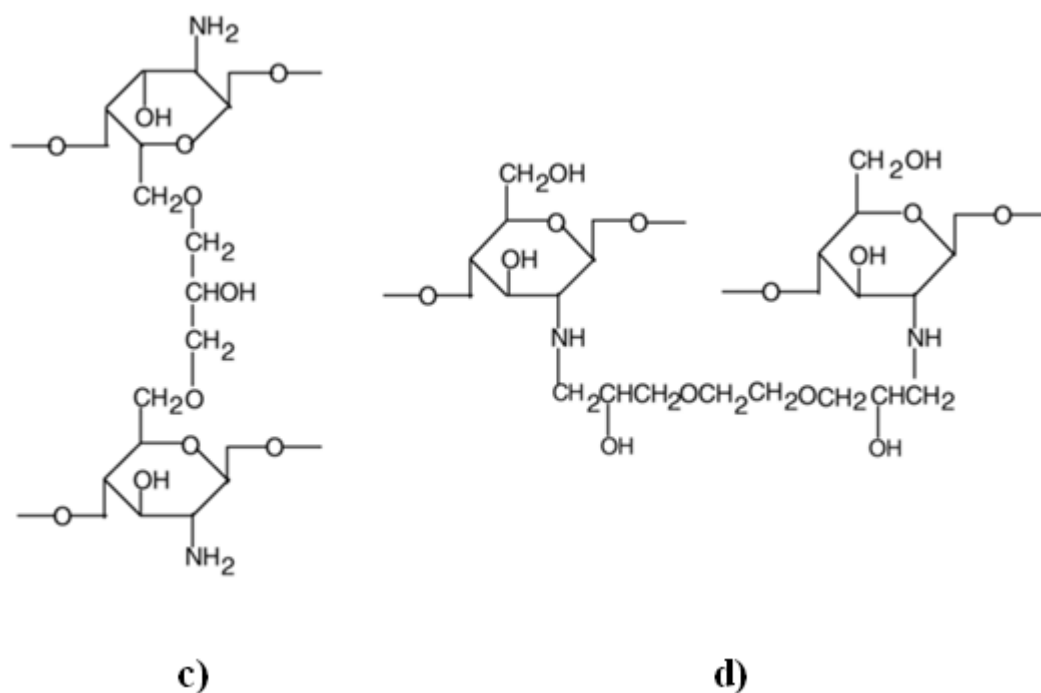


**Figure 2.3 Schematic representation of the chitosan and cross-linked chitosan beads: (a) chitosan, (b) chitosan-glutaraldehyde (c) chitosan-epichlorohydrin (d) chitosan-ethylene glycol diglycidyl ether (Source: Ngah et al. 2002).**

Varma et al. (2004) reviewed the different categories of chitosan derivatives and compared their metal removal capabilities under different conditions. They also reported on the analytical methods employed to analyze the chitosan derivatives, the adsorption mechanisms, and the structural analyses of the metal complexes by several methods.

Kurita (2006) in a review paper, published the basic features of chitin and chitosan such as their preparation, crystallography, degree of N-acetylation and various other properties. The literature on elemental modification reactions including acylation (Hirano and Ohe 1975), alkylation (Kurita et al. 2002b), carboxyalkylation, phthaloylation (Kurita et al. 2000; Kurita et al. 2002a), silylation (Kurita et al. 2004), tosylation (Zou and Khor 2005), quaternary salt formation (Lang et al. 1997), sulfation and thiolation (Nishimura et al. 1998) were discussed. The authors concluded that chitosan showed great promise as a material for use in many diverse applications.

Webster et al. (2007) investigated the physicochemical characterization of metal complexed with chitosan and its glutaraldehyde cross-linked derivative. Complexation products with seven metal ions (Cr (VI), Mn (II), Fe (III), Co (II), Ni (II), Cu (II), and Zn (II)) were synthesized. The mechanism of metal interaction with polymer was reported. Studies using solid-state NMR spectroscopy and XRPD (X-ray powder diffraction) supported by ESR (Electron spin resonance) spectroscopy, ICP-OES (inductively couple plasma-optical emission spectroscopy) and far-FTIR spectroscopy for metal interaction with nitrogen sites at C-2 of the metal-polymer complexes were performed. Computations of the metal-polymer ratio, the approximate charges on N atom for both amine and imine groups, and the hydrogen bonding between an alcohol group from the polymer and an amino/imine group were investigated.

Osifo et al. (2008) investigated the effect of degree of cross linking (DCL) on the adsorption properties of cross linked chitosan beads compared to pure chitosan beads. They reported that the degree of cross-linking significantly altered adsorption and other properties of the beads. Beads which were not cross-linked and beads with a DCL of 8.2% dissolved in hydrochloric and acetic acid at low pH between 2 and 4, while beads with a DCL of 18.4 and 34.7% were stable in this pH region. A rise in DCL reduced both the concentration of amino groups and aqueous retention in the beads. This was ascribed to the bonding of glutaraldehyde with the amino groups of the chitosan to form compact polymeric linkages inside the bead. The observed decrease in maximum adsorption capacity was attributed to the reduction in the number of amino groups in the polymer after the cross linking operation. The authors also showed that the bond between the nitrogen atom and the metal ion in cross-linked chitosan was weaker as compared to the one in the case of un-crosslinked chitosan and metal ion. The diffusivity of the copper ion was found to decrease with increase in DCL in cross-linked chitosan which was explained based on a simultaneous decrease in aqueous retention which occurs in the beads after cross-linking.

Vasconcelos et al. (2008) modified chitosan by crosslinking it with the complexing agent N-N'-[bis(2-hydroxy-3-formyl-5-methylbenzyl-dimethyl)]-ethylenediamine (H2fmbme). The new synthesized product was utilized in the adsorption of Cu (II) ions from aqueous solution. The adsorption was observed to be

pH dependent with an optimum value of 6.0. The kinetics study revealed that the experimental data was well correlated to the pseudo-second-order model. The adsorption equilibrium data gave excellent fit with the Langmuir isotherm from which a maximum monolayer adsorption capacity of 113.6 mg of metal ion per gram of the new adsorbent material ( $1.79 \text{ mmol g}^{-1}$ ) was obtained.

Wu et al. (2010) reviewed the reported adsorption capacities of pure and modified chitosan for the removal of selected heavy metals (Cu (II), Zn (II), Ni (II), Cd (II), Pb (II), Hg (II), and Cr (VI)) from aqueous solutions. They observed that crosslinking or substitution of chitosan led to a significant decrease in adsorption capacity. The decrease in capacity was strongly dependent on the type and degree of crosslinking. They reported that for the modification of chitosan to be practically attractive, the decrease in adsorption capacity should be compensated with other improvements in properties of chitosan such as the resistance in acidic solutions ( $\text{pH} < 2$ ). They also reported that there is always a potential for improving the adsorption efficiency through the choice of complexing agents that contain new functional groups such as hydroxyl (OH), carboxyl ( $-\text{COOH}$ ), and amino ( $-\text{NH}_2$ ) groups for efficient adsorption of heavy metals.

Khan et al. (2011) modified chitosan with glycidylmethacrylate followed by diethylenetriamine. The final characterized biopolymers established the incidence of suspended chains having basic nitrogen and oxygen centres for divalent cation removal. The crystallinity of the final product was less than that of chitosan due to decrease in intra and inter hydrogen bonding between chitosan strands. The new biopolymers were thermally less stable than original chitosan as observed by thermogravimetric analysis. The Langmuir isotherm model provided the best fit of equilibrium data, revealing maximum sorption capacities for Cu (II), Pb (II) and Cd (II) of 188.73, 414.4 and  $31.475 \text{ mg g}^{-1}$  respectively.

Chethan and Vishalakshi (2015) obtained chitosan as microspheres after cross linking with glutaraldehyde and investigated its adsorption characteristics for the removal of metal ions. The modification produced a derivative with extra nitrogen sites which functioned as prospective binding sites. The adsorbent was used in batch experiments to evaluate the adsorption of Cu (II), Zn (II), Pb (II) and Cr (VI) in aqueous solutions. The product showed greater preference for Cu (II) and least for Cr

(VI) ions. The adsorption data were interpreted based on Langmuir and Freundlich isotherm models. The maximum monolayer adsorption capacity obtained was 60.9 mg g<sup>-1</sup>. The spent adsorbent was efficiently regenerated using 0.5 N NaOH solution.

### 2.5.2.1 Schiff base derivatives of chitosan

The reaction of chitosan with aromatic aldehydes in acetic acid to form the resultant Schiff bases has been described by some researchers. Tirkistani (1998) synthesised many chitosan Schiff bases using such techniques. The products were analysed by infra-red spectroscopy. Thermal methods showed that the Schiff bases were thermally less stable compared to chitosan. The reduction in stability was attributed to the decrease in free amino groups in the Schiff base. Two chitosan derivatives (CTB and CCTS) and two novel polymeric ligands (CCTS-ECH-DHSalophen and CCTS-ECH-DHDPE) were studied for their effectiveness in heavy metal removal by Kocak et al. (2012) The studied adsorbents were found to be effective for Cr (VI) removal.

Santos et al. (2005) investigated the grafting of salicylaldehyde and derivatives at the C-2 nitrogen position of chitosan with low degree of acetylation. Chitosan was grafted with salicylaldehyde and its 5-bromo, 5-chloro, 5-nitro, 5-methyl and 5-methoxy derivatives. The chitosan Schiff bases formed were characterized by elemental analysis (C, H, and N), FTIR, proton NMR spectroscopy and conductimetric titration. The degree of substitution was impacted by inductive and resonance effects.

Justi et al. (2005a) synthesized two new Schiff-base chitosan derivatives by grafting complexation agents 2[-bis-(pyridylmethyl) aminomethyl]-4-methyl-6-formyl-phenol (BPMAMFF) and 2-[2-(hydroxybenzyl)-2-(pyridylmethyl) aminomethyl] - 4-methyl-6-formyl-phenol (HBPAMFF) and used them as new adsorbent materials for the removal of metal ions. The synthesized derivatives were found to have higher thermal stability which was attributed to the presence of imine bonds.

Donia et al. (2008) studied the selective removal of Hg (II) from aqueous solution using a magnetic chitosan biopolymer modified by Schiff base derived from thiourea and glutaraldehyde. The resin synthesized was used for the separation of Hg (II) from aqueous solution having six other heavy metal ions. The mechanism of adsorption of the metal on the resin was found to be dependent upon the pH of the solution. The adsorbent was successfully recovered with 0.1M potassium iodide. A maximum monolayer adsorption capacity of  $2.8 \text{ mmol g}^{-1}$  was obtained. The prepared adsorbent presented superior adsorption behaviour towards Hg (II) compared to a commercial resin.

Krishnapriya and Kandaswamy (2009) prepared a chitosan derivative (CCTSL) by crosslinking a metal complexing ligand, [6,60-piperazine-1,4-diyl dimethylenebis (4-methyl-2-formyl) phenol] (L), with chitosan. Adsorption experiments (pH dependency, kinetics, and equilibrium) of CCTSL toward various metal ions such as Mn (II), Fe (II), Co (II), Cu (II), Ni (II), Cd (II), and Pb (II) were carried out. The optimum pH for the adsorption was found to lie between pH values 6.5-8.5. The maximum adsorption capacity obtained was  $1.21 \text{ mmol g}^{-1}$  for Cu (II) and the order of adsorption capacities for the metal(II) ions studied was found to be Cu (II) > Ni (II) > Cd (II) > Co (II) > Mn (II) > Fe (II) > Pb (II).

In a different study, Krishnapriya and Kandaswamy (2010) prepared a new chitosan derivative (CTSL) by grafting a new vanillin-based complexing ligand, 4-hydroxy-3-methoxy-5-[(4-methylpiperazin-1-yl) methyl] benzaldehyde, (L) with chitosan by a Schiff base reaction. Adsorption of many heavy metals viz. Mn (II), Fe (II), Co (II), Cu (II), Ni (II), Cd (II), and Pb (II) were investigated. The CTSL displayed good adsorption capacity towards heavy metals studied in the order Cu (II) > Ni (II) > Cd (II) > Co (II) > Mn (II) > Fe (II) > Pb (II).

Chethan and Vishalakshi (2013) incorporated ethylene-1,2-diamine molecule into chitosan using N-phthaloyl-chitosan and chloro-6-deoxy N-phthaloyl-chitosan as precursor materials. The alteration created additional nitrogen centres which function as potential sites for adsorption where complexation of metal ions could occur. The derivative ethylene-1, 2-diamine-6-deoxy-chitosan and its phthaloylated precursor were

investigated for the adsorption of divalent cations. The former was found to have superior adsorption capacity owing to the existence of extra  $\text{NH}_2$  group. The modified resin showed maximum affinity for Cu and minimum for Zn. Approximately 80% of the adsorbed material could be recovered in a medium of pH 1.2. The interaction between acidic metal centres and basic nitrogen centres on surface of the adsorbent appeared to govern adsorption. Intra-chain and inter-chain co-ordinate bonding involving NH and  $\text{NH}_2$  groups was suggested to be the adsorption mechanism.

Monier et al. (2012) conducted batch studies in the adsorption of Cu (II), Cd (II) and Ni (II) ions from aqueous solution by cross-linked magnetic chitosan- 2-aminopyridine glyoxal Schiff base polymer. The removal of Cu (II), Cd (II) and Ni (II) ions was found to be pH dependent and the highest adsorption was observed at pH 5.0. The adsorption was fast with estimated initial rate of 2.7, 2.4 and 1.4  $\text{mg g}^{-1} \text{min}^{-1}$  for Cu (II), Cd (II) and Ni (II) respectively. The adsorption data could be well interpreted by the Langmuir, Freundlich and Temkin models. The maximum monolayer adsorption capacities were  $124 \pm 1$ ,  $84 \pm 2$  and  $67 \pm 2 \text{ mg g}^{-1}$  for Cu (II), Cd (II) and Ni (II) respectively. The adsorption kinetics data fitted the pseudo-second-order model well. Thermodynamic study showed that the adsorption was feasible, spontaneous and exothermic in nature. The metal ions were effectively desorbed from the resin using EDTA and HCl solutions.

#### **2.5.2.2 Composite materials with chitosan**

Recently Yuvaraja et al. (2017) synthesized magnetic-epichlorohydrin crosslinked chitosan Schiff base (m-ECCSB) by doping iron oxide ( $\text{Fe}_3\text{O}_4$ ) nano particles with chitosan cross-linked with epichlorohydrin. They used this derivative to study the adsorptive removal of Cu (II). The FTIR analysis revealed that N and O atoms of the adsorbent were responsible for the metal complexation. The maximum monolayer adsorption capacity obtained was 123.1 mg/g.

El-Reash (2016) synthesized new magnetic beads using crosslinked magnetic chitosan beads modified with cystein-glutaraldehyde Schiff base (Chi-CG). The precursor magnetic chitosan beads were prepared by encapsulating magnetic  $\text{Fe}_3\text{O}_4$  as core in chitosan micro spheres. The blend product exhibited superior adsorption

capacity and mechanical properties compared to chitosan. The blending process caused an increase in the number of active sites (e.g. -COOH, >C=N- and -SH), that could interact with metal ions. Additionally, no significant reduction in the sorption performance of either Cu (II) or Cr (VI) was observed in the presence of solutions containing  $K^+$ ,  $Na^+$ ,  $Mg^{2+}$ ,  $Ca^{2+}$ ,  $Cl^-$ ,  $NO_3^-$ ,  $SO_4^{2-}$  or  $PO_4^{3-}$  ions. In case of Cr (VI), the maximum adsorption occurred at pH 2, but it decreased with increasing the pH of studied solution. This behaviour was ascribed to the protonation of both  $-NH_2$  and ( $>C=N-$ ) of Chi-CG, which leads to an electrostatic interaction with the anionic  $CrO_4^{2-}$  and  $HCrO_4^-$  from the Cr (VI) solution. At higher pH, protonation decreases and consequently Cr (VI) removal is reduced. The adsorption of Cu (II) was the highest at pH 5. This result was attributed to the presence of free lone pair of electrons on nitrogen atoms of ( $-NH_2$  and  $>C=N-$ ) and facile de-protonation of both carboxylic and -SH groups which facilitate the coordination with Cu (II) ions on Chi-CG and formation of a complex via surface chelation ion exchange rather than electrostatic interaction.

Since their discovery in 1991, carbon nanotubes have made enormous impact in most fields of science and engineering attributable to their extraordinary physical and chemical properties. The superlative mechanical, thermal, and electronic properties attributed to them are quite unparalleled by any other material. These properties position nanotubes as a perfect material for a variety of uses (Baughman et al. 2002). In particular, this blend of properties renders them most suitable as a superior filler material in nanocomposites. A promising area of nanocomposites research involves the reinforcement of polymers like chitosan and its derivatives by carbon nanotubes as reinforcing filler material. Coleman et al. (2006) in a review article explored the advances made in the area of mechanical reinforcement of polymers using carbon nanotubes. The authors dealt with the mechanical properties of carbon nanotubes and the optimum requirements needed to maximize reinforcement. The important approaches reported in the literature to make and process polymer–nanotube composites were deliberated and analyzed. Further, the mechanical properties of different nanotube–polymer composites made by different methods have been critically analyzed and evaluated in this article.



Wang et al. (2005) incorporated multi walled carbon nanotubes (MWCNT) into chitosan matrix and demonstrated that when compared with pure chitosan, with only about 0.8 wt % MWCNT, mechanical properties of the nanocomposites, including the tensile modulus and strength, greatly improved by about 93% and 99%, respectively. Chatterjee et al. (2010) prepared a chitosan-carbon nanotube (CNT) hydrogel bead that had excellent mechanical properties as well as enhanced adsorption capacity to congo red dye. They elucidated the importance of this technology and postulated that the CNT technology would be able to greatly increase the applicability of chitosan in environmental and separation industries.

Li et al. (2015) synthesized chitosan/sulfhydryl-functionalized graphene oxide composite (CS/GO-SH) material and the same was used as an adsorbent for removal of Cu (II), Pb (II) and Cd (II) in single and multi-metal ions systems. It was found that the CS/GO-SH had potential applications in fields of adsorptive materials due to its superiority of the chemical characteristic and the specific surface area. The adsorbent (CS/GO-SH) had functional groups such as  $-OH$ ,  $-COOH$ ,  $-SH$ , and  $-NH_2$  which could effectively bind with the metal ions.

Shen et al. (2013) prepared chitosan supported on porous glass beads with the intention to enhance the accessibility of its binding sites, and improve its mechanical and chemical properties. The adsorption properties of the sample for the removal of Ni (II), Cu (II), Ag (II), Cd (II) and Pb (II) were investigated. The prepared samples exhibited high mechanical strength, large specific surface area, and no swelling in water, offering possibilities for practical use.

Clay materials such as bentonite are inexpensive, plentiful, and exhibit a higher specific surface area, which renders them beneficial support material for chitosan. Futralan et al. (2011a) investigated the removal of Ni (II) from aqueous solutions using chitosan-coated bentonite (CHB). The BET specific surface area for chitosan, bentonite and CHB were 2.1, 84, 33  $m^2 \cdot g^{-1}$  respectively; hence CHB showed many fold increase in specific surface area over chitosan.

Shariful et al. (2017) synthesized chitosan/Poly Ethylene Oxide nanofibrous bead-less membrane having mesopores and high specific surface area by the method

of electrospinning. Bead-less fibres tend to show the lowest contact angle (hence, higher hydrophilicity) and high specific surface area, which are beneficial for the adsorption process. The maximum monolayer adsorption capacity for Cu (II), Zn (II) and Pb (II) ions were found to be 120, 117 and 108 mg g<sup>-1</sup> respectively.

Other substances reported as prop materials for chitosan were perlite for Cu (II) adsorption (Hasan et al. 2008), calcium alginate for Ni (II) adsorption (Vijaya et al. 2008), polyvinyl acetate beads for Cu (II) adsorption (Ngah et al. 2004), PVC beads for Cu (II) and Ni (II) adsorption (Popuri et al. 2009) and sand for Cu (II) and Pb (II) adsorption (Wan et al. 2010).

### **2.5.2.3 Miscellaneous derivatives of chitosan**

Dendrimers are a category of hyperbranched polymers holding different functional groups where they have the capability to interact with various functional units of other molecules in nanometer range. In comparison to regular polymers, dendrimers have exceptional physical properties such as viscosity, flexibility, and density distribution (Shimei et al. 2006). For any specifically desired properties, the spread of functional groups in the dendrimer structure performs a key role (Astruc et al. 2010). Zarghami et al. (2016) grafted chitosan with polyamidoamine (PAMAM) dendrimer as a new sorbent. The prepared material was used as an adsorbent for the removal of Pb (II) from aqueous media. Effects of different variables on the adsorption capacity of the sorbents were assessed. Adsorption capacity of the prepared material increased by up to 18 times compared to that of pure chitosan.

Lately, a few studies have been directed towards enhancing the preferential adsorption of specific metal ion in a mixture of metal ions from aqueous solutions. Molecular imprinting technique is one such promising affinity separation technique available since the 1990s. The monomers are first copolymerized with a cross-linking agent and template ions, after which the template ions are removed to form imprinting sites that could completely match the template ions on space positions and binding sites. Therefore, the molecular imprinted polymer could preferentially adsorb specific ions based on 'memory effects' (Jiang et al. 2010; Zhang et al. 2016).

Lu et al. (2013) successfully synthesized Pb (II) imprinted chitosan (Pb (II)-CS) beads with uniform size and porous structure. A combination of a microfluidics technique with crosslinking solidification was used to make the Pb (II)-CS beads. The adsorbent was used after removing the chelated Pb (II) by EDTA and exposing the imprinted sites. The FTIR analysis showed that the reversible chelation of Pb (II) with amino group was responsible in amino group protection and Pb (II) adsorption. A maximum adsorption capacity of 79.2 mg/g was obtained after optimising the preparation conditions of the adsorbent. Moreover, the repeated reuse of the Pb (II)-CS bead exhibited insignificant variation in the adsorption capacity- a point in favour of reusability of the adsorbent.

Huo et al. (2009) used the surface molecular imprinting technique for preparing the Ag (I) imprinted biosorbent for handling of the wastewater laden with Ag (I), which displayed superior adsorption affinity and selectivity towards the imprinting ion (Ag (I)) than the other non-imprinting metal ions. It was also demonstrated that the biosorbent could be easily desorbed by using 0.1M Na<sub>2</sub>S<sub>2</sub>O<sub>3</sub> solution with an efficiency of 99%.

An exhaustive list of reported studies providing details of adsorption characteristics using chitosan and its derivatives as adsorbents for the removal of Cu (II), Pb (II) and Cr (VI) is presented in Table 2.1.

## **2.6 ADSORPTION STUDIES**

### **2.6.1 Adsorption isotherms**

Originally used to model gas-solid phase adsorption onto activated carbon, the Langmuir adsorption isotherm has now been extensively used to assess the equilibrium adsorption performance of biosorbents. In its development, the Langmuir adsorption isotherm (Langmuir 1916) assumes monolayer adsorption with all adsorption sites being equivalent. This isotherm represents adsorption on homogeneous surface with each active adsorption site displaying equal affinity towards the adsorbate with no interaction between the adsorbate molecules even among the adjacent ones. Langmuir isotherm is characterised by a plateau in

adsorption capacity at higher concentrations of the adsorbate as equilibrium is attained. The equation for the Langmuir isotherm is as given in Eq. 2.1.

$$Q_e = \frac{Q_o b C_e}{b C_e + 1} \quad (2.1)$$

where, 'Q<sub>e</sub>' and 'Q<sub>o</sub>' represent equilibrium and maximum monolayer adsorption capacities (mg/g) respectively, 'b' is the Langmuir constant (L/mg), and 'C<sub>e</sub>' is the adsorbate concentration in aqueous solution at equilibrium (mg/L). At very low concentrations of the adsorbate, the equation is reduced to a linear form (Henry's law).

$$Q_e = Q_o b C_e \quad (2.2)$$

The basic features of the Langmuir isotherm can be elaborated by a dimensionless number 'R<sub>L</sub>' which was originally defined by Hall et al. (1964) is given by the following equation.

$$R_L = \frac{1}{1 + b C_o} \quad (2.3)$$

'R<sub>L</sub>', called the separation parameter, gives insight into the nature of adsorption; adsorption is variously, irreversible (R<sub>L</sub>=0), favourable (0 < R<sub>L</sub> < 1), linear (R<sub>L</sub>=1) and unfavourable (R<sub>L</sub> > 1).

Freundlich isotherm (Freundlich 1906) which was initially proposed as an empirical model can also be derived on the basis of rigorous theoretical underpinnings. It has the following form.

$$Q_e = K_f C_e^{1/n} \quad (2.4)$$

where 'K<sub>f</sub>' stands for Freundlich adsorbent constant (mg/g) and 'n' the dimensionless Freundlich exponent related to the propensity for adsorption.

Freundlich isotherm is applied to multilayer adsorption with non-uniform surface reactivity and heat of adsorption on the adsorbent surface. It is obtained by assuming that the surface is heterogeneous in the sense that the adsorption energy is

distributed and the surface has many areas having the same adsorption energy, these areas are grouped together into one patch. Such an isotherm is another form of Langmuir isotherm which was applicable for amorphous surfaces. The amount adsorbed is summation of the adsorption of all sites. This isotherm predicts that the adsorbate concentration on the adsorbent will increase as long as there is an increase of ion concentration in the liquid. This isotherm has the limitation of not following the Henry's law at very dilute concentrations (Do 1998).

Many hybrid isotherms that combine aspects of both the Langmuir and Freundlich equations have also been proposed. Redlich-Peterson isotherm is one such isotherm which incorporates three parameters in the model.

Redlich-Peterson isotherm (Redlich and Peterson 1959) represents adsorption equilibria across a broad concentration span, has practical uses in homogeneous or heterogeneous systems owing to its adaptability. The mathematical form of this isotherm is given by Eq. 2.5.

$$Q_e = \frac{K_R C_e}{1 + a_R C_e^{b_R}} \quad (2.5)$$

where, ' $K_R$ ' ( $L g^{-1}$ ), ' $a_R$ ' ( $L mg^{-1}$ ) and ' $b_R$ ' are parameters. Exponent ' $b_R$ ' has no exact physical significance; values of ' $b_R$ ' between 0 and 1 indicate favourable adsorption and higher values may reflect weaker interactions between the adsorbent and the adsorbate (Boddu et al. 2008).

when  $b_R = 1$ , this equation changes to Langmuir isotherm

$$Q_e = \frac{K_R C_e}{1 + a_R C_e} \quad (2.6)$$

when  $b_R = 0$ , it changes to Henry equation which is defined as follows

$$Q_e = \frac{K_R C_e}{1 + a_R} \quad (2.7)$$

The Redlich–Peterson isotherm model combines elements from both the Langmuir and Freundlich equations and the mechanism of adsorption is a hybrid one and does not follow ideal monolayer adsorption.

### 2.6.2 Adsorption kinetics

The kinetic analysis is of great importance in evaluating the rate at which the adsorbate is removed from the solution which helps determine the time for completion of the adsorption process. The kinetic parameters also help establish the size of the equipment of a fixed bed continuous contact system. Further, the kinetic data is of great value in understanding the underlying mechanism of sorption. A review article of the important kinetic models used in adsorption systems has been published by Qiu et al. (2009).

In order to determine the adsorption kinetics of the uptake of metal ions by modified chitosan adsorbents, three kinetic models have been widely employed.

The pseudo-first order rate equation of Lagergren has the mathematical form as in Eq. 2.8 (Zhang et al. 2016).

$$\ln(Q_e - Q_t) = \ln(Q_e) - k_1 t \quad (2.8)$$

where ‘ $Q_e$ ’ and ‘ $Q_t$ ’ represent the quantity adsorbed (mg/g) at equilibrium and time ‘ $t$ ’ (min) respectively. ‘ $k_1$ ’ is the pseudo-first order adsorption rate constant ( $\text{min}^{-1}$ ).

The pseudo-second order rate equation is expressed as given in Eq. 2.9 (Qiu et al. 2009).

$$\frac{t}{Q_t} = \frac{t}{Q_e} + \frac{1}{k_2 Q_e^2} \quad (2.9)$$

where ‘ $Q_e$ ’ and ‘ $Q_t$ ’ represent the quantity adsorbed (mg/g) at equilibrium and time ‘ $t$ ’ (min) respectively, and ‘ $k_2$ ’ is the adsorption rate constant ( $\text{g mg}^{-1} \text{min}^{-1}$ ).

The terms ‘pseudo’ first order and ‘pseudo’ second order equations are used to distinguish between kinetic equations based on adsorption capacity and equations in reaction engineering based on solution concentration (Qiu et al. 2009).

In some sorption systems, the amount of adsorbate removed varies almost linearly with square root of the time of contact. This phenomenon described by the Weber-Morris model commonly known as intra particle diffusion model is given by Eq. 2.10 (Qiu et al. 2009).

$$Q_t = K_{id}t^{\frac{1}{2}} + C \quad (2.10)$$

where, ' $K_{id}$ ' is the intraparticle diffusion rate constant ( $\text{mg g}^{-1}.\text{min}^{-\frac{1}{2}}$ ) and ' $C$ ' is the intercept ( $\text{mg g}^{-1}$ ). This model is applicable if the adsorption is governed by pore diffusion in the particles and convective diffusion in the solution.

In some systems three linear regions may be observed in the plot of  $Q_t$  v/s  $t^{0.5}$  indicating that the adsorption process is a three step process. The first region which is very steep represents the initial stages of adsorption when the adsorbate diffuses from the bulk to the adsorbent surface through a boundary layer. The second region represents the slow diffusion of the adsorbate molecules in the pores filled with aqueous solution or through lateral diffusion along the pore walls of the adsorbent, which together is called the intraparticle diffusion. The third region represents the equilibrium stage during which the adsorbate concentration gets depleted to a low value in the solution present inside the pores (Cheung et al. 2007).

### 2.6.3 Adsorption thermodynamics

The feasibility of adsorption is governed by the Gibb's free energy change ( $\Delta G$ ). Negative values of  $\Delta G$  means the sorption occurs spontaneously. The Gibb's free energy change was determined employing the thermodynamic equilibrium constant ' $K_o$ ' (Gunay et al. 2007).

$$K_o = \frac{a_s}{a_e} = \frac{v_s Q_e}{v_e C_e} \quad (2.11)$$

where ' $a_s$ ' is activity of the adsorbed metal ion, ' $a_e$ ' is the activity of the metal ion in the solution at equilibrium, ' $v_s$ ' and ' $v_e$ ' represent activity coefficients of the adsorbate on the adsorbent surface and the equilibrated solution. ' $Q_e$ ' and ' $C_e$ ' represent surface concentrations of metal ions ( $\text{mg g}^{-1}$ ) and concentration of metal

ions in solution at equilibrium ( $\text{mg mL}^{-1}$ ) respectively. Since for dilute aqueous solutions ( $\text{mg mL}^{-1}$ ) is nearly equal to ( $\text{mg g}^{-1}$ ),  $K_o$  becomes dimensionless. At vanishing concentrations of the metal ion in the solution, both the activity coefficients ' $v_s$ ' and ' $v_e$ ' approach unity (Khan and Singh 1987).

$$\lim_{Q_e \rightarrow 0} \frac{a_s}{a_e} = \frac{Q_e}{C_e} = K_o \quad (2.12)$$

' $K_o$ ' may be obtained by plotting a straight line of  $\ln (Q_e/C_e)$  versus  $Q_e$  and extending  $Q_e$  to zero. The change in standard free energy ( $\Delta G^\circ$ ) can be determined from the Van't Hoff Equation given below (Van't Hoff 1894).

$$\Delta G^\circ = -RT \ln K_o \quad (2.13)$$

where, R is the universal gas constant (8.314 J/mol.K), T is the temperature (K).

The standard change in enthalpy ( $\Delta H^\circ$ ) and standard change in entropy ( $\Delta S^\circ$ ) are then related to the change in standard Gibbs free energy, ( $\Delta G^\circ$ ) through Eq. 2.14.

$$\Delta G^\circ = \Delta H^\circ - T\Delta S^\circ \quad (2.14)$$

From which follows the Eq. 2.15

$$\ln K_o = \frac{\Delta S^\circ}{R} - \frac{\Delta H^\circ}{RT} \quad (2.15)$$

' $K_o$ ' was obtained from Eq. 2.12 and the values of  $\Delta H^\circ$  and  $\Delta S^\circ$  were determined as per Eq. 2.15 from the slope and intercept of the plot of  $\ln K_o$  v/s  $1/T$  respectively.

## 2.7 POLYSULFONE MEMBRANES

Membrane processes have steadily gained prominence in the purification of water over the last few decades. Ultrafiltration membranes are used as pretreatment membranes prior to reverse osmosis in the desalination process. Polysulfone polymer qualifies as an excellent ultrafiltration membrane material because of its superior chemical and thermal stability, its stability in wide pH ranges, high mechanical strength and high film forming properties (Cho et al. 2011). The surface hydrophilicity and the porous structure are of great significance in the membrane



separation technique. A suitable porous membrane must have high permeability, good hydrophilicity and excellent chemical resistance towards the feed solution (Lau et al. 2012). Polysulfone membranes are extensively used to make asymmetric membranes for microfiltration and nanofiltration applications (Sikder et al. 2009).

An important drawback of polysulfone membrane is its low hydrophilic nature which leads to inferior permeation characteristics and poor anti-fouling properties (Dong et al. 2009). Increase in surface hydrophilicity has been obtained by chemical grafting, surface coating or by blending the casting solution with hydrophilic agents (Kumar et al. 2013d). Of these, blending is an established method for membrane alteration that can bring about a desired change in pore size and permeation characteristics of the membrane. Polymeric additives like polyvinylpyrrolidone, poly(ethylene glycol), polyaniline, and inorganic additives like TiO<sub>2</sub> nanoparticles, carbon nanotubes have been used to improve PSf ultrafiltration properties (Kumar et al. 2013c). Direct blending of hydrophilic macromolecules like chitosan or its derivatives with polysulfone is a simple method to achieve the desired membrane improvement (Amiji 1995).

Polysulfone and chitosan are good candidates for the proper blend composite membranes (Wan et al. 2006). To enhance the performance of membranes, many studies have been devoted towards chemical modification of chitosan to further improve its properties for preparing composite membranes with better hydrophilicity, surface charge and biological compatibility (Yuan et al. 2008). The structural modification of the chitosan enhances its solubility. Modified chitosan provides better hydrophilicity whereas polysulfone would ensure structural stability of the composite blend (Padaki et al. 2011a). Many studies related to polysulfone and chitosan or modified chitosan–polysulfone blend membranes have been reported (Kumar et al. 2013d; Kumar et al. 2013b; Kumar et al. 2013a; Padaki et al. 2011a; Padaki et al. 2012; Padaki et al. 2011b; Kumar et al. 2014; Miao et al. 2006; Miao et al. 2008).

Kumar et al. (2013d) used pure chitosan as an additive for the preparation of a polysulfone ultrafiltration membrane. Two different compositions of polysulfone in N-methylpyrrolidone (NMP) and chitosan in 1% acetic acid were blended to prepare

PSf–CS ultrafiltration membranes by the diffusion induced phase separation (DIPS) method. The membrane hydrophilicity was determined by contact angle measurements. The PSf–CS membrane presented an improved hydrophilicity compared to a PSf ultrafiltration membrane. The pure water permeation studies showed the increased flux of PSf–CS membranes. The membranes were tested for their anti-fouling property by using bovine serum albumin (BSA). The antifouling behavior for PSf–CS blend membranes was markedly better when compared to neat PSf ultrafiltration membranes. The maximum FRR of 56% was observed for PSf-CS blend membranes when compared to 30% for neat PSf membranes.

Kumar et al. (2013b) used N-succinyl chitosan (NSCS) as an additive with polysulfone to obtain blend membranes. Pure water flux, water uptake and contact angle of the PSf/NSCS blend membranes were measured and compared with neat polysulfone membrane. The PSf/NSCS blend membranes displayed improved hydrophilicity and permeation fluxes when contrasted with pristine polysulfone membrane. The membrane antifouling property was measured by filtering the bovine serum albumin (BSA) solution. The maximum flux recovery ratio (FRR) of 70% was observed by the PSf/NSCS blend membrane with 20% NSCS content. The hydrophilic derivative of chitosan NSCS acted as an excellent additive in improving PSf ultrafiltration properties.

Kumar et al. (2013a) synthesized polysulfone (PSf) and chitosan (CS) blend membranes using titanium dioxide nanotubes (TiO<sub>2</sub>NT) in various proportions. The influence of nanotubes on morphology of membranes was investigated. The change in hydrophilicity of the membranes was examined by water swelling studies and contact angle measurements. The permeation property of PSf/CS/TiO<sub>2</sub>NT membranes was evaluated by measuring the time dependent pure water flux (PWF). Bovine serum albumin (BSA) protein rejection studies revealed that the antifouling properties for PSf/CS/TiO<sub>2</sub>NT membranes were the best compared to PSf/CS and neat PSf ultrafiltration membranes with a high FRR of 76%. The PSf/CS/TiO<sub>2</sub>NT membranes also exhibited improved permeation flux compared to the other two membranes.

Padaki et al. (2012) prepared sulfonated polysulfone (sPSf) by the sulfonation of polysulfone and used it as a polymer matrix for cation-exchange membranes. Blend composite membranes were prepared using different ratios of sulfonated polysulfone and modified chitosan. Membrane properties were studied in terms of water flux, water swelling ratio, molecular weight cut off (MWCO), ion-exchange capacity and contact angle measurement. During the rejection experiments using sPSf: CS, a maximum rejection of 93%, 89% and 69% for  $\text{MgSO}_4$ ,  $\text{Na}_2\text{SO}_4$  and  $\text{NaCl}$  respectively, was obtained.

Kumar et al. (2014) studied heavy metal rejection properties of chitosan based polysulfone/chitosan (PSf/CS), polysulfone/N-succinyl chitosan (PSf/NSCS) and polysulfone/N-propylphosphonyl chitosan (PSf/NPPCS) ultrafiltration membranes. The retention of Cu (II), Cd (II) and Ni (II) ions by the membrane was evaluated with and without using polyethyleneimine (PEI) as the complexing agent by polymer enhanced ultrafiltration (PEUF) techniques. The flux change during the UF process and the effect of pH on the rejection were determined. The observed percentages of rejection of different metal ions without using any complexation agents were Cu (75-78%), Ni (66-73%) and Cd (66-68%). However, using complexation by PEI, a maximum rejection of 98%, 95% and 92% rejection for Cu, Ni and Cd respectively, were reported. The reusability study for the membrane after PEUF process showed good results. The increase in membrane recycling property after the metal ion rejection was primarily credited to the hydrophilicity of CS, NSCS and NPPCS.

### **2.7.1 Mechanism of electrolyte separation by membranes**

Possible mechanisms for the separation of electrolytes by membranes are i) sieving, ii) electrostatic interactions, iii) differences in diffusivity and solubility, or a combination of these (Peeters et al. 1998). The membrane separation process is governed by a size exclusion mechanism, solute-solute and solute-membrane interactions that are dependent on membrane surface characteristics such as hydrophilic/hydrophobic balance, electrostatic charges on both membranes, and on the solute (Padaki et al. 2011b). The sieving effect is linked to the pore size, solute size besides molecular weight of the solute and refers to separation of electrolytes by

size exclusion. The charge effect is due to electrostatic interactions between the ion and the membrane, and so it only appears with charged membranes. The Donnan effect appears when two compartments containing electrolytes are separated by a membrane which is impermeable to at least one electrolyte. This electrolyte modifies the mobility of the other electrolytes through the membrane; this phenomenon itself is called Donnan effect (Pontalier et al. 1997). Membrane separations in ultrafiltration are governed by a complex combination of both steric exclusion and surface force interactions. UF membranes bearing formal surface charges can display unusual selectivity behaviour not predicated on the physical pore size alone (Rudie et al. 1993).

The adsorptive UF membranes provide the benefits of high rejection for metal ions, along with the advantages of energy efficiency and high permeate flux. Recently, Salehi et al. (2016) have authored an article in which they reviewed the preparation methods and uses of chitosan-based adsorptive membranes. Important factors including thermo kinetic analyses of adsorption and regeneration capacity of the membrane adsorbents have been overviewed in this paper. Many published works related to blended and supported membranes, composite membranes and imprinted membranes have been dealt with in this article.

The presence of reactive functional groups on the membrane is very important for the binding of heavy metal ions. Biopolymer such as chitosan has a chelation ion exchange property that removes ions of a specific size in the presence of large quantities of other ions. The amine groups are able to sorb metals through several mechanisms including chemical interactions such as chelation, electrostatic interactions, ion exchange or the formation of ion pairs (Kumar et al. 2014).

**Table 2.1 Main characteristics and adsorption capacities of chitosan/ chitosan based derivatives for the removal of Cu (II), Pb (II), Cr (VI)**

Sl. No.	Adsorbent	Characterization	Metal Ion	Q <sub>o</sub> (mg/g)	Sorption Variables				$\Delta H^\circ$ kJ/mol	Kinetic Model	Isotherm	RPM	Reference
					pH	T (°C) or K	t (min/h)	dz (mg/L)					
1	Magnetic-epichlorohydrin crosslinked chitosan schiff's base	XRD, FTIR, SEM, Elemental analysis, TEM, <sup>1</sup> H NMR, VSM,	Cu(II)	123.1	6	323 K	60 min	2-10	15.674	PSO	L	200	(Yuvaraja et al. 2017)
2	Chitosan/poly (ethylene oxide) nanofibres	FESEM, FTIR, XRD, BET	Cu(II) Pb(II)	120.0 108.0	NA	25°C	60 min	2.5	NA	PSO	L	NA	(Shariful et al. 2017)
3	Poly(itaconic acid) modified cross-linked chitosan	FT-IR, XRD, SEM, TEM, TGA	Pb(II)	1320.0	5	293.2–333.2 K	3h	0.2 - 1	-9.859	PSO	L	150	(Ge et al. 2017)
4	Cross-linked chitosan aerogel (CsA)	FTIR TG-DTG compressive strength	Cu (II)	35.08	NA	25°C	12h	0.2	NA	Nil	L	150	(Li et al. 2016)

5	Fungal chitosan	FTIR	Cu (II) Pb (II)	113.44 286.46	NA	25°C	7.5h	NA	NA	NA	NA	120	(Tayel et al. 2016)
6	Polyamidoamine (PAMAM) dendrimer-grafted chitosan	FTIR, XRD, Zeta potential	Pb (II)	44.0	6	298 K	24h	0-20	NA	PSO	L	NA	(Zarghami et al. 2016))
7	Magnetic chitosan beads modified with cystein glutaraldehyde's schiff base	FTIR, SEM, XPS, TGA	Cu (II) Cr(VI)	156.49 138.53	5 2	293-313 K	110 min 90 min	0.4	48.56 80.67	PSO PSO	L L	150	(El-Reash et al., 2016)
8	Chitosan-poly(vinyl alcohol)/attapulgate nanocomposite	SEM, FTIR, XRD, Spectrophotometer	Cu(II)	64.67	5.5	25, 45, 55°C	24h	0.5-10	NA	PSO	F	NA	(Wang and Wang, 2016)
9	Chitosan/Sulfydryl-functionalized graphene oxide composite (CS/GO-SH)	FTIR, SEM, Raman spectroscopy, TG, XRD	Cu(II) Pb(II)	425.0 447.0	5 5	20°C	90 min	0.8	endothermic endothermic	PSO PSO	F F	NA	(Li et al. 2015)
10	Polyaniline grafted chitosan	FTIR, SEM, EDX, XRD, TGA, DSC	Pb(II)	17.54	6	50°C	90 min	1.0-3.0	33.67	PSO	L	150	(Karthk and Meenakshi, 2015)
11	Ethylenediamine modified chitosan microspheres	FTIR, SEM	Pb(II) Cr(VI)	46.511 28.812	7 3	NA	2h	0.4	NA	NA	L L	NA	(Chethan and Vishalakshi, 2015)
12	Pollen-chitosan microcapsules	SEM, FTIR, TGA, EA	Cu(II)	67.1	5.18	25,35, 45°C	4h	4	-1.403	NA	L,F	200	(Sargin et al. 2015)

13	Heterocycle modified chitosan	FTIR, XRD, TGA, SEM, and swelling tests	Cu(II) Pb(II)	10.0 12.0	5 5	25°C	10h	0.1	NA	NA	NA	NA	(Kandile et al. 2015)
14	Cross linked chitosan-g-acrylonitrile copolymer	FTIR, XRD	Cr(VI) Cu(II)	122.83 230.79	5 5	30°C	300 min	10	NA	PSO PSO	F F	160	(Shankar et al. 2014)
15	Chitosan-dialdehyde hydrogel A1 & A-2	FTIR, TGA, SEM, X-ray	Cu(II) Pb(II)	18 , 20 73, 80	5 5	RT	10h	1	NA	NA	NA	NA	(Kandile and Nasr 2014)
16	Sulfate-crosslinred chitosan	FTIR, SEM, XRD, EDX	Cr(VI)	156.85	6	298 K	45 min	1.0- 16.0	-59.39	PSO	F	NA	(Kahu et al. 2014)
17	Chitosan-coated cotton gauze	SEM, EDX, FTIR-ATR	Cr(VI) Cu(II)	12.4 14.1	3 5	20,30,40,50 °C	300 min	10	NA	PSO	L F	NA	(Ferrero et al. 2014)
18	Pb(II) imprinted chitosan (Pb(II)-CS)	SEM, FTIR	Pb(II)	79.2	5.33	25°C	30h	0.4	-15.57	PSO	L	200	(Lu et al. 2013)
19	Chitosan supported on porous glass beads	SEM,FTIR,TGA,BET	Cu(II) Pb(II)	462.0 1831.0	NA	303K	24h	1	NA	PSO	NA	160	(Shen et al. 2013)
20	Ethylenediamine modified chitosan microspheres CtsEn and PtCtsEn	FTIR, TGA, SEM	Cu(II) Pb(II)	38.0 30.57 30.57, 24.40	NA	25°C	2h	0.5	NA	NA	L,L L,L	NA	(Chethan and Vishalakshi, 2013)

21	Chitosan -cross-linked and grafted with N-(2-carboxybenzyl)	SEM, FTIR, BET	Cu(II) Cr(VI)	308.0 175.0	5	25°C	24h	1	NA	NA	L-F	140	(Kyzas et al. 2013)
22	Cross-linked magnetic chitosan-2-aminopyridine glyoxal Schiff's base	SEM, FTIR, XRD, TGA, VSM, <sup>1</sup> HNMR	Cu(II)	124.0	5	30°C	8h	1	-78.71	PSO	L	150	(Monier et al. 2012)
23	Thiocarbamoyl chitosan	SEM, EDX, BET, FTIR	Cr(VI)	434.8	2	RT	4h	1	1.86	PSO	L	100	(Chauhan et al. 2012)
24	Chitosan/FeO-nanoparticles beads	SEM, FTIR, EDX, TGA	Cr(VI)	6.67	6.7	25°C	60 min	3	NA	PFO	NA	NA	(Liu et al. 2012)
25	Chitosan immobilized on bentonite	BET, TGA	Pb(II) Cu(II)	26.38 21.55	4	25,35,45, 55°C	24h	6.67	NA	PSO	F	50	(Futalan et al. 2011b)
26	Glutaraldehyde cross-linked chitosan beads	BET, FTIR, SEM	Pb(II)	204.0	5	35°C	4h	1	25.93	PSO, E	L, L-F	200	(Suguna et al. 2011)
27	Surfactant-modified chitosan bead	NA	Cu(II)	221.46	5.4	313 K	NA	0.5	24	PFO	L	NA	(Sarkar and Majumdar, 2011)
28	EDTA-modified chitosan-silica hybrid	FTIR, SEM	Pb(II)	49.73	3	22°C	24h	2	NA	PSO	L-F	NA	(Repo et al. 2011)



29	Chitosan modified with glycidylmethacrylate and diethylenetriamine	FTIR, TGA, XRD, SEM, <sup>13</sup> CNMR	Cu(II) Pb(II)	188.73 414.4	7	298 K	7h	0.8	NA	NA	L	NA	(Khan et al. 2011)
30	Chitosan with polyaspartic acid as complexing agent	FTIR-ATR, AFM, SEM, EDX	Pb(II) Cu(II)	79.05 85.21	5 1	295 K	3h	10	NA	PSO PSO	L	180	(Kołodzyńska, 2011)
31	Ethylenediamine-modified cross-linked magnetic chitosan	SEM	Cr(VI)	51.813	4	20,30,40°C	60 min	5	NA	PSO	L	250	(Hu et al. 2011)
32	a)raw chitosan beads b)protonated chitosan beads c)carboxylated chitosan beads d)grafted chitosan beads	FTIR, SEM	Cu(II)	40.0 52.0 86.0 126.0	6	303, 313, 323 K	5h	1	- 1.736 0.813 11.418	NA	L	200	(Gandhi et al. 2011)
33	a)protonated chitosan beads b)carboxylated chitosan beads c)grafted chitosan beads	FTIR, SEM, EDX	Cr(VI)	323.9, 364.7 405.7	7	303, 313, 323 K	10h	2	3.99 15.69 15.99	NA	F L L	200	(Kousalya et al. 2010)
34	Chitosan grafted with vanillin-based ligand	FTIR, XRD, <sup>13</sup> CNMR, <sup>1</sup> HNMR, CHN analyzer, SEM, DSC, TGA	Cu(II) Pb(II)	56.5 51.8	6.5 6	25°C	2h	2.5	NA	PSO	L	200	(Krishnapriya and Kandaswamy, 2010)

35	Chitosan-tripolyphosphate beads	FTIR, XRD, EDX, CHN analyzer, SEM,	Cu(II) Pb(II)	26.06 51.33	4.5	300-343K	100 min	4	32.64 16.26	PSO	L	400	(Nghah and Fatinathan, 2010)
36	Cross-linked magnetic chitosan-isatin Schiff's base	FTIR, TGA, WAXRD, <sup>1</sup> HNMR	Cu(II)	103.16	5	28°C	8h	1.5	NA	PSO	L	150	(Monier et al. 2010)
37	Chitosan-coated sand	SEM, TGA, BET	Cu(II) Pb(II)	8.18 12.32	4.5	RT	4h	83.33	-42.969	PSO	L	50	(Wan et al., 2010)
38	Gel beads of hydrolyzed polyacrylamide and chitosan	Nil	Cu(II) Pb(II)	49.07 353.09	4.2	10-60°C	2h	2.5- 12.5	endothermic endothermic	NA	F F	NA	(Cao et al. 2010)
39	Chitosan electrospun nanofiber	SEM, FTIR	Cu(II) Pb(II)	485.44 263.15	NA	25°C	24h	0.52	NA	NA	L	NA	(Haider and Park, 2009)
40	Chitosan cross-linked and grafted with amido or carboxyl groups a) Ch-g-Aa b) Ch-g-Aam	FTIR	Cu(II) Cr(VI)	397, 184 613,1254	6 4	25, 45, 65°C	24h	1	32.89, 15.73 14.02, 19.14	NA	L-F	160	(Kyzas et al., 2009)
41	Chitosan flakes	Nil	Cr(VI)	7.943	3	303-333K	24h	5	-50.782	PSO	L	120	(Aydin and Aksoy, 2009)
42	Chitosan-crosslinked agent	CHN, FTIR, TGA, DTA, <sup>13</sup> CNMR, SEM, XRD	Cu(II) Pb(II)	76.88 84.95	8.5 8.5	25°C	4h	1	NA	PSO PSO	L L	200	(Krishnapriya and Kandaswamy, 2009)

43	Magnetic chitosan microspheres modified with thiourea	XRD, FTIR, Elemental analysis, Zeta potential, SEM, TGA, VSM	Cu(II)	66.7	5	28°C	8h	1.5	NA	NA	L	150	(Zhou et al., 2009)
44	Chitosan coated PVC beads	FTIR, BET	Cu(II)	87.9	4	RT	6h	0.5-5	NA	PSO	L	120	(Popuri et al., 2009)
45	Epichlorohydrin-crosslinked chitosan	SEM, FTIR,	Cu(II) Pb(II)	35.46 34.13	6	RT	4h	0.1	NA	PSO PSO	L L	NA	(Chen et al., 2008)
46	Chitosan cross-linked with (H2fmbme) Schiff base	Raman, TGA	Cu(II)	113.6	6	25°C	4h	2	NA	PSO	L	230	(Vasconcelos et al., 2008)
47	Chitosan coated on ceramic alumina	BET, SEM, FTIR, ATR	Cu(II)	86.2	4	25°C	24h	NA	NA	NA	RP	200	(Boddu et al. 2008)
48	Cross linked chitosan with epichlorhydrin	<sup>13</sup> CNMR, FTIR, SEM	Cu(II) Pb(II)	35.46 34.13	6	RT	4h	1	NA	PSO PSO	F L	NA	(Chen et al. 2008)
49	Aminated chitosan	FTIR	Cr(VI)	28.7	NA	RT	12h	3	NA	NA	L	NA	(Yan et al. 2007)
50	Chitosan modified with reactive blue	Raman, TGA, SEM	Cu(II)	57.0	7	25°C	4h	2	NA	PSO	L	230	(Vasconcelos et al., 2007)
51	Chitosan from silkworm chrysalides	SEM, TGA	Pb(II)	150.42	5	20°C	24h	3	NA	NA	F	200	(Paulino et al. 2007)

52	Chitosan beads	BET, FTIR	Cr(VI)	76.92	5	NA	50 min	0.1	NA	NA	L	500	(Ngah et al. 2006)
53	Cross linked xanthated chitosan a) CMCB b) CMCF	XRD, FTIR, EPR	Cr(VI)	625.0 256.4	3	25°C	16h	1	NA	PSO PSO	L	NA	(Sankararamakrishnan et al. 2006)
54	Cross linked chitosan (glutaraldehyde)	Nil	Cr(VI)	215	4	RT	96h	0.1g/L	NA	NA	L	250	(Rojas et al. 2005)
55	Chitosan modified with complexing agent BPMAMF	Nil	Cu(II)	109	6	25°C	200 min	2	NA	PSO	L	200	(Justi et al. 2005a)
56	a)chitosan b)chitosan/PVA beads	Nil	Cu(II)	33.4 47.9	6	RT	50 min 70 min	0.2	NA	NA	L L	NA	(Ngah et al. , 2004)
57	Alginate-chitosan hybrid gel beads	Nil	Cu(II)	8.38	3.5	25°C	3h	25	NA	NA	F	NA	(Gotoh et al. 2004)
58	Quaternary chitosan salt	FTIR, <sup>1</sup> H NMR, TGA	Cr(VI)	68.3	4.5	25°C	5h	0.25-5	NA	PSO	L	150	(Spinelli et al. 2004)
59	Chitosan pure	Nil	Pb(II)	34.78- 115.06	4.5	20°C	14d	1	NA	NA	RP	200	(Ng et al. 2003)
60	Chitosan pure	SEM, TGA, DSC, BET, NMR	Cu(II)	81.78- 122.58	3.5	20°C	14d	1	NA	NA	L, RP	200	(Ng et al. 2002)

61	a) chitosan beads b) cross-linked chitosan beads (GLA) c) -do- (ECH) d) -do- (EGDE)	FTIR	Cu(II)	80.71 59.67 62.47 45.94	6	NA	60-90 min	0.1	NA	NA	L	500	(Ngah et al. 2002)
62	Cross-linked chitosan-crown ethers a) Chitosan b) CCTS-1 c) CCTS-2	XRD FTIR	Cu(II) Pb(II)	16.8, 23.9; 31.3 24.0; 29.1, 60.2.	5.6	RT	12h	1	NA	NA	NA	NA	(Tan et al. 1999)
63	Chitosan pure	Nil	Cu(II)	16.8	5	25°C	24h	0.05	NA	NA	L	150	(Huang et al., 1996)
64	Chitosan from crab shells	Nil	Cr(VI)	34.9	3	25°C	12h	0.5	NA	PFO	L	NA	(Udaybhaskar et al., 1990)



**CHAPTER 3**  
**MATERIALS AND**  
**METHODS**





*This chapter provides details about materials, chemicals and the analytical instruments used in achieving the objectives of the present work. The synthesis procedures adopted for the preparation of four ligands (L-1, L-2, L-3 and L-4) and four chitosan derivatives (CTSL-1, CTSL-2, CTSL-3 and CTSL-4) have been presented here. The methodologies and the equations used in adsorption experiments encompassing equilibrium, kinetic and thermodynamic studies are also presented. Finally, the methods and equations used in membrane synthesis, characterization and permeation experiments have been described.*

### 3.1 MATERIALS

#### 3.1.1 Chitosan

The chitosan used for this research was procured in the form of powder (30 mesh) from Seafresh Industry Public Co., Ltd. Thailand. The degree of deacetylation was 90%. The structure of chitosan with complete deacetylation and partial deacetylation is shown in Figure 3.1 a and Figure 3.1 b respectively. The properties and characteristics of the chitosan used in the present study are tabulated in Table 3.1. A photograph of the chitosan powder is shown in Figure 3.2.

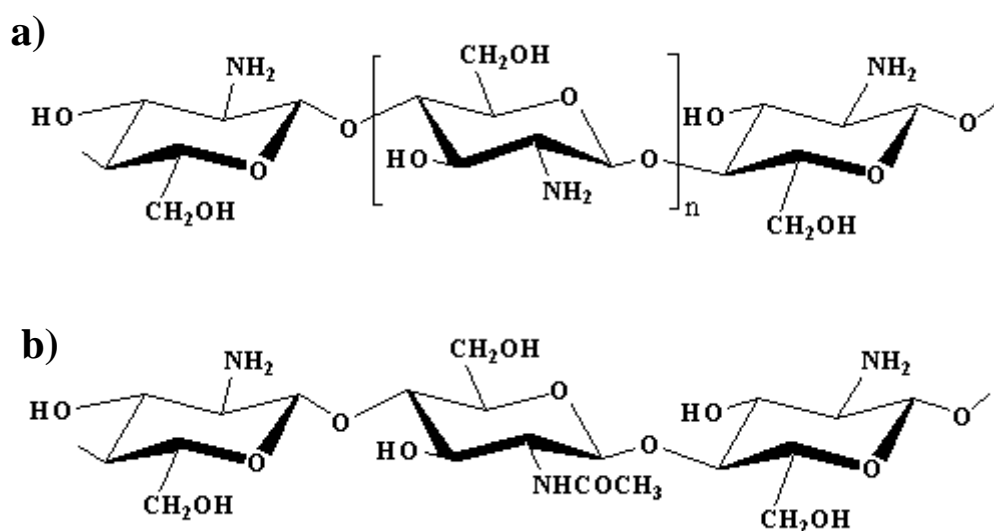


**Figure 3.1 Structure of chitosan a) with complete deacetylation and b) with partial deacetylation**

**Table 3.1 Properties and characteristics of chitosan (Data provided by the supplier)**

<b>Sl. No.</b>	<b>Parameters</b>	<b>Analysis</b>
<b>1</b>	Raw Material	Shrimp
<b>2</b>	Powder appearance	Cream
<b>3</b>	Particle size (mesh #)	30 (95%)
<b>4</b>	Ash content (%)	0.3
<b>5</b>	Moisture content (%)	8-10
<b>6</b>	Deacetylation (%)	90
<b>7</b>	Insoluble (%)	0.3
<b>8</b>	Viscosity at 25°C (mPa.s)	600
<b>9</b>	Molecular Wt. at 25°C	$5.0 \times 10^5$
<b>10</b>	Heavy metal content	Nil
<b>11</b>	Molecular formula of monomer unit	$C_6H_{11}NO_4$
<b>12</b>	Molecular mass of monomer unit	161



**Figure 3.2 Photograph of chitosan powder**

### 3.1.2 Chemicals used

The chemicals used in this study along with their suppliers are tabulated in Table 3.2

**Table 3.2 Chemicals used and their suppliers**

Sl. No.	Chemical Used	Supplier
1	$K_2Cr_2O_7$	Thomas Baker, India
2	$Pb(NO_3)_2$	NICE chemicals, Cochin, India
3	$CuSO_4 \cdot 5H_2O$	Merck Specialities India Ltd.
4	Semicarbazide hydrochloride	Merck Schuchardt OHG, Germany
5	4-methoxy acetophenone	Merck KGaA, Germany
6	Acetophenone	Merck Specialities, India Ltd.
7	4-Methyl acetophenone	Sigma-Aldrich Chemie-GmbH
8	4-Chloro acetophenone	Sigma-Aldrich, USA
9	Sodium acetate	Finar Ltd. India
10	Sodium bicarbonate	Finar Ltd. India
11	Sodium hydroxide	Finar Ltd. India
12	Hydrochloric Acid	Finar Ltd. India
13	$POCl_3$	Spectrochem Ltd, India.
14	Di methyl formamide	Finar Ltd. India
15	Ethyl acetate	Finar Ltd. India
16	Chloroform	Merck specialities India Ltd.

<b>17</b>	Polysulfone beads	Sigma Aldrich USA
<b>18</b>	PEG-1000	Hi Media Laboratories, Mumbai, India.
<b>19</b>	Bovine serum albumin	Central Drug House, New Delhi.
<b>20</b>	N-Methyl-2-Pyrrolidone	Merck India Ltd.
<b>21</b>	Formic acid	Merck India Ltd.

### 3.1.3 Instruments used

The various instruments used in this study along with purpose of use are presented in Table 3.3.

**Table 3.3 List of instruments used**

<b>Sl. No.</b>	<b>Instrument</b>	<b>Model and Make</b>	<b>Purpose</b>
<b>1</b>	Fourier transformed infrared spectrometer (FTIR)	FTIR RX-1, Shimadzu	To find chemical groups in the adsorbent; to find groups responsible for sorption.
<b>2</b>	<sup>13</sup> C NMR Nuclear magnetic resonance spectrometer	ECX400 - Jeol 400 MHz High Resolution Multinuclear FT-NMR Spectrometer for solids.	To determine the environment of the carbon atoms
<b>3</b>	<sup>1</sup> H NMR spectrometer	400MHz Bruker Ascend	To determine the proton environment
<b>4</b>	Atomic absorption spectrometer	Thermo-Scientific iCE 3000 series flame atomic absorption spectrometer	To determine heavy metal concentration.
<b>5</b>	Powder X-ray diffractometer	Rigaku Miniflux-600	To find molecular structure, crystallinity.

<b>6</b>	Scanning electron microscope	Jeol JED 2300 Analysis Station scanning electron microscope.	To determine surface morphology
<b>7</b>	pH meter	Systronics digital pH meter-335	pH measurement
<b>8</b>	Incubator shaker	Lead instruments	Agitation, temperature control.
<b>9</b>	Differential scanning calorimeter	NETZSCH DSC 404F1	To determine thermal properties.

### **3.2 SYNTHESSES OF CHITOSAN DERIVATIVES.**

The syntheses of the ligands (L-1, L-2, L-3 and L-4) were carried out following a previously reported method (Lebedev et al. 2005; Malladi et al. 2013). Pure chitosan powder (CTS) was then reacted with four ligands (L-1, L-2, L-3 and L-4) separately to form four derivatives of chitosan (CTSL-1, CTSL-2, CTSL-3 and CTSL-4) respectively. The following sections describe in detail the syntheses of the chitosan derivatives.

#### **3.2.1 Synthesis of CTSL-1**

CTSL-1 was synthesized in two steps viz. synthesis of the ligand L-1, 3-(4-methoxyphenyl)-1H-pyrazole-4-carbaldehyde, which was followed by the grafting of this ligand on to chitosan.

The synthesis of the ligand L-1 was carried out in the following two steps:

##### **3.2.1.1 Synthesis of semicarbazone-1**

In the first step 4-methoxyacetophenone (20 g, 0.13 mol) was added to 400 mL ethanol in a 1 litre round bottom flask. Semicarbazide hydrochloride powder (13.38 g, 0.12 mol) and sodium acetate (16.32 g, 0.20 mol) were added to this mixture and the contents were kept under stirring and refluxed at atmospheric pressure at 78°C for 4h. The reaction scheme is as shown in Figure 3.3.

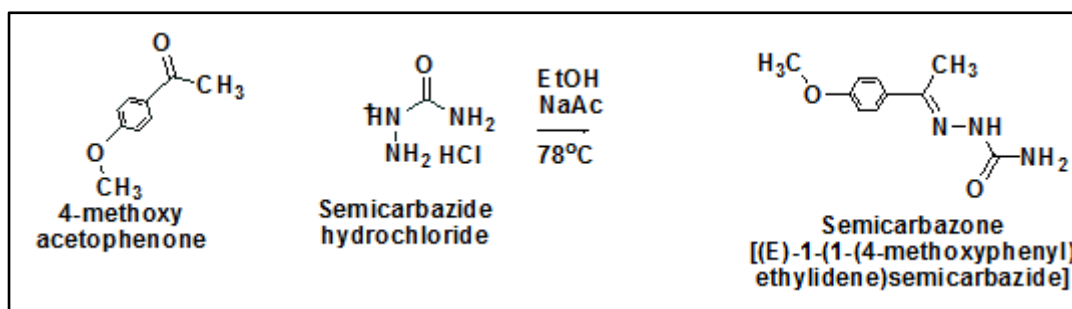


**Figure 3.3 Synthesis of semicarbazone-1 from 4-methoxyacetophenone**

The reaction mass was cooled to room temperature and the off-white precipitate was filtered and washed with additional ethanol and water to remove impurities. The solid mass was taken in 1 litre of distilled water, washed and filtered, and dried at 50°C. (Yield: 20 g, 80.5%), C<sub>10</sub>H<sub>13</sub>N<sub>3</sub>O<sub>2</sub>, MW=207). The experimental set up is shown in Figure 3.4.



**Figure 3.4 Experimental set up for the synthesis of semicarbazone intermediate**

### 3.2.1.2 Synthesis of ligand (L-1)

Dimethyl Formamide (40 mL, 0.52 mol) was added drop-wise to ice-cold phosphorous oxychloride (19.8 mL, 0.21 mol) in a 250 mL round bottomed flask. Semicarbazone (20 g, 0.097 mol) was added portion-wise over 10 min to the previous

mixture. The reaction mass was brought to room temperature and gradually heated to 70°C and maintained for 4h. The scheme for the reaction is as shown in Figure 3.5.

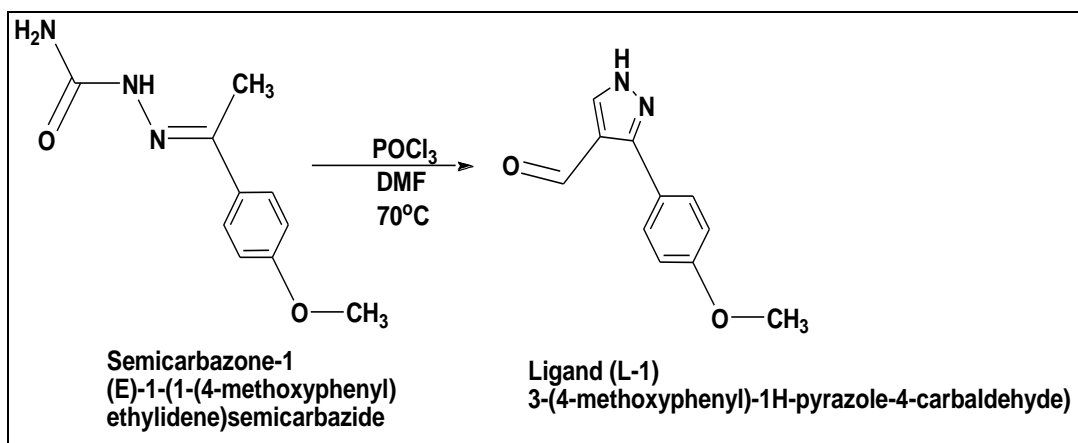


**Figure 3.5 Synthesis of ligand (L-1) from semicarbazone-1**

The red viscous liquid was poured into 500 mL of ice cold water with constant stirring. The pH of the mixture is then brought to 7.0 by a portion-wise addition of sodium carbonate solution. The greenish yellow precipitate obtained was filtered and washed with water and dried at 50°C. The experimental setup for the synthesis of the ligand (L-1) is shown in Figure 3.6. The reaction mass is kept under inert atmosphere by connecting a nitrogen filled balloon into the septum attached to the neck of the round bottom flask. This precaution was taken to avoid the possible interference of atmospheric moisture with the reaction. (Yield: 13.5 g, 69.2%, C<sub>11</sub>H<sub>10</sub>O<sub>2</sub>N<sub>2</sub>, MW=202).

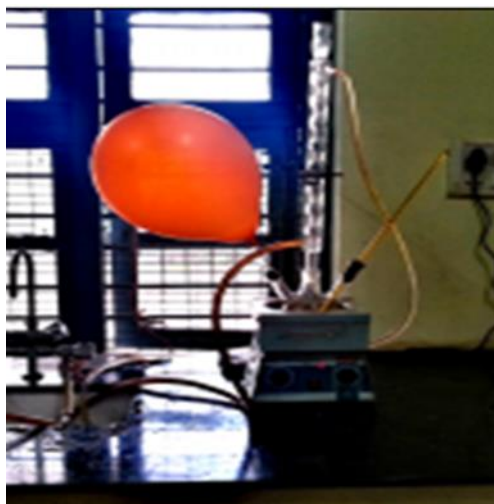


**Figure 3.6 Experimental set up for the synthesis of the ligand (L-1) under nitrogen atmosphere**

### **3.2.1.3 Grafting of L-1 on chitosan to form CTSL-1**

Chitosan in powder form (3 g) was taken with 1% acetic acid (76 mL) and kept under stirring at room temperature for one hour. Further, the thick solution was diluted by adding methanol (350 mL) and stirred for an additional 16h. ligand (L-1) (6 g) was dissolved in chloroform (60 mL) and added to the previous mixture over a period of 10 min at room temperature. Agitation was continued for a further period of 16h at room temperature.



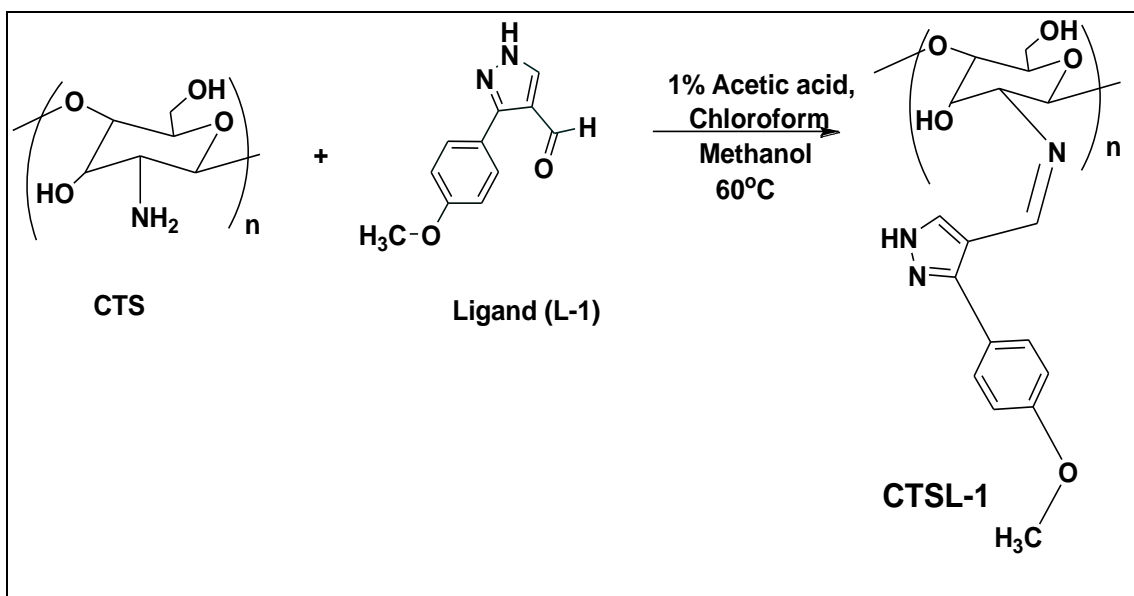


**Figure 3.7 Synthesis of chitosan derivative CTSL-1**

The reaction mixture was then heated to 60°C and refluxed for 18h under agitation. The product was brought down to room temperature; chloroform (75 mL) was added to the reaction mass and stirred for 10 min to remove any unreacted components. The yellow mass (CTSL-1) obtained was filtered, washed with chloroform and dried at 50°C. The reaction scheme is as shown in Figure 3.7 (Yield: 6 g, 93.3%). In Figure 3.8, the images of CTSL-1 in the wet and dry forms are shown.

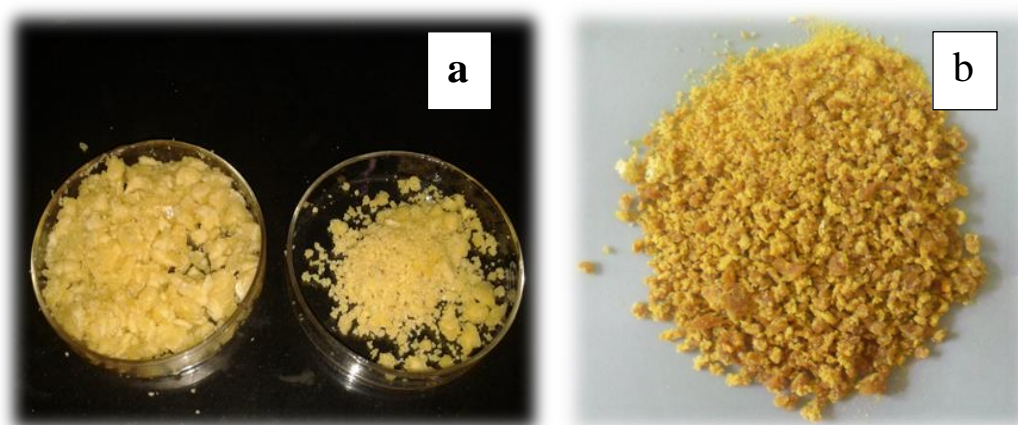


**Figure 3.8 CTSL-1 a) in wet form before drying, b) after drying.**

### 3.2.2 Synthesis of CTSL-2

The synthesis of the chitosan derivative CTSL-2 was carried out in three steps (Figure 3.9). In the first two steps, ligand L-2 (3-phenyl-1H-pyrazole-4-carbaldehyde) was synthesized as per procedure reported in literature (Lebedev et al. 2005, Malladi et al. 2013).

Briefly, to 125 mL ethanol, acetophenone (15.6 mL, 0.13 mol), semicarbazide hydrochloride powder (13.38 g, 0.12 mol) and sodium acetate (16.32 g, 0.20 mol) were added and refluxed at 78°C for 4h to yield semicarbazone-2 (Yield: 17.4 g, 82%). To dimethyl formamide (40.38 mL, 0.525 mol), phosphorous oxychloride (20 mL, 0.21 mol) was added drop-wise under nitrogen atmosphere, to which semicarbazone-2 (17.4 g, 0.098 mol) was added portion wise over 10 min. The reaction mass was then heated to 80°C in a gradual manner and maintained for 4h. After the completion of the reaction, the pH was adjusted to 7 by adding sodium carbonate. It was then extracted with ethyl acetate in three stages using 75 mL in each stage to recover the ligand L-2. (Yield: 12.1 g , 83.43%).

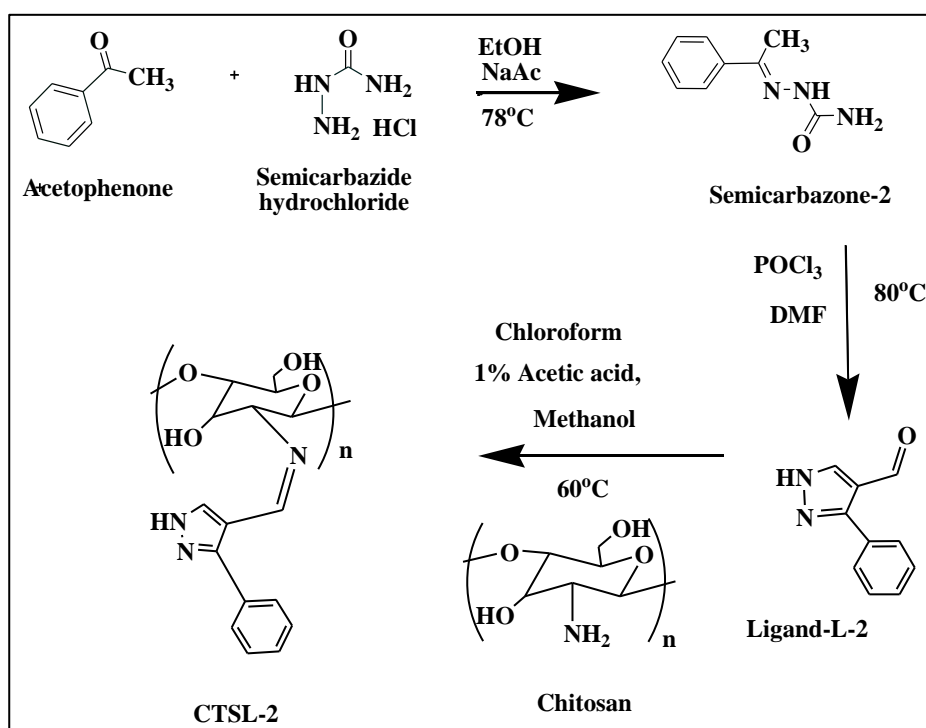


Figure 3.9 Reaction scheme for the synthesis of CTSL-2

In the last step, 150 mL of acetic acid (1%) was used to dissolve 6 g of chitosan powder. To this mixture, 600 mL of methanol was added and agitated for 16h. To this, L-2, (10.25 g) dissolved in 60 mL of chloroform was added over 10 min. After this, the reaction mixture was maintained at 60°C for 18h under agitation. The product obtained was further washed with 75 mL of chloroform and the yellow mass obtained was filtered and dried at 50°C (Yield: 9.3 g)

### 3.2.3 Synthesis of CTSL-3

CTSL-3 was synthesized by first preparation of the ligand L-3, 3-p-tolyl-1H-pyrazole-4-carbaldehyde followed by the grafting of this ligand on to the chitosan backbone.

#### 3.2.3.1 Synthesis of semicarbazone-3

The ligand L-3 was prepared as per the two step reaction scheme given below in Figure 3.10 and Figure 3.11. In the first step, semicarbazone-3 (*E*)-1-(1-*p*-tolylethylidene) semicarbazide was prepared by reacting 4 methyl acetophenone with semicarbazide by refluxing in alcoholic medium. 4 methyl acetophenone (17.4 mL, 0.13 mol) was added to 125 mL ethanol taken in a 1 L round bottom flask. Semicarbazide hydrochloride powder (13.38 g, 0.12 mol) and sodium acetate (16.32 g, 0.20 mol) were added to this mixture and the contents were kept under stirring and refluxed at 78°C for 4h.

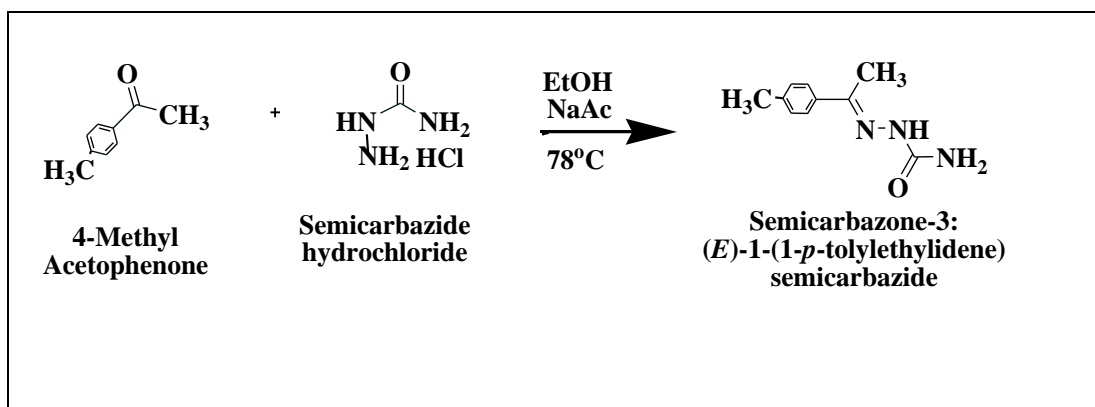


**Figure 3.10** Reaction scheme for the synthesis of semicarbazone-3.

The post-reaction mass was cooled to room temperature and the off-white precipitate was filtered and washed with additional ethanol to remove organic impurities. The solid mass was taken in 1 L of distilled water, stirred and filtered, and dried at 50°C. Yield: 17.2 g (75.0%) (C<sub>10</sub>N<sub>3</sub>H<sub>13</sub>O, MW=191.23)

The experimental setup used for the synthesis of semicarbazone-3 is shown in Figure 3.4.

### 3.2.3.2 Synthesis of the ligand-L-3: 3-*p*-tolyl-1H-pyrazole-4-carbaldehyde

Dimethyl formamide (37 mL, 0.48 mol) was added drop-wise to ice-cold phosphorous oxychloride (18.4 mL, 0.18 mol) taken in a 250 mL round bottomed flask. An inert atmosphere was maintained by using a nitrogen filled balloon pierced into a septum and connected to one neck of the round bottomed flask. This precaution was taken to avoid the interference of atmospheric moisture with the reaction. To this semicarbazone-3 (17.2 g, 0.09 mol) was added portion wise over 10 min. The reaction mass was brought to room temperature and gradually heated to 78°C and maintained for 4h.

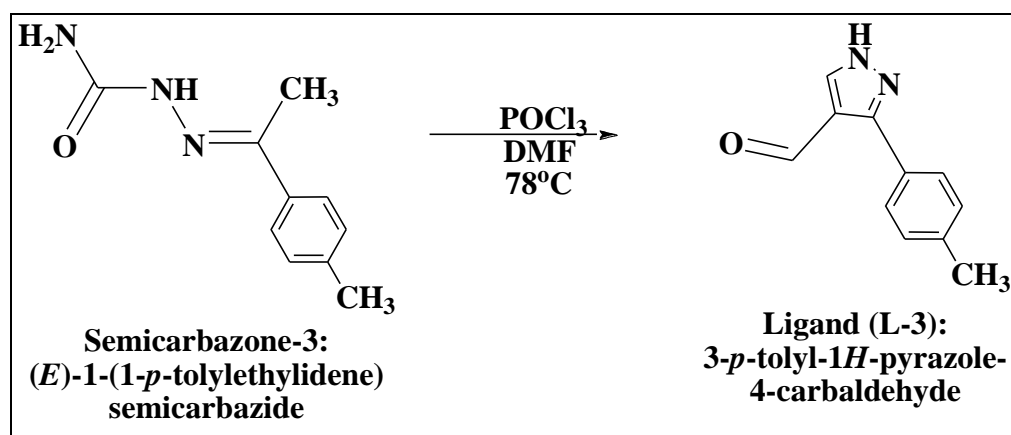


**Figure 3.11 Reaction scheme for the synthesis of the ligand (L-3)**

The red viscous liquid was cooled to room temperature and added portion wise to 500 mL of ice cold water with constant stirring. The pH of this mixture was brought to 7 by the portion-wise addition of sodium carbonate solution. It was then extracted with ethyl acetate in three stages using 75 mL in each stage to recover the ligand-3 (3-*p*-tolyl-1H-pyrazole-4-carbaldehyde) which is in the form of a reddish

brown viscous mass. It was then dried at 50°C. Yield: 16.75 g (75.2%) ( $C_{11}H_{10}N_2O$ , MW=186.21)

The experimental set up used for the reaction is as shown in Figure 3.6.

### 3.2.3.3 Grafting of L-3 on chitosan to form chitosan derivative CTSL-3

Chitosan (CTS) powder (6 g) was dissolved in 1% acetic acid (150 ml) and stirred at room temperature for one hour. The thick solution was diluted by adding methanol (700 mL) and stirring was continued for an additional 16h. 3-p-tolyl-1H-pyrazole-4-carbaldehyde (11.1 g) was dissolved in chloroform (110 mL) and added to the previous mixture over a period of 10 min at room temperature. Stirring was continued for a further period of 16h at room temperature. The reaction scheme is as shown in Figure 3.12.

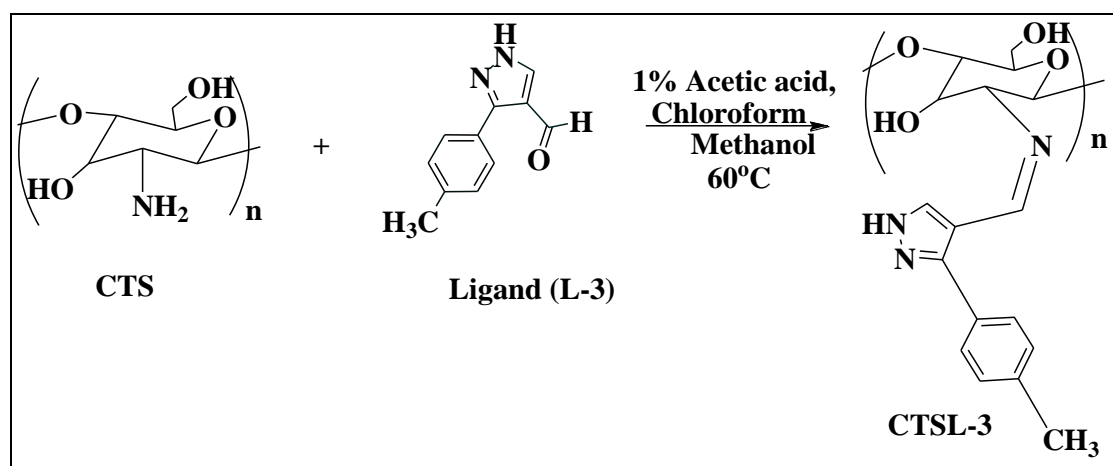


**Figure 3.12** Reaction scheme for grafting L-3 on chitosan to form CTSL-3

The reaction mixture was heated to 60°C and stirred for 18h. The product was brought to room temperature. Chloroform (75 mL) was added to the reaction mass and stirred for 10 min. The yellow solid mass obtained was filtered, washed with chloroform and dried at 50°C. Yield: 9.5 g (77.5%).

### 3.2.4 Synthesis of the chitosan derivative CTSL-4

The synthesis of the CTSL-4 was carried out by first preparing the ligand L-4 followed by the grafting of this ligand on the chitosan. The steps are enumerated as follows.

### 3.2.4.1 Synthesis of Semicarbazone-4: (*E*)-1-(1-(4-chlorophenyl) ethylidene) semicarbazide)

4-Chloro Acetophenone (16.86 mL, 0.13mol) was added to 150 mL ethanol taken in a 1 L round bottom flask. Semicarbazide hydrochloride powder (13.38 g, 0.12mol) and sodium acetate (16.32 g, 0.20mol) were added to this mixture and the contents were kept under stirring and refluxed at 78°C for 4h. The scheme of the reaction is as shown below in Figure 3.13.

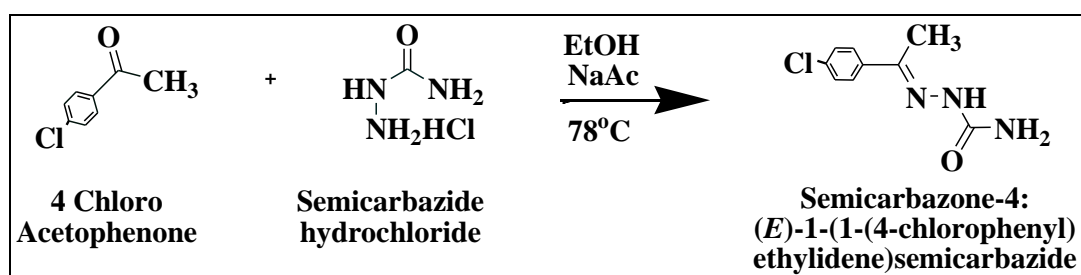


**Figure 3.13** Reaction scheme for the synthesis of semicarbazone-4 intermediate

The post-reaction mass was cooled to room temperature and the white precipitate was filtered and washed with additional ethanol to remove organic impurities. The solid mass was taken in 1L of distilled water, stirred and filtered, and dried at 50°C. Yield: 20.3 g (79.9%) (C<sub>9</sub>N<sub>3</sub>H<sub>10</sub>OCl, MW=211.65)

The experimental setup for the synthesis of semicarbazone-4 is shown in Figure 3.4.

### 3.2.4.2 Synthesis of L-4 (3-(4-chlorophenyl)-1H-pyrazole-4-carbaldehyde)

Dimethyl formamide (39.2 mL, 0.51 mol) was added drop-wise to ice-cold phosphorous oxychloride (19.4 mL, 0.20 mol) taken in a 250 mL round bottomed flask. An inert atmosphere was maintained by using a nitrogen filled balloon pierced into a septum and connected to one neck of the round bottomed flask. This precaution was taken to avoid the interference of atmospheric moisture with the reaction. To this semicarbazone-4 (20.3 g, 0.095 mol) was added portion wise over 10 min. The reaction mass was brought to room temperature and gradually heated to 80°C and maintained for 4h. The scheme for the reaction is as shown in Figure 3.14.

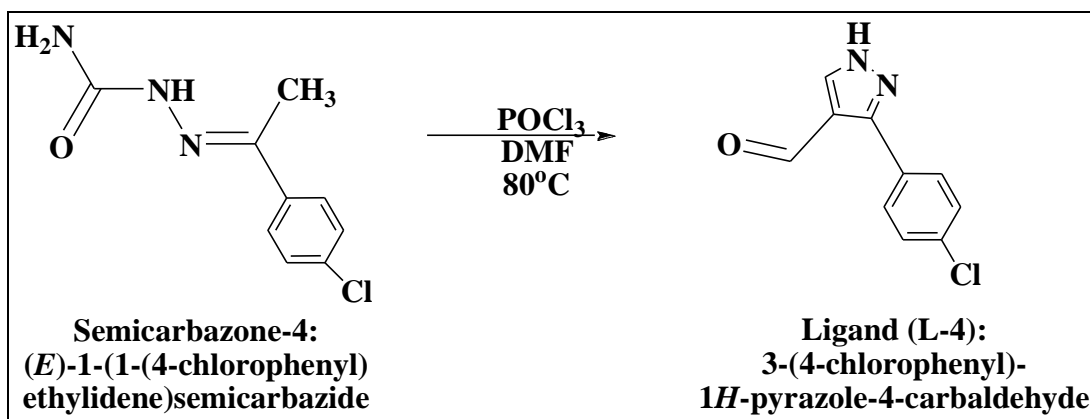


**Figure 3.14** Reaction scheme for the synthesis of the ligand (L-4)

The red viscous liquid was cooled to room temperature and added portion wise to 500 mL of ice cold water with constant stirring. The pH of this mixture was brought to 7 by portion wise adding of sodium carbonate solution. The yellow precipitate obtained was filtered and washed with water and dried at 50°C. Yield: 16.6 g (83.8%) (C<sub>10</sub>H<sub>7</sub>ClN<sub>2</sub>O, MW=206.63). The experimental setup for the synthesis of the ligand (L-4) is shown in Figure 3.6

#### 3.2.4.3 Reaction of ligand L-4 with chitosan to form CTSL-4

Chitosan (CTS) powder (6 g) was dissolved in 1% acetic acid (150 mL) and stirred at room temperature for one hour. The thick solution was diluted by adding methanol (700 mL) and stirring was continued for an additional 16h. 3-(4-chlorophenyl)-1H-pyrazole-4-carbaldehyde (12.3 g) was dissolved in chloroform (120 mL) and added to the previous mixture over a period of 10 min at room temperature. Stirring was continued for a further period of 16h at room temperature. The reaction scheme is as shown in Figure 3.15.

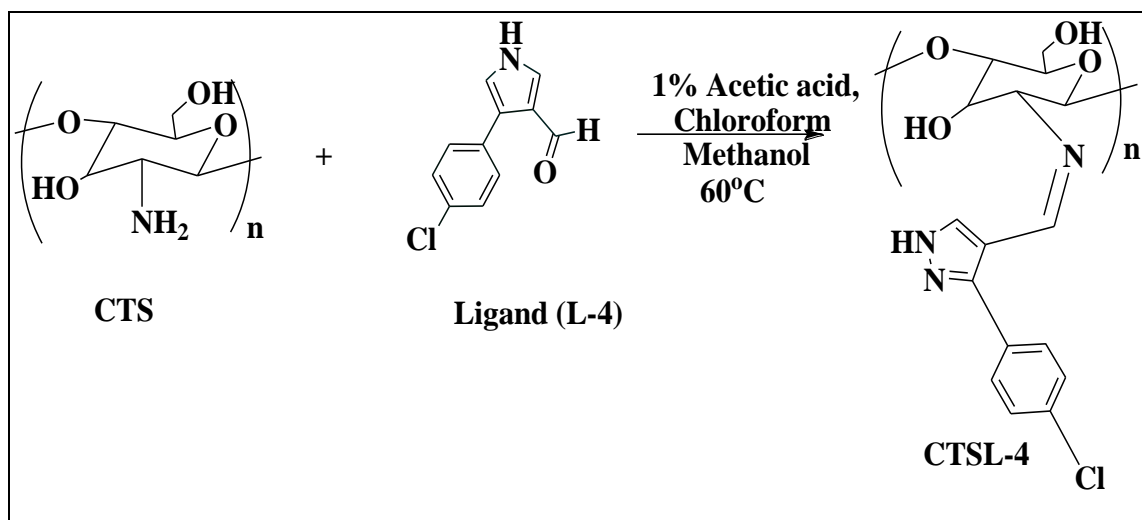


**Figure 3.15 Reaction scheme for synthesis of CTSL-4**

The reaction mixture was heated to 60°C and stirred for 18h. The product was brought to room temperature. Chloroform (75 mL) was added to the reaction mass and stirred for 10 min. The yellow solids obtained were filtered, washed with chloroform and dried at 50°C. Yield: 10.82 g (83.1%).

### 3.3 ADSORPTION STUDIES

#### 3.3.1 Preparation of stock solutions of metal ions

##### 3.3.1.1 Preparation of 1000 mg/L stock solution of Cr (VI)

2.828 g of  $K_2Cr_2O_7$  salt was first dissolved in adequate amount of double distilled water in a 1 L standard flask and the water level was brought up to the mark. The contents were then vigorously shaken to make a uniform solution.

##### 3.3.1.2 Preparation of 1000 mg/L stock solution of Cu (II)

3.929 g of  $CuSO_4 \cdot 5H_2O$  salt was first dissolved in required amount of double distilled water in a 1 L standard flask and the water level was brought up to the mark. The contents were then vigorously shaken to make a uniform solution.



### **3.3.1.3 Preparation of 1000 mg/L stock solution of Pb (II)**

1.598 g of  $\text{Pb}(\text{NO}_3)_2$  salt was first dissolved in enough quantity of double distilled water in a 1 L standard flask and the water level was brought up to the mark. The contents were then vigorously shaken to make a uniform solution.

## **3.3.2 Characterization and Analysis**

### **3.3.2.1 Fourier transformed infrared (FTIR) spectroscopic studies**

The FTIR images were obtained for chitosan, ligands (L-1, L-2, L-3, L-4) and adsorbents (CTSL-1, CTSL-2, CTSL-3, CTSL-4) using FTIR (Shimadzu) spectroscope. KBr disks having approximately 2% by wt. of sample were prepared and the images were recorded in the range of  $400\text{-}4000\text{ cm}^{-1}$ .

### **3.3.2.2 Proton Nuclear Magnetic Resonance ( $^1\text{H}$ NMR) studies**

$^1\text{H}$  NMR spectra of the ligands (L-1, L-2, L-3 and L-4) were recorded using Bruker Ascend 400 NMR Spectrometer. The samples were first dissolved in deuterated DMSO (Di-methyl sulfoxide- $d_6$ ) before recording the images.

### **3.3.2.3 Solid state $^{13}\text{C}$ NMR studies**

The  $^{13}\text{C}$  NMR of the chitosan derivatives CTSL-1, CTSL-2, CTSL-3, CTSL-4 were recorded on ECX400 - Jeol 400 MHz high resolution multinuclear FT-NMR spectrometer for solids. Since the afore-mentioned derivatives were not soluble in commonly used deuterated solvents such as DMSO,  $\text{CDCl}_3$  and  $\text{CD}_3\text{COOD}$ , solid state  $^{13}\text{C}$  NMR method was employed to extract the structural details.

### **3.3.2.4 Scanning electron microscopy (SEM) studies**

The scanning electron micrographs were recorded using a Jeol JED 2300 Analysis Station scanning electron microscope. The samples were first prepared by sputter coating with gold before recording the images.

### 3.3.2.5 Powder X-ray diffraction (XRD) studies

The X-Ray Diffraction spectral images of chitosan, CTSL-1, CTSL-2, CTSL-3, CTSL-4 were recorded by using Rigaku Miniflux-600 X-ray diffractometer. The structure of the sample was investigated by X-ray diffraction at  $2\theta$  angle values in the range of  $5-80^\circ$  with a step size of  $0.02^\circ$ .

### 3.3.2.6 Differential scanning calorimetry (DSC) studies

The DSC thermal stability tests for the samples were performed with NETZSCH DSC 404F1 analyzer and the results were recorded in a temperature range of  $25^\circ\text{C} - 600^\circ\text{C}$

### 3.3.3 Effect of initial pH on adsorption

Ionic solutions of Cr (VI), Cu (II) and Pb (II) having a concentration of 100 mg/L were prepared at the required pH values (3 to 7) and 25 mL of each was taken in 50 mL Erlenmeyer flasks and agitated with 50 mg of adsorbent for a duration of 24h in an incubator shaker at  $30 \pm 1^\circ\text{C}$  and 150 rpm. After adsorption, samples were drawn using a syringe and filtered with syringe filter of 0.2 micron size. They were then diluted and analysed by atomic absorption spectrometer (AAS). The amount of metal ions adsorbed was calculated using Eq.3.1 (Krishnapriya and Kandaswamy 2010).

$$Q_e = \frac{(C_o - C_e)V}{W} \quad (3.1)$$

where ' $Q_e$ ' is the equilibrium adsorption capacity of the adsorbent (mg/g of adsorbent), ' $C_o$ ' and ' $C_e$ ' are the initial and equilibrium concentrations of the solute (mg/L) in aqueous solution respectively, ' $V$ ' is the volume of the solution (mL) and ' $W$ ' is the mass of the sorbent used (g).

### 3.3.4 Adsorption equilibrium studies

25 mL of solutions having metal ions Cr (VI), Cu (II) and Pb (II) with initial concentration in the range of 10 mg/L to 1000 mg/L at the optimum pH for adsorption were taken in Erlenmeyer flasks and to each, 50 mg of the adsorbent was added. The samples were then kept under agitation for 24h in an incubator shaker at 150 rpm and  $30 \pm 1^\circ\text{C}$ . Samples were drawn, filtered through syringe filter of 0.2 micron size,

diluted and their concentration was analysed by AAS. The amount of metal ions adsorbed was calculated using Eq.3.1.

### 3.3.5 Adsorption kinetic studies

The kinetic study was conducted by taking a volume of 125 mL of the metal ion (Cr (VI), Cu (II) and Pb (II)) solutions having initial concentration of 100 mg/L at the optimum pH corresponding to each metal ion with an adsorbent dose of 250 mg. The solutions were agitated in an orbital shaker for 24h and samples were drawn at predetermined time intervals, filtered, diluted and their concentration analysed by AAS. The amount of metal ion adsorbed ( $Q_t$ , mg/g) at time  $t$  (min) was calculated by Eq. 3.2 (Shariful et al. 2017).

$$Q_t = \frac{(C_o - C_t)V}{W} \quad (3.2)$$

where ' $C_t$ ' (mg/L) is the concentration of the metal ion at time ' $t$ ' (min).

### 3.3.6 Adsorption thermodynamic studies

Thermodynamic studies were carried out for different initial concentrations of metal ions ranging from 10 mg/L to 100 mg/L, each at 5 different temperatures in the range of 283.15 K to 323.15 K (10°C, 20°C, 30°C, 40°C, 50°C). Volume of each metal ion solution taken was 25 mL with an adsorbent dose of 50 mg. The solution was agitated for 24h in an orbital shaker. The initial pH of the solution corresponded to the optimum pH obtained during the pH study for the particular metal ion.

## 3.4 MEMBRANE STUDIES

### 3.4.1 Preparation of neat polysulfone membrane (P-0)

1.8 g of polysulfone was taken with 8 mL of N-Methyl-2-pyrrolidone (NMP) in a 20 mL beaker and kept under stirring for over 3h till polysulfone completely dissolved after which 0.2 g of PEG-1000 was added to the previous mixture and was stirred for over 24h until a homogeneous solution was obtained. The stirring was then stopped and the temperature was maintained at 50°C for 2h to remove the air bubbles. This solution was then cast over a glass plate and then dipped into a coagulation bath of distilled water (27°C) acting as the non-solvent, when the membrane is formed by phase inversion (Kumar et al. 2013c).

### 3.4.2 Preparation of PSf: CTSL-2 blend membranes

The PSf: CTSL-2 (98:2) (P-2) blend membranes were prepared by the method of wet phase inversion following the procedure given in the literature (Kumar et al. 2014). 1.8 g of polysulfone was taken with 8 mL of NMP in a 20 mL beaker and kept under stirring for over 3h at 60°C until the polysulfone completely dissolved after which 0.2 g of PEG-1000 was added to the previous mixture and agitation was continued till a clear solution was obtained.

Accurately weighed 0.36 g of chitosan derivative (CTSL-2) was taken in another 20 mL beaker with 3.0 mL of formic acid and kept under stirring for 45 min at 60°C until a clear solution was obtained. The solution was poured into the first beaker and the contents were kept under gentle stirring for over 24h till a clear solution was obtained. The homogeneous solution was maintained at 50°C for a further period of 2h without stirring to remove the air bubbles entrapped in the solution. This solution was then cast over a glass plate and then dipped into a coagulation bath of distilled water (27°C) acting as the non-solvent when the membrane gets formed by phase inversion.

To ensure complete phase inversion, the membrane was kept immersed under water for 24h after which it was taken out and rinsed several times with distilled water and finally dried at 30°C. In a similar manner, following the same procedure, the membrane with the ratio of PSf: CTSL-2 (99:1) (P-1) was also prepared. The prepared membranes had an average thickness of 143  $\mu\text{m}$ . The chemical structures of polysulfone and CTSL-2 are shown in Figure 3.16.

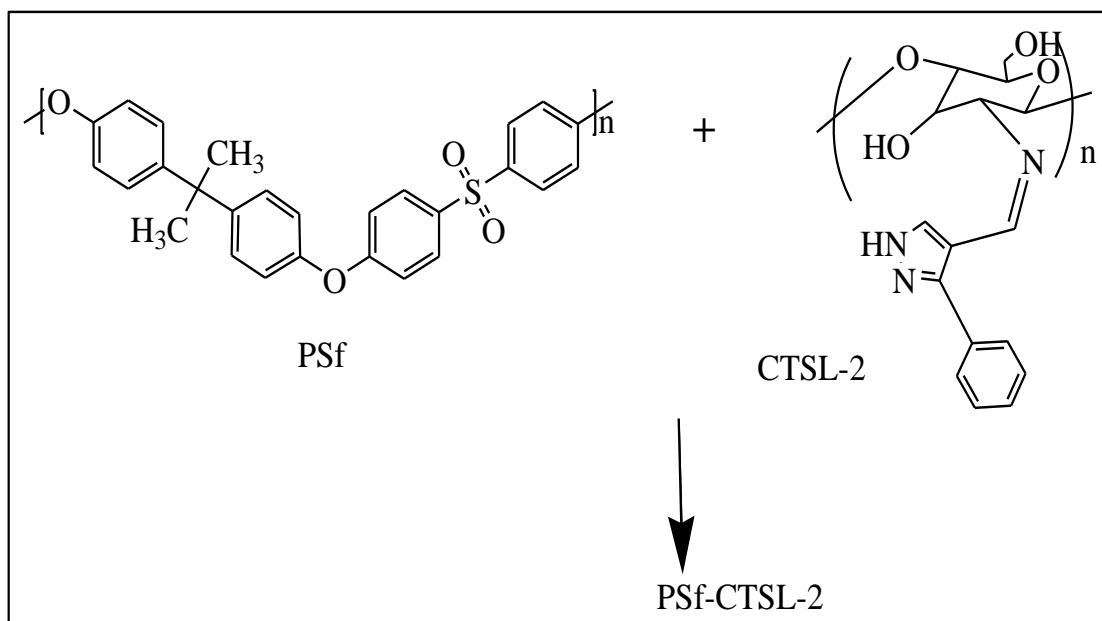


**Figure 3.16 Chemical structure of polysulfone and CTSL-2**

### 3.4.3 Membrane characterization

#### 3.4.3.1 Scanning Electron Microscopy (SEM) studies

To record the cross-sectional image of the membrane, the sample was prepared by first immersing in liquid nitrogen, followed by fracturing and then sputtering with gold dust. Jeol JED 2300 Analysis Station scanning electron microscope was used to record the membrane morphology.

#### 3.4.3.2 Contact angle measurement

The surface contact angle was measured by FTA-200 Dynamic contact angle analyzer based on the sessile droplet method.

#### 3.4.3.3 Powder XRD analysis

The membrane samples were characterized by Bruker D8 Advance X-ray powder diffractometer employing Cu K-radiation (operating specifications: 40 keV, 40 mA) in a scanning range of  $2\theta = 5-80^\circ$ .

### 3.4.4 Membrane experiments

#### 3.4.4.1 Pure water flux study

A self-fabricated dead-end filtration kit was used for measuring the pure water flux (PWF) (Figure 3.17). The membrane sample used in permeation experiments was in the form of a circular disc with an effective diameter of 5 cm. The pure water flux  $J_w$  ( $L m^{-2} h^{-1}$ ), was calculated using the Eq. 3.3 (Dejardin 2006).

$$J_w = \frac{Q}{A \Delta t} \quad (3.3)$$

where ' $Q$ ' is the volume of water collected (L), ' $A$ ' is the effective membrane area available for permeation ( $m^2$ ) and ' $\Delta t$ ' is the time duration of permeation (h).

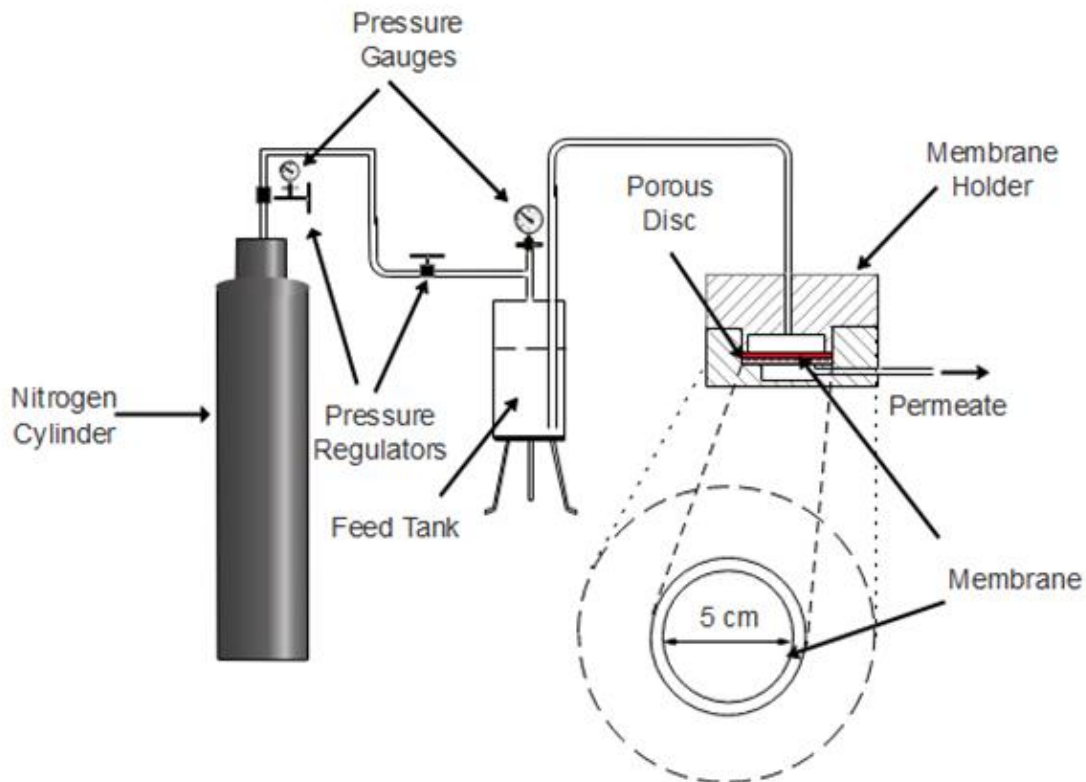


Figure 3.17 Schematic view of the filtration cell.

#### 3.4.4.2 Membrane hydraulic resistance

Flux through an ultrafiltration membrane is related to the trans membrane pressure (TMP) by the Darcy's Law (Li et al. 2017).

$$J_w = \frac{\Delta P}{\mu R_m} \quad (3.4)$$

$J_w$  is the flux;  $\Delta P$ , the TMP in MPa;  $\mu$  is the viscosity in Pa.sec and  $R_m$  is the hydraulic resistance.

At a given temperature viscosity may be considered to be constant and taking the product of  $\mu$  and  $R_m$  as ' $R_h$ ', which is the resistance offered by the membrane to the flow of feed, Eq. 3.4 may be re-written as follows: (Li et al. 2011; Waheed 2014).

$$R_h = \frac{\Delta P}{J_w} \quad (3.5)$$

where ' $\Delta P$ ' is the TMP in MPa and ' $J_w$ ' is the pure water flux ( $L m^{-2} h^{-1}$ ) and ' $R_h$ ', the hydraulic resistance ( $MPa. L^{-1} m^2 h$ ).

#### 3.4.4.3 Anti-fouling studies

The anti-fouling property of the membrane was studied by using Bovine Serum Albumin (BSA) solution having a concentration of 0.8% by wt. Initially, the PWF ' $J_{w1}$ ' ( $L m^{-2} h^{-1}$ ) of the membrane was determined at a TMP of 0.8 MPa with pure water for 60 min. This was followed by the permeation study to find the flux ' $J_p$ ', ( $L m^{-2} h^{-1}$ ) using 0.8% BSA solution for 60 min at the same pressure. The membrane was then flushed with distilled water for 15 min to remove the lightly adhering molecules of protein. Subsequently, the flux through the cleaned membrane was measured for 60 min at 0.8 MPa and recorded as ' $J_{w2}$ ', ( $L m^{-2} h^{-1}$ ). The anti-fouling nature of the membrane was assessed by calculating the flux recovery ratio (FRR) using Eq.3.6 (Dejardin 2006).

$$FRR (\%) = \frac{J_{w2}}{J_{w1}} \times 100 \quad (3.6)$$

To further analyze the fouling behavior, three more equations Eq.3.7, Eq.3.8, Eq.3.9 were used to determine the three dimensionless recovery ratios  $R_t$ ,  $R_r$  and  $R_{ir}$  (Dejardin 2006; Vatanpour et al. 2011).

$$R_t(\%) = \frac{(J_{w1} - J_p)}{J_{w1}} \times 100 \quad (3.7)$$

' $R_t$ ' is a measure of total loss of flux due to membrane fouling.

$J_{w1}$  ( $Lm^{-2} h^{-1}$ ) is the initial flux;  $J_p$  ( $Lm^{-2} h^{-1}$ ) is the flux after fouling of the membrane;  $J_{w2}$  ( $Lm^{-2}h^{-1}$ ) is the flux after washing of the membrane. An illustrative representation of these three fluxes is shown in Figure 3.18.

$$R_r(\%) = \frac{(J_{w2} - J_p)}{J_{w1}} \times 100 \quad (3.8)$$

' $R_r$ ' provides a measure of flux recovery as a percentage initial flux.

$$R_{ir}(\%) = \frac{(J_{w1} - J_{w2})}{J_{w1}} \times 100 \quad (3.9)$$

' $R_{ir}$ ' gives the permanent loss of flux due to fouling, as a percentage of initial flux.

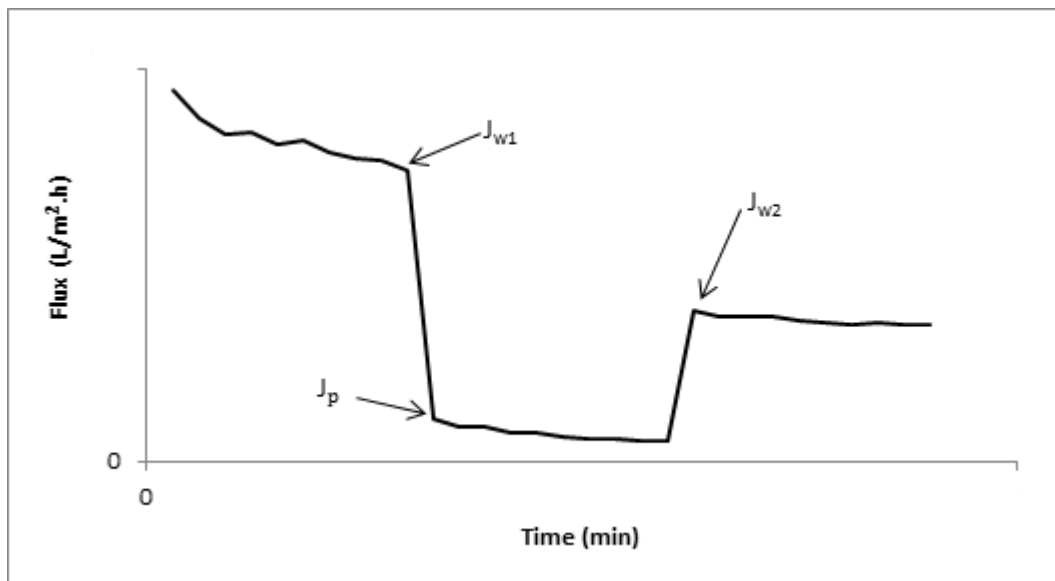


**Figure 3.18 Illustration of flux before fouling ( $J_{w1}$ ), after fouling ( $J_p$ ) and after the post-fouling wash ( $J_{w2}$ )**



# **CHAPTER 4**

## **RESULTS AND DISCUSSION**



# **PART A**

## **Adsorption Studies**



*In Part A, the results of the adsorption studies for all the four chitosan derivatives (CTSL-1, CTSL-2, CTSL-3 and CTSL-4) are presented in a serial manner, one after another. For every derivative, firstly, the analysis of the respective ligand by <sup>1</sup>H NMR is presented followed by the characterization of each derivative by various instrumental analyses such as <sup>13</sup>C NMR, FTIR, DSC and XRD. The results of the adsorption studies viz. pH study; equilibrium study, kinetic study and thermodynamic study are presented next. Post-adsorption analyses by FTIR and XRD are presented and possible mechanisms for metal sequestration have been proffered. A brief summary of all the adsorption studies carried out is then presented. This is followed by the results of the swelling studies.*

#### **4.1 STUDIES USING CHITOSAN DERIVATIVE CTSL-1**

##### **4.1.1 Characterization of ligand L-1**

The proton NMR spectrum of the ligand (L-1) exhibited the following chemical shifts (Figure 4.1). <sup>1</sup>H NMR (DMSO-d<sub>6</sub>) δ (ppm): 13.651 (1 H, Pyrazole NH), 9.873 (1 H, Aldehyde), 7.080-7.787 (4 H, Ar. Ring), 8.290 (1 H, Pyrazole 5H), 3.825 (3 H, Methoxy). The chemical shift for NH observed at 13.65 ppm was broad with low intensity which may be attributed to the rapid exchange of the NH proton with the solvent DMSO-d<sub>6</sub> or water present (Anderson et al. 2004). The chemical shifts obtained validate the successful synthesis of the ligand L-1.

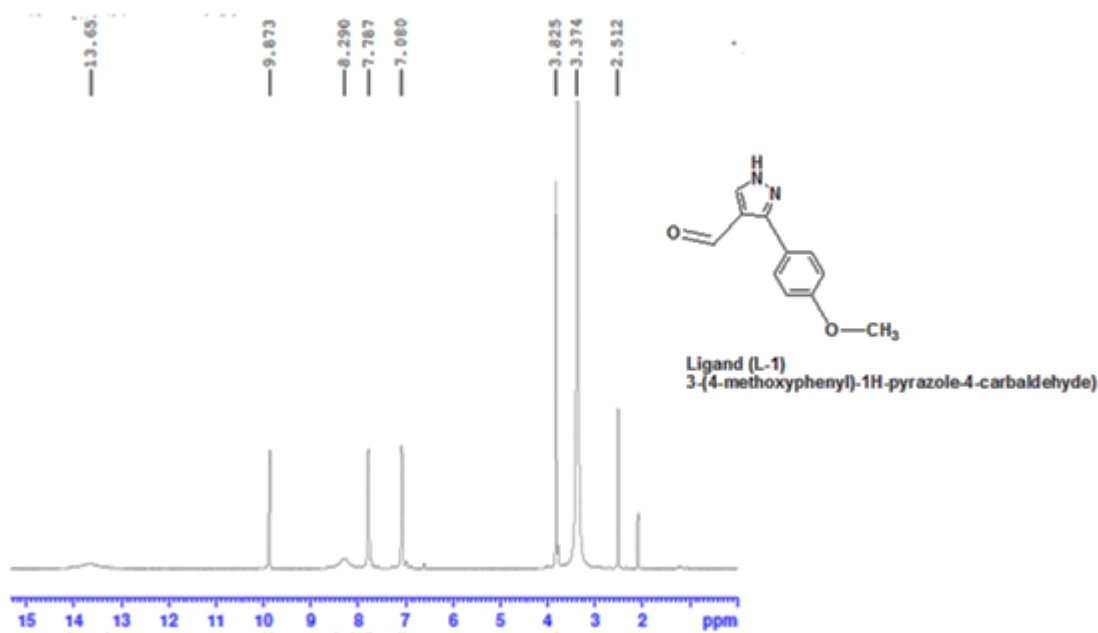


**Figure 4.1** <sup>1</sup>H NMR spectrum of the ligand (L-1)

#### 4.1.2 Characterization of the chitosan derivative CTSL-1

##### 4.1.2.1 Solid state <sup>13</sup>C NMR analysis of CTSL-1

The solid state <sup>13</sup>C NMR spectrum for neat chitosan is shown in Figure 4.2 a, where the chemical shifts along with the carbon atoms corresponding to these peaks are labelled (Chen et al. 2008a). The spectrum for CTSL-1 shown in Figure 4.2 b displays a peak at 161.357 ppm which is assigned to imine (>C=N) formed during the Schiff reaction (Xiao and Zhou 2008). The aromatic rings were represented by signals between 116.493 ppm and 131.362 ppm. The peaks obtained are in agreement with those reported in literature. The appearance of new peaks in the aromatic region and the changes in peak intensity for CTSL-1 when compared to chitosan confirm the successful grafting of the ligand on chitosan (Bekircan and Bektas 2008; Krishnapriya and Kandaswamy 2009).

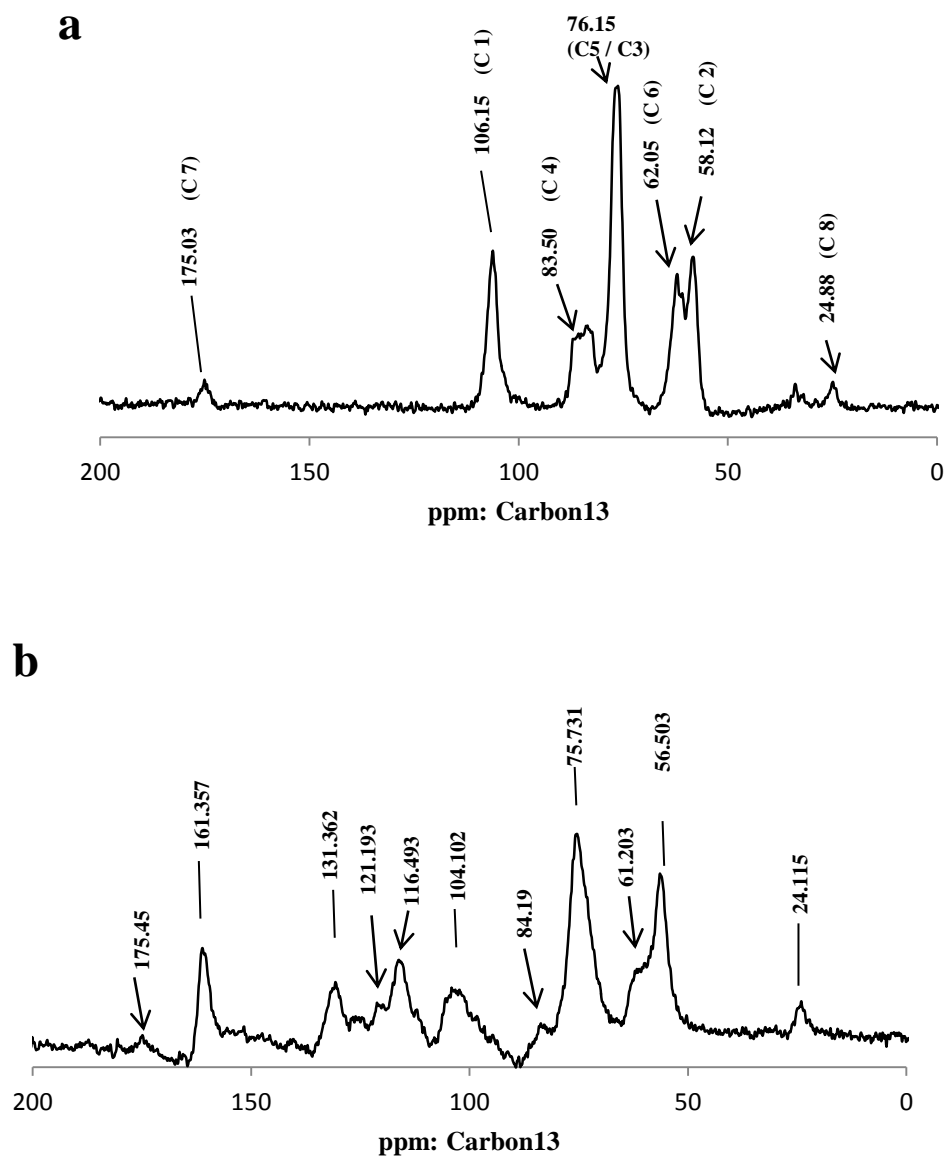


**Figure 4.2 Solid state  $^{13}\text{C}$  NMR spectra of a) Chitosan and b) CTSL-1**

#### **4.1.2.2 FTIR analysis of CTSL-1**

The FTIR spectra for pure chitosan and CTSL-1 are shown in Figure 4.3 a and b respectively.

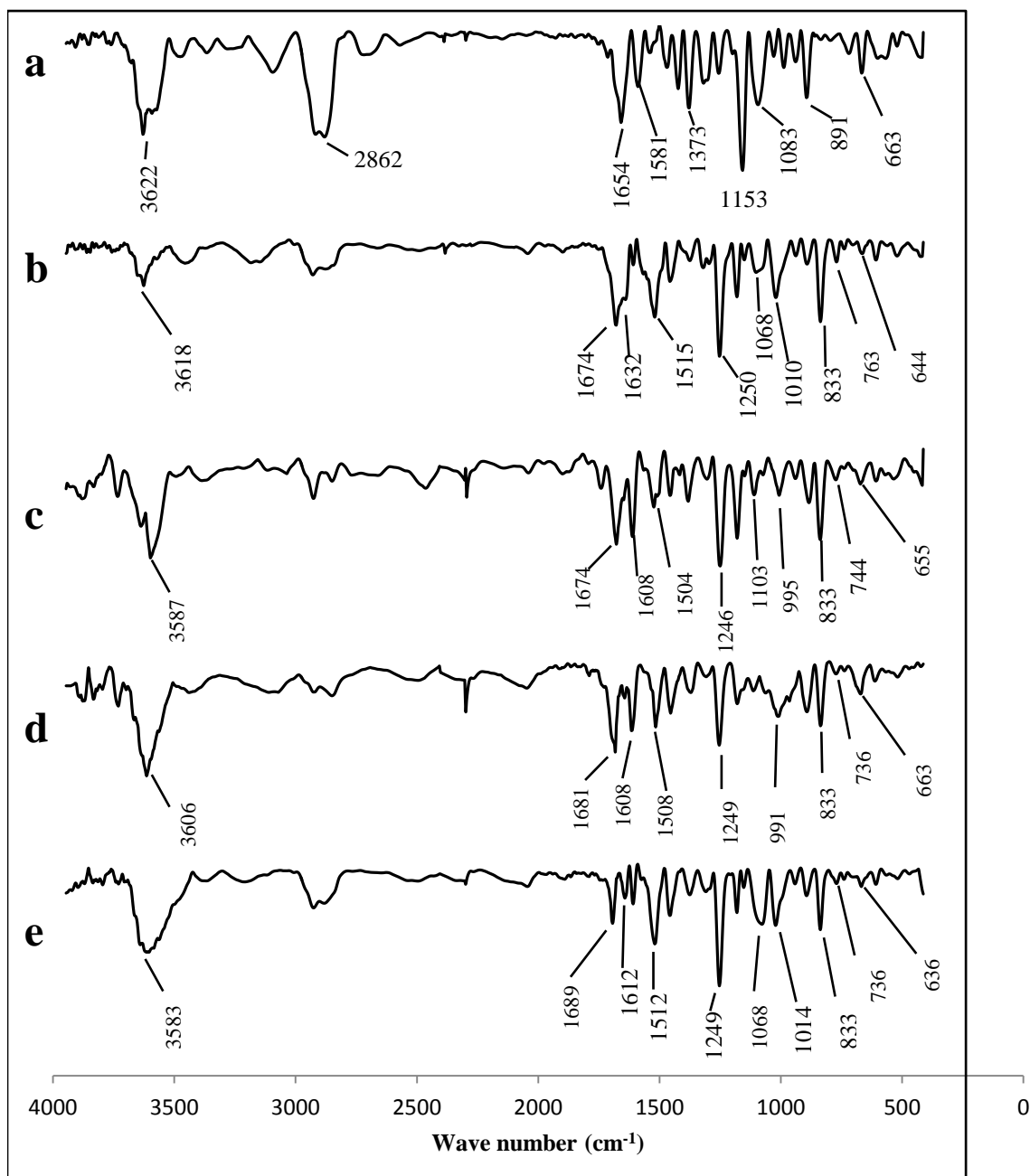


**Figure 4.3 FTIR spectra of a) Chitosan b) CTSL-1 c) CTSL-1-Pb d) CTSL-1-Cu e) CTSL-1-Cr**

The major bands for pure chitosan were assigned as follows:  $3400\text{cm}^{-1}$  to  $3630\text{cm}^{-1}$  (br, O-H and  $\text{NH}_2$  stretching vibrations);  $2862\text{cm}^{-1}$  (-CH) stretching vibration in (-CH) and (- $\text{CH}_2$ );  $1654\text{cm}^{-1}$  ( $>\text{C}=\text{O}$ ) stretching vibration of remaining acetyl units of CTS-NHAc;  $1581\text{cm}^{-1}$  amide II band of CTS-NHAc;  $1373\text{cm}^{-1}$  (-CH) symmetric bending vibration in (-CHOH-),  $1153\text{cm}^{-1}$  stretching vibration in (C-O-C bridge),



1080  $\text{cm}^{-1}$  (s, -C-O) stretching vibration in (-COH), 891  $\text{cm}^{-1}$  (C-H) out of plane bending, 663  $\text{cm}^{-1}$  (N-H) secondary wagging vibrations (Li and Bai 2005; Kamari et al. 2011).

The FTIR pattern for CTSL-1 has a broad band at 3548-3687  $\text{cm}^{-1}$  attributed to the (-OH) stretch. The presence of a band around 1674  $\text{cm}^{-1}$  is due to ( $>\text{C}=\text{O}$ ) stretch of acetyl units of CTS-NHAc. The splitting of the band at 1632  $\text{cm}^{-1}$  is attributed to the imine ( $>\text{C}=\text{N}-$ ) stretch. Our results are in agreement with Santos et al. (2005), who have reported FTIR peak values of imine groups in the range of 1631.5-1640.2  $\text{cm}^{-1}$ . The band between 1469  $\text{cm}^{-1}$  and 1593  $\text{cm}^{-1}$  is due to ( $>\text{C}=\text{C}<$ ) stretch. It may be observed that this band is absent in the FTIR spectrum of pure chitosan, which is as expected as chitosan lacks any aromatic or heterocyclic groups. The band at 1199-1272  $\text{cm}^{-1}$  is due to alkyl-aryl (C-O) stretch. The vibrations at 1010  $\text{cm}^{-1}$  is assigned to stretching vibrations of primary alcohol of C-6 (C-OH). The band at 794-856  $\text{cm}^{-1}$  is due to aromatic (-CH) out of plane bending (Borsagli et al. 2015).

The analysis of post-adsorption FTIR spectrum of CTSL-1 is presented under section 4.1.3.5.

#### **4.1.2.3 Scanning electron microscope analysis of CTSL-1**

The scanning electron micrographs of the pure chitosan and CTSL-1 surface are presented in Figure 4.4 The morphology exhibits the decreased surface flakiness in CTSL-1 as compared to CTS. The sturdy and bulky appearance of CTSL-1 particles as compared to flaky and flat particles of CTS is also discernible from the micrograph. The increase in bulk density of CTSL-1 by 2.8 times as compared to CTS (bulk density of 691.02 and 247.13  $\text{kg/m}^3$ , for CTSL-1 and CTS respectively, under section 4.6) is consistent with this observed compactness of CTSL-1.

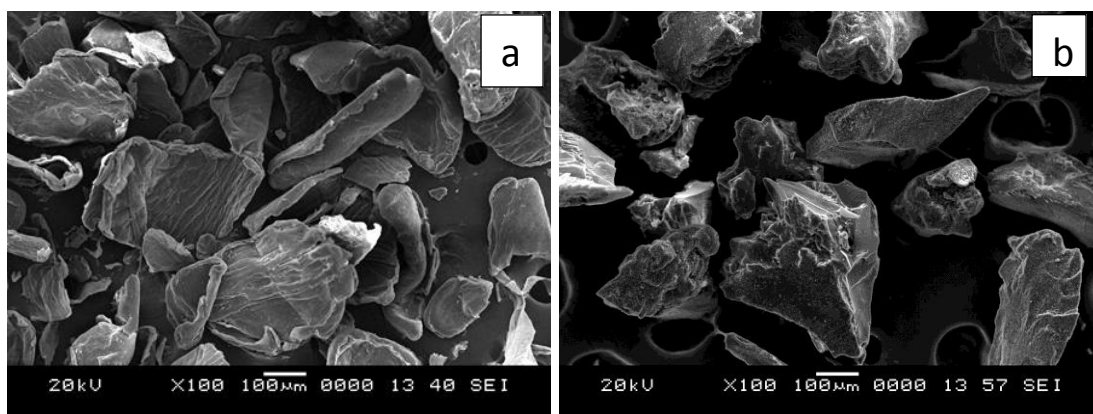


**Figure 4.4 Scanning electron micrographs of a) CTS b) CTSL-1**

#### 4.1.2.4 XRD analysis of CTSL-1

The XRD pattern of CTS (Figure 4.5 a) shows the characteristic peaks around  $2\theta=10^\circ$ ,  $2\theta=19^\circ$  and  $2\theta=21^\circ$  (Li and Bai 2005). The disappearance of the peak at  $2\theta=10^\circ$  in the spectrum for CTSL-1 (Figure 4.5 b) attributed to (-NH<sub>2</sub>) group is further evidence for the Schiff base reaction at the (-NH<sub>2</sub>) group (Webster et al. 2007). The decrease in the intensity and broadening of the spectrum in the section around  $2\theta=20^\circ$  for CTSL indicates the decrease in crystallinity and increased amorphous nature of CTSL-1 as compared to pure CTS (Krishnapriya and Kandaswamy 2010).

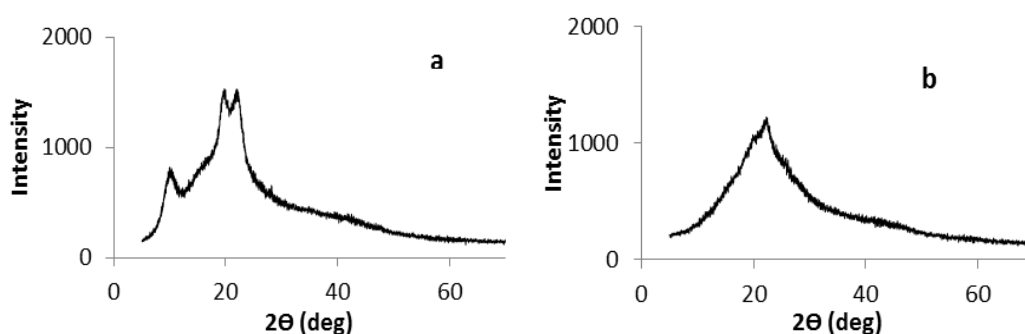
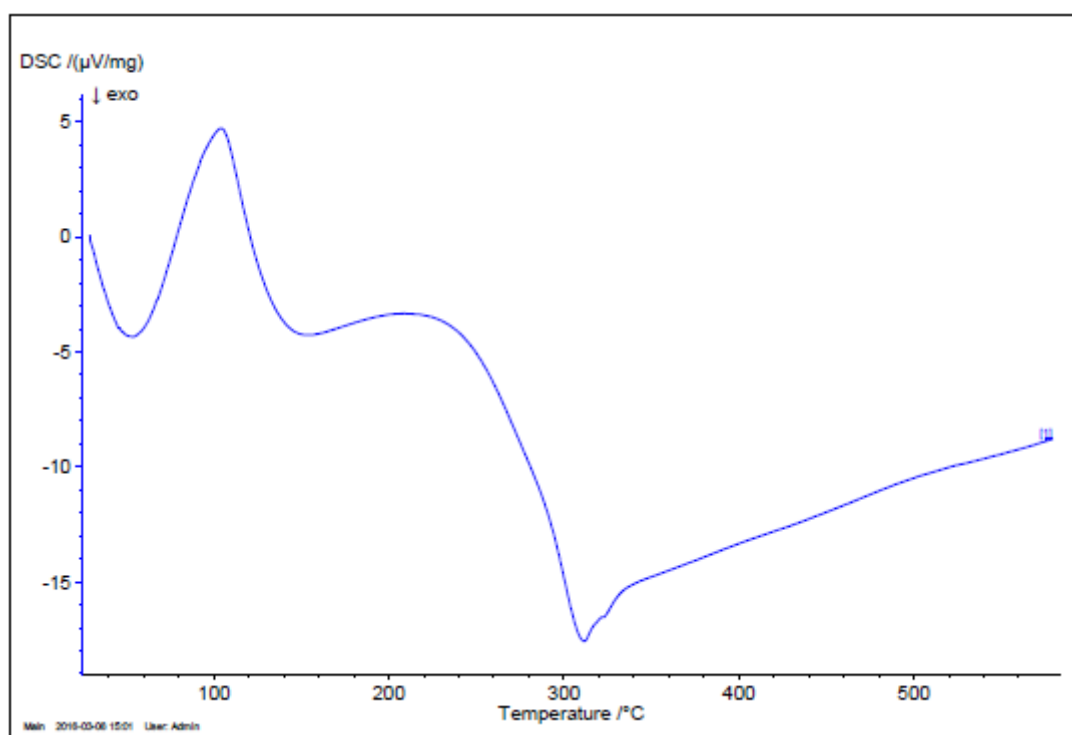


**Figure 4.5 a) XRD spectrum of chitosan b) XRD spectrum of CTSL-1**

#### 4.1.2.5 DSC analysis of CTS and CTSL-1

The DSC thermograms of CTS and CTSL-1 were used to study the thermal properties of chitosan and CTSL-1. The thermogram for chitosan shows a sharp exothermic peak  $\sim 70^\circ\text{C}$  and a mild peak  $\sim 165^\circ\text{C}$  (Figure 4.6 a). The former peak is attributed to the removal of loosely bound free moisture and the latter to the removal

of tightly bound moisture. In comparison, the thermogram of CTSL-1 (Figure 4.6 b) shows three exothermic peaks at 60, 230 and 260°C. The first peak is attributed to the moisture removal, the second one is probably due to the degradation of the grafted ligand and the last one due to the degradation of the polymer. The DSC thermogram shows that CTSL-1 is thermally stable upto a temperature of ~200°C which is slightly lower than that of chitosan. This difference between the two could be due to the grafting of the ligand L-1 on to the chitosan which might have caused a breakage of hydrogen bonds in the crystalline regions thereby marginally decreasing the thermal stability of CTSL-2 (Krishnapriya and Kandaswamy 2010; Jing et al. 2016).



**a)**

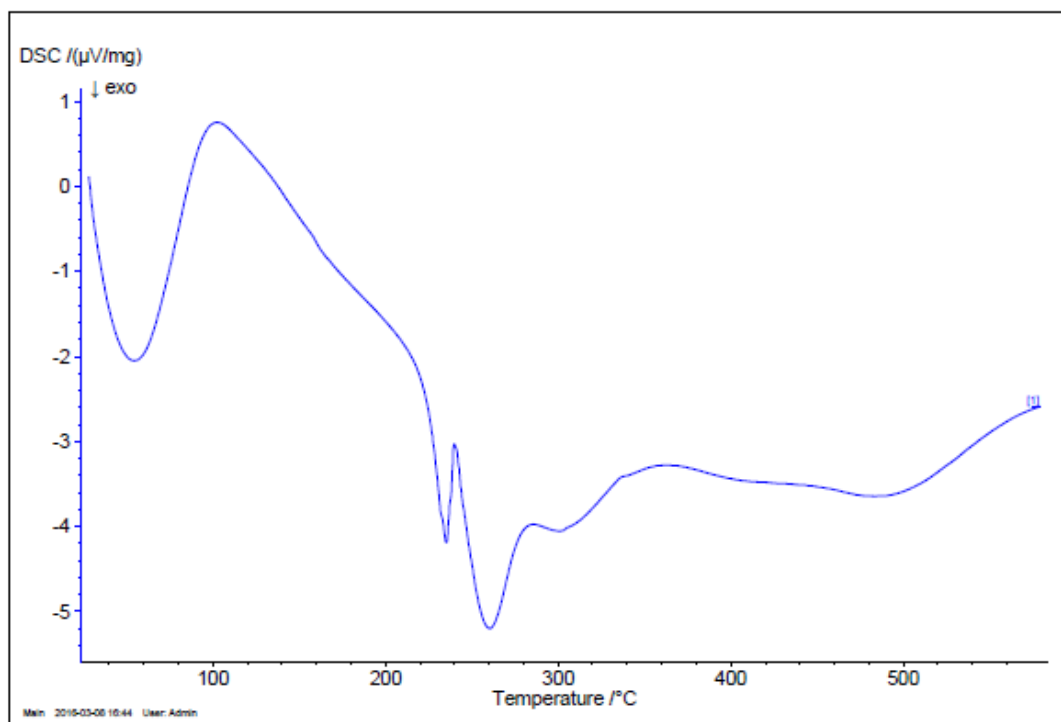


**Figure 4.6 DSC thermograms of a) Chitosan and b) CTSL-1**

### **4.1.3 Adsorption Studies with CTSL-1**

#### **4.1.3.1 Effect of pH**

The pH of metal ion solution is an important factor to be considered in the process of adsorption. The effect of pH on sorption of the metal ions on CTSL-1 in the pH range of 3-7 is shown in Figure 4.7. At very low pH values (<3), there was evidence of fragmentation of the adsorbent. At higher values of pH much above 7, there was indication of precipitation of the metals as hydroxides, as observed by cloudiness of solution. This is consistent with literature reports (Nghah and Isa 1998; Gunay et al. 2007).

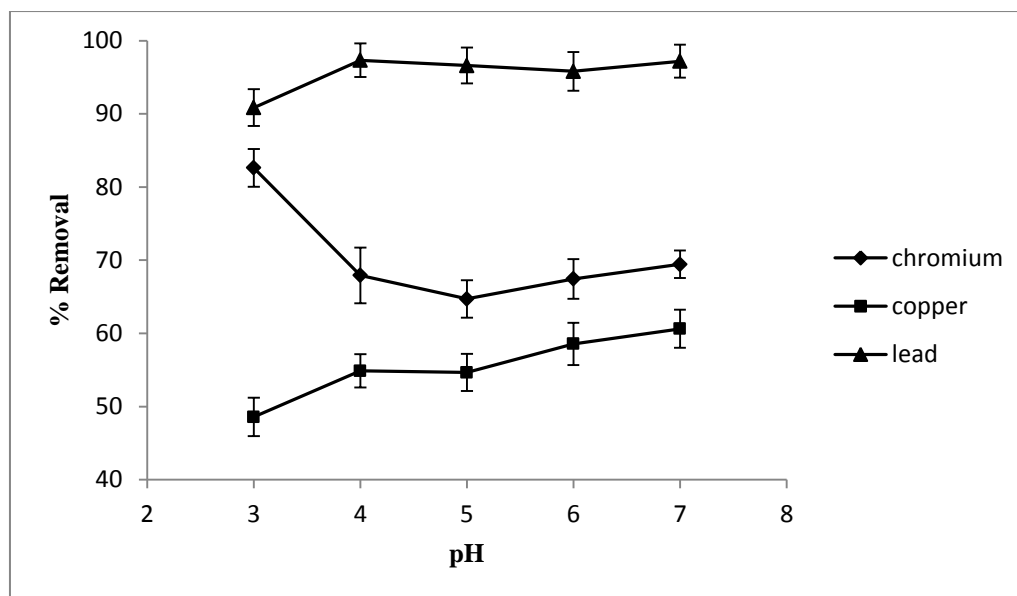


**Figure 4.7 Effect of pH on % removal (Initial concentration=100 mg/L; Temperature=303K; Ads. Dose= 4g/L; Agitation speed=150 rpm; Contact time=24h)**

The adsorption uptake of Cr (VI) onto CTSL-1 was found to be the maximum at a pH of 3. According to Qin et al. (2003), in aqueous phase, the various anionic forms of Cr (VI) present themselves as  $\text{Cr}_2\text{O}_7^{2-}$ ,  $\text{HCrO}_4^-$ ,  $\text{CrO}_4^{2-}$  and  $\text{HCr}_2\text{O}_7^-$  depending upon the ionic concentration and pH in the solution. At low concentrations within the pH range of 2–4, the main fraction is  $\text{HCrO}_4^-$ , while the concentration of  $\text{CrO}_4^{2-}$  moiety rises with increase in pH value, turning out to be the predominant form at a pH > 7.0. Anions of  $\text{Cr}_2\text{O}_7^{2-}$  and  $\text{HCr}_2\text{O}_7^-$  are present only at higher concentration (> 1 g/L) of Cr (VI). In the present study at pH=3 and Cr (VI) < 1 g/L, the predominant form is  $\text{HCrO}_4^-$  (Mohan and Pittman 2006). The anions present in solution can interact with protonated amine functional groups. At low pH, electrostatic interactions between the protonated sites of the sorbent and  $\text{HCrO}_4^-$  ions support high chromium removals. At higher pH values, however, the  $\text{OH}^-$  ion competes with the oxyanions of Cr (VI) ( $\text{HCrO}_4^-$  and  $\text{CrO}_4^{2-}$ ) for the protonated sites and hence the adsorption capacity decreases (Zhang et al. 2016).

For the adsorption of Pb (II) and Cu (II), the optimal pH values were observed to be 4 and 7 respectively. At pH < 4, protonation occurs at the nitrogen atoms of CTSL-1 which results in positive charges on the surface of the adsorbent causing

electrostatic repulsion with the positively charged Cu (II) and Pb (II) ions. However, for  $\text{pH} > 4$ , the adsorption sites get deprotonated, when metal binding can occur by chelation, leading to increase in adsorption efficiency (Bhatnagar and Sillanpää 2009). Based on the results of the pH study, the optimum values of pH to be used for the equilibrium, kinetic and thermodynamic studies were fixed as 3 for Cr (VI), 7 for Cu (II) and 4 for Pb (II).

#### **4.1.3.2 Adsorption equilibrium**

The experiments in adsorption equilibrium were conducted following the method outlined in section 3.3.4 under Chapter 3; the quantity of metal ion removal was determined using the Eq. 3.1; the mathematical expressions of the adsorption isotherms used are given under section 2.6.1.

In order to establish the applicable adsorption equilibrium isotherm, three models viz. Langmuir, Freundlich, and Redlich-Peterson were employed. Langmuir and Freundlich isotherms represent monolayer and multilayer adsorptions respectively. The Langmuir and Freundlich isotherms have two parameters in the model compared with Redlich-Peterson isotherm which has three parameters. The Redlich Peterson isotherm was used because its application to certain systems has been very successful because of its dual features representing both Langmuir and Freundlich isotherms. This applies particularly to adsorbents that are heterogeneous. Chitosan-metal ion systems have been analysed using the Redlich-Peterson and the results have been good. The systems include single-component copper and lead, and they give results that are better than the results obtained from the Langmuir analysis of the same data (Gerente 2007).

Non-linear analysis with minimization of sum of squared errors method was employed with MICROSOFT EXCEL Solver add-in for fitting the Langmuir, Freundlich and Redlich-Peterson isotherm models. The results are tabulated in Table 4.1. The corresponding plots are as per Figures 4.8, 4.9 and 4.10. For the removal of Cu (II), Langmuir and Redlich-Peterson isotherm models gave better results ( $r^2=0.962$  and  $0.963$  respectively), whereas for the removal of Pb (II), the Freundlich and Redlich-Peterson isotherm models were better ( $r^2=0.927$  and  $0.929$  respectively). For

the removal of Cr (VI), the Langmuir and the Redlich-Peterson isotherms ( $r^2 = 0.971$ ) both provided a satisfactory fit to the data. The maximum monolayer adsorption capacities ( $Q_0$ ) were 52.1 mg/g for Cr (VI), 40.62 mg/g for Cu (II) and 71.99 mg/g for Pb (II). The Langmuir separation factor  $R_L$  which was within 0-1 and the Freundlich exponent 'n' which was between 1 and 10 indicated that the adsorption was favourable (Nethaji et al. 2010). Details regarding the factors ' $R_L$ ' and 'n' are described under section 2.6.1. It has been reported that values of ' $b_R$ ' between 0 and 1 in the Redlich-Peterson model (described under section 2.6.1) indicate a favourable adsorption, and higher values may indicate a milder sorptive interaction between adsorbent and adsorbate (Boddu et al. 2008). The values obtained in this study for  $b_R$  (~1.0 for Cr (VI), 0.984 for Cu (II), and 0.670 for Pb (II) ) point towards adsorption being favourable.

**Table 4.1 Equilibrium model parameters of adsorption of Cu (II), Pb (II) and Cr (VI) on CTSL-1**

<b>Isotherm</b>	<b>Cu (II)</b>	<b>Pb (II)</b>	<b>Cr (VI)</b>
<b>Langmuir Isotherm</b>			
$Q_0$ (mg g <sup>-1</sup> )	40.62	71.99	52.10
b (L mg <sup>-1</sup> )	0.0161	0.011	0.171
$r^2$	0.962	0.891	0.9708
$R_L$	0.71-0.0584	0.784-0.0833	0.1895-0.00581
<b>Freundlich Isotherm</b>			
$K_f$ (mg g <sup>-1</sup> )	4.874	5.672	18.942
n	3.132	2.628	6.081
$r^2$	0.896	0.927	0.7824
<b>Redlich-Peterson Isotherm</b>			
$K_R$ (L g <sup>-1</sup> )	0.678	4.918	8.55
$a_R$ (L mg <sup>-1</sup> )	0.018	0.619	0.155
$b_R$	0.984	0.670	1.009
$r^2$	0.963	0.929	0.9709

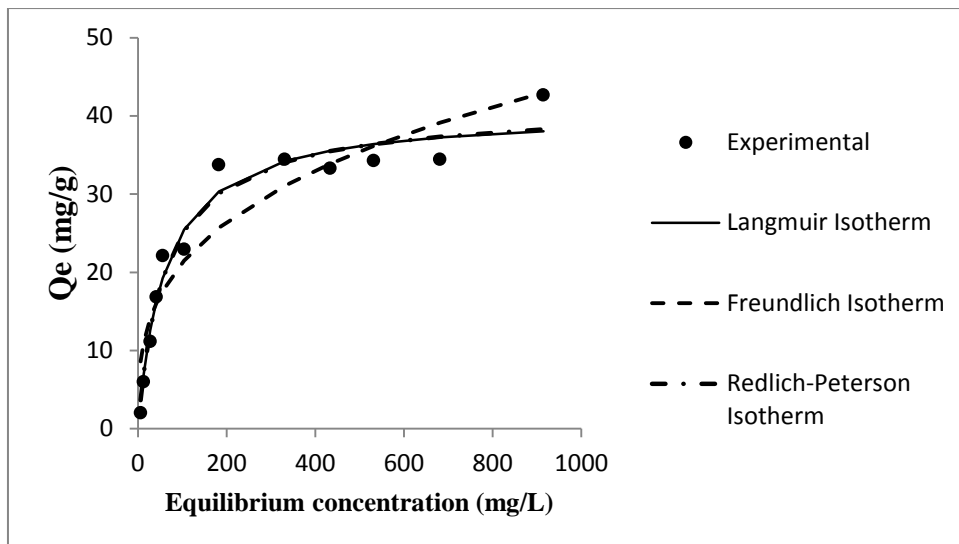


**Figure 4.8** Plot of various adsorption isotherms to CTSL-1-Cu (II) adsorption data (Initial conc. =100 mg/L; T=303 K; pH 7; Ads. Dose=2g/L; Stirring speed =150 rpm; t =24 h)

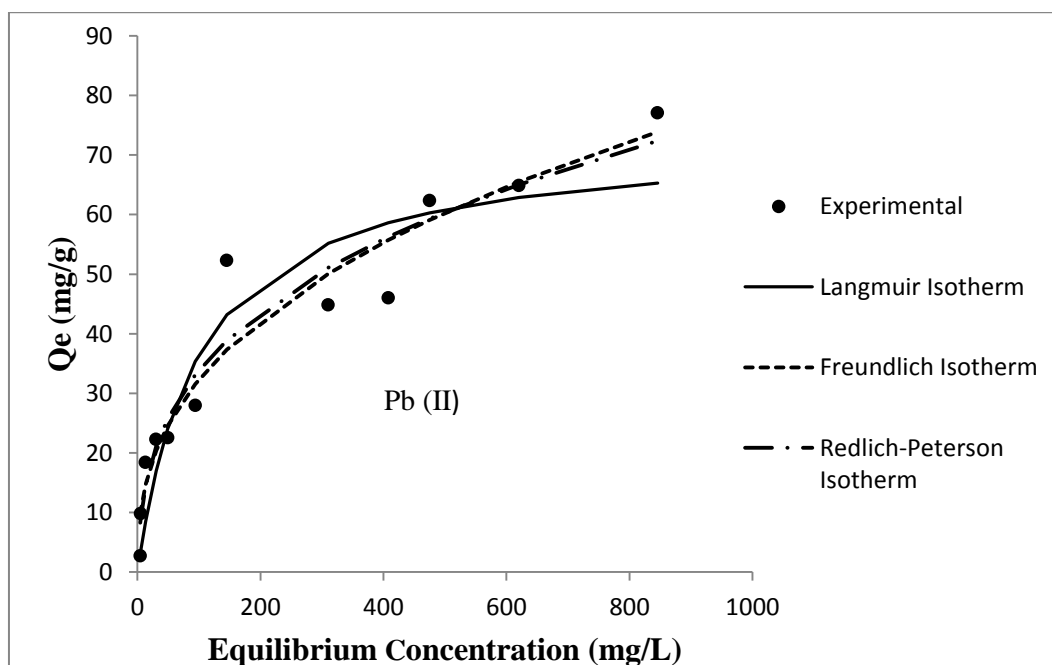


**Figure 4.9** Plot of various adsorption isotherms to CTSL-1-Pb (II) adsorption data (Initial conc. =100 mg/L; T =303 K; pH 4; Ads. Dose=2 g/L; Stirring speed=150 rpm, t=24 h)



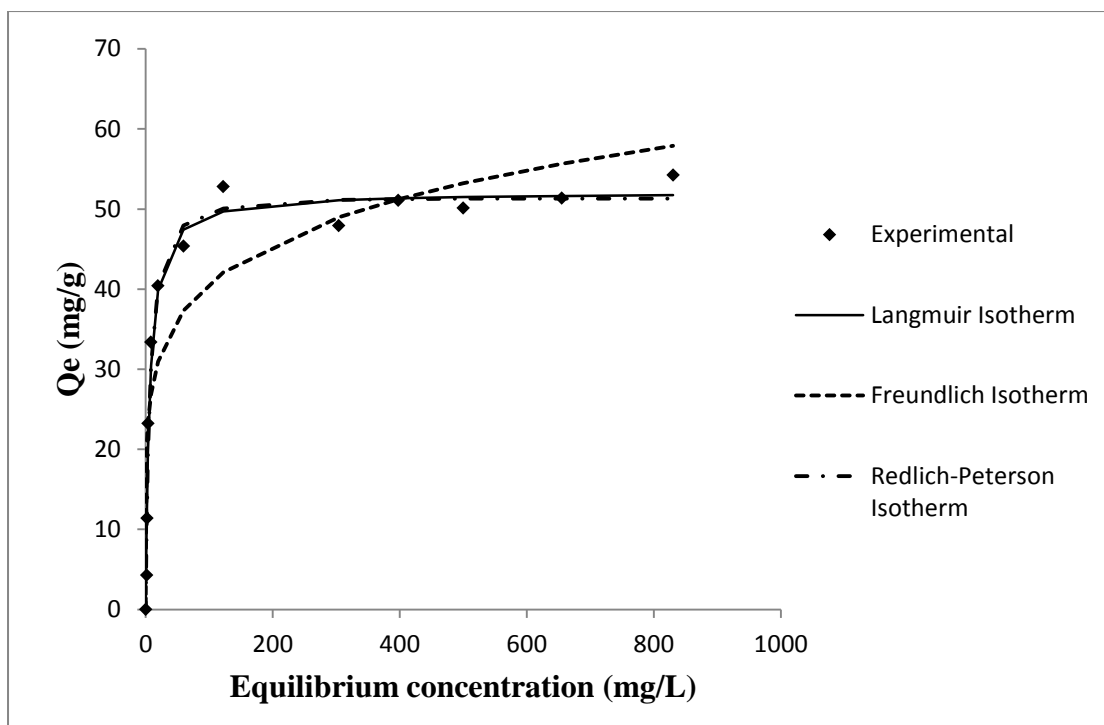


**Figure 4.10 Fit of various isotherms to CTSL-1-Cr (VI) adsorption data (Initial conc.=100 mg/L; T=303 K; pH 3; Ads. Dose=2g/L; Agitation speed=150 rpm; Contact time=24 h)**

The photographic images of the CTSL-1 before adsorption and CTSL-1-metal complexes after adsorption are shown in Figure 4.11. The colours exhibited by the metal complexes respectively are, CTSL-1(sand-brown), CTSL-1-Pb (light brown), CTSL-1-Cu (greenish) and CTSL-1-Cr (rust colour). Mende et al. (2016) studied the surface of chitosan before and after the metal adsorption process by SEM and SEM-EDX. By these analyses they found crystal-like structures of copper sulfate and iron sulfate on the surface which were the salts they had used to make the metal solutions. It was also shown by these researchers that both metal cations and anions were adsorbed on the adsorbent surface, and they together formed crystals of the salt used to make the metal solution.

The colors of salts used in the present study for making the metal solutions were white ( $\text{PbNO}_3$ ), blue ( $\text{CuSO}_4 \cdot 5\text{H}_2\text{O}$ ) and orange ( $\text{K}_2\text{Cr}_2\text{O}_7$ ). When the metal ions are adsorbed on the CTSL-1, the final color obtained was a combination color obtained by mixing sand-brown color of the CTSL-1 with the color of the metal salt, consistent with the principle of color mixing. Hence the observed colors were light

brown for CTSL-1-Pb (sand brown+white), greenish for CTSL-1-Cu (sand brown+blue), and rust-color for CTSL-1-Cr (sand brown+orange). During subsequent equilibrium studies with CTSL-2, CTSL-3 and CTSL-4, the corresponding metal complexes obtained with the three metals (Pb, Cu and Cr) also displayed similar colors as their corresponding metal complexes with CTSL-1 as explained above.

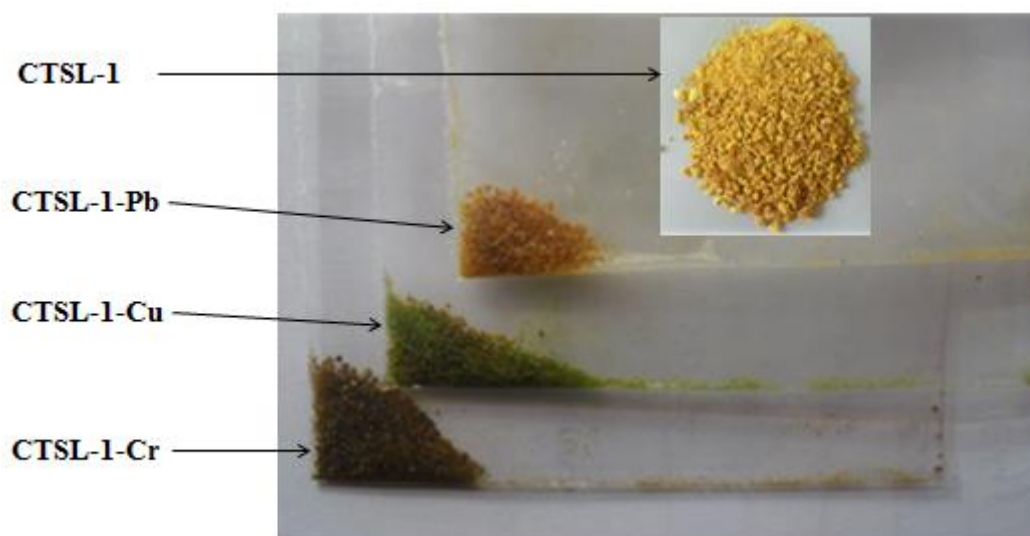


**Figure 4.11 Photographic images of CTSL-1 (before adsorption) and CTSL-1-Metal complexes (after adsorption)**

#### 4.1.3.3 Adsorption kinetics

The adsorption kinetic study was conducted by following the procedure explained in section 3.3.5; Eq. 3.2 was used to determine the instantaneous, non-equilibrium adsorption capacity ( $Q_t$ ); the mathematical expressions of the kinetic models employed to fit the experimental data are given in section 2.6.2 under Chapter 2.

In order to determine the adsorption kinetics of the metal sequestration process, three models were investigated viz. pseudo first order, pseudo second order and intraparticle diffusion models. Among the three models, the pseudo second order model was found to best represent the adsorption kinetics for the metal ions Cr (VI), Cu (II) and Pb (II) (Figure 4.12, Figure 4.13 and Figure 4.14). Very high values of regression coefficient are obtained for pseudo second order model (0.9999 for Cr (VI),

0.9901 for Cu (II) and 0.9941 for Pb (II)) indicates that chemisorption may be the rate controlling step for the metal removal (Ho and Mckay 1999).

For all the three metals, the predicted value of the maximum adsorption capacity  $Q_{e, \text{calc}}$  obtained from the pseudo-second order model was very close to  $Q_{e, \text{expt}}$ , the experimental value (Table 4.2). Nghah and Fatinathan (2010) have reported that the pseudo-second order model is more likely to predict the behavior over the full contact range of time. Our data was also consistent with their report, and we observed that the pseudo-second order model was applicable over the entire range of contact for all the three metals studied. The pseudo-second order rate constant ( $k_2$ ) obtained for Cr (VI), Cu (II) and Pb (II) were  $8.3 \times 10^{-3}$ ,  $0.34 \times 10^{-3}$  and  $1.4 \times 10^{-3} \text{ g mg}^{-1} \text{ min}^{-1}$  respectively. In the case of pseudo-first order model, a large difference between the predicted and experimental values of the maximum capacity was observed indicating that this model was unsuitable for predicting the kinetic data. The intraparticle diffusion model did not show satisfactory linear correlation to the experimental data for all metals indicating that the adsorption process was controlled by multiple resistances (Cheung et al. 2007).

**Table 4.2 Comparison of kinetic model parameters for Cr (VI), Cu (II) and Pb (II) on to CTSL-1**

<b>Kinetic Model</b>	<b>Cr (VI)</b>	<b>Cu (II)</b>	<b>Pb (II)</b>
<b>Pseudo first order</b>			
$Q_{e, \text{calc}} (\text{mg g}^{-1})$	12.791	24.293	27.871
$Q_{e, \text{expt.}} (\text{mg g}^{-1})$	44.21	32.418	48.302
$k_1 (\text{min}^{-1})$	0.0153	0.0024	0.0207
$r^2$	0.6519	0.9421	0.8793
<b>Pseudo second order</b>			
$Q_{e, \text{calc.}} (\text{mg g}^{-1})$	43.103	32.415	47.619
$Q_{e, \text{expt.}} (\text{mg g}^{-1})$	44.21	32.418	48.302
$k_2 (\text{g mg}^{-1} \text{ min}^{-1})$	0.0083	0.00034	0.0014
$r^2$	0.9999	0.9901	0.9941
<b>Intraparticle diffusion</b>			
$K_{id} (\text{mg g}^{-1} \text{ min}^{-1/2})$	2.337	0.8862	3.357
$C (\text{mg g}^{-1})$	20.447	4.1506	13.529
$r^2$	0.5454	0.9166	0.8078

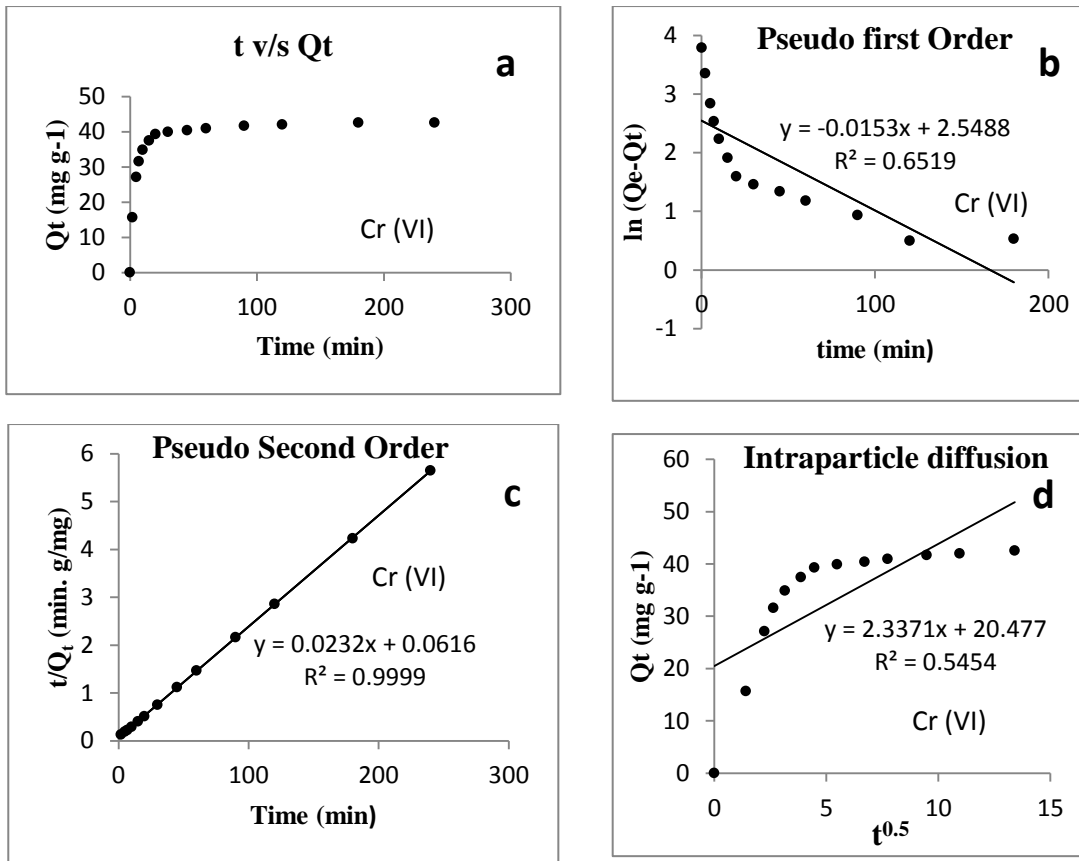
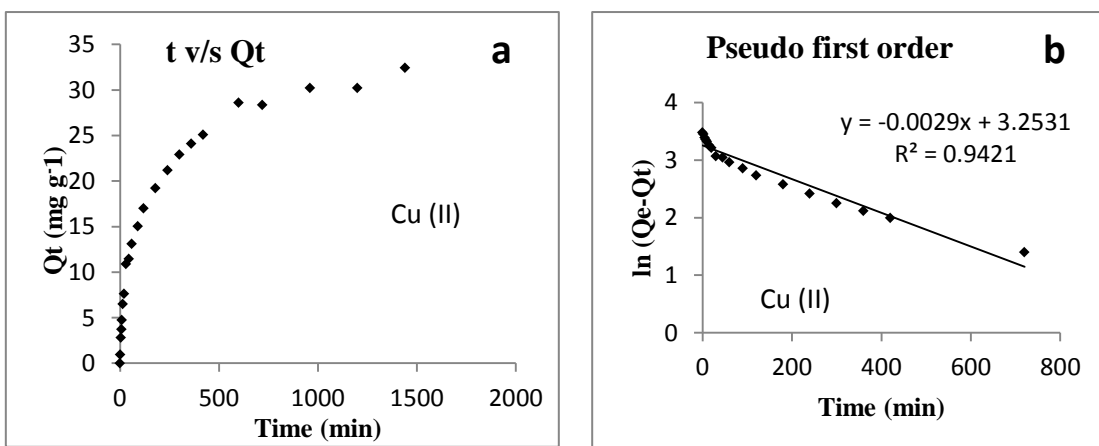
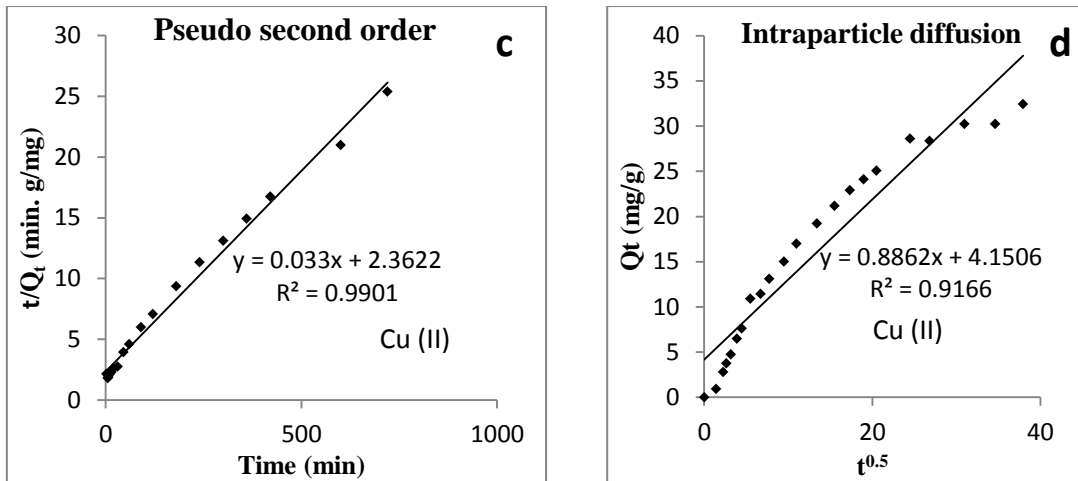
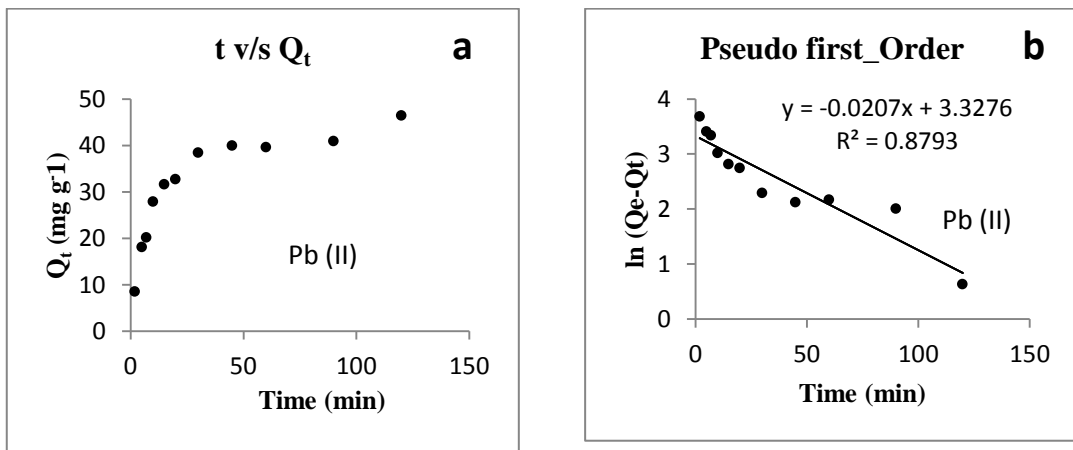


Figure 4.12 Plot of CTSL-1-Cr (VI) kinetic study data [a] Quantity adsorbed v/s time b) Pseudo-first order c) Pseudo-second order d) Intraparticle diffusion] (Initial concentration=100mg/L; Temperature=303K; pH=3; Ads. Dose=2g/L; Agitation speed=150rpm)





**Figure 4.13 Plot of CTSL-1-Cu (II) kinetic study data [a) Quantity adsorbed v/s time b) Pseudo-first order c) Pseudo-second order d) Intraparticle diffusion] (Initial concentration=100mg/L; Temperature=303K; pH=7; Ads. Dose=2g/L; Agitation speed=150rpm)**



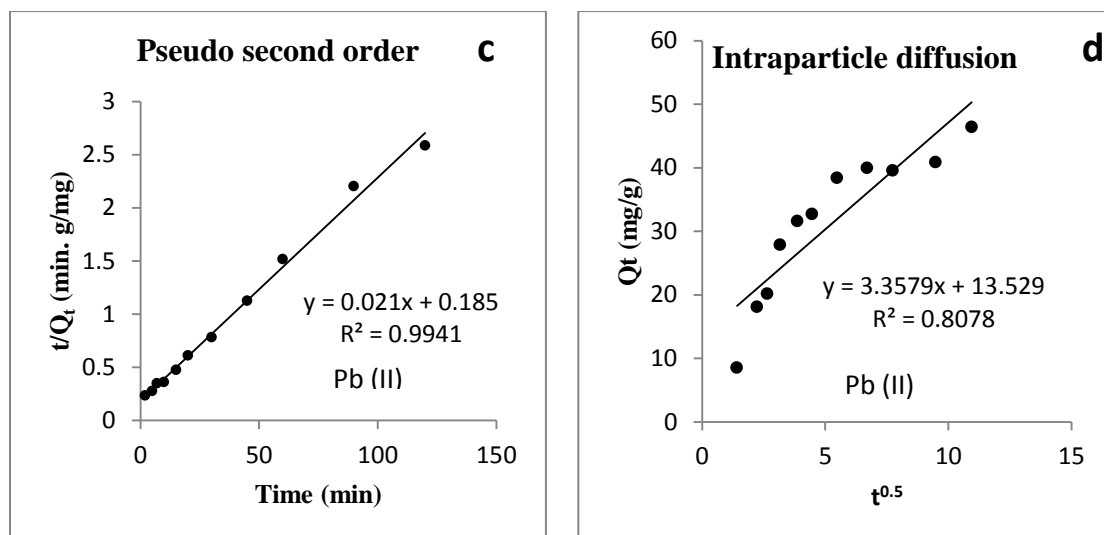


**Figure 4.14** Plot of CTSL-1-Pb (II) kinetic study data [a) Quantity adsorbed v/s time b) Pseudo-first order c) Pseudo-second order d) Intraparticle diffusion] (Initial concentration=100mg/L; Temperature=303K; pH=4; Ads. Dose=2g/L; Agitation speed=150rpm)]

#### 4.1.3.4 Adsorption Thermodynamics

The thermodynamic studies were conducted following the experimental method described in section 3.3.6; further explanation on the equations used in calculations is provided in section 2.6.3 under Chapter 2.

The results of the thermodynamic study are tabulated in Table 4.3. The change in standard Gibb's free energy,  $\Delta G^\circ$  of adsorption for all the three metals studied had negative values which suggests that the adsorption process was spontaneous (Liu et al. 2015).

**Table 4.3** Results of thermodynamic study for the adsorption of Cr (VI), Cu (II) and Pb (II) on to CTSL-1

T (K)	$K_o$	$\Delta G^\circ$ (kJ.mol <sup>-1</sup> )	$\Delta H^\circ$ (kJ.mol <sup>-1</sup> )	$\Delta S^\circ$ (J.mol <sup>-1</sup> .K <sup>-1</sup> )
<b>Cr (VI)</b>				
283.15	4012.62	-19.522	-11.126	29.88
293.15	3476.91	-19.863		
303.15	3285.91	-20.399		
313.15	2517.70	-20.379		
323.15	2261.08	-20.741		

<b>Cu (II)</b>				
283.15	210.38	-12.585	25.22	133.80
293.15	301.42	-13.906		
303.15	494.43	-15.627		
313.15	562.11	-16.477		
323.15	811.27	-17.988		
<b>Pb (II)</b>				
283.15	792.59	-15.706	14.87	107.80
293.15	980.24	-16.779		
303.15	1471.44	-18.375		
313.15	732.53	-17.166		
323.15	2399.22	-20.900		

The enthalpy change ( $\Delta H^\circ$ ) for Cr (VI) was negative indicating that the adsorption process was exothermic. On the other hand, the values for enthalpy change ( $\Delta H^\circ$ ) for both Pb (II) and Cu (II) were positive implying the adsorption process was endothermic in nature (Deng et al. 2006).

For Cu (II) and Pb (II), the adsorption increased at higher temperatures in the range of 10°C to 50°C. According to Rodda et al. (1993) there were two reasons for the adsorption to be favoured at higher temperatures. First, the adsorption of many of the divalent cations is endothermic in nature i.e. the equilibrium constants for such adsorptions increase with temperature. Second, the positive charge on the surface of the adsorbent at a given pH decreases with increase in temperature, thus increasing the temperature reduces the repulsive forces between the cations and the adsorbent surface allowing higher interactions between the two.

For Cr (VI), the adsorption was favoured at lower temperatures in the range of 10°C to 50°C. Possible reason for the decrease in adsorption at higher temperature could be the decrease in the number of protonated sites at higher temperature thereby decreasing the number of active sites for adsorbate sequestration.

The net change in standard entropy ( $\Delta S^\circ$ ) for sorption for all the metals were positive, signifying that net disorderliness increased post adsorption. During the adsorption process the water molecules which are coordinated with the adsorbent surface are displaced by the metal ions. According to Kyzas et al. (2013), even though the entropy of the adsorbed ions decreases after the adsorption on the surface of the

adsorbent, the translational entropy gained by the displaced water molecules is higher than the entropy lost by the metal ions so that the net entropy increases.

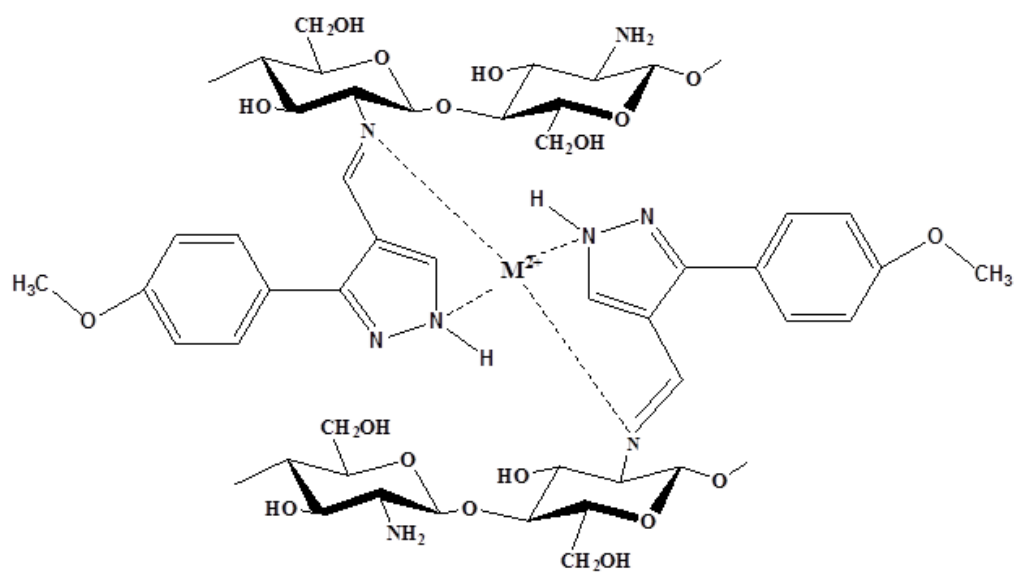
#### 4.1.3.5 Proposed mechanism of metal removal

##### a) Cu (II) and Pb (II) adsorption

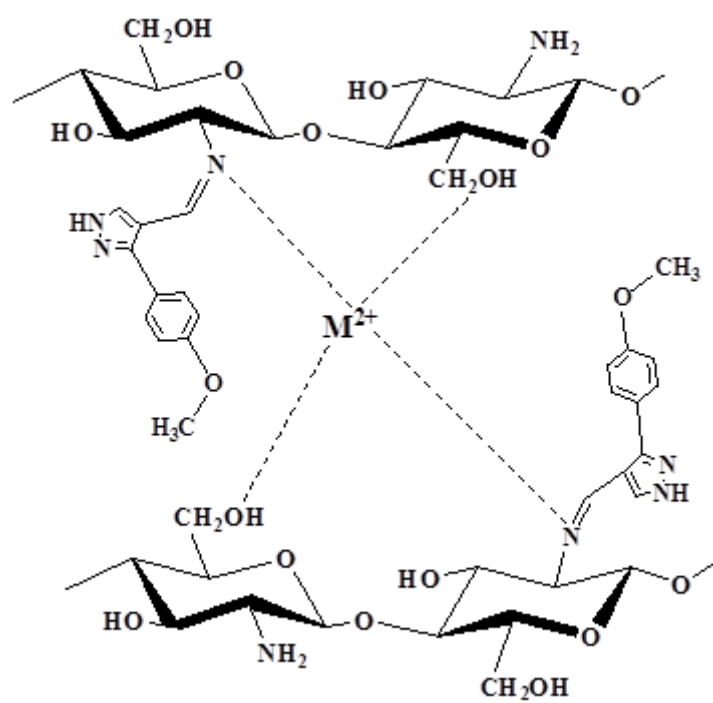
The FTIR spectra of CTSL-1 and CTSL-1 metal complexes are depicted in Figure 4.3 b, c and d. The comparison of the spectra reveals the following differences: The broad peak at wave number  $3618\text{ cm}^{-1}$  due to (OH) stretching is shifted to  $3587\text{ cm}^{-1}$  for CTSL-1-Pb and  $3606\text{ cm}^{-1}$  for CTSL-1-Cu. Further, a shoulder band in CTSL-1 around  $1632\text{ cm}^{-1}$  which is assigned to imine group ( $>\text{C}=\text{N}-$ ) is shifted to  $1608\text{ cm}^{-1}$  both for CTSL-1-Pb and CTSL-1-Cu. The peak at  $1515\text{ cm}^{-1}$  due to NH bending is shifted to  $1504\text{ cm}^{-1}$  for CTSL-1-Pb and to  $1508\text{ cm}^{-1}$  for CTSL-1-Cu; the stretching vibrations of the C-O group in the primary alcohol ( $-\text{C}-\text{O}-\text{H}$ ) is shifted from  $1010\text{ cm}^{-1}$  to  $995$  and  $991\text{ cm}^{-1}$  respectively in case of CTSL-1-Pb and CTSL-1-Cu; the NH secondary wagging peak at  $644\text{ cm}^{-1}$  is shifted to  $655\text{ cm}^{-1}$  and  $663\text{ cm}^{-1}$  for CTSL-1-Pb and CTSL-1-Cu respectively (Borsagli et al. 2015; Yuvaraja et al. 2017). It may be noted that after adsorption there is very little change in the peak at  $1250\text{ cm}^{-1}$  assigned to the stretching vibrations in C-O of the alkyl-aryl C-O-C bridge of the methoxy group indicating that the oxygen atom is unavailable for forming the coordination bond.

Webster et al. (2007) reported that nitrogen had a greater tendency to donate its pair of electrons to form a complex compared to oxygen, where the attraction of the electron pair to the atom's nucleus was stronger. Zarghami et al. (2016) have also expressed a similar view that oxygen has a stronger attraction to its electron pair compared to nitrogen which has a better tendency of donating it to a cation. Based on the considerations discussed and the changes observed in FTIR, the imine, amine and the hydroxyl groups are implicated in metal ( $\text{M}^{2+}$ ) removal. In a recent study involving removal of heavy metal ions using a chitosan derivative, Lv et al. (2017) have demonstrated the binding of Pb (II) or Cu (II) ions with N atoms through coordination bonds. Proposed mechanisms of the Cu (II) and Pb (II) removal by chelation are shown in Figure 4.15 a, b and c. (Zhao et al. 2007; Kyzas et al. 2009).





(a)



(b)

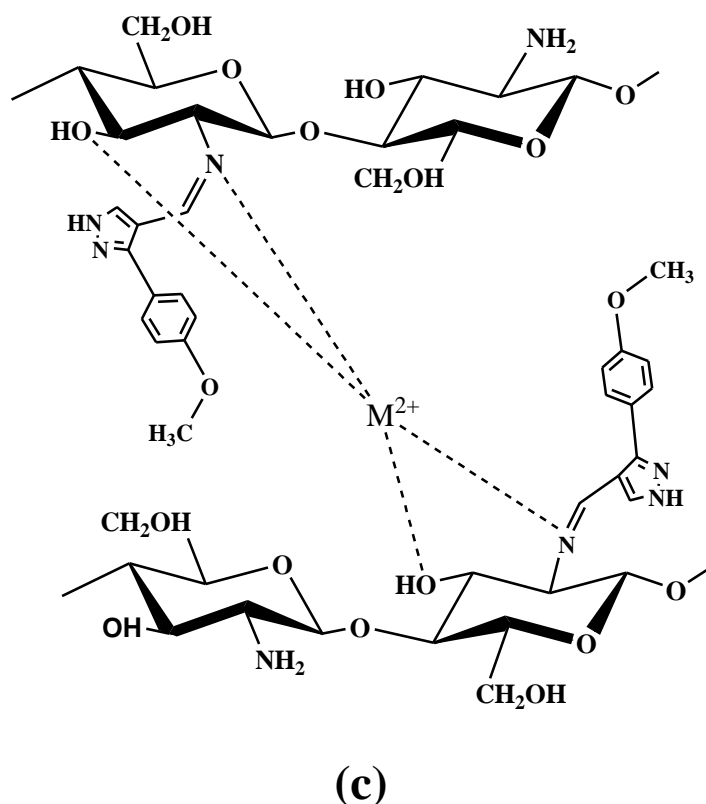


**Figure 4.15 a, b and c. Proposed mechanisms of adsorbate uptake.**  
**( $M^{2+}$  =Pb (II) or Cu (II))**

b) Cr (VI) adsorption

At low pH values during the adsorption ( $\text{pH} < 3$ ), the different N-atom and hydroxyl bearing groups get protonated (Wang and Wang 2016; Janciauskaite et al. 2008; Webster et al. 2007).



The positive electrical charges are formed on the N bearing groups due to protonation and hence the adsorbent surface gets charged. The sorbate Cr (VI) which exists

mostly in the form of  $\text{HCrO}_4^-$  anions under the experimental conditions gets attracted to these sites and the binding takes place by electrostatic interaction.

When the FTIR pattern of CTSL-1 (Figure 4.3 b) is compared with CTSL-1-Cr (Figure 4.3 e), the wide band around  $3618\text{ cm}^{-1}$  corresponding to the stretching vibrations of the hydroxyl group is shifted to  $3583\text{ cm}^{-1}$ ; the peak at  $1674\text{ cm}^{-1}$  ascribed to the bending vibrations of the carbonyl group (C=O) of acetamide units is shifted to  $1689\text{ cm}^{-1}$ ; the absorption peak at  $1632\text{ cm}^{-1}$  ascribed to the stretching vibrations of the imine group (C=N) is shifted to  $1612\text{ cm}^{-1}$ ; the band due to C-O stretching vibrations of the C-O-H group is shifted to  $1014\text{ cm}^{-1}$ . The spectrum also displays a shift of the NH secondary wagging vibrations from  $644$  to  $636\text{ cm}^{-1}$ . From the preceding considerations, it is concluded that imine, NH and hydroxyl groups took part in the binding of Cr (VI). A schematic diagram of the possible mechanism of Cr (VI) interaction is presented in Figure 4.16.

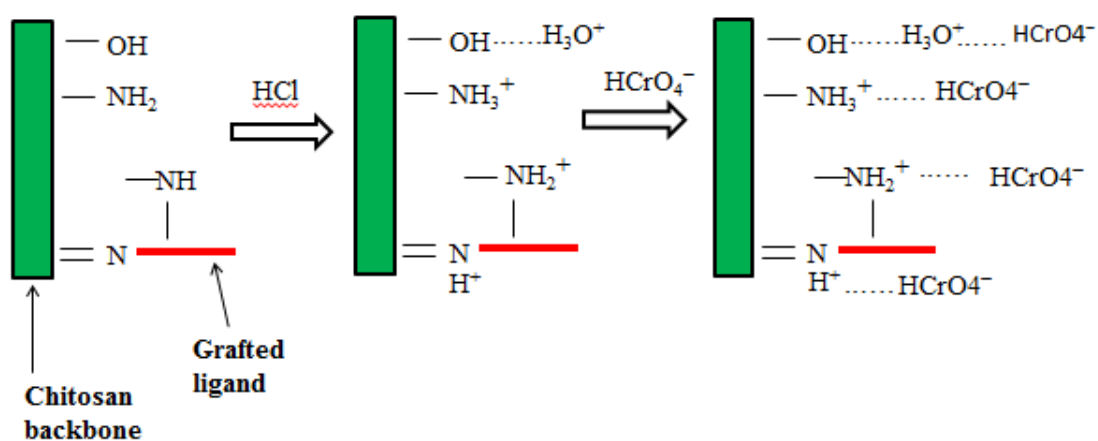


**Figure 4.16 Proposed mechanism of adsorption for Cr (VI) removal**

The interpretation of observed changes in FTIR absorption peaks after the adsorption is presented in Table 4.4.

**Table 4.4 FTIR peak vibrations before and after adsorption on to CTSL-1**

<b>Adsorbent: CTSL-1</b>			
<b>Metal ion</b>	<b>Group</b>	<b>Wavenumber (cm<sup>-1</sup>) before adsorption</b>	<b>Wavenumber (cm<sup>-1</sup>) after adsorption</b>
<b>Pb (II)</b>	Hydroxyl-OH stretching	3618	3587
	Imine (C=N) stretching	1632	1608
	C-O stretch of secondary alcohol (C-O-H) at C-3 position	1068	1103
	C-O stretch of primary alcohol (C-O-H) at C-6 position	1010	995
	NH Secondary wagging	644	655
<b>Cu (II)</b>	Hydroxyl-OH stretching	3618	3606
	C=O bending of NHCOCH <sub>3</sub>	1674	1681
	Imine (C=N) stretching	1632	1608
	C-O stretching of primary alcohol (C-O-H) at C-6 position	1010	991
	NH secondary wagging	644	663
<b>Cr (VI)</b>	Hydroxyl-OH stretching	3618	3583
	C=O bending of NHCOCH <sub>3</sub>	1674	1689
	Imine (C=N) stretching	1632	1612
	C-O stretch of primary alcohol (C-O-H) at C-6 position	1010	1014
	NH Secondary wagging	644	636

#### **4.1.3.6 Post adsorption XRD analysis of CTSL-1-Metal complexes**

The XRD spectra of CTSL-1 and the CTSL-1-Metal complexes obtained after the adsorption process are presented in Figure 4.17. When the XRD spectra of CTSL-1 is compared with that of CTSL-1-Cr and CTSL-1-Cu, a general weakening of

intensity and a broadening of the peak around  $2\Theta=20^\circ$  is observed. This may be attributed to the decrease in crystallinity after the metal complex formation. Sankararamakrishnan et al. (2006) reported similar results for the removal of Cr (VI) for a chitosan derivative. In addition to the broadening of the peak, the XRD spectrum for CTSL-1-Pb shows a few extra peaks which may be evidence of formation of new crystals of  $Pb^{2+}$  is generated in CTSL-1-Pb. Trimukhe and Varma (2008) have reported similar extra peaks for chitosan-Pb complexes.

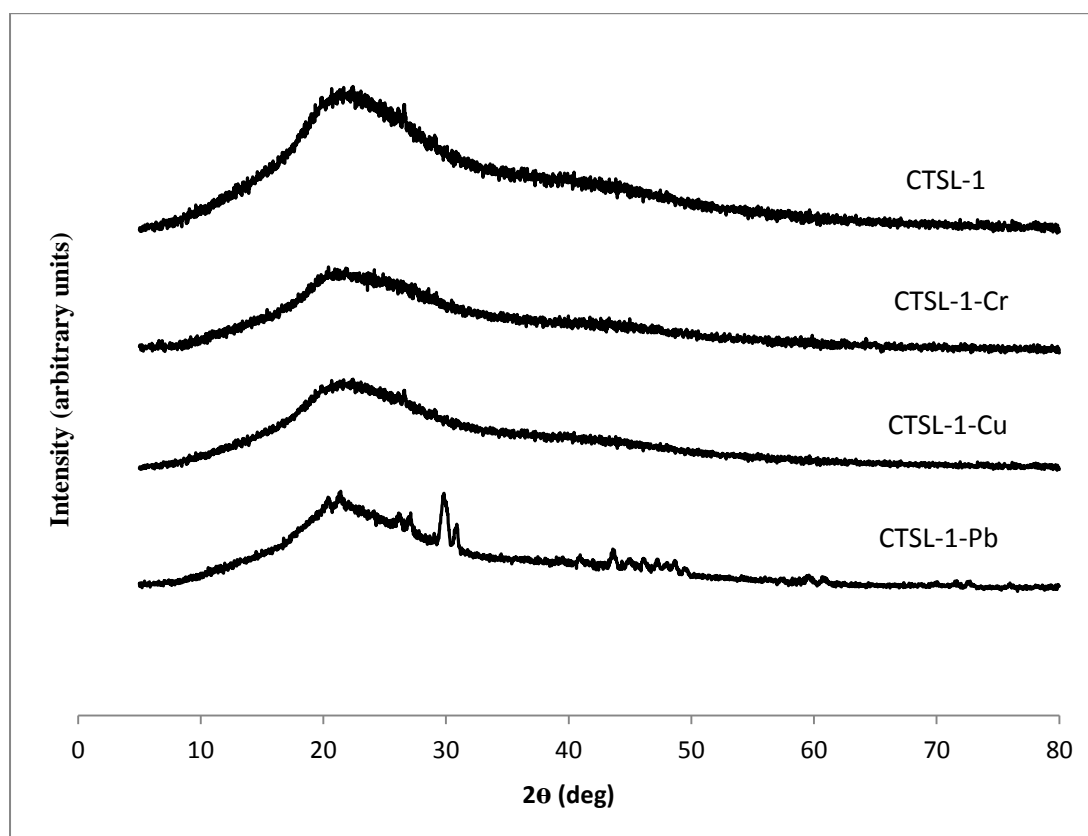


**Figure 4.17 XRD spectra of a) CTSL-1 b) CTSL-1-Cr c) CTSL-1-Cu  
d) CTSL-1-Pb**

## 4.2 STUDIES USING CHITOSAN DERIVATIVE CTSL-2

### 4.2.1 Characterization of ligand L-2

The  $^1\text{H}$  NMR spectrum of the ligand (L-2) exhibited the following peaks (Figure 4.18).  $^1\text{H}$  NMR (DMSO- $d_6$ )  $\delta$  (ppm): 13.70 (1 H, Pyrazole NH), 9.904 (1 H, Aldehyde), 7.498-7.822 (4 H, Ar. Ring), 8.380 (1 H, Pyrazole 5H). When the  $^1\text{H}$  NMR spectrum of ligand L-2 is compared with that of L-1, it is observed that the shift at 3.825 ppm (3 H, Methoxy) is absent, as would be expected, due to the unsubstituted C-4 position in the aromatic ring. The chemical shifts at 3.377 and 2.512 ppm are the shifts due to water and the solvent DMSO respectively. The proton NMR signals obtained validate the successful formation of the ligand L-2.

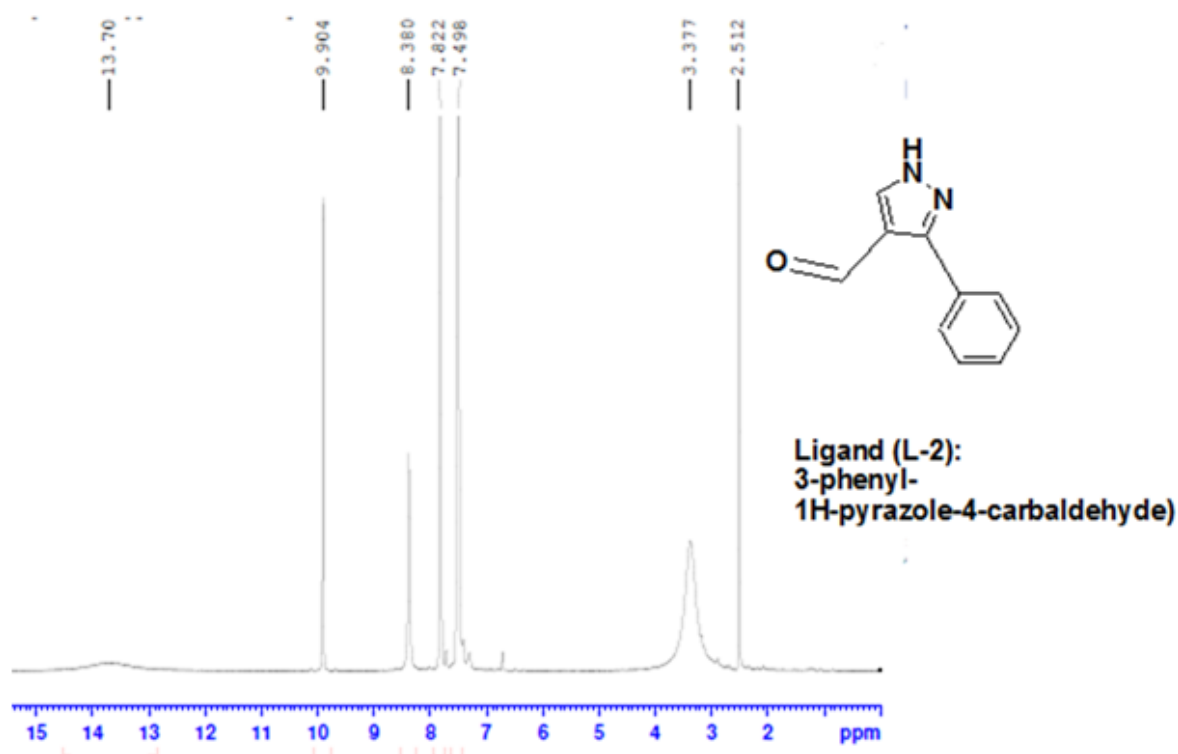


Figure 4.18  $^1\text{H}$  NMR spectrum of the ligand (L-2)

## 4.2.2 Characterization of the chitosan derivative CTSL-2

### 4.2.2.1 Solid state $^{13}\text{C}$ NMR analysis of CTSL-2

The spectrum of CTSL-2 as presented in Figure 4.19 shows the characteristic peak for imine (C=N) at 163.1, and the aromatic and heterocyclic rings are represented between 118.9 and 150.3. When compared to the spectrum of chitosan which is shown in Figure 4.2 a, the appearance of the new peak assigned to the imino-linker group along with new peaks for aromatic and heterocyclic groups validates the anchoring of the L-2 to the chitosan strand by the Schiff reaction to form the new chitosan derivative CTSL-2 (Xiao and Zhou 2008).

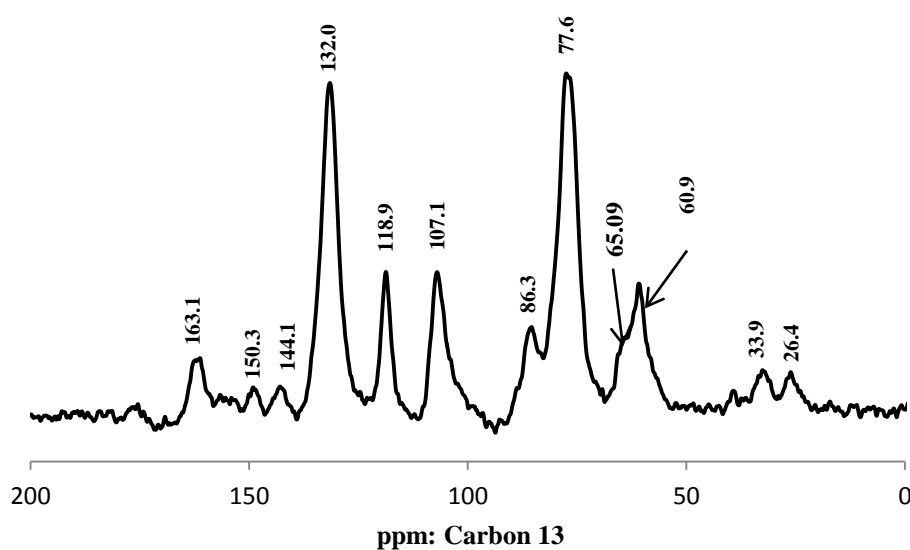


Figure 4.19  $^{13}\text{C}$  NMR of CTSL-2

### 4.2.2.2 FTIR analysis of CTSL-2

The FTIR spectra for pure chitosan and CTSL-2 are shown in Figure 4.20 a and b. The major bands for pure chitosan are described under section 4.2.2.2.

The FTIR pattern for CTSL-2 has an absorption signal at  $3627\text{ cm}^{-1}$  attributed to the (-OH) stretching vibrations. The presence of a peak around  $1639\text{ cm}^{-1}$  is due to the ( $>\text{C}=\text{O}$ ) stretch of acetyl units of CTS-NHAc. The splitting of the band at 1633

$\text{cm}^{-1}$  is attributed to imine ( $>\text{C}=\text{N}-$ ) stretch. As would be expected, the strong peak observed at  $1250 \text{ cm}^{-1}$  observed in case of CTSL-1 due to alkyl-aryl (C-O) stretch is absent in case of CTSL-2. The peak around  $1062 \text{ cm}^{-1}$  is assigned to the stretching vibrations of the secondary alcohol C-O-H. The peak around  $1002 \text{ cm}^{-1}$  is assigned to the stretching vibrations of the primary alcohol C-O-H. The band at  $777\text{-}802 \text{ cm}^{-1}$  is due to aromatic (-CH) out of plane bending. The shoulder band around  $648 \text{ cm}^{-1}$  is assigned to secondary amide wagging (Stuart 2004).

The analysis of the post-adsorption FTIR spectra is presented under section 4.2.3.5.



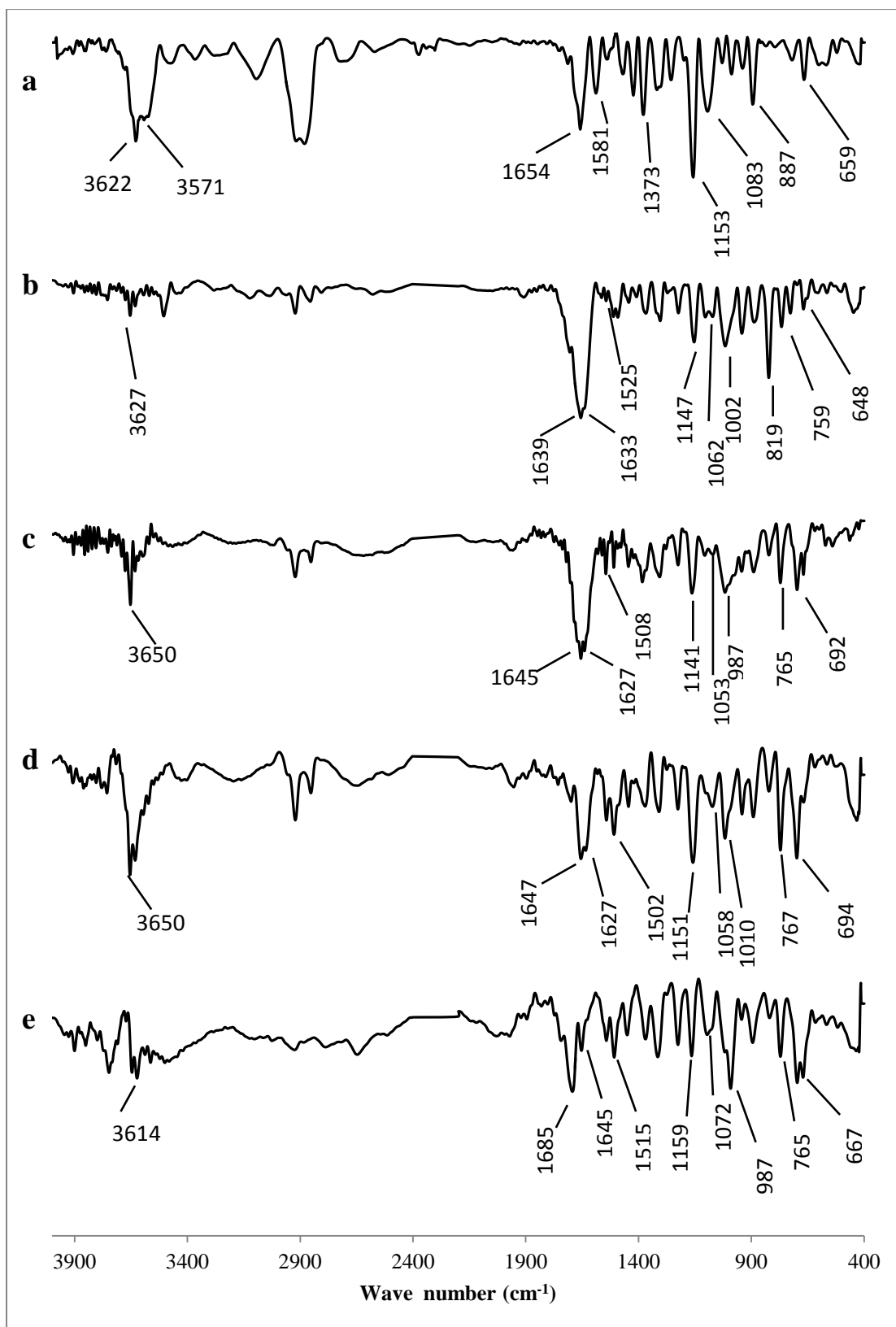


**Figure 4.20** FTIR spectra of a) Chitosan b) CTSL-2 c) CTSL-2-Pb d) CTSL-2-Cu e) CTSL-2-Cr

#### 4.2.2.3 XRD analysis

The powder X-ray diffraction plot of CTSL-2 is presented in Figure 4.21. When compared to XRD spectrum of CTS (Figure 4.5 a), the disappearance of the peak at  $2\Theta=10^\circ$  which is attributed to  $(-\text{NH}_2)$  group is further evidence for the Schiff base reaction at the  $(-\text{NH}_2)$  group (Webster et al., 2007; Hussein et al., 2012). The decrease in the intensity of the peak around  $2\Theta=20^\circ$  and the broadening of the peak for CTSL-2 indicates the decrease in crystallinity and increase in amorphous nature of CTSL-2 as compared to pure CTS. This was probably due to the weakening of hydrogen bonding interactions between the hydroxyl and amino groups of chitosan as a result of stereochemical hindrance of the side chains or the diminished concentrations of those groups (Liu, et al. 2015). According to Jing et al. (2016), crystallinity plays an important part in the adsorption performance of polymeric adsorbents such as chitosan. The crystalline areas of the polymer are not available for metal ion infiltration, while the metal ions can access the amorphous region. Hence, the amorphous areas provide easier access to the adsorbate species creating conducive conditions for adsorption thus increasing the adsorption capacity. It was very evident from the comparison of XRD patterns of chitosan and CTSL-2 (Figure 4.5 a and Figure 4.21 respectively) that the crystallinity of CTSL-2 had decreased thereby increasing the amorphous regions present in the polymer which in turn created better conditions for adsorption.

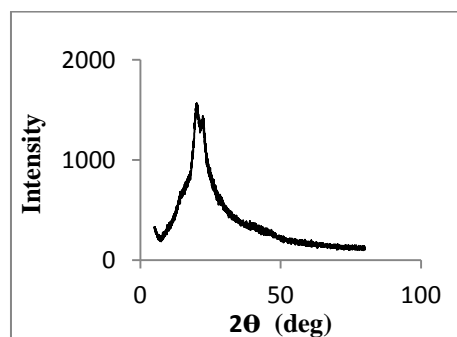


**Figure 4.21 XRD spectrum of CTSL-2**

#### 4.2.2.4 DSC thermogram studies of CTSL-2

The DSC thermogram of CTSL-2 (Figure 4.22) shows two major exothermic peaks; a peak around 70°C culminating in the endothermic peak at 100°C is attributed to vaporisation of water present; a peak around 300°C is due to the degradation of the biopolymer derivative CTSL-2. When the thermograms of CTS (Figure 4.6 a) and CTSL-2 (Figure 4.22) are compared it is evident that the derivative CTSL-2 has retained the thermal stability of the CTS in spite of grafting of the ligand L-2 on to it. Further, when the thermograms of CTSL-1 and CTSL-2 (Figure 4.6 b and Figure 4.22) are compared, CTSL-1 presented a lower thermal stability with the derivative displaying degradation at a relatively lower temperature. This may be due to the relatively bulky and extra methoxy (-O-CH<sub>3</sub>) group present in CTSL-1 which is absent in CTSL-2.

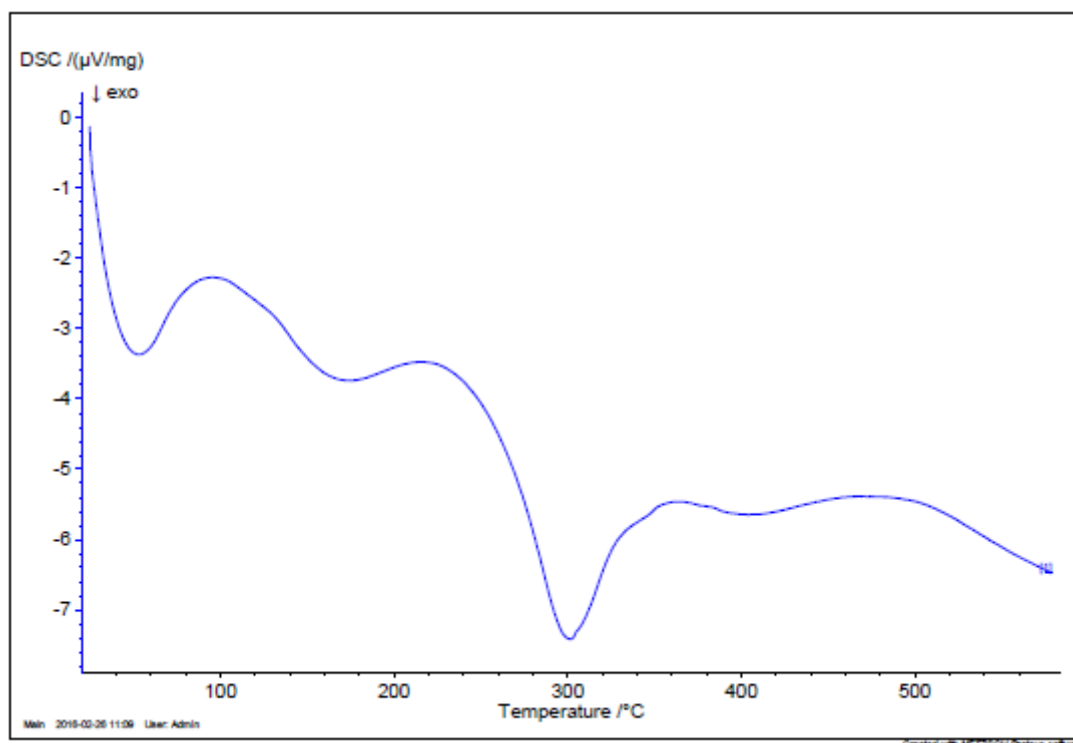


**Figure 4.22 DSC thermogram of CTSL-2**

## 4.2.3 Adsorption studies with CTSL-2

### 4.2.3.1 Effect of pH

The pH effect on adsorption was studied in the pH range of 2-7. Higher pH values were not considered in order to avoid the risk of possible metal hydroxide precipitation at those pH values (Nghah and Isa 1998; Gunay et al. 2007). The effect of pH on sorption of the metal ions on CTSL-2 is shown in Figure 4.23.

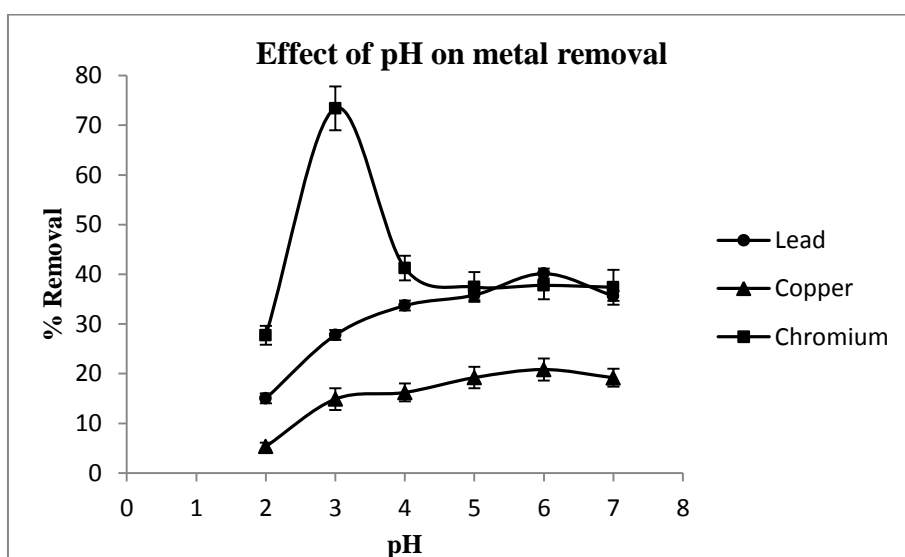


**Figure 4.23 Effect of pH on % removal (Initial concentration=100mg/L; Temperature=303K; Ads. Dose=4 g/L; Agitation speed=150rpm; Contact time=24h)**

The adsorption uptake of Cr (VI) onto CTSL-2 was found to be the highest at a pH of 3, and for both Pb (II) and Cu (II), the optimal pH value was observed to be 6. At very low pH values ( $\leq 2$ ), there was evidence of fragmentation of the adsorbent, which caused a steep fall in % removal.

### 4.2.3.2 Adsorption equilibrium

The experiments in adsorption equilibrium were conducted following the method outlined in section 3.3.4 of Chapter 3; the quantity of metal ion removal was determined using the Eq. 3.1; the mathematical expressions of the adsorption isotherms used are given under section 2.6.1.

The results of the equilibrium studies are presented in Table 4.5 and Figures 4.24, Figure 4.25 and Figure 4.26. The adsorption equilibria were best represented by Redlich-Peterson isotherm for CTSL-2-Cr (VI) ( $r^2=0.9849$ ) and CTSL-2-Cu (II) ( $r^2=0.9676$ ) and by Freundlich isotherm for CTSL-2-Pb (II) ( $r^2=0.9716$ ). The maximum monolayer adsorption capacities ( $Q_o$ ) were 63.465 mg/g for Cr (VI), 37.038 mg/g for Cu (II) and 91.745 mg/g for Pb (II). The Langmuir separation factor  $R_L$  which was within 0-1 and the Freundlich exponent (n) (both described under section 2.6.1) which was in the range of 1-10 indicated that the adsorption process was favourable (Nethaji et al. 2010). It has been stated elsewhere that values of  $b_R$  between 0 and 1 in the Redlich-Peterson model (described under section 2.6.1) indicate a favourable adsorption and higher values may indicate a weaker interaction between the adsorbent and the adsorbate (Boddu et al. 2008). The values obtained in this study for  $b_R$  were 0.858, 0.689 and 0.505 for the adsorption of Cr (VI), Cu (II) and Pb (II) respectively, which indicated that the adsorption was favourable.

**Table 4.5 Equilibrium model parameters for adsorption of Cr (VI), Cu (II) and Pb (II) on CTSL-2**

<b>Isotherm</b>	<b>Cr (VI)</b>	<b>Cu (II)</b>	<b>Pb (II)</b>
<b>Langmuir Isotherm</b>			
$Q_o(\text{mg g}^{-1})$	63.465	37.038	91.745
$b(\text{L mg}^{-1})$	0.0968	0.0039	0.003
$r^2$	0.9390	0.9603	0.9628
$R_L$	0.0160- 0.000162	0.4105-0.0069	0.2612-0.0035
<b>Freundlich Isotherm</b>			
$K_f(\text{mg g}^{-1})$	16.445	1.078	2.158
n	4.440	2.025	1.937
$r^2$	0.9569	0.9622	0.9716
<b>Redlich-Peterson Isotherm</b>			
$K_R(\text{L g}^{-1})$	14.789	0.284	16.476
$a_R(\text{L mg}^{-1})$	0.540	0.069	6.648
$b_R$	0.858	0.689	0.505
$r^2$	0.9849	0.9676	0.9708

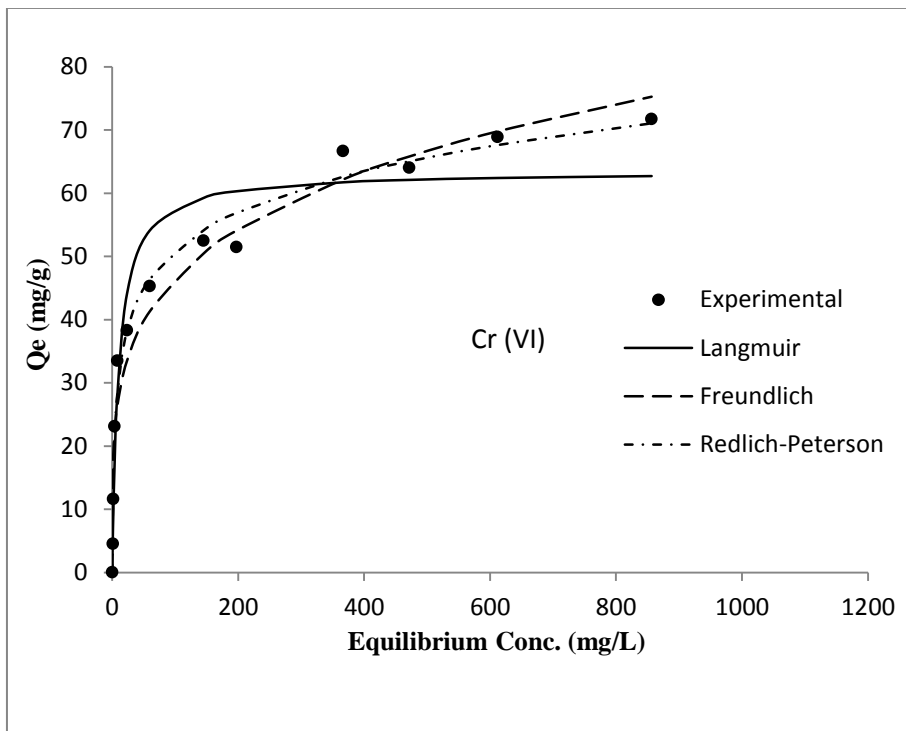


**Figure 4.24** Plot of various adsorption isotherms to CTSL-2-Cr (VI) adsorption data (Initial concentration=100 mg/L; Temperature=303K; pH=3; Ads. Dose=2g/L; Agitation speed=150 rpm; Contact time=24 h)

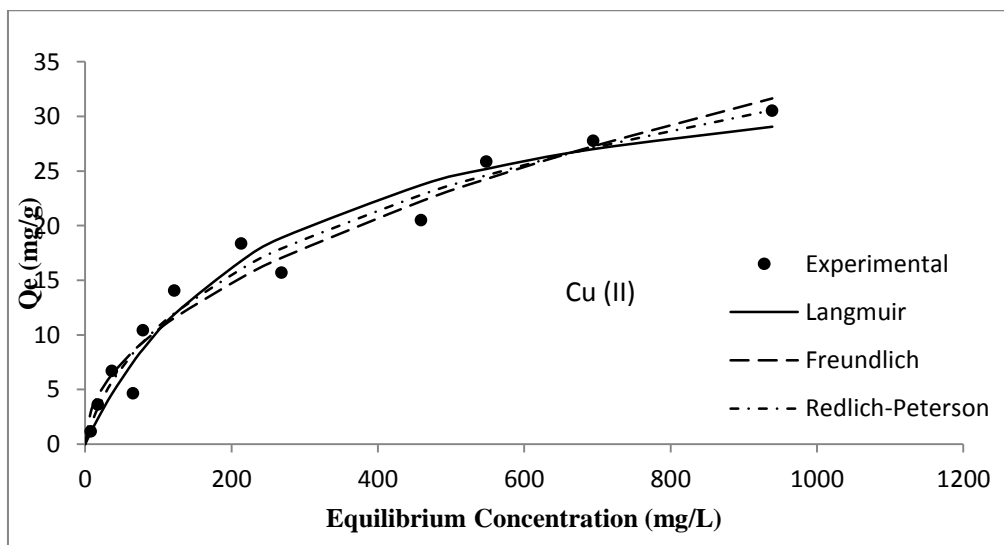


**Figure 4.25** Plot of various adsorption isotherms to CTSL-2-Cu (II) adsorption data (Initial concentration=100 mg/L; Temperature=303K; pH=6; Ads. Dose=2g/L; Agitation speed=150 rpm; Contact time=24 h)

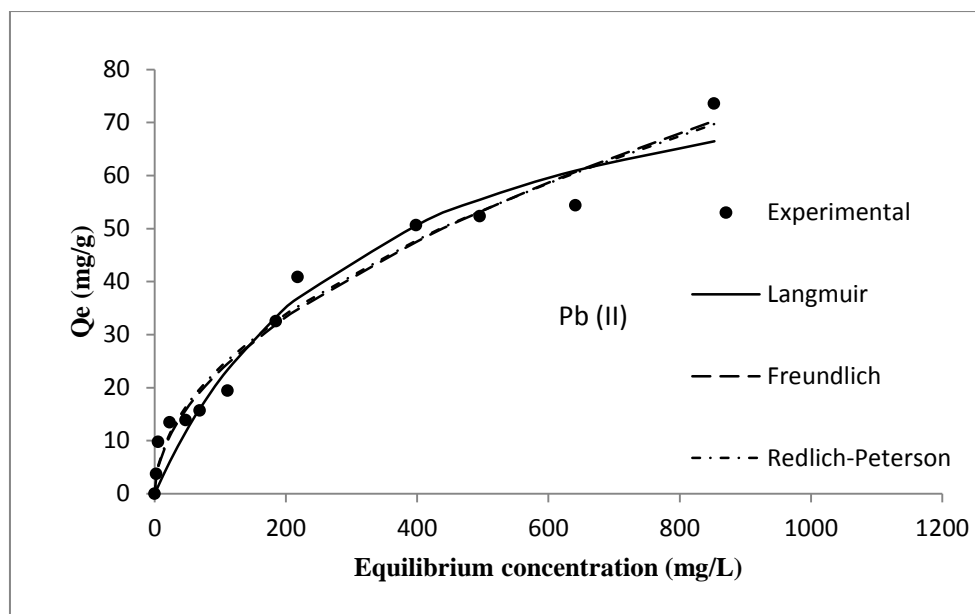


**Figure 4.26 Plot of various adsorption isotherms to CTSL-2-Pb (II) adsorption data (Initial concentration=100 mg/L; Temperature=303K; pH=6; Ads. Dose=2g/L; Agitation speed=150 rpm, Contact time=24 h)**

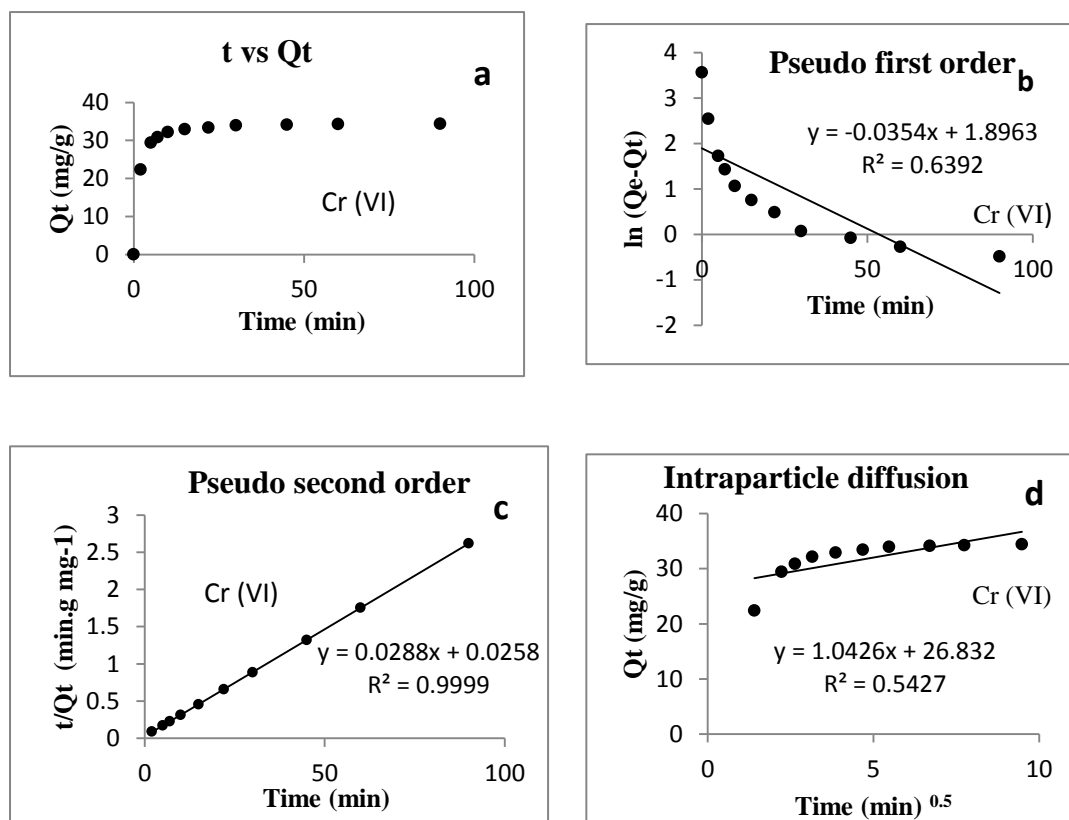
#### 4.2.3.3 Adsorption kinetics

The adsorption kinetic study was conducted by following the procedure explained in section 3.3.5; Eq. 3.2 was used to determine the instantaneous, non-equilibrium adsorption capacity ( $Q_t$ ); the mathematical expressions of the kinetic models employed to fit the experimental data are given in section 2.6.2.

In order to determine the adsorption kinetics of the metal ions, three models were examined for suitability for fitment with data. They were pseudo first order, pseudo second order and intraparticle diffusion models. Among these, the pseudo second order model was found to best represent the adsorption kinetics in all the three metal ions. (Cr (VI)  $r^2 = 0.9999$ ; Cu (II)  $r^2 = 0.9978$ ; Pb (II)  $r^2 = 0.9978$ ). The pseudo-second order rate constant ( $k_2$ ) obtained for Cr (VI), Cu (II) and Pb (II) were  $32.2 \times 10^{-3}$ ,  $17.4 \times 10^{-3}$  and  $7.2 \times 10^{-3} \text{ g mg}^{-1} \text{ min}^{-1}$  respectively. The results are presented in Table 4.6 and graphically shown in Figure 4.27, Figure 4.28 and Figure 4.29. The close agreement between the calculated and the experimental values of  $Q_e$  in case of the pseudo-second order model is further evidence of its applicability to the kinetics of the adsorption process.

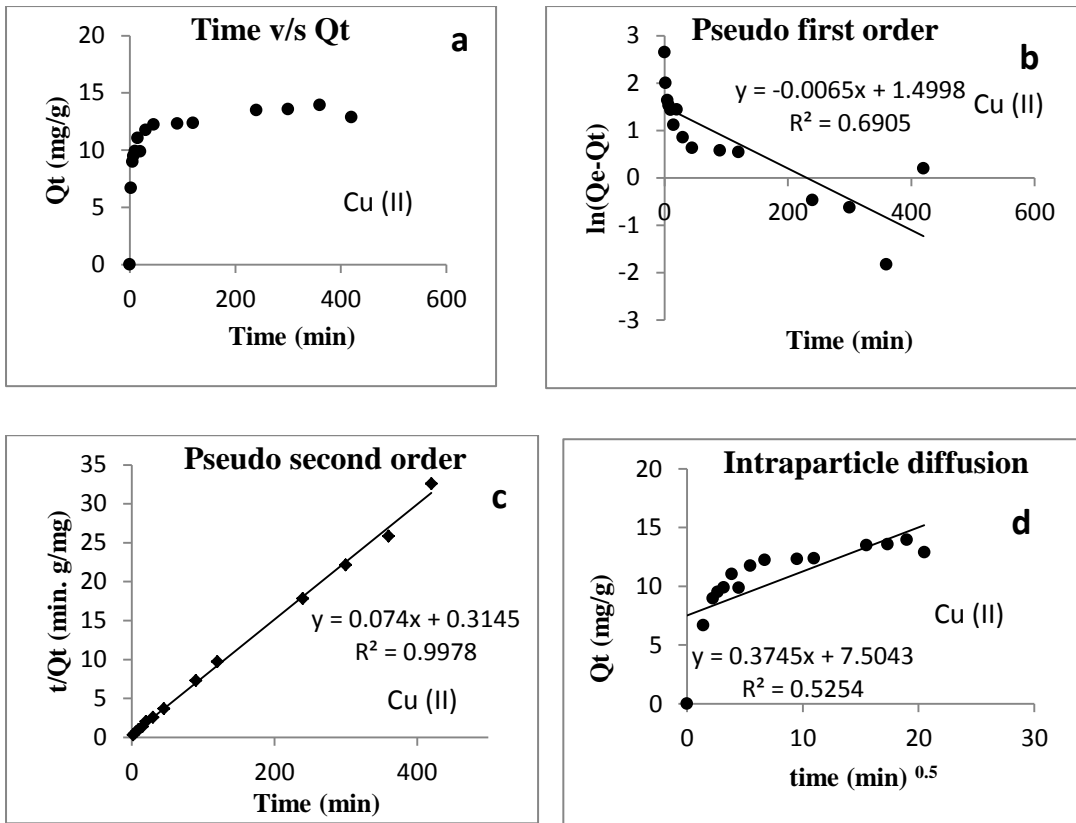
**Table 4.6 Kinetic model parameters for adsorption of Cr (VI), Cu (II) and Pb (II) onto CTSL-2**

Kinetic Model	Cr (VI)	Cu (II)	Pb (II)
<b>Pseudo First order</b>			
$Q_e, \text{ calc. (mg g}^{-1}\text{)}$	6.674	4.479	6.248
$Q_e, \text{ expt (mg g}^{-1}\text{)}$	35.014	14.102	25.893
$k_1(\text{min}^{-1})$	0.0354	0.0065	0.0066
$r^2$	0.6392	0.6905	0.4918
<b>Pseudo second order</b>			
$Q_e, \text{ calc (mg g}^{-1}\text{)}$	34.722	13.514	25.580
$Q_e, \text{ exp (mg g}^{-1}\text{)}$	35.014	14.102	25.893
$k_2(\text{g mg}^{-1}\text{min}^{-1})$	0.0322	0.0174	0.0072
$r^2$	0.9999	0.9978	0.9978
<b>Intraparticle diffusion</b>			
$K_{id}(\text{mg g}^{-1}\text{min}^{-1/2})$	1.0426	0.3745	0.7619
$C(\text{mg g}^{-1})$	26.832	7.5043	13.622
$r^2$	0.5427	0.5254	0.4879

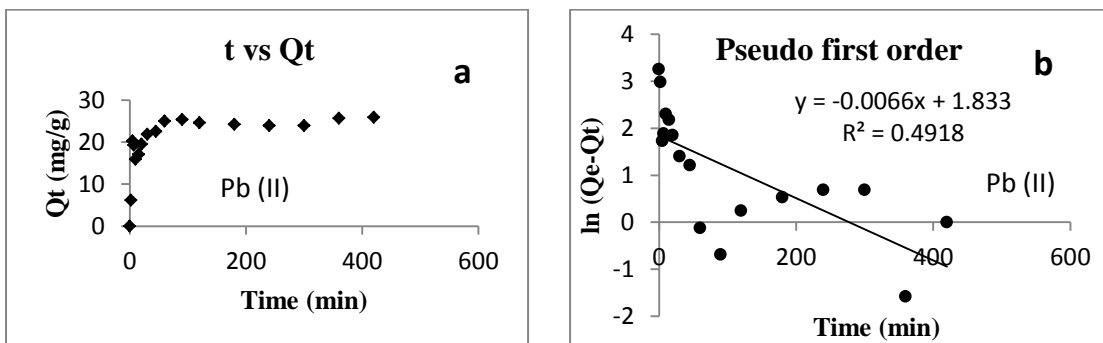


**Figure 4.27 Plot of CTSL-2-Cr (VI) kinetic study data [a) Quantity adsorbed v/s time b) Pseudo-first order c) Pseudo-second order d) Intraparticle diffusion] (Initial concentration=100mg/L; Temperature=303K; pH=3; Ads. Dose=2g/L; Agitation speed=150rpm)**





**Figure 4.28** Plot of CTSL-2-Cu (II) kinetic study data [a) Quantity adsorbed v/s time b) Pseudo-first order c) Pseudo-second order d) Intraparticle diffusion] (Initial concentration=100mg/L; Temperature=303K; pH=6; Ads. Dose=2g/L; Agitation speed=150rpm)



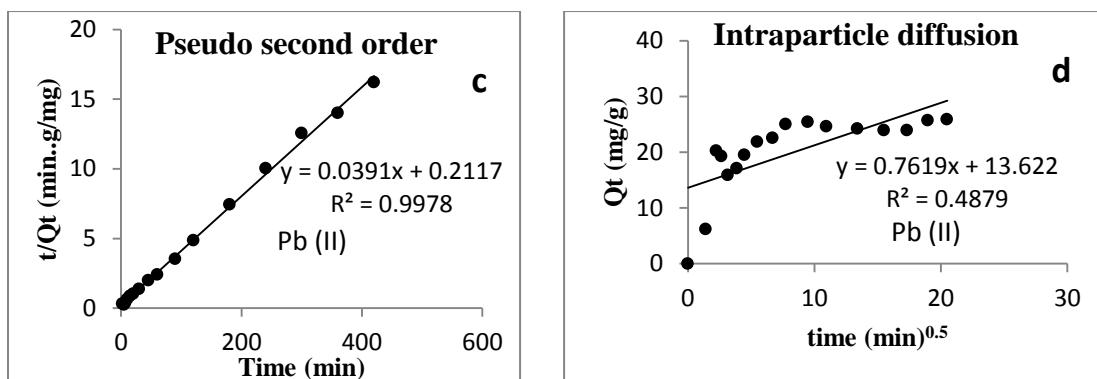


**Figure 4.29 Plot of CTSL-2-Pb (II) kinetic study data [a] Quantity adsorbed v/s time b) Pseudo-first order c) Pseudo-second order d) Intraparticle diffusion] (Initial concentration=100mg/L; Temperature=303K; pH=6; Ads. Dose=2g/L; Agitation speed=150rpm)**

#### 4.2.3.4 Adsorption thermodynamics

The thermodynamic studies were conducted following the experimental method described under section 3.3.6; further explanation on the equations used in calculations is provided under section 2.6.3.

The feasibility of the sorption of the adsorbate with the adsorbent is determined by the change in standard Gibb's free energy ( $\Delta G^\circ$ ). Negative values of  $\Delta G^\circ$  indicate that the adsorption occurs spontaneously.

The results of the thermodynamic study are presented in the Table 4.7. It is observed that the change in standard Gibb's free energy of adsorption is negative for all the three metals studied which indicates that the adsorption of all the metal ions on CTSL-2 is spontaneous.

**Table 4.7 Thermodynamic parameters for the adsorption of Cr (VI), Cu (II) and Pb (II) onto CTSL-2**

T (K)	K <sub>o</sub>	$\Delta G^{\circ}$ (kJ.mol <sup>-1</sup> )	$\Delta H^{\circ}$ (kJ.mol <sup>-1</sup> )	$\Delta S^{\circ}$ (J.mol <sup>-1</sup> .K <sup>-1</sup> )
<b>Chromium</b>				
283.15	10499.679	-21.797	-11.606	35.514
293.15	7878.557	-21.867		
303.15	7091.839	-22.348		
313.15	6007.716	-22.653		
323.15	5639.214	-23.206		
<b>Copper</b>				
283.15	82.187	-10.379	41.336	182.534
293.15	147.025	-12.163		
303.15	307.231	-14.436		
313.15	290.906	-14.770		
323.15	889.803	-18.245		
<b>Lead</b>				
283.15	119.355	-11.258	58.417	245.421
293.15	157.228	-11.655		
303.15	1091.709	-17.631		
313.15	1063.478	-18.145		
323.15	2102.327	-20.555		

From the results of the study, it is evident that the change in standard enthalpy ( $\Delta H^{\circ}$ ) for the adsorption of Cr (VI) onto CTSL-2 is exothermic and for the adsorption of Pb (II) and Cu (II) it is endothermic in nature. For Cu (II) and Pb (II), the adsorption capacity increased with increase in temperature in the range of 10 °C to 50 °C, whereas for Cr (VI), it decreased in the same temperature range. The net entropy change values obtained for Cr (VI), Cu (II) and Pb (II) were positive indicating that the net disorderliness increased after the adsorption process. The enthalpy change values are also useful for distinguishing between physisorption and chemisorption. Physisorption is typically associated with  $\Delta H$  in the range of 2.1-20.9 kJ/mol, whereas chemisorption is associated with  $\Delta H$  in the range of 20.9-418.4 kJ/mol (Liu et al.

2015). This supports the interpretation that adsorption of Cu (II) and Pb (II) onto CTSL-2 may be due to chemisorption.

#### 4.2.3.5 Post-adsorption CTSL-2 characterization

The FTIR spectra of CTSL-2 and CTSL-2 metal complexes are depicted in Figure 4.20 b, c, d and e. The broad peak at wave number  $3627\text{ cm}^{-1}$  due to (OH) stretching is shifted to  $3650\text{ cm}^{-1}$  for both CTSL-1-Pb and CTSL-1-Cu. The band in CTSL-2 around  $1633\text{ cm}^{-1}$  which is assigned to imine group ( $>\text{C}=\text{N}-$ ) is shifted to  $1627\text{ cm}^{-1}$  in case of both CTSL-1-Pb and CTSL-1-Cu. The stretching vibrations of the C-O group in the secondary alcohol (-C-O-H) is shifted from  $1062\text{ cm}^{-1}$  to  $1053\text{ cm}^{-1}$  (CTSL-1-Pb) and  $1058\text{ cm}^{-1}$  (CTSL-1-Cu). The stretching vibrations of the C-O group in the primary alcohol (-C-O-H) is shifted from  $1002\text{ cm}^{-1}$  to  $987\text{ cm}^{-1}$  (CTSL-1-Pb) and  $1010\text{ cm}^{-1}$  (CTSL-1-Cu); the NH secondary wagging peak at  $648\text{ cm}^{-1}$  is shifted to  $692\text{ cm}^{-1}$  and  $694\text{ cm}^{-1}$  for CTSL-1-Pb and CTSL-1-Cu respectively.

When the FTIR pattern of CTSL-2 (Figure 4.20 b) is compared with CTSL-2-Cr (Figure 4.20 e), the wide band absorption peak around  $3627\text{ cm}^{-1}$  due to hydroxyl group is shifted to  $3614\text{ cm}^{-1}$ ; the peak at  $1639\text{ cm}^{-1}$  ascribed to the stretching vibrations of the carbonyl group (C=O) of acetamide units is shifted to  $1685\text{ cm}^{-1}$ ; the absorption peak at  $1633\text{ cm}^{-1}$  ascribed to the stretching vibrations of the imine group ( $>\text{C}=\text{N}-$ ) is shifted to  $1645\text{ cm}^{-1}$ . The band at  $1062\text{ cm}^{-1}$  assigned to the C-O stretching vibrations of the secondary alcohol C-O-H is shifted to  $1072\text{ cm}^{-1}$ . Similarly, the band at  $1002\text{ cm}^{-1}$  assigned to the C-O stretching vibrations of the primary alcohol C-O-H is shifted to  $987\text{ cm}^{-1}$ . The band at  $648\text{ cm}^{-1}$  assigned to the secondary wagging vibrations of the NH group is shifted to  $667\text{ cm}^{-1}$  (Borsagli et al. 2015; Yuvaraja et al. 2017). From the preceding considerations, it is inferred that imine, NH and hydroxyl groups took part in the binding of Cr (VI). The observed changes in FTIR peak vibrations after the adsorption is presented in Table 4.8.

**Table 4.8 FTIR peak vibrations before and after adsorption on to CTSL-2**

<b>Adsorbent: CTSL-2</b>			
<b>Metal ion</b>	<b>Group</b>	<b>Wavenumber (cm<sup>-1</sup>) before adsorption</b>	<b>Wavenumber (cm<sup>-1</sup>) after adsorption</b>
<b>Pb (II)</b>	Hydroxyl-OH stretching	3627	3650
	C=O bending of N <sub>2</sub> HCOCH <sub>3</sub>	1639	1645
	Imine (C=N) stretching	1633	1627
	C-O stretching of secondary alcohol (C-O-H)	1062	1053
	C-O stretching of primary alcohol (C-O-H)	1002	987
	NH Secondary wagging	648	692
<b>Cu (II)</b>	Hydroxyl-OH stretching	3627	3650
	C=O bending of N <sub>2</sub> HCOCH <sub>3</sub>	1639	1647
	Imine (C=N) stretching	1633	1627
	C-O stretching of secondary alcohol (C-O-H)	1062	1058
	Primary Alcohol (C-O-H) C-O stretch	1002	1010
	NH Secondary wagging	648	694
<b>Cr (VI)</b>	Hydroxyl-OH stretching	3627	3614
	C=O bending of N <sub>2</sub> HCOCH <sub>3</sub>	1639	1685
	Imine (C=N) stretching	1633	1645
	C-O stretching of secondary alcohol (C-O-H)	1062	1072
	C-O stretching of primary alcohol (C-O-H)	1002	987
	NH Secondary wagging	648	667

The XRD spectra of CTSL-2 and the CTSL-2 metal complexes obtained after the adsorption process are presented in Figure 4.30. When compared to CTSL-2, the XRD spectra of CTSL-2-Cr and CTSL-2-Cu show broadening of the peak around  $2\theta=20^\circ$ . This may be attributed to the decrease in crystallinity after the metal complex formation. As per the literature, the decrease in crystallinity after the metal complex formation is due to the grafting reactions, breaking of hydrogen bonds and interaction with ions (Hussein et al. 2012; Jing et al. 2016). The XRD pattern for CTSL-2-Pb however, shows a few additional pronounced peaks at  $2\theta$  values of  $29.6^\circ$  and  $30.1^\circ$  indicating crystalline phase structure of CTSL-2-Pb complex.

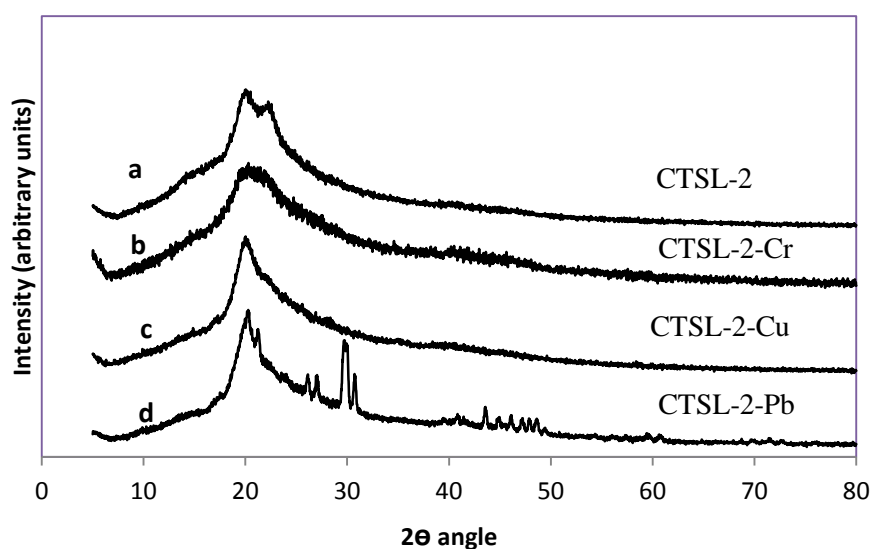


**Figure 4.30 XRD spectra of a) CTSL-2 b) CTSL-2-Cr c) CTSL-2-Cu d) CTSL-2-Pb**

### 4.3 STUDIES USING CHITOSAN DERIVATIVE CTSL-3

#### 4.3.1 Characterization of ligand L-3

The  $^1\text{H}$  NMR spectrum of the ligand (L-3) exhibited the following peaks.  $^1\text{H}$  NMR ( $\text{DMSO-d}_6$ )  $\delta$  (ppm): 13.622 (1 H, Pyrazole NH), 9.890 (1 H, Aldehyde), 7.220-7.702 (4 H, Ar. Ring), 8.290 (1 H, Pyrazole 5H), 2.370 (3 H, Methyl). The observed chemical shifts validated the successful synthesis of the ligand L-3.

### 4.3.2 Characterization of the chitosan derivative CTSL-3

#### 4.3.2.1 Solid state $^{13}\text{C}$ NMR analysis of CTSL-3

The  $^{13}\text{C}$  NMR of CTSL-3 (Figure 4.31) shows the characteristic peak for imine (C=N) at 162.6 ppm. The peaks assigned to carbon atoms in the aromatic and heterocyclic rings are represented between 119.6 ppm and 142.5 ppm. The intensity of the peak at 24.4 ppm is much more pronounced in the spectrum of CTSL-3 than in the spectrum of CTS (shown in Figure 4.2 a). This is attributed to the methyl group attached to the aromatic ring in the ligand L-3 due to which the overall concentration of the methyl group increased in CTSL-3. The analysis of peaks for CTSL-3 against CTS (Figure 4.31 and Figure 4.2 a respectively) reveals that the adsorbent (CTSL-3) has been successfully prepared.

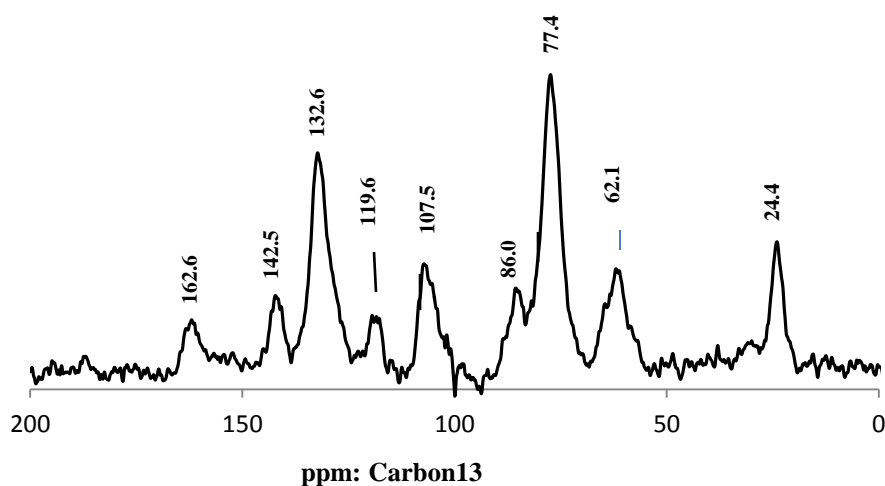


Figure 4.31  $^{13}\text{C}$  NMR of CTSL-3

#### 4.3.2.2 FTIR analysis

The FTIR spectra for CTSL-3 are shown in Figure 4.32 b. The various FTIR bands of CTSL-3 are as follows: the peak at  $3627\text{ cm}^{-1}$  is assigned to the stretching vibration of (-OH); the vibrations at  $1641\text{ cm}^{-1}$  and  $1633\text{ cm}^{-1}$  making up a shoulder band are assigned to amide I band of the acetamide units and the imine linker respectively (Zhang et al. 2016). The band at  $1485\text{ cm}^{-1}$  is due to aromatic ( $>\text{C}=\text{C}<$ )

stretch and ( $>C=N-$ ) stretching of the heterocyclic five-membered ring (Janssen and Ruyschaert 1958). The peak at  $1145\text{ cm}^{-1}$  is due to the C-O-C bridge vibrations. The peak at  $1080\text{ cm}^{-1}$  is assigned to the stretching vibrations of  $-C-O-H$  of the secondary alcohol. Similarly, the peak at  $1004\text{ cm}^{-1}$  is assigned to the stretching vibrations of  $-C-O-H$  of the primary alcohol. The band at  $817\text{ cm}^{-1}$  is due to aromatic ( $-CH$ ) out of plane bending. The peak at  $649\text{ cm}^{-1}$  is assigned to the secondary amide NH wagging vibrations (Stuart 2004).

The analysis of the post-adsorption FTIR spectrum is presented under section 4.3.3.5.



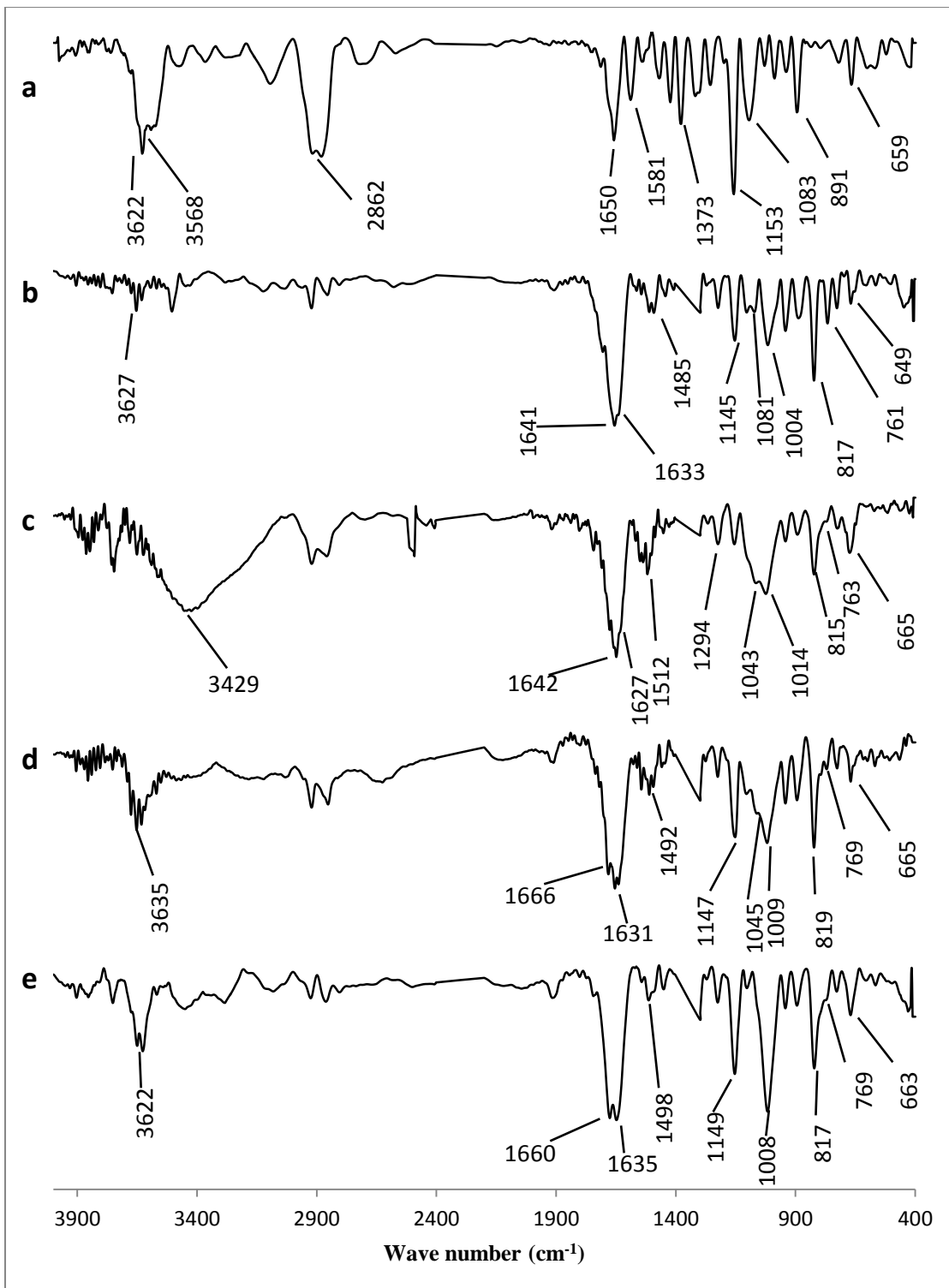


**Figure 4.32** FTIR spectra of a) Chitosan b) CTSL-3 c) CTSL-3-Pb d) CTSL-3-Cu e) CTSL-3-Cr

#### 4.3.2.3 XRD analysis

The powder X-ray diffraction pattern of CTSL-3 is presented in Figure 4.33. The disappearance of the peak at  $2\Theta=10^\circ$  which was present in the spectrum of CTS (refer figure 4.5 a), attributed to (-NH<sub>2</sub>) group is further evidence for the Schiff base reaction at the (-NH<sub>2</sub>) group (Webster et al. 2007; Hussein et al. 2012). The decrease in the intensity of the peak around  $2\Theta=20^\circ$  and the broadening of the peak for CTSL-3 indicates the decrease in crystallinity and increase in amorphous nature of CTSL-3 as compared to pure CTS. This was probably due to the weakening of hydrogen bonding interactions between the hydroxyl and amino groups of chitosan as a result of stereochemical hindrance of the side chains or the diminished concentrations of those groups (Liu et al. 2015).

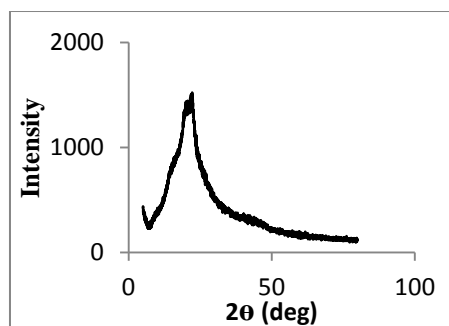


**Figure 4.33 XRD spectrum of CTSL-3**

#### 4.3.2.4 DSC Thermogram of CTSL-3

The DSC thermogram of CTSL-3 (Figure 4.34) shows two major exothermic peaks; a peak around 100°C is attributed to vaporisation of water present; a peak around 300°C is due to the degradation of the biopolymer derivative CTSL-3. Hence the CTSL-3 showed good thermal stability up to a temperature of about 250°C.

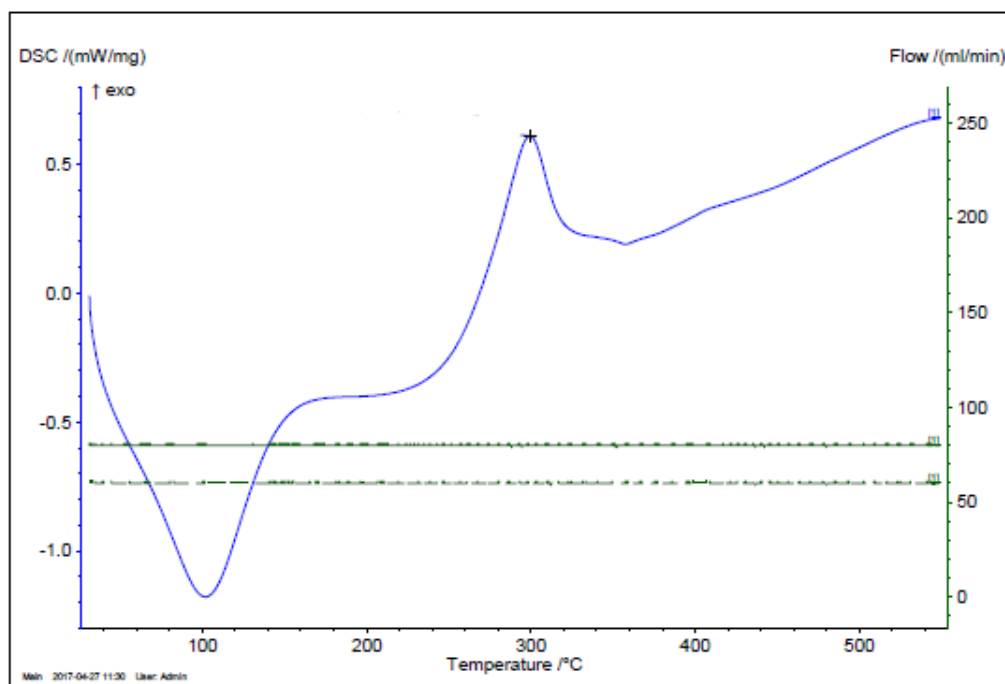


**Figure 4.34 DSC thermogram of CTSL-3**

### **4.3.3 Adsorption studies with CTSL-3**

#### **4.3.3.1 Effect of pH**

The initial pH is an important factor to be considered in the process of adsorption. The effect of pH on the sorption of the metal ions in the pH range on CTSL-3 is depicted in Figure 4.35.

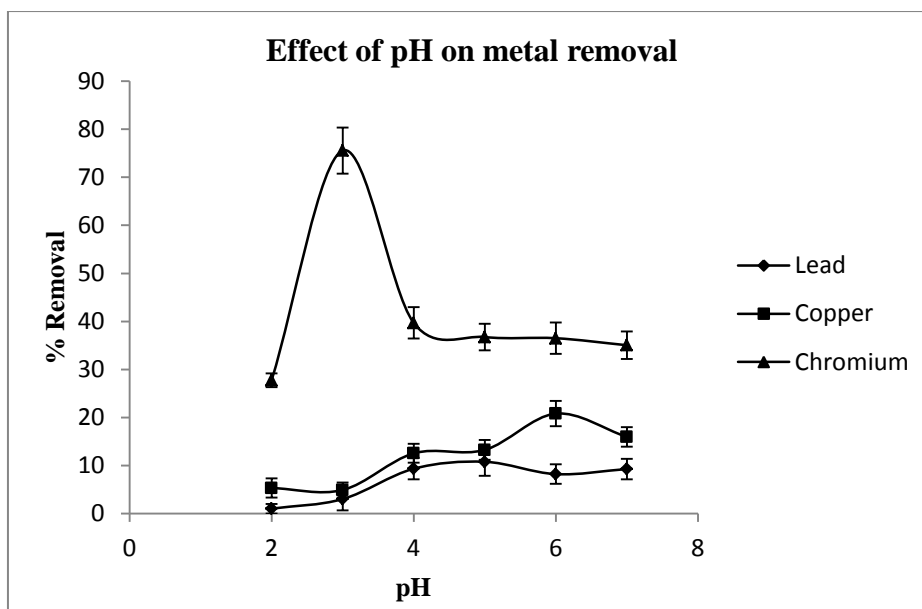


**Figure 4.35 Effect of pH on % removal (Initial concentration=100 mg/L; Temperature=303K; Ads. Dose=4 g/L; Agitation speed=150rpm; Contact time=24 h)**

The adsorption uptake of Cr (VI) onto CTSL-3 was found to be the highest at a pH of 3. For Pb (II) and Cu (II), the optimal pH values were observed to be 5 and 6 respectively. The optimum values of pH to be used for the equilibrium, kinetic and thermodynamic studies were taken as 3 for Cr (VI), 6 for Cu (II) and 5 for Pb (II).

#### 4.3.3.2 Adsorption equilibrium

The experiments in adsorption equilibrium were conducted following the method outlined in section 3.3.4 under Chapter 3; the quantity of metal ion removal was determined using the Eq. 3.1; the mathematical expressions of the adsorption isotherms used are given under section 2.6.1.

The experimental data were fitted to Langmuir, Freundlich and Redlich-Peterson isotherm models and the best fitting isotherm was determined by minimizing the sum of the squared errors. The results of the equilibrium studies are presented in Table 4.9, Figure 4.36, Figure 4.37 and Figure 4.38. The adsorption equilibria were best represented by Redlich Peterson isotherm in all the three metals- CTSL-3-Cr (VI) ( $r^2=0.9469$ ), CTSL-3-Cu (II) ( $r^2=0.9653$ ) and CTSL-3-Pb (II) ( $r^2=0.9782$ ). The maximum monolayer adsorption capacities ( $Q_0$ ) were 55.783 mg/g for Cr (VI), 45.614 mg/g for Cu (II) and 86.229 mg/g for Pb (II). The Langmuir separation factor  $R_L$

which was within 0-1 and the Freundlich exponent (n) which was in the range of 1-10 indicated that the adsorption process was favorable. The values obtained in this study for the parameter  $b_R$  in the Redlich-Peterson isotherm model were 0.881, 1.098 and 1.149 respectively, for the adsorption of Cr (VI), Cu (II) and Pb (II).

**Table 4.9 Equilibrium model parameters for adsorption of Cr (VI), Cu (II) and Pb (II) on CTSL-3**

Isotherm	Cr (VI)	Cu (II)	Pb (II)
<b>Langmuir Isotherm</b>			
$Q_o(\text{mg g}^{-1})$	55.783	45.614	86.229
$b(\text{L mg}^{-1})$	0.040	0.003	0.001
$r^2$	0.9241	0.9640	0.9762
$R_L$	0.0430-0.0004	0.4214-0.0072	0.4561-0.0083
<b>Freundlich Isotherm</b>			
$K_f(\text{mg g}^{-1})$	11.237	0.918	0.4718
n	3.935	1.861	1.457
$r^2$	0.9072	0.9412	0.9621
<b>Redlich-Peterson Isotherm</b>			
$K_R(\text{L g}^{-1})$	3.883	0.128	0.113
$a_R(\text{L mg}^{-1})$	0.147	0.0014	0.0004
$b_R$	0.881	1.098	1.149
$r^2$	0.9469	0.9653	0.9782

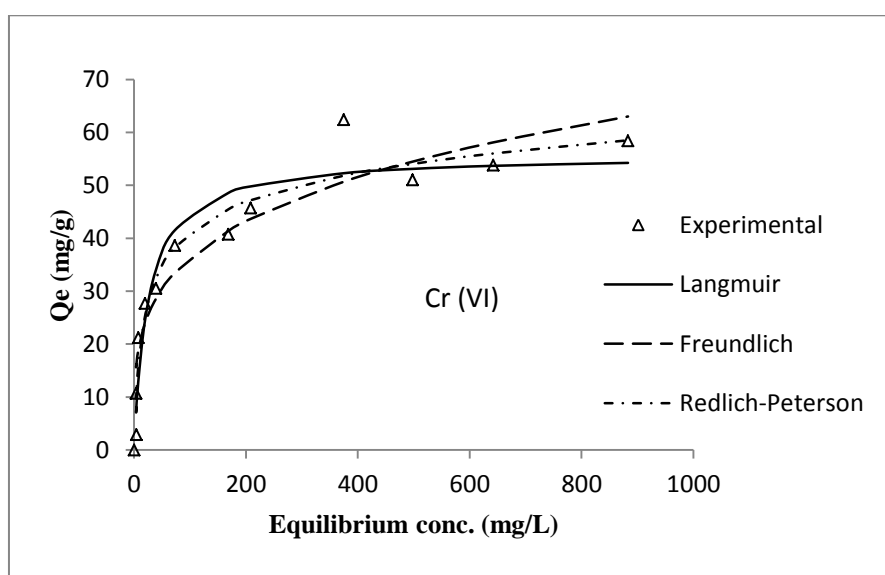


**Figure 4.36 Plot of various adsorption isotherms to CTSL-3-Cr (VI) adsorption data (Initial concentration=100 mg/L; Temperature=303K; pH=3; Ads. Dose=2g/L; Agitation speed=150rpm; Contact time=24h)**

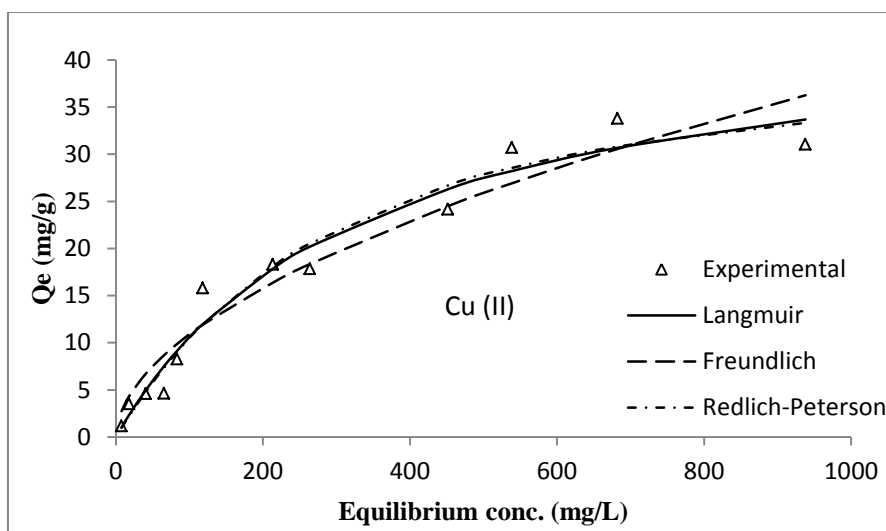


**Figure 4.37** Plot of various adsorption isotherms to CTSL-3-Cu (II) adsorption data (Initial concentration=100 mg/L; Temperature=303K; pH=6; Ads. Dose=2g/L; Agitation speed=150 rpm; Contact time=24 h)

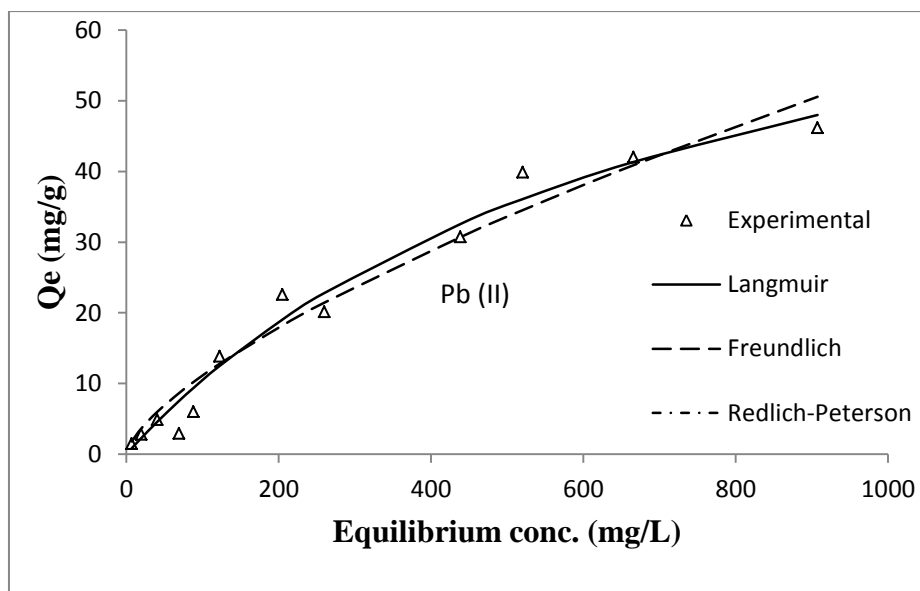


**Figure 4.38** Plot of various adsorption isotherms to CTSL-3-Pb (II) adsorption data (Initial concentration=100 mg/L; Temperature=303K; pH=5; Ads. Dose=2g/L; Agitation speed=150 rpm; Contact time=24 h)

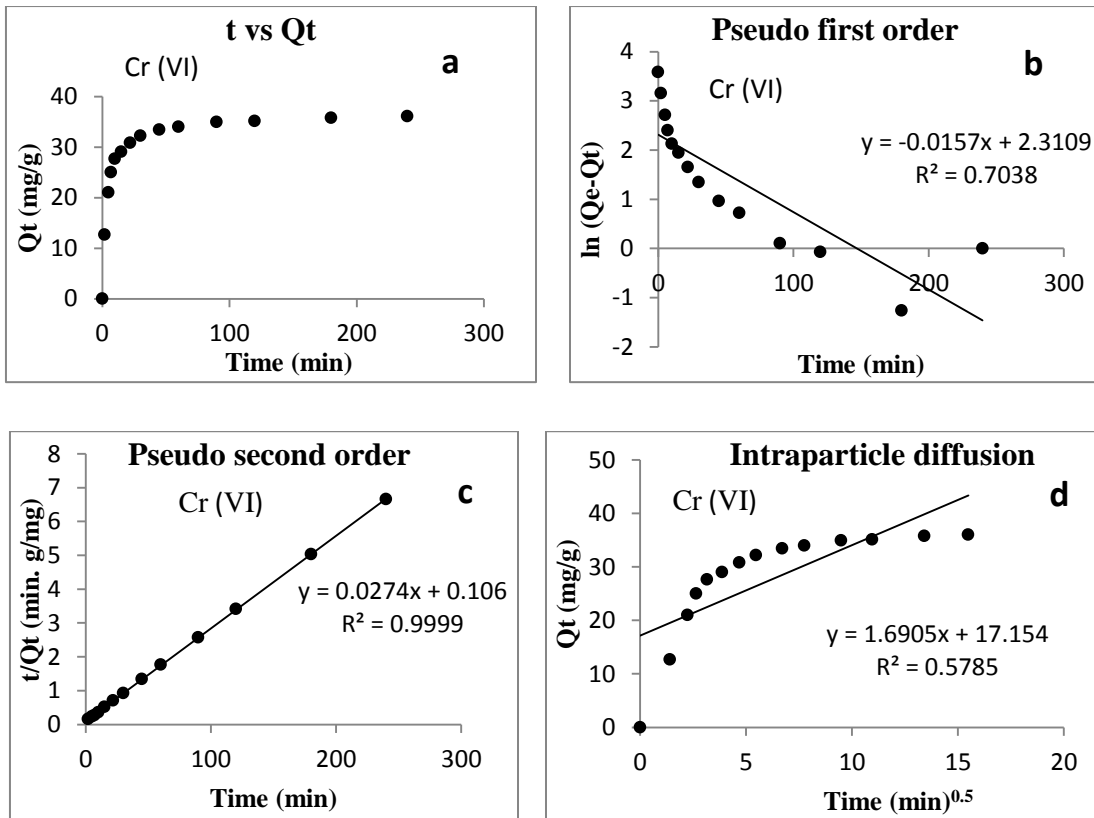
### 4.3.3.3 Adsorption kinetics

The adsorption kinetic study was conducted by following the procedure explained in section 3.3.5; Eq. 3.2 was used to determine the instantaneous, non-equilibrium adsorption capacity ( $Q_t$ ); the mathematical expressions of the kinetic models employed to fit the experimental data are given under section 2.6.2.

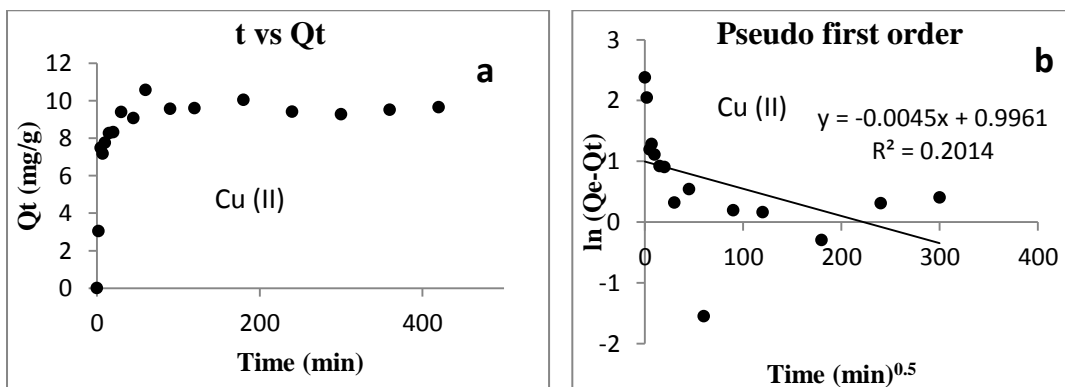
Among the three models which were investigated for the best fit with experimental data, the pseudo second order model gave excellent regression coefficient for all three metals (Cr (VI)  $r^2=0.9999$ ; Cu (II)  $r^2=0.9981$ ; Pb (II)  $r^2=0.9980$ ). The pseudo-second order rate constant ( $k_2$ ) obtained for Cr (VI), Cu (II) and Pb (II) were  $7.1 \times 10^{-3}$ ,  $136.0 \times 10^{-3}$  and  $11.2 \times 10^{-3} \text{ g mg}^{-1}\text{min}^{-1}$  respectively. The results of the kinetic study are presented in Table 4.10 and shown graphically in Figure 4.39, Figure 4.40 and Figure 4.41. The close correlation between the experimental and calculated values of  $Q_e$  in case of the pseudo-second order model further validates its applicability in describing the kinetics of the process. Low regression coefficients  $r^2$  were obtained for pseudo-first-order model and intraparticle diffusion models (Table 4.10). Large differences between the calculated adsorption capacities ( $Q_{e, \text{cal}}$ ) and the experimental adsorption capacities ( $Q_{e, \text{exp}}$ ) were observed indicating that this model is unsatisfactory in describing the kinetics of the adsorption process.

**Table 4.10 Kinetic model parameters for adsorption of Cr (VI), Cu (II) and Pb (II) onto CTSL-3**

<b>Kinetic Model</b>	<b>Cr (VI)</b>	<b>Cu (II)</b>	<b>Pb (II)</b>
<b>Pseudo First order</b>			
$Q_{e, \text{calc.}} (\text{mg g}^{-1})$	10.0750	2.7070	5.6110
$Q_{e, \text{expt}} (\text{mg g}^{-1})$	36.0460	10.7800	18.8390
$k_1 (\text{min}^{-1})$	0.0158	0.0045	0.0082
$r^2$	0.7038	0.2014	0.4940
<b>Pseudo second order</b>			
$Q_{e, \text{calc}} (\text{mg g}^{-1})$	36.4900	9.5100	18.4840
$Q_{e, \text{exp}} (\text{mg g}^{-1})$	36.0460	10.7800	18.8390
$k_2 (\text{g mg}^{-1}\text{min}^{-1})$	0.0071	0.1360	0.0112
$r^2$	0.9999	0.9981	0.9980
<b>Intraparticle diffusion</b>			
$K_{\text{id}} (\text{mg g}^{-1}\text{min}^{-1/2})$	1.6905	0.3449	0.8197
$C (\text{mg g}^{-1})$	17.1540	5.5303	7.9551
$r^2$	0.5785	0.4219	0.6106



**Figure 4.39** Plot of CTSL-3-Cr (VI) kinetic study data [a) Quantity adsorbed v/s time b) Pseudo-first order c) Pseudo-second order d) Intraparticle diffusion] (Initial concentration=100 mg/L; Temperature=303K; pH=3; Ads. Dose=2g/L; Agitation speed=150rpm)





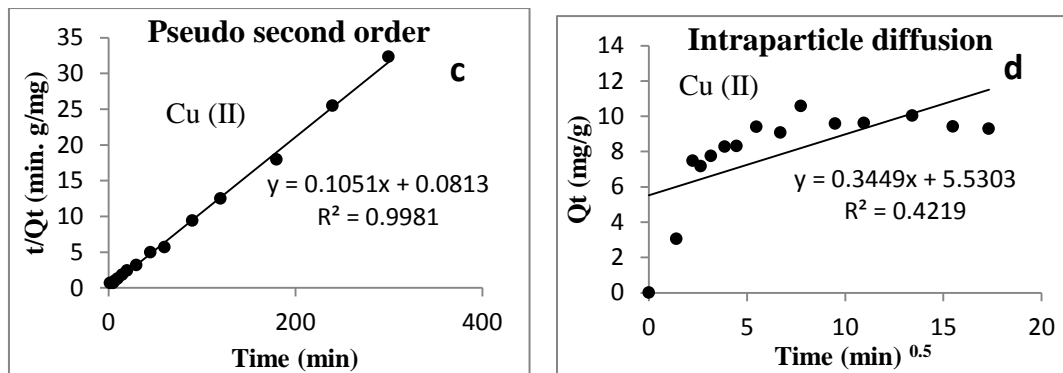


**Figure 4.40** Plot of CTSL-3-Cu (II) kinetic study data [a) Quantity adsorbed v/s time b) Pseudo-first order c) Pseudo-second order d) Intraparticle diffusion] (Initial concentration=100 mg/L; Temperature=303K; pH=6; Ads. Dose=2g/L; Agitation speed=150rpm)

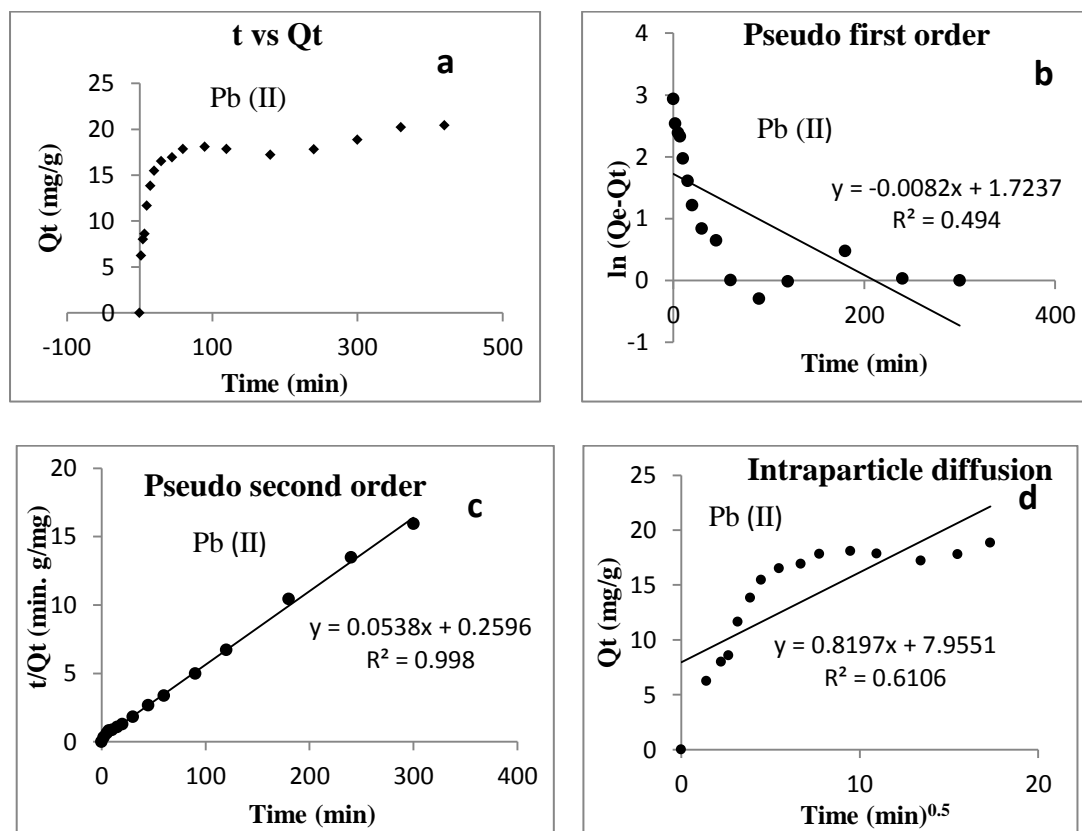


**Figure 4.41** Plot of CTSL-3-Pb (II) kinetic study data [a) Quantity adsorbed v/s time b) Pseudo-first order c) Pseudo-second order d) Intraparticle diffusion] (Initial concentration=100 mg/L; Temperature=303K; pH=5; Ads. Dose=2g/L; Agitation speed=150rpm)

#### 4.3.3.4 Adsorption thermodynamics

The thermodynamic studies were conducted following the experimental method outlined in section 3.3.6; further the equations used in calculations are provided under section 2.6.3.

The results of the thermodynamic study are presented in the Table 4.11. It is observed that the change in standard Gibb's free energy of adsorption is negative for the adsorption of all the three metal ions on to CTSL-3. This indicates that the adsorption process is spontaneous for all the metal ions that were studied.

**Table 4.11 Thermodynamic parameters for the adsorption of Cr (VI), Cu (II) and Pb (II) onto CTSL-3**

T (K)	$K_o$	$\Delta G^\circ$ (kJ.mol <sup>-1</sup> )	$\Delta H^\circ$ (kJ.mol <sup>-1</sup> )	$\Delta S^\circ$ (J.mol <sup>-1</sup> .K <sup>-1</sup> )
<b>Chromium</b>				
283.15	13992.825	-22.473	-13.109	32.619
293.15	9947.733	-22.435		
303.15	9561.501	-23.101		
313.15	7655.656	-23.284		
323.15	6762.852	-23.694		
<b>Copper</b>				
283.15	39.437	-8.651	31.317	145.487
293.15	175.195	-12.591		
303.15	244.203	-13.857		
313.15	188.991	-13.647		
323.15	284.377	-15.180		
<b>Lead</b>				
283.15	55.279	-9.446	0.334	36.740
293.15	125.186	-9.779		
303.15	63.854	-10.476		
313.15	53.330	-10.353		
323.15	86.194	-11.973		

The negative values of the change in standard enthalpy ( $\Delta H^\circ$ ) for the adsorption of Cr (VI) onto CTSL-3 signifies an exothermic process. The positive values of  $\Delta H^\circ$  indicate that the adsorption of Pb (II) and Cu (II) are endothermic in

nature. The net entropy change values obtained for Cr (VI), Cu (II) and Pb (II) were positive indicating that the net disorderliness increased after the adsorption process.

#### 4.3.3.5 Post-adsorption CTSL-3 characterization

The FTIR spectra of CTSL-3 and CTSL-3 metal complexes after adsorption are presented in Figure 4.32 b, c, d and e. The comparison of the FTIR spectra of CTSL-3 and CTSL-3 metal complexes shows the following differences. An adsorption peak in CTSL-3 around  $1641\text{ cm}^{-1}$  which is attributed to C=O of the acetamide group gets shifted to  $1642\text{ cm}^{-1}$  (CTSL-3-Pb),  $1666\text{ cm}^{-1}$  (CTSL-3-Cu) and  $1660\text{ cm}^{-1}$  (CTSL-3-Cr). A shoulder band in CTSL-3 around  $1633\text{ cm}^{-1}$  which is attributed to imine group ( $>\text{C}=\text{N}-$ ) gets shifted to  $1627\text{ cm}^{-1}$  (CTSL-3-Pb),  $1631\text{ cm}^{-1}$  (CTSL-3-Cu) and  $1635\text{ cm}^{-1}$  (CTSL-3-Cr); this is attributed to the participation of the imine group in metal complexation. (Wang et al. 2009b). The vibrations due to C-O stretching in the secondary alcohol (C-O-H) which was originally at  $1081\text{ cm}^{-1}$  is shifted to  $1043\text{ cm}^{-1}$  (CTSL-3-Pb), to  $1045\text{ cm}^{-1}$  (CTSL-3-Cu) and to  $1047\text{ cm}^{-1}$  (CTSL-3-Cr). Similarly, peak due to C-O stretching vibrations in the primary alcohol (C-O-H) at  $1004\text{ cm}^{-1}$  is shifted to  $1014\text{ cm}^{-1}$  (CTSL-3-Pb), to  $1009\text{ cm}^{-1}$  (CTSL-3-Cu) and to  $1008\text{ cm}^{-1}$  (CTSL-3-Cr) respectively. The peak at  $649\text{ cm}^{-1}$  which is assigned to secondary wagging vibrations of the NH group is shifted to  $665\text{ cm}^{-1}$  (CTSL-3-Pb), to  $665\text{ cm}^{-1}$  (CTSL-3-Cu) and  $663\text{ cm}^{-1}$  (CTSL-3-Cr) respectively (Borsagli et al. 2015; Yuvaraja et al. 2017). The preceding interpretations indicate that imine, hydroxyl and amine groups are responsible for heavy metal interactions. The observed changes in FTIR peak vibrations after the adsorption is presented in Table 4.12.

**Table 4.12 FTIR peak vibrations before and after adsorption on to CTSL-3**

<b>Adsorbent: CTSL-3</b>			
<b>Metal ion</b>	<b>Group</b>	<b>Wavenumber (cm<sup>-1</sup>) before adsorption</b>	<b>Wavenumber (cm<sup>-1</sup>) After adsorption</b>
<b>Pb (II)</b>	Hydroxyl-OH stretching	3627	3429
	C=O bending of NHCOCH <sub>3</sub>	1641	1642
	Imine (C=N) stretching	1633	1627
	C-O stretching of secondary alcohol (C-O-H)	1081	1043
	C-O stretching of primary alcohol (C-O-H)	1004	1014
	NH Secondary wagging	649	665
<b>Cu (II)</b>	Hydroxyl-OH stretching	3627	3635
	C=O bending of NHCOCH <sub>3</sub>	1641	1666
	Imine (C=N) stretching	1633	1631
	Secondary alcohol (C-O-H) C-O stretching	1081	1045
	Primary Alcohol (C-O-H) C-O stretch	1004	1009
	NH Secondary wagging	649	665
<b>Cr (VI)</b>	Hydroxyl-OH stretching	3627	3622
	C=O of NHCOCH <sub>3</sub> bending	1641	1660
	Imine (C=N) stretching	1633	1635
	Secondary alcohol (C-O-H) C-O stretching	1081	Combined single peak at 1008
	Primary Alcohol (C-O-H) C-O stretch	1004	
	NH Secondary wagging	649	663

The XRD spectra of CTSL-3 and the CTSL-3 metal complexes obtained after the adsorption process are presented in Figure 4.42. When compared to CTSL-3, the XRD spectra of CTSL-3-Cr and CTSL-3-Cu show broadening of the peak around  $2\theta=20^\circ$ . This may be attributed to the decrease in crystallinity after the metal complex formation. The XRD spectrum for CTSL-3-Pb however, shows a few small extra peaks which may be evidence of increase in crystallinity of CTSL-3-Pb as compared to CTSL-3.

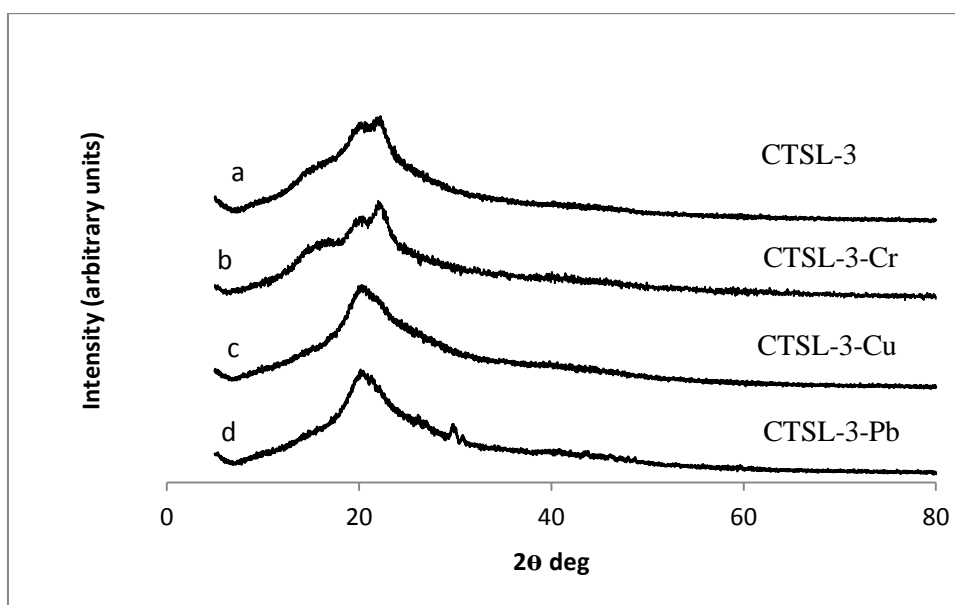


**Figure 4.42 XRD spectra of a) CTSL-3 b) CTSL-3-Cr c) CTSL-3-Cu d) CTSL-3-Pb**

#### 4.4 STUDIES USING CHITOSAN DERIVATIVE CTSL-4

##### 4.4.1 Characterization of ligand L-4

The ligand (L-4) was characterized by  $^1\text{H}$  NMR. (Figure 4.43) which exhibited the following peaks.  $^1\text{H}$  NMR ( $\text{DMSO-d}_6$ )  $\delta$  (ppm): 9.908 (1 H, Aldehyde), 7.556-7.914 (4 H, Ar. Ring), 8.484 (1 H, Pyrazole 5H). The expected broad peak at around 13.70 (1 H, Pyrazole NH) was not exhibited. Such disappearance of the peaks of labile groups like NH and OH is well known; it is attributed to the exchange of hydrogen atom of these groups by the deuterium atom present in the deuterated

solvent or in D<sub>2</sub>O. The observed proton NMR chemical shifts validate the successful formation of the ligand L-4.

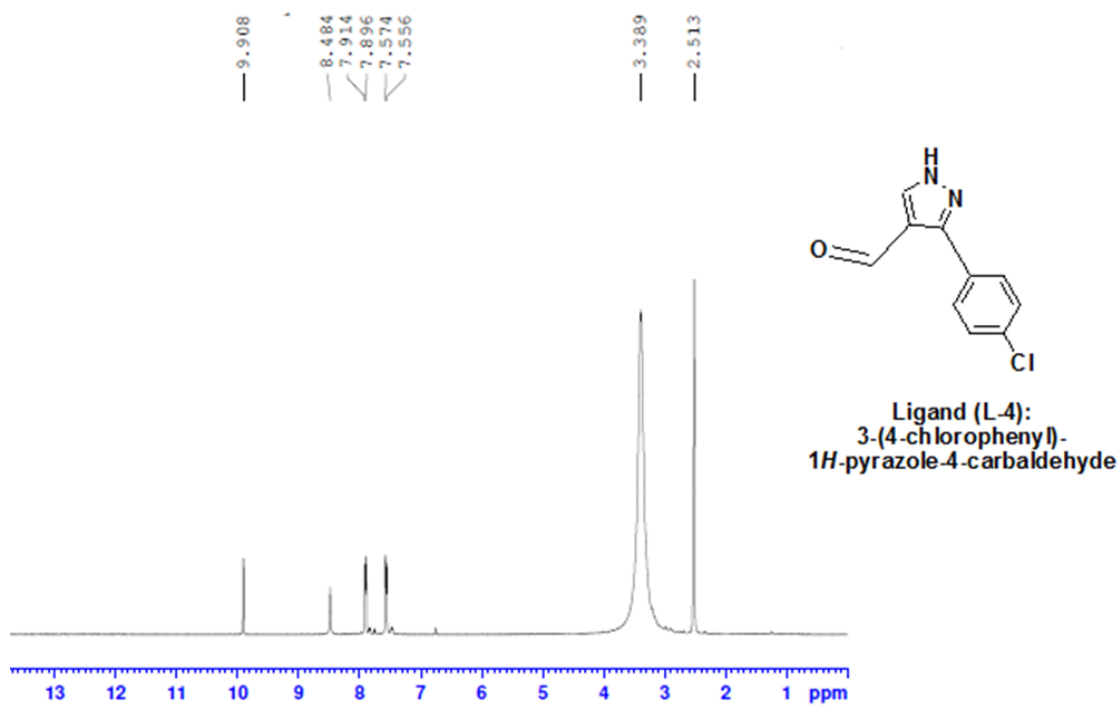
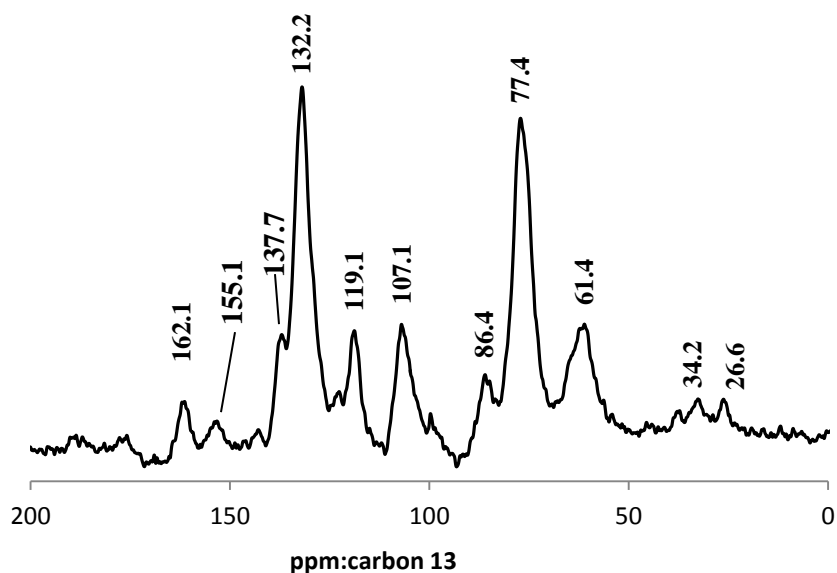


Figure 4.43 <sup>1</sup>H NMR spectrum of the ligand (L-4)

#### 4.4.2 Characterization of the chitosan derivative CTSL-4

##### 4.4.2.1 Solid state <sup>13</sup>C NMR analysis of CTSL-4

The <sup>13</sup>C NMR spectrum for CTSL-4 is as shown in Figure 4.44. When compared to the <sup>13</sup>C NMR of CTS (Figure 4.2 a), the spectrum of CTSL-4 shows an additional peak belonging to the imine (C=N) group at 162.1 ppm (Xiao and Zhou 2008). Further, a few more new peaks appear at 155.1, 137.77, 132.2 and 119.1 ppm which are signatures of the carbon in aromatic and the pyrazole ring. The new peaks validate the formation of the chitosan derivative CTSL-4 (Bekircan and Bektas 2008).



**Figure 4.44**  $^{13}\text{C}$  NMR of CTSL-4

#### 4.4.2.2 FTIR analysis

The FTIR spectra for CTSL-4 are shown in Figure 4.45 b. The peak at  $3629\text{ cm}^{-1}$  is due to the stretching vibrations of the hydroxyl group. The peak at  $1635\text{ cm}^{-1}$  represents the combined stretching vibrations of the C=O of the acetamide group and the stretching vibrations of the imine ( $>\text{C}=\text{N}-$ ) group. The peak at  $1149\text{ cm}^{-1}$  is assigned to the stretching vibrations of the C-O-C. The peaks at  $1091$  and  $1002\text{ cm}^{-1}$  are assigned to the stretching vibrations of the C-O-H in the secondary and primary alcohols of the polymer respectively. The peak at  $829\text{ cm}^{-1}$  is due to the out of plane bending vibrations of the benzene ring (Li et al. 2010). The peak at  $651\text{ cm}^{-1}$  is assigned to the secondary wagging vibrations of the  $\text{NH}_2$  group. The analysis of the post-adsorption FTIR spectrum is presented under section 4.4.3.5.

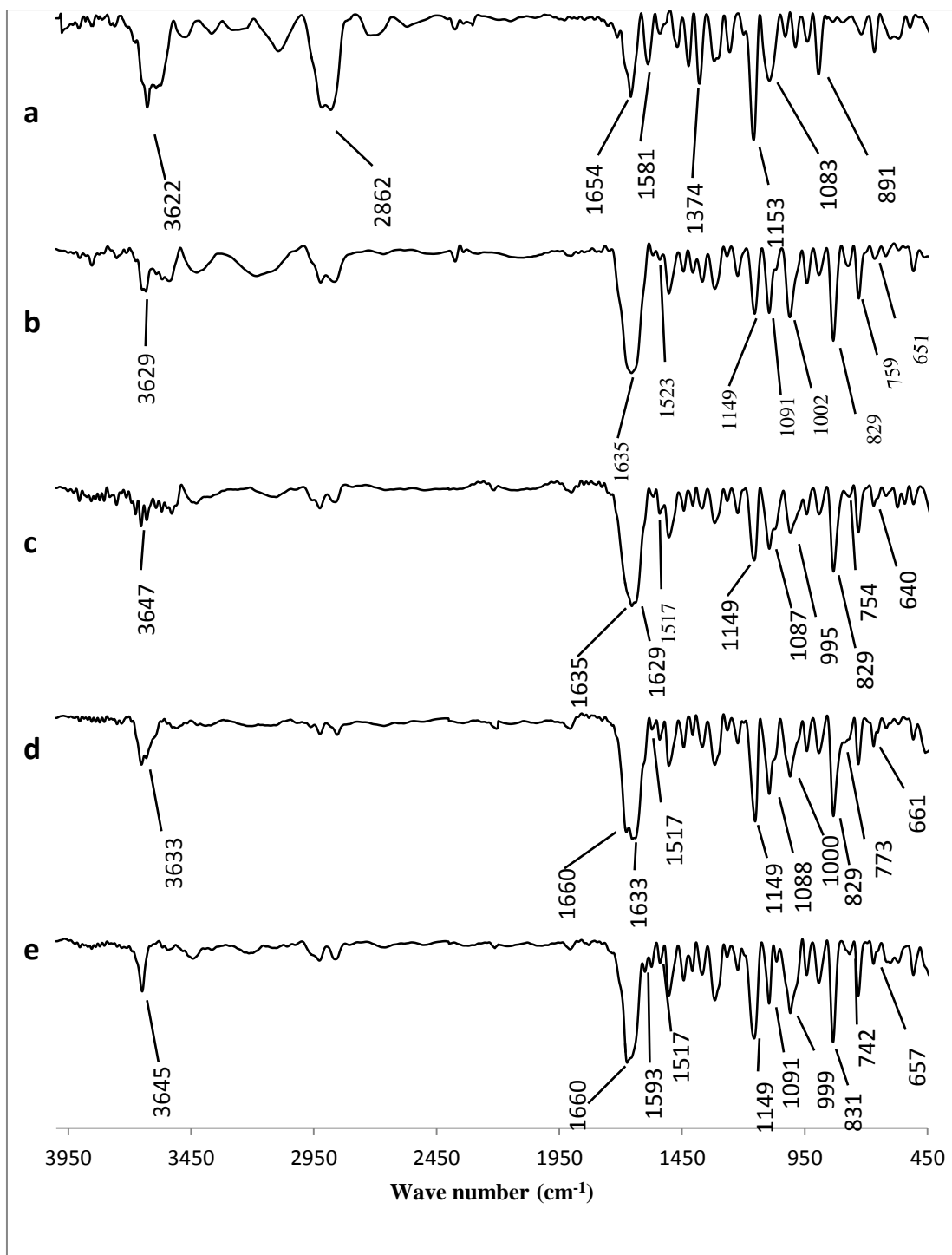


**Figure 4.45** FTIR spectra of a) Chitosan b) CTSL-4 c) CTSL-4-Pb d) CTSL-4-Cu  
e) CTSL-4-Cr



#### 4.4.2.3 XRD analysis

The powder X-ray diffraction plot of CTSL-4 is presented in Figure 4.46. When compared to the XRD spectrum of chitosan (Figure 4.5 a), the disappearance of the peak at  $2\theta=10^\circ$  which is attributed to (-NH<sub>2</sub>) group is further evidence for the Schiff base reaction at the (-NH<sub>2</sub>) group (Hussein et al. 2012). Further, the drastic decrease in peak intensity is evidence of strong decrease in the crystallinity of the CTSL-4 after the incorporation of the ligand L-4 in CTS, which in turn may be attributable to the weakening of the intermolecular hydrogen bonds between the hydroxyl and amino groups of the polymer chain after the grafting of the ligand (Jing et al. 2016).

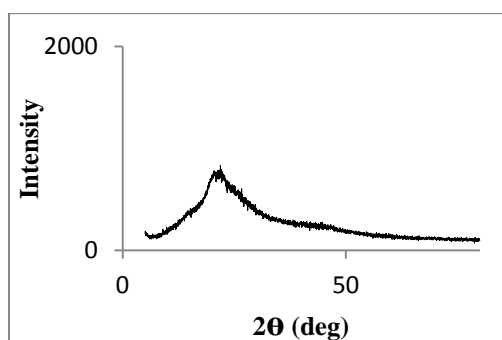


**Figure 4.46 XRD spectrum of CTSL-4**

#### 4.4.2.4 DSC Thermogram of CTSL-4

The DSC thermogram of CTSL-4 (Figure 4.47) shows two major exothermic peaks; a peak starting around 100°C is attributed to vaporisation of water present; a peak around 280°C is due to the degradation of the biopolymer derivative CTSL-4. When the thermograms of CTS (Figure 4.6 a) and CTSL-4 (Figure 4.47) are compared it is evident that the derivative CTSL-4 retains the thermal stability in spite of grafting of the ligand L-4 up to a temperature of ~240°C.

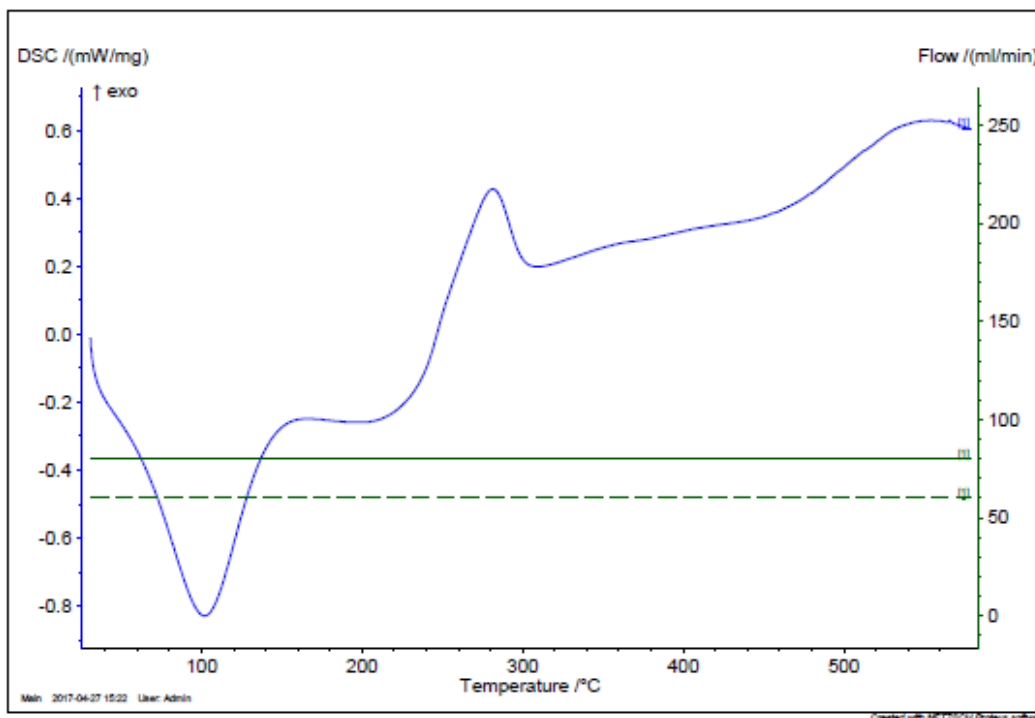


**Figure 4.47 DSC thermogram of CTSL-4**

### **4.4.3 Adsorption studies using CTSL-4**

#### **4.4.3.1 Effect of pH**

The effect of pH on sorption of the metal ions on CTSL-4 in the pH range 3-7 is shown in Figure 4.48. This pH range was selected because at pH < 3, the fragmentation of the adsorbent was observed and at pH > 7 metal precipitation may occur.

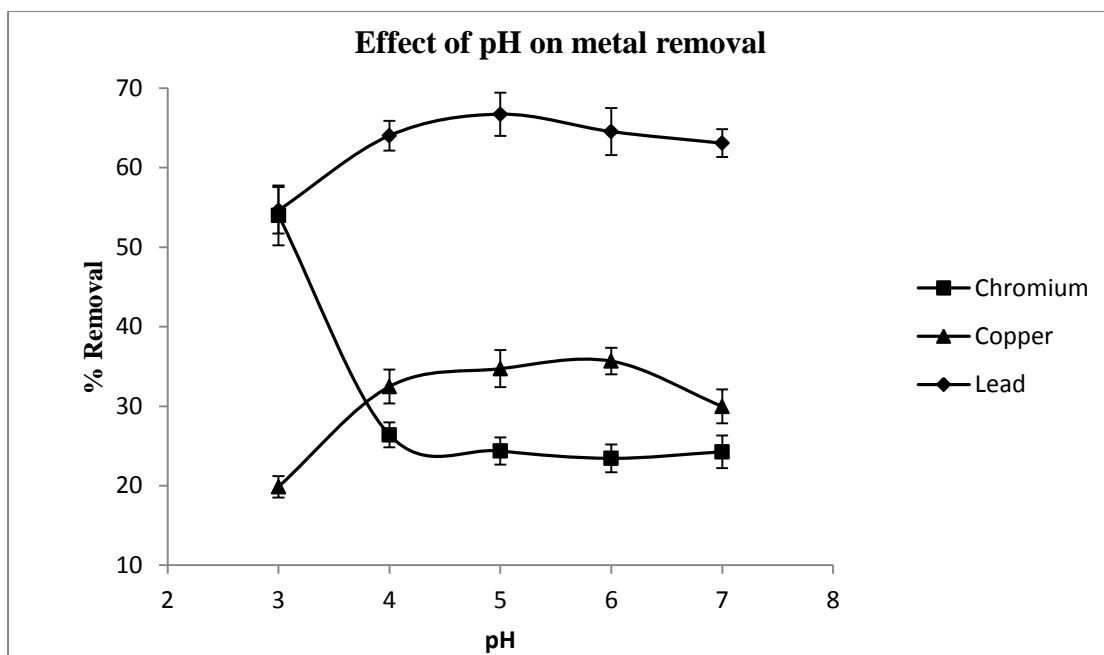


**Figure 4.48 Effect of pH on % removal (Initial concentration=100 mg/L; Temperature=303K; Ads. Dose=4 g/L; Agitation speed=150 rpm; Contact time=24h)**

The adsorption uptake of Cr (VI) onto CTSL-4 was found to be the highest at a pH of 3. For Pb (II) and Cu (II), the optimal pH values were observed to be 5 and 6 respectively. Based on the results of the pH study, the optimum values of pH to be used for the equilibrium, kinetic and thermodynamic studies were fixed as 3 for Cr (VI), 6 for Cu (II) and 5 for Pb (II).

#### 4.4.3.2 Adsorption equilibrium

The experiments in adsorption equilibrium were conducted following the method outlined in section 3.3.4 under Chapter 3; the quantity of metal ion removal was determined using the Eq. 3.1; the mathematical expressions of the adsorption isotherms used are given under section 2.6.1.

The results of the equilibrium studies are presented in Table 4.13, Figure 4.49, Figure 4.50 and Figure 4.51. For the removal of chromium and copper by CTSL-4, the adsorption equilibria were best represented by Redlich-Peterson isotherm. ( $r^2=0.9306$  for Cr (VI) and  $r^2=0.9621$  for Cu (II)). However, for the removal of lead, Langmuir isotherm best represented the experimental data ( $r^2=0.9608$ ).

**Table 4.13 Equilibrium model parameters for adsorption of Cr (VI), Cu (II) and Pb (II) on CTSL-4**

<b>Isotherm</b>	<b>Cr (VI)</b>	<b>Cu (II)</b>	<b>Pb (II)</b>
<b>Langmuir Isotherm</b>			
$Q_o(\text{mg g}^{-1})$	58.525	17.108	56.459
$b (\text{L mg}^{-1})$	0.0339	0.042	0.033
$r^2$	0.8908	0.9608	0.9608
$R_L$	0.0479-0.0005	0.1219-0.0014	0.0208-0.00013
<b>Freundlich Isotherm</b>			
$K_f(\text{mg g}^{-1})$	10.315	4.828	13.191
$n$	3.636	5.101	4.480
$r^2$	0.9062	0.8478	0.9138
<b>Redlich-Peterson Isotherm</b>			
$K_R (\text{L g}^{-1})$	4.843	0.633	5.702
$a_R (\text{L mg}^{-1})$	0.247	0.030	0.256
$b_R$	0.826	1.033	0.858
$r^2$	0.9306	0.9621	0.8928

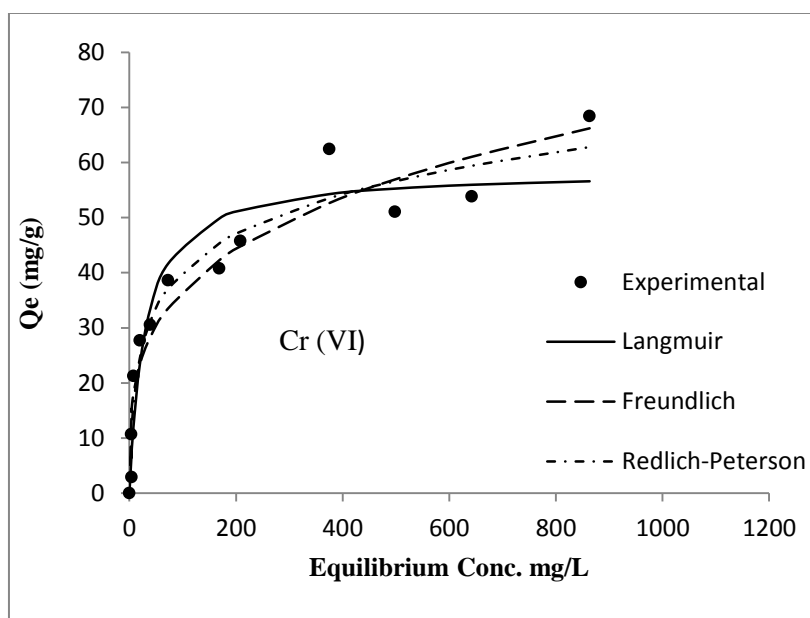


**Figure 4.49 Plot of various adsorption isotherms to CTSL-4-Cr (VI) adsorption data (Initial concentration=100 mg/L; Temperature=303K; pH=3; Ads. Dose=2g/L; Agitation speed=150 rpm; Contact time=24 h)**

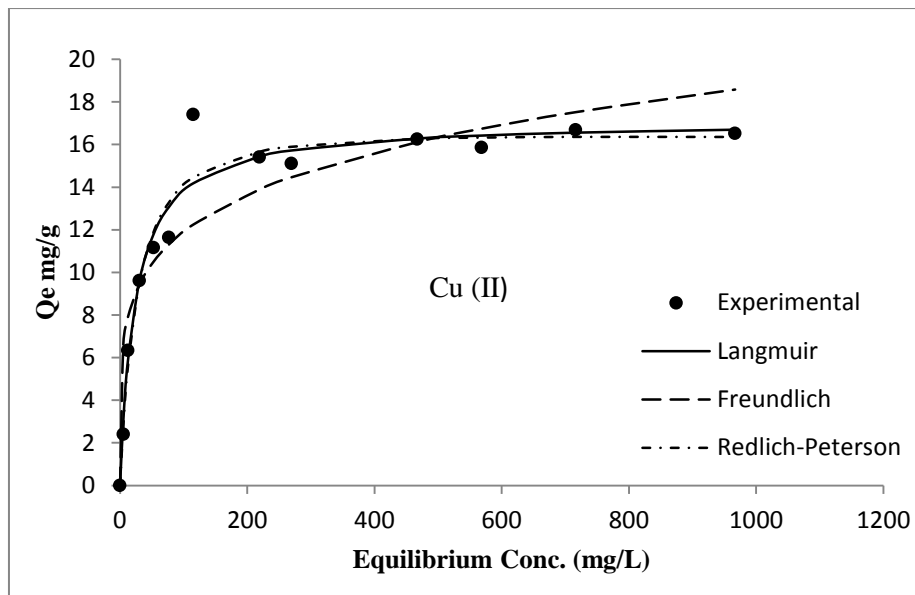


**Figure 4.50** Plot of various adsorption isotherms to CTSL-4-Cu (II) adsorption data (Initial concentration=100mg/L; Temperature=303K; pH=6; Ads. Dose=2g/L; Agitation speed=150rpm; Contact time=24h)

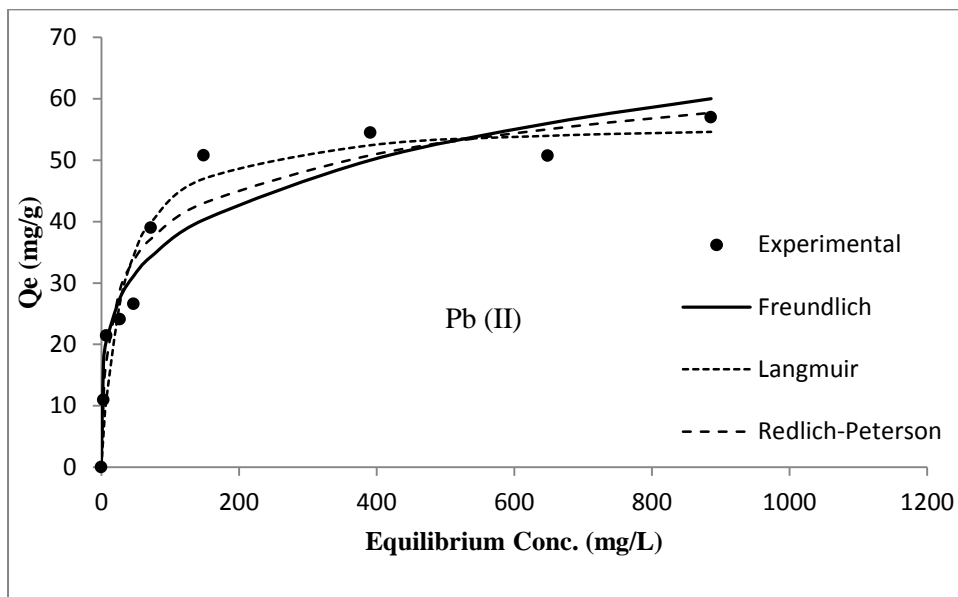


**Figure 4.51** Plot of various adsorption isotherms to CTSL-4-Pb (II) adsorption data (Initial concentration=100mg/L; Temperature=303K; pH=5; Ads. Dose=2g/L; Agitation speed=150rpm, Contact time=24h)

#### 4.4.3.3 Adsorption kinetics

The adsorption kinetic study was conducted by following the procedure explained in section 3.3.5; Eq. 3.2 was used to determine the instantaneous non-equilibrium adsorption capacity ( $Q_t$ ); the mathematical expressions of the kinetic

models employed to fit the experimental data are given in section 2.6.2 under Chapter 2.

The validity of three kinetic models was investigated for fitment with experimental data. The results of this study are presented in Table 4.14 and shown graphically in Figure 4.52, Figure 4.53, and Figure 4.54. The pseudo second order model was found to best represent the adsorption kinetics for all the three metal ions. (Cr (VI):  $r^2=0.9481$ ; Cu (II):  $r^2=0.9973$ ; Pb (II):  $r^2=0.9965$ ). In comparison, the pseudo-first order and the intraparticle diffusion models did not fit the experimental data satisfactorily. The calculated and experimental values of  $Q_e$  were far better correlated with each other in the case of the pseudo-second order model than with the pseudo-first order model. The pseudo-second order rate constants ( $k_2$ ) obtained for Cr (VI), Cu (II) and Pb (II) were  $7.9 \times 10^{-3}$ ,  $8.3 \times 10^{-3}$  and  $2.9 \times 10^{-3} \text{ g mg}^{-1}\text{min}^{-1}$  respectively.

**Table 4.14 Kinetic model parameters for adsorption of Cr (VI), Cu (II) and Pb (II) onto CTSL-4**

<b>Kinetic Model</b>	<b>Cr (VI)</b>	<b>Cu (II)</b>	<b>Pb (II)</b>
<b>Pseudo First order</b>			
$Q_{e, \text{ calc.}} (\text{mg g}^{-1})$	27.379	5.238	17.253
$Q_{e, \text{ expt.}} (\text{mg g}^{-1})$	38.049	9.827	34.121
$k_1 (\text{min}^{-1})$	0.0103	0.0132	0.0129
$r^2$	0.7267	0.9098	0.8789
<b>Pseudo second order</b>			
$Q_{e, \text{ calc}} (\text{mg g}^{-1})$	34.480	10.020	34.130
$Q_{e, \text{ exp}} (\text{mg g}^{-1})$	38.040	9.827	34.121
$k_2 (\text{g mg}^{-1}\text{min}^{-1})$	0.0079	0.0083	0.0029
$r^2$	0.9481	0.9973	0.9965
<b>Intraparticle diffusion</b>			
$K_{id} (\text{mg g}^{-1}\text{min}^{-1/2})$	2.3626	0.3938	1.5724
$C (\text{mg g}^{-1})$	2.2203	3.4558	11.938
$r^2$	0.8819	0.7497	0.6756

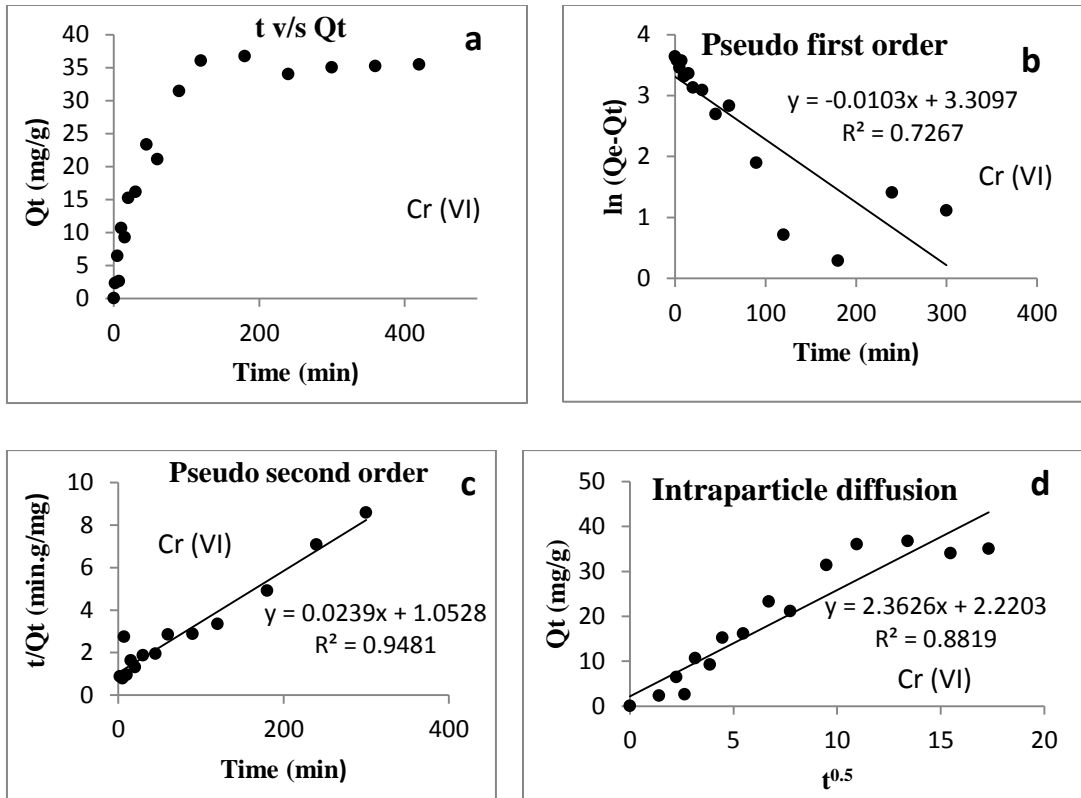
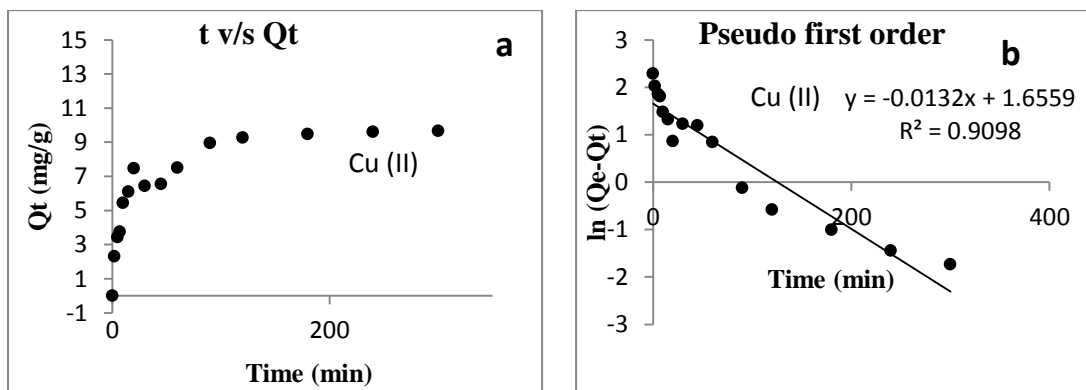
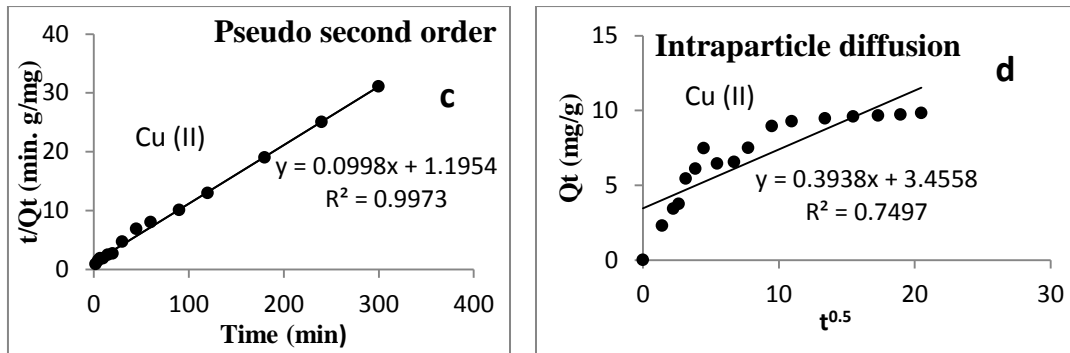
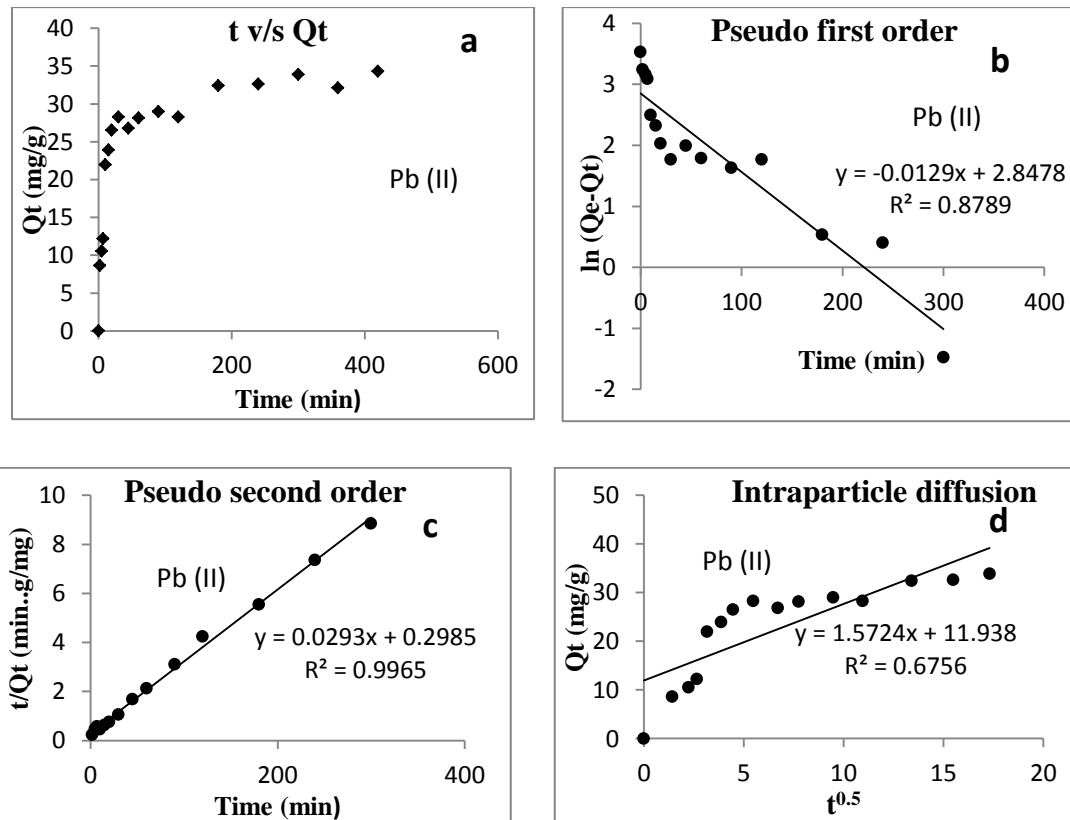


Figure 4.52 Plot of CTSL-4-Cr (VI) kinetic study data [a) Quantity adsorbed v/s time b) Pseudo-first order c) Pseudo-second order d) Intraparticle diffusion] (Initial concentration=100mg/L; Temperature=303K; pH=3; Ads. Dose=2g/L; Agitation speed=150rpm)





**Figure 4.53 Plot of CTSL-4-Cu (II) kinetic study data [a) Quantity adsorbed v/s time b) Pseudo-first order c) Pseudo-second order d) Intraparticle diffusion] (Initial concentration=100 mg/L; Temperature=303K; pH=6; Ads. Dose=2g/L; Agitation speed=150 rpm)**



**Figure 4.54 Plot of CTSL-4-Pb (II) kinetic study data [a) Quantity adsorbed v/s time b) Pseudo-first order c) Pseudo-second order d) Intraparticle diffusion] (Initial concentration=100 mg/L; Temperature=303K; pH=5; Ads. Dose=2g/L; Agitation speed=150rpm)**



#### 4.4.3.4 Adsorption thermodynamics

The thermodynamic studies were conducted following the experimental method outlined in section 3.3.6; the equations used in calculations are given under section 2.6.3 under Chapter 2.

The results of the thermodynamic study are presented in the Table 4.15. It is observed that the change in standard Gibb's free energy of adsorption is negative for all the three metals studied. This indicates that the adsorption process is spontaneous for all the metals that were studied.

**Table 4.15 Thermodynamic parameters for the adsorption of Cr (VI), Cu (II) and Pb (II) onto CTSL-4**

<b>T (K)</b>	<b>K<sub>o</sub></b>	<b>ΔG° (kJ.mol<sup>-1</sup>)</b>	<b>ΔH° (kJ.mol<sup>-1</sup>)</b>	<b>ΔS° (J.mol<sup>-1</sup>.K<sup>-1</sup>)</b>
<b>Chromium</b>				
283.15	5729.594	-20.371	-11.272	34.155
293.15	5414.306	-20.514		
303.15	3698.194	-20.707		
313.15	3935.133	-21.511		
323.15	4678.814	-22.705		
<b>Copper</b>				
283.15	98.820	-10.813	34.896	162.48
293.15	171.417	-12.537		
303.15	450.204	-15.399		
313.15	446.304	-15.884		
323.15	593.300	-17.156		
<b>Lead</b>				
283.15	2885.634	-18.756	12.592	110.476
293.15	3286.900	-20.300		
303.15	3598.240	-20.637		
313.15	5348.653	-22.350		
323.15	5181.760	-22.979		

The change in standard enthalpy ( $\Delta H^\circ$ ) for the adsorption of Cr (VI) onto CTSL-4 is negative which means that the adsorption process is exothermic. For the adsorption of Pb (II) and Cu (II) the positive values of  $\Delta H^\circ$  indicate that the adsorption is endothermic in nature. The change in standard entropy is positive for all the three metals which means that disorderliness increased after the adsorption process.

#### 4.4.3.5 Post-adsorption CTSL-4 characterization

The FTIR spectra of CTSL-4 and metal complexes CTSL-4-Pb, CTSL-4-Cu and CTSL-4-Cr after adsorption are presented in Figure 4.45 b, c, d and e. The comparison of the spectra shows the following differences: A combined broad band in CTSL-4 around  $1635\text{ cm}^{-1}$  which is attributed to combined imine group ( $>\text{C}=\text{N}-$ ) stretching vibrations with  $\text{C}=\text{O}$  bending vibrations of the acetamide group gets split into  $1635\text{ cm}^{-1}$  and  $1629\text{ cm}^{-1}$  in the case of CTSL-4-Pb;  $1660\text{ cm}^{-1}$  and  $1633\text{ cm}^{-1}$  in the case of CTSL-4-Cu;  $1660\text{ cm}^{-1}$  and  $1593\text{ cm}^{-1}$  in the case of CTSL-4-Cr. Further, the peak at  $1002\text{ cm}^{-1}$  assigned to C-O stretching vibrations of the primary alcohol (C-O-H) is shifted to  $995\text{ cm}^{-1}$  (CTSL-4-Pb),  $1000\text{ cm}^{-1}$  (CTSL-4-Cu) and  $999\text{ cm}^{-1}$  (CTSL-4-Cr). The peak at  $651\text{ cm}^{-1}$  attributed to the secondary NH wagging vibrations is also shifted to  $640\text{ cm}^{-1}$  (CTSL-4-Pb),  $661\text{ cm}^{-1}$  (CTSL-4-Cu) and  $657\text{ cm}^{-1}$  (CTSL-4-Cr) (Borsagli et al. 2015; Yuvaraja et al. 2017). The observed changes in FTIR peak vibrations after the adsorption are presented in Table 4.16.

**Table 4.16 FTIR peak vibrations before and after adsorption on to CTSL-4**

<b>Adsorbent: CTSL-4</b>			
<b>Metal ion</b>	<b>Group</b>	<b>Wavenumber (<math>\text{cm}^{-1}</math>) before adsorption</b>	<b>Wavenumber (<math>\text{cm}^{-1}</math>) after adsorption</b>
<b>Pb (II)</b>	Hydroxyl-OH stretching	3629	3647
	C=O bending of $\text{NHCOCH}_3$ group	1635	1635
	imine (C=N) stretching	1635	1629
	C-O stretching of secondary alcohol (C-O-H)	1091	1087
	C-O stretching of primary alcohol (C-O-H)	1002	995
	NH Secondary wagging	651	640

<b>Cu (II)</b>	Hydroxyl-OH stretching	3629	3633
	C=O bending of N <sub>2</sub> HCOCH <sub>3</sub> group	1635	1660
	imine (C=N) stretching	1635	1633
	C-O stretching of secondary alcohol (C-O-H)	1091	1088
	C-O stretching of primary alcohol (C-O-H)	1002	1000
	NH Secondary wagging	651	661
<b>Cr (VI)</b>	Hydroxyl-OH stretching	3629	3645
	C=O bending of N <sub>2</sub> HCOCH <sub>3</sub>	1635	1660
	Imine (C=N) stretching	1635	1593
	C-O stretching of secondary alcohol (C-O-H)	1091	1091 (no change)
	C-O stretching of primary alcohol (C-O-H)	1002	999
	NH Secondary wagging	651	657

The XRD spectra of CTSL-4 and the CTSL-4 metal complexes obtained after the adsorption process are presented in Figure 4.55. When compared to CTSL-4, the XRD spectra of all the three complexes show broadening of the peak around  $2\theta=20^\circ$ . This may be attributed to the decrease in crystallinity after the metal complex formation. The XRD spectrum for CTSL-4-Pb however, shows a few extra peaks including a high intensity peak at  $2\theta=29.94^\circ$  which may be evidence of increase in crystallinity of CTSL-4-Pb as compared to CTSL-4. Trimukhe and Varma (2008) have reported similar XRD pattern for chitosan-Pb complexes.

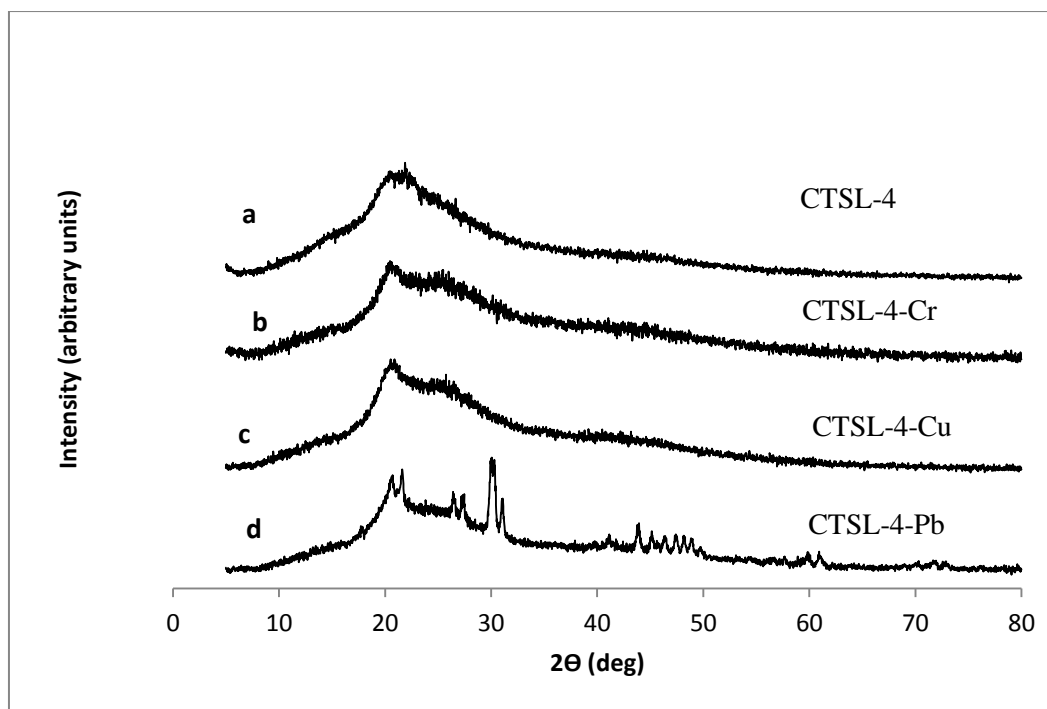


**Figure 4.55 XRD spectra of a) CTSL-4 b) CTSL-4-Cr c) CTSL-4-Cu  
d) CTSL-4-Pb**

#### **4.5 SUMMARY OF ADSORPTION STUDIES CARRIED OUT**

Four new chitosan derivatives CTSL-1, CTSL-2, CTSL-3 and CTSL-4 were synthesized employing the Schiff base reaction by reacting chitosan with 4 new 1H-pyrazole-4-carbaldehyde bearing ligands (L-1, L-2, L-3, L-4). The chemical structures of the ligands (L-1, L-2, L-3 and L-4) were validated from the  $^1\text{H}$  NMR analysis. The new chitosan derivatives were characterized by  $^{13}\text{C}$  NMR, FTIR, powder XRD spectra and DSC analysis. The  $^{13}\text{C}$  NMR study confirmed the successful synthesis of the chitosan derivatives. Pre and post adsorption comparison of the adsorbent by FTIR and XRD analysis was carried out. There was a general decrease in the intensity, and broadening of the XRD spectrum for the chitosan derivatives which meant that there was a general reduction in crystallinity, and increase in amorphous nature as compared to pure chitosan. Equilibrium, kinetic and thermodynamic batch studies were carried out to investigate the suitability of the new derivatives as adsorbents for the removal of Cr (VI), Cu (II) and Pb (II) from aqueous solutions. In the equilibrium study the Langmuir, Freundlich and Redlich-Peterson isotherm models were fitted to experimental data and the best isotherm model was identified. In

the kinetics study, three kinetic models viz. pseudo-first order, pseudo-second order and intraparticle diffusion models were fitted to the experimental kinetic data to determine the best fitting model. In the thermodynamic study, the feasibility, the changes in standard enthalpy and entropy of the adsorption process was investigated and various important thermodynamic parameters have been estimated. Possible mechanisms for the metal uptake by the adsorbent have been proposed by us from the FTIR study.

In the pH study, the pH range of 3-7 was chosen. This was because at very low pH values ( $\leq 2$ ), there was evidence of fragmentation of the adsorbent and at higher pH values outside the range, there was indication of metal precipitation. This is consistent with reported literature. The adsorption equilibrium was favoured at pH=3 for Cr (VI), pH=6 to 7 for Cu (II) and pH=4 to 6 for Pb (II). Ng et al. (2003) have shown that for fitting equilibrium isotherm models, nonlinear method of analysis with error values gives better results as isotherms are essentially nonlinear entities. For this reason nonlinear method of analysis using MICROSOFT EXCEL was chosen for fitting isotherm models. A comparison of monolayer adsorption capacities  $Q_o$  of CTSL-1, CTSL-2, CTSL-3 and CTSL-4 is obtained for the adsorption of Cu (II), Pb (II) and Cr (VI) are presented in Table 4.17 along with other results.

The pseudo-second order kinetic model was observed to best describe the adsorption kinetics for all three metals studied for all four derivatives. The consistently high values of regression coefficient ( $r^2$ ) obtained provide conviction to the applicability of this model. This model was successful in predicting the kinetics of the adsorption process over the entire contact time range of 24 h. From the FTIR analysis, the removal of metals was attributed to the imine, amine and hydroxyl functional groups.

The maximum monolayer adsorption capacities obtained for the three metals and the derivatives were 63.5 mg/g for Cr (VI) (by CTSL-2), 91.7 mg/g for Pb (II) (by CTSL-2) and 45.6 mg/g for Cu (II) (by CTSL-3). The regression coefficients obtained in fitting the adsorption isotherms for the experimental equilibrium data for the four adsorbents are tabulated in Table 4.18. The values shown in boldface correspond to the best fitting adsorption isotherm to the equilibrium experimental data, for a particular metal and a given adsorbent. The results of the thermodynamic study

indicated the spontaneous nature of adsorption. It was observed that the adsorption of chromium was exothermic and favoured at lower temperatures whereas that of copper and lead were endothermic in nature and favoured at higher temperatures.

The results of all the adsorption studies are summarily presented in Table 4.17. The values entered in boldface refer to the highest monolayer adsorption capacity obtained for the removal of a given metal across all the four chitosan derivatives studied.

**Table 4.17 Summary of results of adsorption studies**

Adsorbent (M.Wt.)	Metal	Optimum pH	Maximum monolayer adsorption capacity (mg/g)	Best fitting isotherm model	Best fitting kinetic model	Thermodynamic parameters	
						$\Delta H^\circ$ (kJ/mol <sup>-1</sup> )	$\Delta S^\circ$ (J/mol <sup>-1</sup> K)
<b>CTSL-1</b> (345)	Cr (VI)	3.0	57.9	Langmuir	Pseudo second order	-10.898	30.460
	Pb (II)	4.0	72.0	Redlich-Peterson	-do-	21.044	129.797
	Cu (II)	7.0	40.6	Redlich-Peterson	-do-	33.293	158.765
<b>CTSL-2</b> (315)	Cr (VI)	3.0	<b>63.5</b>	Redlich-Peterson	-do-	-11.606	35.514
	Pb (II)	6.0	<b>91.7</b>	Freundlich	-do-	58.417	245.421
	Cu (II)	6.0	37.0	Redlich-Peterson	-do-	41.336	182.534
<b>CTSL-3</b> (329)	Cr (VI)	3.0	55.8	Redlich-Peterson	-do-	-13.109	32.619
	Pb (II)	5.0	86.2	Redlich-Peterson	-do-	0.334	36.740
	Cu (II)	6.0	<b>45.6</b>	Redlich-Peterson	-do-	31.317	145.487
<b>CTSL-4</b> (349.5)	Cr (VI)	3.0	58.5	Redlich-Peterson	-do-	-11.272	34.155
	Pb (II)	5.0	56.4	Langmuir	-do-	12.592	11.476
	Cu (II)	6.0	17.0	Redlich-Peterson	-do-	34.896	162.48

**Table 4.18 Regression coefficient values obtained for various adsorbents for the fitment of adsorption isotherms to experimental data**

Adsorbent	Isotherm model	Cr (VI)	Cu (II)	Pb (II)
CTSL-1	Langmuir	0.9708	0.9620	0.8910
	Freundlich	0.7824	0.8960	0.9270
	Redlich Peterson	<b>0.9709</b>	<b>0.9630</b>	<b>0.9290</b>
CTSL-2	Langmuir	0.9390	0.9603	0.9628
	Freundlich	0.9569	0.9622	<b>0.9716</b>
	Redlich Peterson	<b>0.9849</b>	<b>0.9676</b>	0.9708
CTSL-3	Langmuir	0.9241	0.9640	0.9762
	Freundlich	0.9072	0.9412	0.9621
	Redlich Peterson	<b>0.9469</b>	<b>0.9653</b>	<b>0.9782</b>
CTSL-4	Langmuir	0.8908	0.9608	<b>0.9608</b>
	Freundlich	0.9062	0.8478	0.9138
	Redlich Peterson	<b>0.9306</b>	<b>0.9621</b>	0.8928

#### 4.6 SWELLING STUDIES AND BULK DENSITY MEASUREMENT

The effect of grafting of the ligands on swelling percentage was determined by conducting swelling experiments which were performed at two different pH values of 3 and 6, as per the procedure reported by Kyzas and Delianni (2013). Accordingly, accurately weighed 1 g of adsorbent was immersed in double distilled water whose pH had been pre-adjusted for the required pH and left to be swollen for 24h. The required pH was achieved with HCl and NaOH solutions. After the specified time, the swollen samples were filtered, and weighed after gently removing the moisture sticking to the surface with filter paper. The swelling percentage (SP, %) was then calculated using Eq. 4.1.

$$SP (\%) = \left( \frac{W_s - W}{W} \right) \cdot 100 \quad (4.1)$$

where 'W<sub>s</sub>' (g) is the weight of the swollen sample, and 'W'(g) is the initial weight of the sample before swelling. The results of the swelling experiments are tabulated in Table 4.19. The values obtained for percentage swelling for pure chitosan were 398.5

at pH 6 and 346.0 at pH 3. In comparison, the corresponding values for the four chitosan derivatives were between 10.6 and 108.5 which were significantly lower. The lowest percentage of swelling obtained at pH=3 was 10.6 for CTSL-1 and at pH=6, it was 19.43 for CTSL-2.

The bulk density was measured by taking samples in a specified size range (-72+170 #) and measuring the weight of a known volume. When compared to pure chitosan (247.17 kg/m<sup>3</sup>), the bulk densities of the chitosan derivatives were found to be higher by a factor of 2.35 to 2.80. It has been reported by No et al. (2000) that the water binding capacity of chitosan and hence its swelling is inversely correlated with bulk density ( $r = -0.939$ ,  $p < 0.01$ ).

**Table 4.19 Percentage of swelling and bulk density of chitosan and chitosan derivatives**

Description	CTS	CTSL-1	CTSL-2	CTSL-3	CTSL-4
% of swelling (pH=6)	398.5 ± 9	<b>10.6 ± 2.0</b>	59.2 ± 1.8	48.5 ± 1.5	84.2 ±
% of swelling (pH=3)	346.0 ± 8.5	26.0 ± 1.6	<b>19.43 ± 1.4</b>	38.6 ± 1.8	108.9 ± 2.5
Bulk Density (kg/m <sup>3</sup> )	247.13 ± 5.0	<b>691.02 ± 12.5</b>	641.66 ± 7.2	580.20 ± 7.2	663.54 ± 7.3
Increase in bulk density of the chitosan- derivative compared to chitosan (X times)	—	<b>2.80</b>	2.60	2.35	2.68



# **PART B**

## **Membrane studies**



*Part B comprises of the results and discussion of the studies performed with polysulfone membranes blended with CTSL-2 as the additive. The characterization of the blend membranes by SEM, contact angle measurement and XRD is presented followed by permeation studies and anti-fouling studies. Finally, heavy metal rejection studies are presented at the end of the chapter.*

#### **4.7 STUDIES USING POLYSULFONE MEMBRANES BLENDED WITH CTSL-2**

Pure polysulfone (PSf) membranes are known to exhibit poor permeability and high fouling. We explored the possibility of improving the permeation characteristics of polysulfone membranes by using the chitosan derivative CTSL-2 as an additive. The choice of CTSL-2 was guided by two factors. First, during the adsorption studies, CTSL-2 gave the maximum monolayer adsorption capacity for the removal of two heavy metals viz. Cr (VI) and Pb (II) among the three metals studied; for Cu (II) removal, CTSL-3 was marginally better than CTSL-2. Second, in its structure CTSL-2 has no alkyl group (CH<sub>3</sub>) unlike CTSL-3. The alkyl group is known to decrease the hydrophilicity of the polymer (Cunha and Gandini 2010). Since we were looking for materials that enhanced hydrophilicity, CTSL-2 was chosen as the additive material for blending purposes.

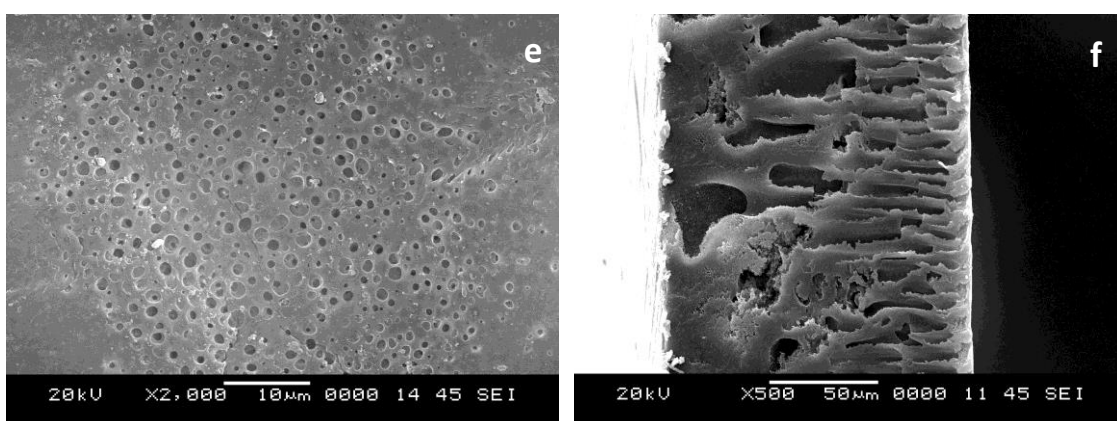
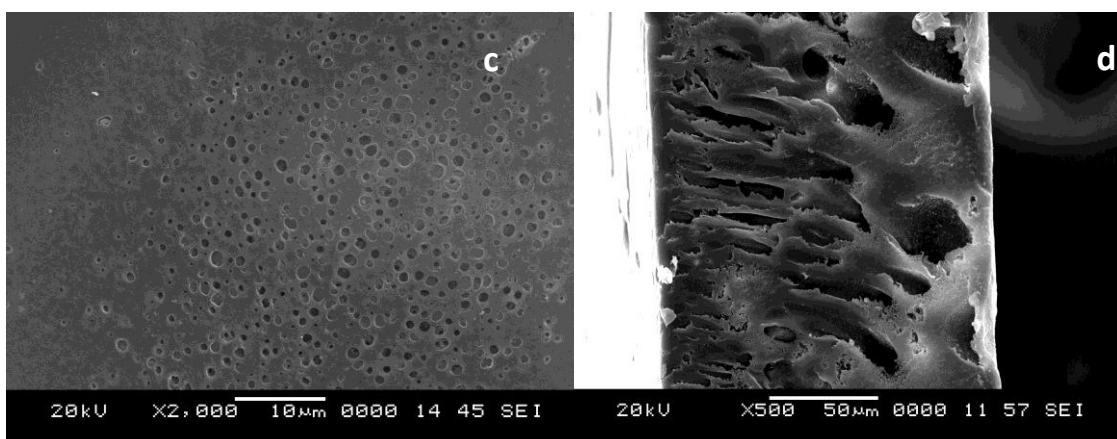
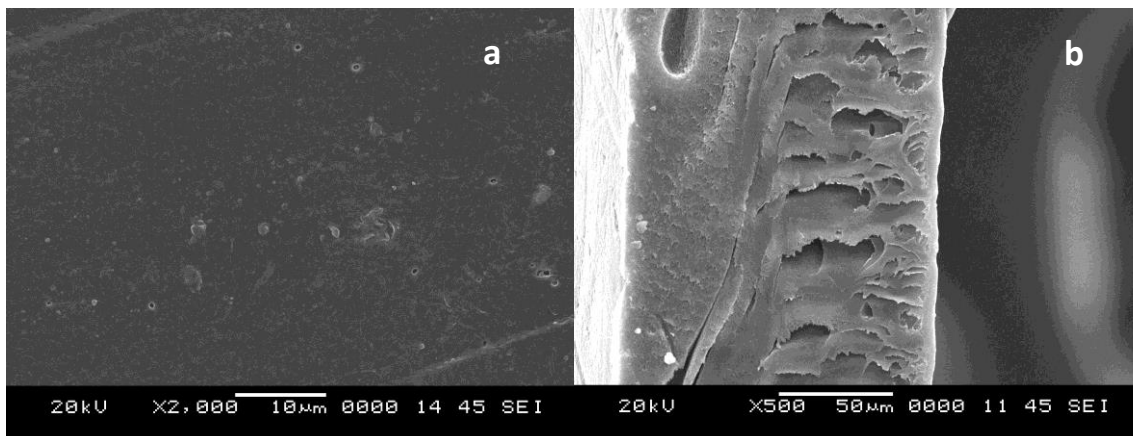
Accordingly, three polysulfone membranes blended with the chitosan derivative CTSL-2, in different proportions of 0%, 1%, and 2% CTSL-2 were prepared by the method of phase inversion by wet coagulation. The membranes were termed P-0, P-1 and P-2 respectively. The method of preparation of the membranes is described under section 3.4.

##### **4.7.1 Study of membrane morphology**

The SEM analysis was carried out to study the membrane pore structure. The membrane cross sectional morphologies are presented in three frames (Figure 4.56 b, d, f). In the case of membranes P-1 and P-2, the morphology exhibits an asymmetric structure with the presence of a dense layer at the top leading to a porous sub layer below it containing numerous finger like-projections which can be prominently seen. However, in the case of the neat membrane (P-0), such projections are virtually

missing forming a thick top skin layer. From the micrograph it is observed that, in case of both P-1 and P-2, the finger like projections start almost from the surface resulting in a top skin layer that is almost nonexistent. The surface images of P-1 and P-2 (Figure 4.56 c and e) also show well developed pores on the surface. The micrograph of the neat membrane P-0 (Figure 4.56 a) however, showed poorly developed porous structure exhibiting an opaque surface. This can be attributed to quick demixing of the polymeric solution due to the presence of formic acid when immersed in the coagulation bath in case of P-1 and P-2. The morphology of the membranes P-0 and P-2 can be further clearly observed from the reconstructed three dimensional images of the membranes presented in Figure 4.57.

According to previously published literature reports, non-solvent additives in the casting solution can significantly influence membrane morphology. The addition of acetic acid to the casting solution decreased the width of the top skin layer (Chuang et al. 2000). Dicarboxylic acids such as glycolic acid and oxalic acid (Chen et al. 2008b) and organic alcohols like propanol and butanol (Lai et al. 1996) have been shown to increase the porosity and have significant bearing on the membrane morphology. In a coagulant/solvent/polymer ternary system (with no additives), instantaneous demixing or very short delay time is required to initiate the formation of macrovoids. It has been reported by Smolders et al. (1992) that macrovoids can be induced when appropriate amount of nonsolvent is added because instantaneous demixing is promoted. The presence of the non-solvent may have produced a quick demixing effect in case of P-2 resulting in higher proportions of macrovoids and corresponding increase in porosity. Further the incorporation of CTSL-2 in the 2% membrane also increased the hydrophilicity which led to improvement in anti-fouling behavior too.



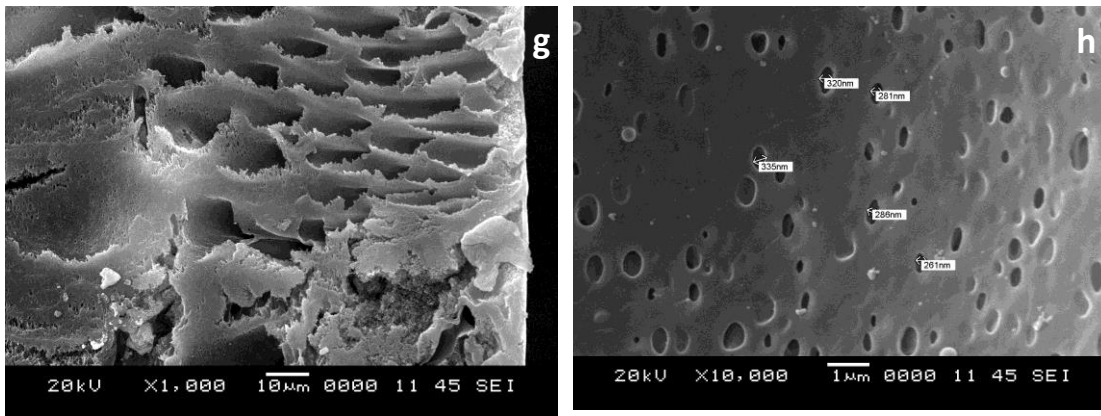


**Figure 4.56 SEM micrographs of membranes: (a) surface of P-0 membrane (b) cross-section of P-0 membrane (c) surface of a PSf : CTSL-2, 99.0: 1.0% membrane d) cross-section of a PSf: CTSL-2, 99.0: 1.0% membrane (e) surface of a PSf: CTSL-2, 98.0: 2.0% membrane (f) cross-section of a PSf: CTSL-2, 98.0: 2.0% membrane , (g) cross section of PSf: CTSL-2, 98: 2% membrane showing macro voids (h) cross section of PSf: CTSL-2, 98: 2% membrane showing microporous structure on the walls of macro voids**

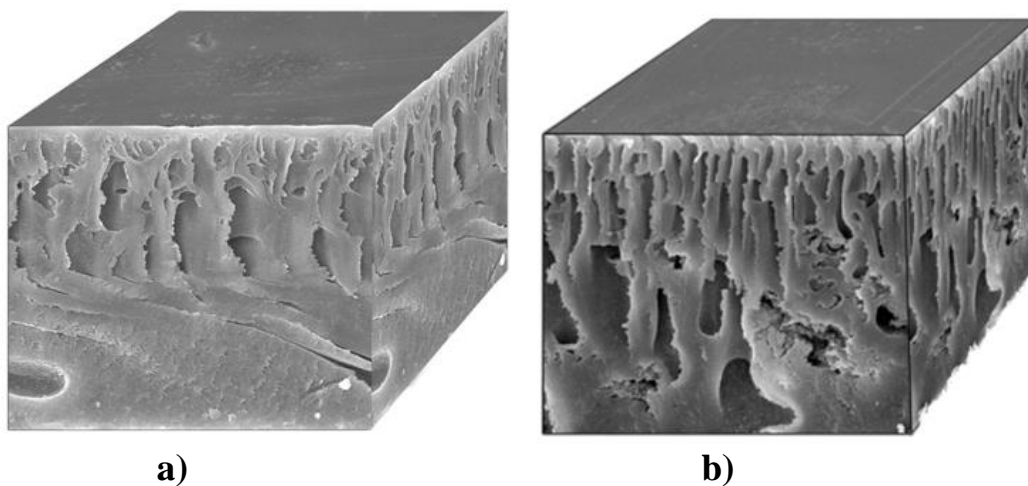


**Figure 4.57 Reconstructed three dimensional view of a) Neat polysulfone membrane (P-0), and b) Polysulfone membrane blended with 2% CTSL-2 (P-2)**

#### 4.7.2 Contact angle

Contact angle is a measure of surface hydrophilicity. In general, a lower contact angle signifies a higher hydrophilicity. As shown in Figure 4.58, the contact angle of the neat polysulfone membrane was  $70.01 \pm 1$  as compared to  $62.55 \pm 1$  for

blended membrane (P-2) having 2 wt % CTSL-2. Hence the blending of the polysulfone membrane with CTSL-2 reduced the contact angle significantly. This is attributed to the hydrophilic groups (imine, amine and hydroxyl) present in the blending material CTSL-2. The blending of the CTSL-2 increased the hydrophilicity and wettability of the membrane surface thereby reducing the contact angle.

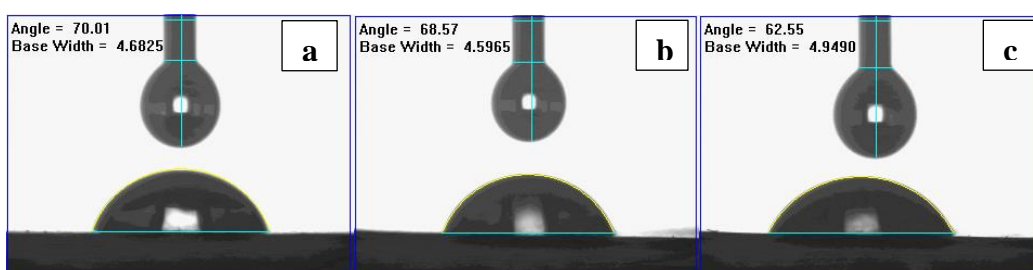


**Figure 4.58 Contact angle of the (a) neat polysulfone membrane (b) PSf: CTSL-2, 99.0: 1.0% membrane (c) PSf: CTSL-2, 98.0: 2.0% membrane**

#### 4.7.3 XRD analysis

The XRD patterns of the chitosan derivative CTSL-2, PSf-CTSL-2 (P-2) membrane (with 2 wt% CTSL-2) and neat PSf (P-0) membrane (with 0% CTSL-2) is presented in Figure 4.59. The XRD pattern for CTSL-2 exhibits peaks at  $19^{\circ}$  and  $21^{\circ}$  which are characteristic of chitosan polymer. The XRD plot of P-0 exhibits a wide peak placed around  $18^{\circ}$  which is consistent with that given in literature (Ganesh et al. 2013).

The general increase in intensity of P-2 spectrum at all  $2\theta$  values and its XRD pattern manifesting in between the patterns for P-0 and CTSL-2 clearly confirms the uniform incorporation of CTSL-2 into the PSf polymer matrix.

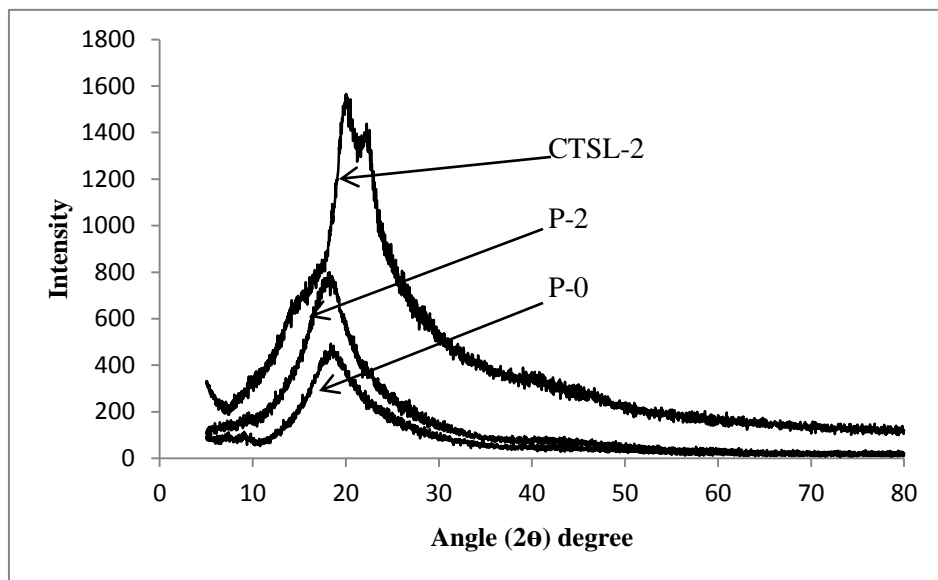


**Figure 4.59 X-ray diffraction patterns of chitosan derivative (CTSL-2), PSf-CTSL-2 blend membrane with 2% CTSL-2 (P-2), and neat PSf (P-0) membrane.**

#### 4.7.4 Permeation studies

The permeation studies were carried out in the dead-end filtration cell given in Figure 3.17, following the procedure described under section 3.4.4.1, at a temperature of 27°C under pH=7 ±0.2 with TMP values in the range of 0.2 to 0.8 MPa. During the permeation experiments, significant increase in flux was observed in case of CTSL-2 blended membranes when compared to the neat membranes (Figure 4.60 and Figure 4.61). Steady state pure water flux values obtained for P-2, P-1 and P-0 were 188 Lm<sup>-2</sup>h<sup>-1</sup>, 101 Lm<sup>-2</sup>h<sup>-1</sup> and 18 Lm<sup>-2</sup>h<sup>-1</sup> respectively, at a TMP of 0.4 MPa. A much smaller skin layer thickness, higher porosity and the increased hydrophilicity due to the presence of CTSL-2 on the membrane surface were responsible for the increase in the flux of the blended membranes P-1 and P-2 when compared to P-0.



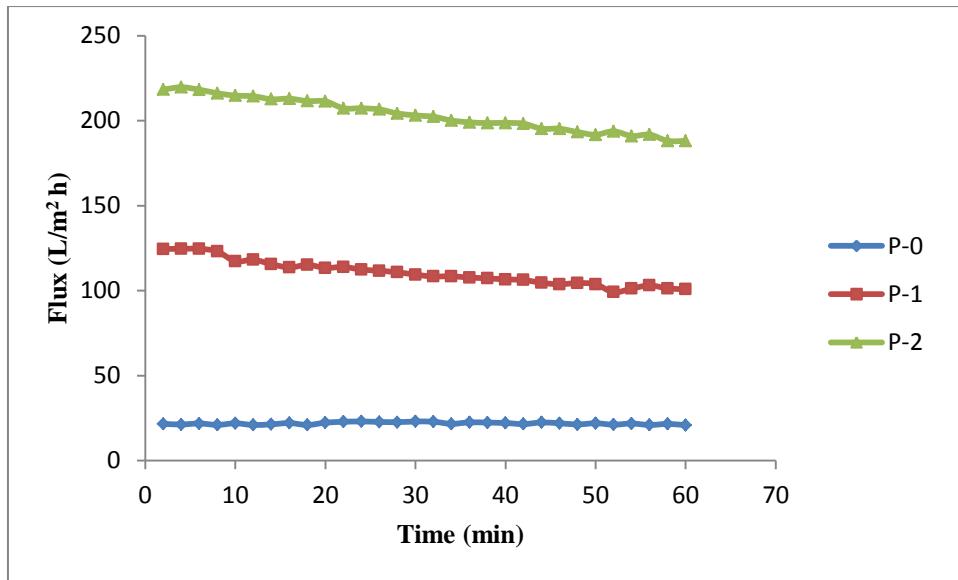


**Figure 4.60** Variation of pure water flux of the membranes at 0.4 MPa TMP and 27°C.

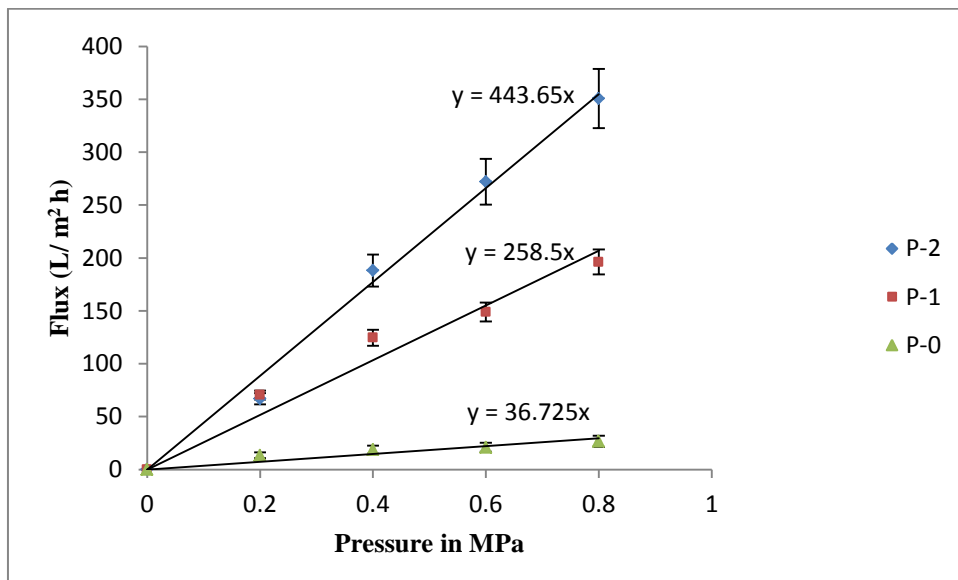


**Figure 4.61** Pure water flux of the membranes as a function of TMP at 27°C.

#### 4.7.5 Membrane hydraulic resistance

The hydraulic resistance is the reciprocal of the slope of the graph obtained by plotting the trans-membrane pressure against the pure water flux (Eq. 3.5). The hydraulic resistances offered by the P-0, P-1 and P-2 membranes were in the order  $P-0 > P-1 > P-2$  ( $0.0272 \text{ MPa/Lm}^{-2}\text{h}^{-1}$ ,  $0.0039 \text{ MPa/Lm}^{-2}\text{h}^{-1}$  and  $0.0023 \text{ MPa/Lm}^{-2}\text{h}^{-1}$ ). The decrease in hydraulic resistance for P-1 and P-2 membranes is attributed to the

increased porous structure and the increase in hydrophilicity of the membrane surface due to the presence of CTSL-2.

#### **4.7.6 Anti-fouling studies**

The anti-fouling studies were carried out following the procedure outlined under section 3.4.4.3. With an increase in membrane surface hydrophobicity, hydrophobic organic molecules gravitate more toward the surface, leading to an increase in surface contamination. In general, membrane fouling refers to an extreme decrease in post-filtration flux that occurs when organic foulants like proteins are present in the permeate solution. Fouling is attributed either to the clogging of the pores by the proteins, or build-up of the proteins on the membrane surface. When the clogging of pores and protein build up is just due to a loose deposition, it is termed as reversible fouling, as it can be cleaned by a facile hydraulic wash. In comparison, when the protein build up is due to strong adsorptive forces, leading to a permanent loss of flux, it is called irreversible fouling (Vatanpour et al. 2011).

It is always desirable to have membranes which have a high degree of resistance to fouling that display self-cleaning behavior. It has been reported that membranes which show a higher hydrophilic characteristic have a higher resistance to fouling (Bowen et al. 2001). The hydroxyl, amine and the imine groups of the CTSL-2 augment hydrophilicity of the membranes P-1 and P-2. These groups present on the membrane surface aided the adsorption of water molecules whereby a hydrated layer was formed on the functioning surface. This layer formed on the top of the membrane surface results in a decrease in protein-membrane interaction.

The catastrophic drop in flux (Figure 4.62) within the initial few seconds of commencement of BSA (Bovine serum albumin) filtration indicated the extremely rapid deposition of the protein molecules on the membrane surface (Shenvi et al. 2014). However, the presence of a hydrated layer on the hydrophilic surface prevented strong bonding between the protein molecules and the membrane surface, thereby making the membrane amenable to simple hydraulic cleaning and recovery in PWF. A higher maximum FRR of 57% was obtained in the case of P-2 membrane compared to 33% of the P-0 membrane. Because of the reasons proffered in the

preceding discussion, the CTSL-2 blended membranes had superior anti-fouling behavior. The results of the anti-fouling studies are provided in Table 4.20 where the dimensionless recovery ratios of FRR,  $R_t$ ,  $R_r$  and  $R_{ir}$  (defined in section 3.4.4.3) are tabulated.

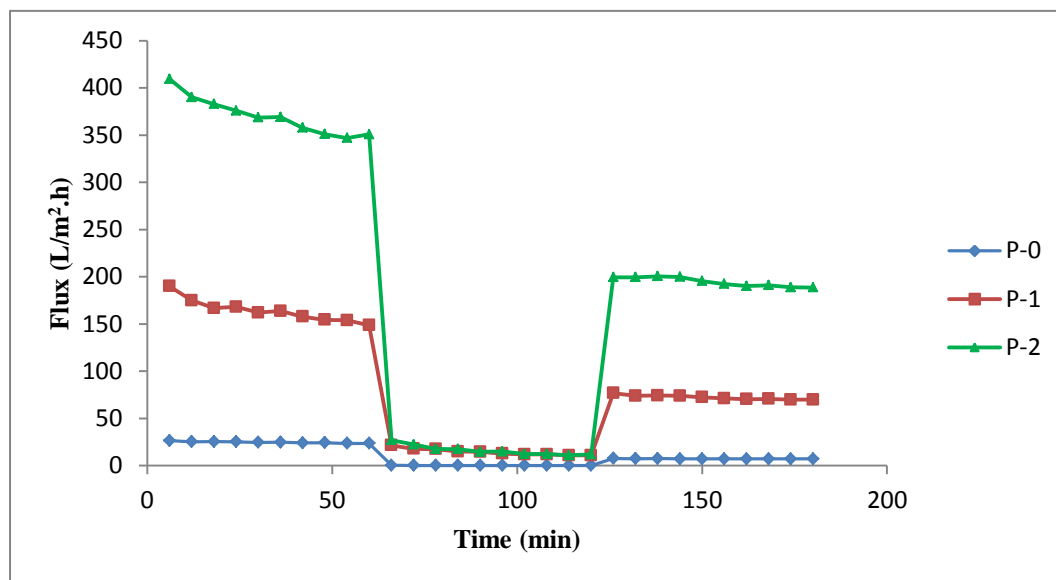


**Figure 4.62 Time dependent flux of PSf-CTSL-2 membranes at 0.8 MPa TMP during three different conditions. PWF for 60 min, BSA flux (pH =7 ± 0.2) for 60 min and water flux for 60 min after 15 min of washing with distilled water.**

**Table 4.20 Filtration and antifouling performances of the membranes**

Membrane	Permeate flux ( $L m^{-2} h^{-1}$ )			FRR and recovery ratios (%)			
	$J_{w1}$	$J_p$	$J_{w2}$	FRR	$R_t$	$R_r$	$R_{ir}$
<b>P-0</b>	24 ± 1.9	0.4 ± 0.2	8 ± 1.2	33	98	31	68
<b>P-1</b>	149 ± 7	22 ± 1.5	77 ± 4.1	52	85	37	48
<b>P-2</b>	351 ± 15	27 ± 1.7	200 ± 9	57	92	49	43

## 4.7.7 Heavy metal rejection studies

### 4.7.7.1 Pb (II) rejection study

The performance of the membranes for Pb (II) rejection was studied with an aqueous solution of  $\text{Pb}(\text{NO}_3)_2$  containing a metal ion concentration of 100 mg/L, at  $\text{pH}=6 \pm 0.2$ , at a temperature of  $27^\circ\text{C}$ . The permeation study was performed at four different pressures between 0.2 MPa to 0.8 MPa. The results of the study are presented in Figure 4.63. The maximum value of 36% rejection of Pb (II) is obtained in the case of P-1 membrane for a TMP of 0.2 MPa. The rejection was ~70% higher than the values obtained with neat membrane (21%). Further, with increase in TMP, the percentage of Pb (II) rejection decreased. In the case of P-2 membrane also, the maximum rejection (29%) occurred at the TMP of 0.2 MPa. However, rejection was lower than that obtained for P-1. For the neat membrane, the rejection remained practically constant at around 21%, at all applied pressures. Thus the addition of CTSL-2 to PSf increased the rejection of Pb (II) in case of P-1 membrane.

Generally, the flux through the membrane is determined by the TMP; as the flux increases, the drag force on the solvent through the pores also increases. Hence, higher the TMP, higher is the drag force. The surface forces (i.e. frictional forces, adsorptive forces) on the pore walls, however, are constant and unchanging with TMP and flux. The surface forces are responsible for the retention of the solute by adsorptive forces (e.g. chelation, electrostatic binding). Comparatively, surface forces are relatively greater than the drag force at lower flux (at lower TMP), than at higher flux (at higher TMP) (Pontalier et al. 1997). Hence it may be inferred that, the blending of PSf with CTSL-2 aided in increasing the retention of metal ions by surface adsorption. The hydroxyl, amine and the imine groups present in the CTSL-2 are the potential sites for the adsorption. The reason for the almost unchanging rejection performance of neat membranes could be the very low prevailing flux rates which change little with increase in TMP there by maintaining a near constant drag force.

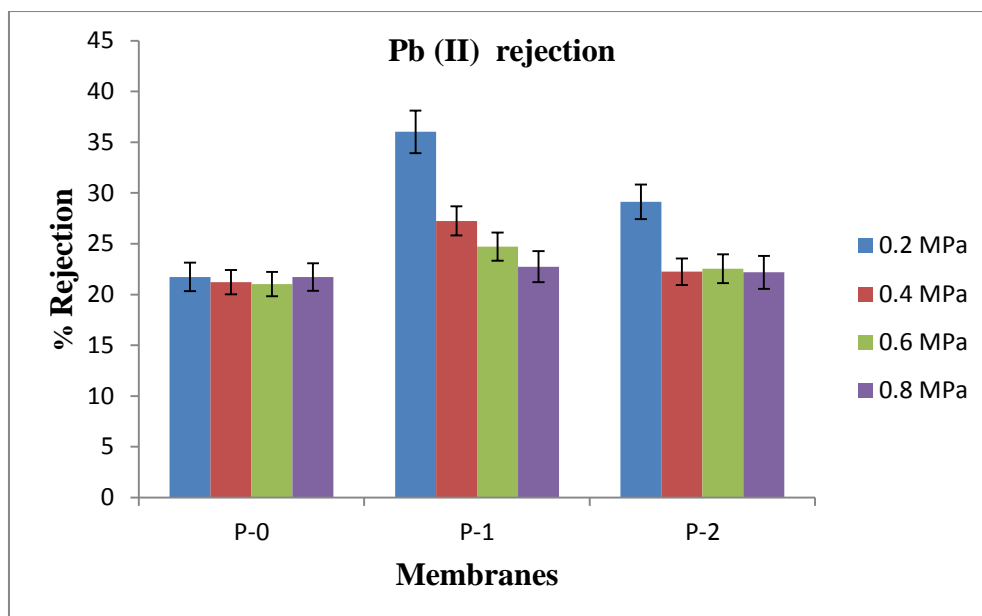


**Figure 4.63 Pb (II) metal rejection of membranes**

#### 4.7.7.2 Cu (II) rejection study

The performance of the membranes for Cu (II) rejection was studied with an aqueous solution of  $\text{CuSO}_4 \cdot 5\text{H}_2\text{O}$  containing a Cu (II) concentration of 100 mg/L, at  $\text{pH} = 6 \pm 0.2$ , at a temperature of  $27^\circ\text{C}$ . The maximum rejection of Cu (II) observed was 29% at 0.2 MPa (Figure 4.64) compared to ~20% rejection of the neat membranes. The blending of CTSL-2 increased the Cu (II) rejection in case of P-1 membrane. Kumar et al. (2014) have obtained a maximum percentage rejection of up to 78% for Cu (II) at pH of 5.5 with a polysulfone-chitosan blend membrane compared to 25% rejection of neat polysulfone membranes.

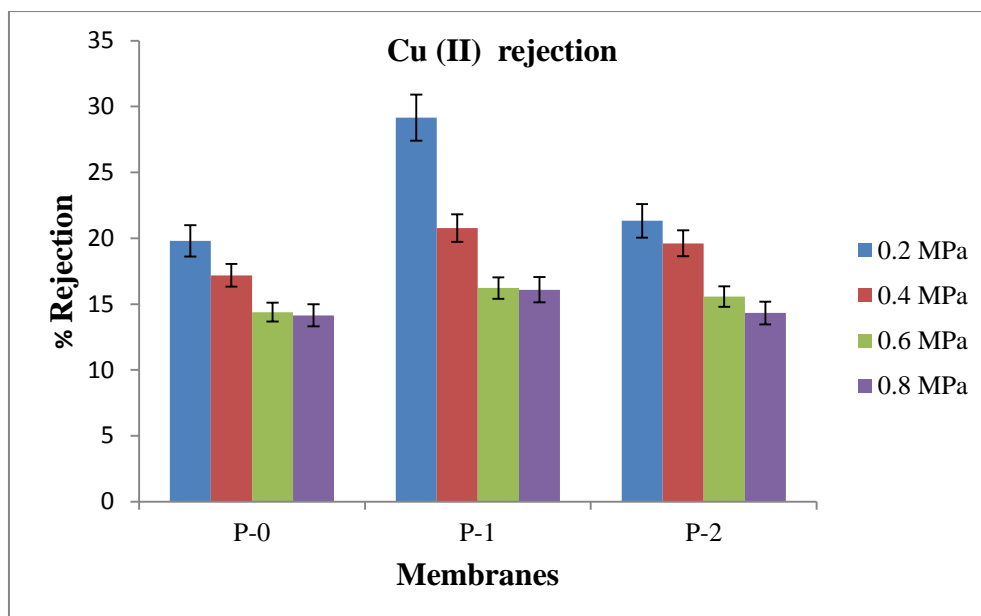


**Figure 4.64 Cu (II) metal rejection of membranes**

#### 4.7.7.3 Cr (VI) rejection study

The performance of the membranes for Cr (VI) rejection was studied using an aqueous solution of  $K_2Cr_2O_7$  having a metal ion concentration of 100 mg/L, at  $pH = 3 \pm 0.1$ , at a temperature of  $27^\circ C$ . Maximum rejection of 61% Cr (VI) was observed at 0.2 MPa for P-1 membrane (Figure 4.65) which was double of the average rejection obtained with neat P-0 membrane (30%). The higher rejection observed for Cr (VI) in comparison to the rejections of Pb (II) and Cu (II) could be due to the higher charge density on the chromium compared to the latter two ions. Presumably, a higher number of macromolecular functional groups may be bound to a heavy metal ion of higher charge density and this higher charge density obstructs the pore more effectually by increased complex volume. Recently, Kanagaraj et al.(2015) have reported similar results.

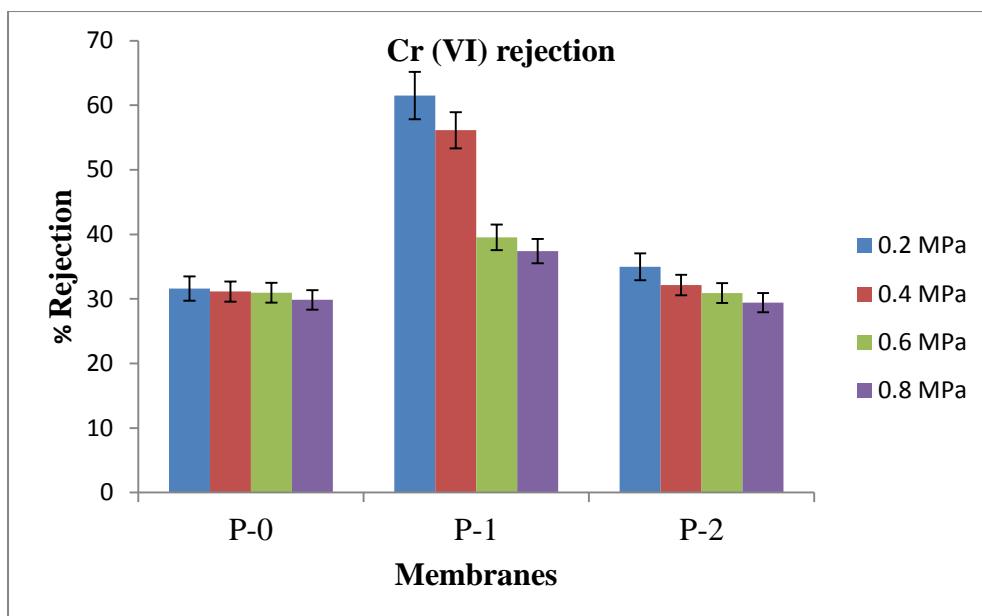


**Figure 4.65 Cr (VI) metal rejection of membranes (Cr<sup>+6</sup>)**

#### **4.7.7.4 Mechanism of metal rejection by membranes**

The heavy metal removal is mainly attributable to adsorption. A pH value >4 is suitable for Pb and Cu removal which occur as divalent cations. The mechanism of removal of divalent metal ions like Pb (II) and Cu (II) is mainly by chelation. However, the hexavalent chromium occurs in the anionic form as  $\text{HCrO}_4^-$ . At pH values < 4 the adsorption surface gets protonated and hence the Cr (VI) are retained by electrostatic interactions. The schematic diagrams describing the proposed mechanisms of metal removal are as shown in Figure 4.66.

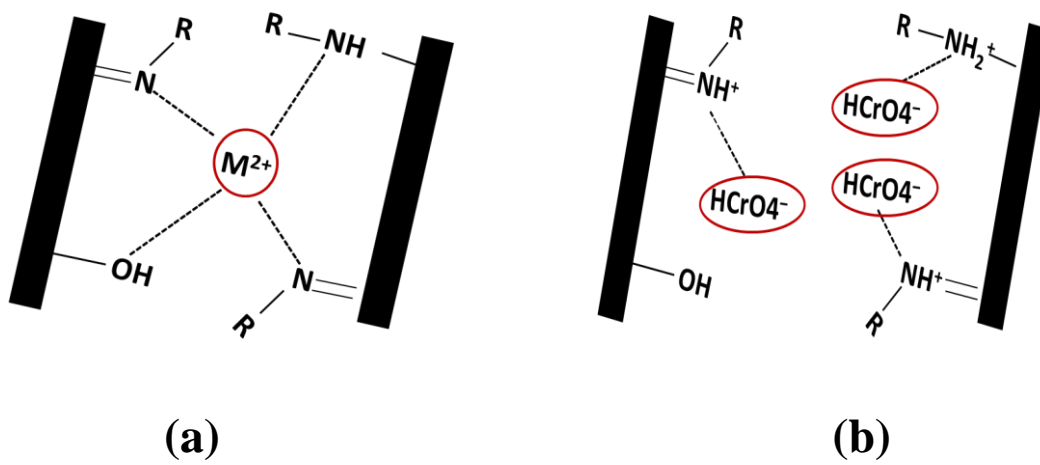


**Figure 4.66** The proposed mechanisms of heavy metal rejection by membranes  
 (a) Pb (II) and Cu (II), and b) Cr (VI)



# **CHAPTER 5**

## **SUMMARY AND CONCLUSIONS**



The salient findings of the present research work are summarized as below:

- Four new chitosan derivatives were successfully synthesized employing the Schiff reaction by grafting chitosan with four new 1H-pyrazole-4-carbaldehyde bearing ligands. Each ligand had a single pyrazole ring with two additional nitrogen atoms which are potential binding sites for heavy metal sequestration. The chemical structure of the four new derivatives which were termed CTSL-1, CTSL-2, CTSL-3 and CTSL-4 are listed below in Figure 5.1. The formation of the ligands and the four derivatives were validated by  $^1\text{H}$  NMR and  $^{13}\text{C}$  NMR analysis respectively. The new derivatives were characterised by FTIR, powder XRD spectra and DSC analysis.

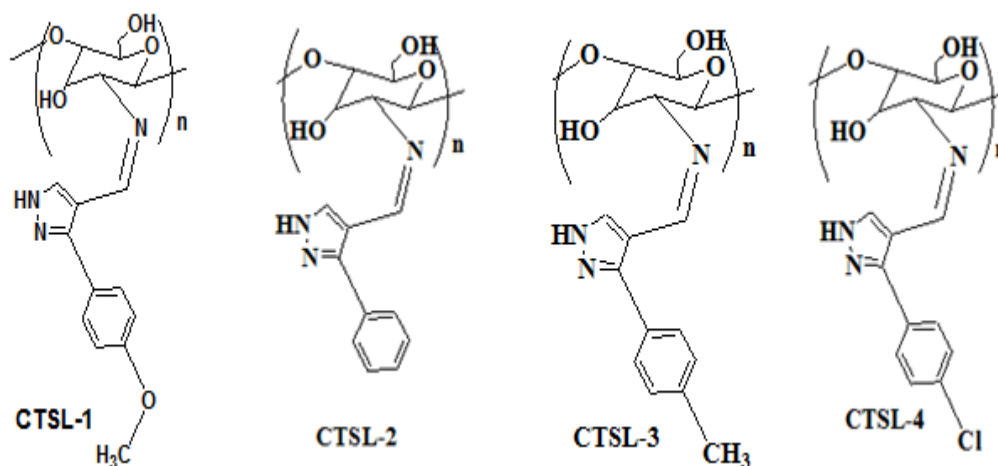


**Figure 5.1 Structure of novel chitosan derivatives**

- The adsorption equilibrium was favoured at pH=3 for Cr (VI), pH= 6 to 7 for Cu (II) and pH = 4 to 6 for Pb (II).
- The maximum monolayer adsorption capacities obtained for the three metals and the derivatives were 63.5 mg/g for Cr (VI) (by CTSL-2), 91.7 mg/g for Pb (II) (by CTSL-2) and 45.6 mg/g for Cu (II) (by CTSL-3).
- In majority of the cases the best fitting isotherm was Redlich Peterson isotherm model which points towards the adsorbent surface to be of heterogeneous nature.

- The pseudo-second order kinetic model was observed to best describe the adsorption kinetics for all three metals studied for all four derivatives. The consistently high values of correlation coefficient ( $r^2$ ) obtained provide conviction to the applicability of this model. This model was successful in predicting the kinetics of the adsorption process over the entire contact-time range.
- The results of the thermodynamic study indicated the spontaneous nature of adsorption. It was observed that the adsorption of chromium was exothermic and favoured at lower temperatures whereas that of copper and lead were endothermic and favoured at higher temperatures. The net change in standard entropy was positive which suggested that the net randomness on the adsorbent surface increased.
- The DSC analysis revealed that the synthesized biopolymer derivatives were stable up to a temperature of  $\sim 200^\circ\text{C}$  which is within the temperature requirement for practical applications of the adsorbent. When compared to that of chitosan, the thermal stability was not affected in a significant manner after the grafting of the ligand on chitosan.
- The XRD study revealed that the crystallinity of the derivatives was generally less than that of chitosan. This was attributed to the break in strong inter particle and intraparticle hydrogen bonds present in chitosan due to the anchoring of the ligand molecule. It was also observed that in case of Pb-chitosan derivative complexes, a few additional peaks appeared after adsorption, an indication of increase in crystallinity in a few areas in such complexes post adsorption.
- Pre and post adsorption comparison of the adsorbent for FTIR was carried out. Based on the FTIR analysis, the metal removal was attributed to the amine, imine and hydroxyl functional groups.
- The possible mechanism of Cu (II) and Pb (II) removal was chelation/complexation whereas for the Cr (VI) removal it was electrostatic interaction.
- The experiments in swelling behavior showed that in comparison to chitosan which had very high swelling percentages of 348.5 at pH 3 and 398.5 at pH 6,

the corresponding values for the derivatives were drastically lower. The lowest percentage of swelling obtained at pH= 3 was 10.6% for CTSL-1 and at pH=6 it was 19.43% for CTSL-2. The major decrease in the swelling percentages of the synthesized derivatives is an important contribution of this research work because the use of chitosan in continuous contact packed columns is practically unfeasible due to its high swelling degree. By virtue of having very low swelling characteristics, the presently synthesized chitosan derivatives are suitable for use in packed column contactors.

- Overall, the results obtained in this study show that three chitosan derivatives CTSL-1, CTSL-2 and CTSL-3 have shown promising results which could enable their application in areas related to purification of water and waste water remediation.
- The CTSL-2 blended polysulfone membranes showed significant increase in pure water flux (PWF) with a maximum flux of  $351 \text{ Lm}^{-2}\text{h}^{-1}$  at 0.8 MPa TMP as compared to  $24 \text{ Lm}^{-2}\text{h}^{-1}$  of the neat polysulfone membrane at the same TMP. From the SEM studies it was observed that finger like projections start almost from the surface resulting in a top skin layer that is almost but nonexistent. The micrograph of the neat membrane P-0, however, showed poorly developed porous structure and a relatively thick top skin layer. It also exhibited an opaque surface. The surface images of CTSL-2 blended membranes show well developed pores on the surface compared to opaque surface of the neat polysulfone membrane. The increase in porosity was attributed to the addition of chitosan derivative into the polymer matrix.
- The contact angle for the 2% CTSL-2 blended membrane decreased to 62.55 compared to 70.01 of the neat polysulfone membrane. Since the hydrophilicity and contact angle were inversely correlated, it was concluded that the hydrophilicity of the blended membranes increased after the blending.
- During the anti-fouling studies using bovine serum albumen, a flux recovery ratio of 56.9 was witnessed for the polysulfone membranes blended with CTSL-2, compared to only 32.5 of the neat membrane. This increase in FRR was attributed to the increase in hydrophilicity in the membrane after blending with CTSL-2 due to the presence of hydrophilic groups such as hydroxyl,

amine and imine which formed a hydrated layer on the hydrophilic surface which prevented strong bonding between the protein molecules and the membrane surface, thereby making the membrane amenable to simple hydraulic cleaning and recovery in PWF.

- During rejection studies of the metal ion solutions through the membrane, the maximum metal rejections observed were 36%, 29% and 61% respectively for the three metals Pb (II), Cu (II) and Cr (VI). The maximum rejections were obtained for the membrane with 1% CTSL-2 for a TMP of 0.2 MPa.
- Hence addition of CTSL2 is an ideal and simple solution for improving the flux, the antifouling resistance and metal rejection performance of the polysulfone ultrafiltration membranes.

## SCOPE FOR FUTURE STUDIES

- Large scale synthesis of the chitosan derivatives with better economies.
- Since the chitosan derivatives have much improved swelling behaviour, they can be tried in continuous column studies for heavy metal removal from aqueous solutions. In all such studies, apart from the heavy metals used in the present study (Cu (II), Pb (II), Cr (VI)), different metals such as mercury and arsenic may be used.
- The effectiveness of the presently synthesized chitosan derivatives as adsorbents for the removal of pollutants other than heavy metals such as dyes and pharmaceutical drugs may be investigated.
- Ligands with other groups having O and S atoms (COOH, SH, SO<sub>3</sub>) which may be effective in metal sequestration may be attempted
- In the membrane studies variations of blending/doping could be another promising idea; the additives may be used in the form of nanoparticles.
- Another way of imparting surface hydrophilicity could be by using a coagulation bath having a small percentage of dissolved derivative instead of plain distilled water. Similar studies using dissolved chitosan in the coagulation bath have been reported in literature (Kumar et al. 2013e).
- In other studies, researchers have reported the use of cross-linked chitosan copper complexes as a versatile, eco-friendly, recyclable solid catalyst (Martina et al. 2011). The copper chitosan derivative complexes obtained in this study may be investigated as a potential catalyst in synthesis reactions.





# **APPENDICES**



## APPENDIX I

### Preparation of Calibration chart for Pb (II) estimation

A stock solution of Pb (II) of 100 mg/L concentration was initially prepared by diluting the standard solution of 1000 mg/L concentration. The standard solution was manufactured by Reagecon Diagnostics Limited Ireland and supplied by Thermo Fisher Scientific India. Using the stock solution of 100 mg/L of Pb (II), working solutions in the range 0-10 mg/L were prepared by diluting several times as per the protocol of the AAS instrument. The various absorption values at a wavelength of 217.0 nm were plotted against the concentrations to get the calibration chart.

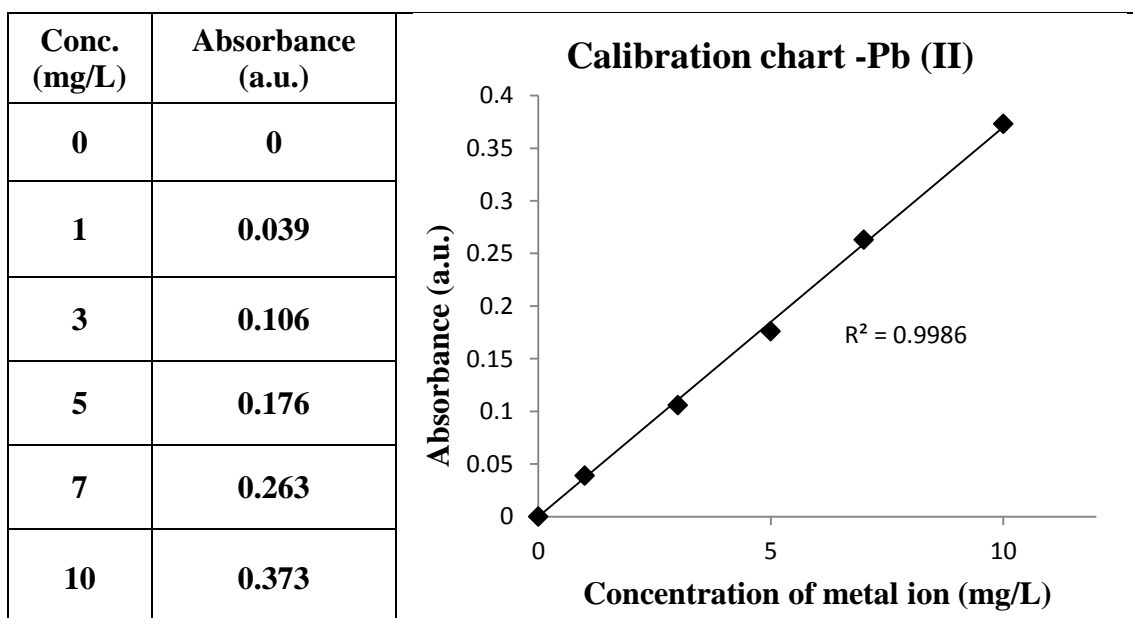


Fig A I (A) Calibration chart for the estimation of Pb (II)

## APPENDIX II

### Preparation of Calibration chart for Cu (II) estimation

A stock solution of Cu (VI) of 100 mg/L concentration was initially prepared by diluting the standard solution of 1000 mg/L concentration. The standard solution was manufactured by Reagecon Diagnostics Limited Ireland and supplied by Thermo Fisher Scientific India. Using the stock solution of 100 mg/L of Cu (VI), working solutions in the range 0-5 mg/L were prepared by diluting several times as per the protocol of the AAS instrument. The various absorption values at a wavelength of 324.8 nm were plotted against the concentrations to get the calibration chart.

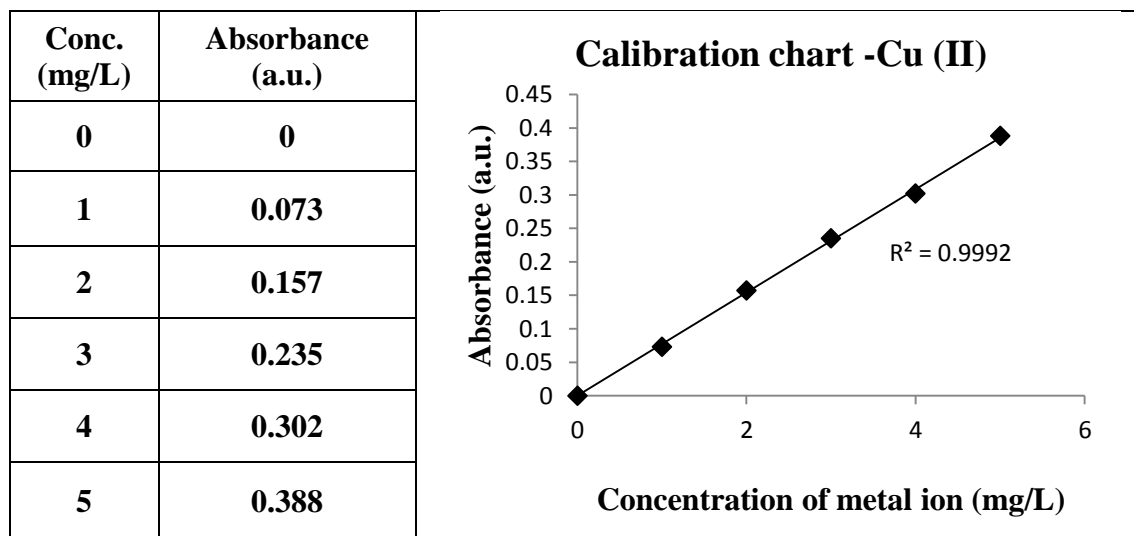


Fig A II (A) Calibration chart for the estimation of Cu (II)

### APPENDIX III

#### Preparation of Calibration chart for Cr (VI) estimation

A stock solution of Cr (VI) of 100 mg/L concentration was initially prepared by diluting the standard solution of 1000 mg/L concentration. The standard solution was manufactured by Reagecon Diagnostics Limited Ireland and supplied by Thermo Fisher Scientific India. Using the stock solution of 100 mg/L of Cr (VI), working solutions in the range 0-7 mg/L were prepared by diluting several times as per the protocol of the AAS instrument. The various absorption values at a wavelength of 357.9 nm were plotted against the concentrations to get the calibration chart.

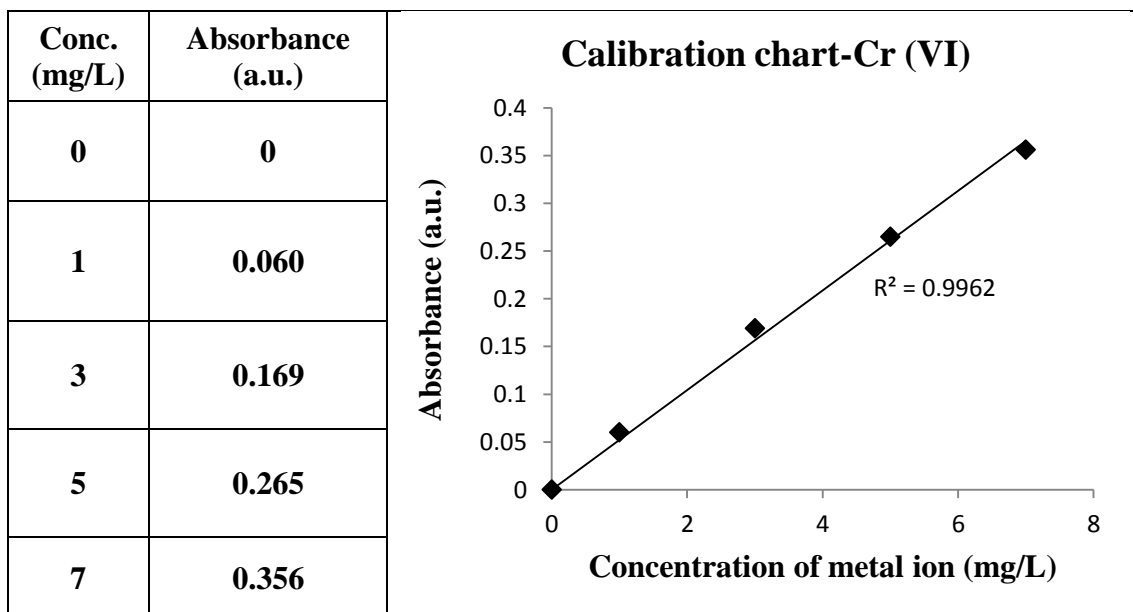


Fig A III (A) Calibration chart for the estimation of Cr (VI)



# **REFERENCES**





Amiji, M.M. (1995). "Permeability and blood compatibility properties of chitosan-poly (ethylene oxide) blend membranes for haemodialysis." *Biomaterials*, 16(8), 593-599.

Anderson, R.J., Bendell, D.J. and Groundwater, P.W. (2004). *Organic spectroscopic analysis*, Vol. 22, Royal Society of Chemistry, UK.

Astruc, D., Boisselier, E. and Ornelas, C. (2010). "Dendrimers designed for functions: from physical, photophysical, and supramolecular properties to applications in sensing, catalysis, molecular electronics, photonics, and nanomedicine." *Chem. Rev.*, 110(4), 1857-1959.

Aydin, Y.A. and Aksoy, N.D. (2009). "Adsorption of chromium on chitosan: Optimization, kinetics and thermodynamics." *Chem. Eng. J.*, 151(1), 188-194.

Baker, R.W. (2000). *Membrane technology*, John Wiley & Sons, Inc.

Baughman, R.H., Zakhidov, A.A. and de Heer, W.A. (2002). "Carbon nanotubes--the route toward applications." *Science*, 297(5582), 787-792.

Bekircan, O. and Bektas, H. (2008). "Synthesis of Schiff and Mannich bases of isatin derivatives with 4-amino-4, 5-dihydro-1H-1, 2, 4-triazole-5-ones." *Molecules*, 13(9), 2126-2135.

Bhatnagar, A. and Sillanpää, M. (2009). "Applications of chitin-and chitosan-derivatives for the detoxification of water and wastewater—a short review." *Adv. Colloid Interface Sci.*, 152(1), 26-38.

Boamah, P.O., Huang, Y., Hua, M., Zhang, Q., Wu, J., Onumah, J., Sam-Amoah, L.K. and Boamah, P.O. (2015). "Sorption of heavy metal ions onto carboxylate chitosan derivatives—a mini-review." *Ecotoxicol. Environ. Saf.*, 116, 113-120.

Boddu, V.M., Abburi, K., Randolph, A.J. and Smith, E.D. (2008). "Removal of copper (II) and nickel (II) ions from aqueous solutions by a composite chitosan biosorbent." *Sep. Sci. Technol.*, 43(6), 1365-1381.

- Borsagli, F.G.M., Mansur, A.A., Chagas, P., Oliveira, L.C. and Mansur, H.S. (2015). "O-carboxymethyl functionalization of chitosan: Complexation and adsorption of Cd (II) and Cr (VI) as heavy metal pollutant ions." *React. Funct. Polym.*, 97, 37-47.
- Bowen, W.R., Doneva, T.A. and Yin, H.B. (2001). "Polysulfone—sulfonated poly (ether ether) ketone blend membranes: systematic synthesis and characterisation." *J. Membr. Sci.*, 181(2), 253-263.
- Cao, J., Tan, Y., Che, Y. and Xin, H. (2010). "Novel complex gel beads composed of hydrolyzed polyacrylamide and chitosan: An effective adsorbent for the removal of heavy metal from aqueous solution." *Bioresour. Technol.*, 101(7), 2558-2561.
- Ceglowski, M. and Schroeder, G. (2015). "Preparation of porous resin with Schiff base chelating groups for removal of heavy metal ions from aqueous solutions." *Chem. Eng. J.*, 263, 402-411.
- Chang, Y.K., Chang, J.E., Lin, T.T. and Hsu, Y.M. (2002). "Integrated copper-containing wastewater treatment using xanthate process." *J. Hazard. Mater.*, 94(1), 89-99.
- Chatterjee, S., Lee, M.W. and Woo, S.H. (2010). "Adsorption of congo red by chitosan hydrogel beads impregnated with carbon nanotubes." *Bioresour. Technol.*, 101(6), 1800-1806.
- Chauhan, D., Jaiswal, M. and Sankararamakrishnan, N. (2012). "Removal of cadmium and hexavalent chromium from electroplating waste water using thiocarbamoyl chitosan." *Carbohydr. Polym.*, 88(2), 670-675.
- Chen, A.H., Liu, S.C., Chen, C.Y. and Chen, C.Y. (2008a). "Comparative adsorption of Cu (II), Zn (II), and Pb (II) ions in aqueous solution on the crosslinked chitosan with epichlorohydrin." *J. Hazard. Mater.*, 154(1), 184-191.
- Chen, G. (2004). "Electrochemical technologies in wastewater treatment." *Sep. Purif. Technol.*, 38(1), 11-41.

- Chen, P.H., Kuo, T.Y., Liu, F.H., Hwang, Y.H., Ho, M.H., Wang, D.M., Lai, J.Y. and Hsieh, H.J. (2008b). "Use of dicarboxylic acids to improve and diversify the material properties of porous chitosan membranes." *J. Agric. Food Chem.*, 56(19), 9015-9021.
- Chethan, P.D. and Vishalakshi, B. (2013). "Synthesis of ethylenediamine modified chitosan and evaluation for removal of divalent metal ions." *Carbohydr. Polym.*, 97(2), 530-536.
- Chethan, P.D. and Vishalakshi, B. (2015). "Synthesis of ethylenediamine modified chitosan microspheres for removal of divalent and hexavalent ions." *Int. J. Biol. Macromol.*, 75, 179-185.
- Cheung, W.H., Szeto, Y.S. and McKay, G. (2007). "Intraparticle diffusion processes during acid dye adsorption onto chitosan." *Bioresour. Technol.*, 98(15), 2897-2904.
- Cho, Y.H., Kim, H.W., Nam, S.Y. and Park, H.B. (2011). "Fouling-tolerant polysulfone-poly (ethylene oxide) random copolymer ultrafiltration membranes." *J. Membr. Sci.*, 379(1), 296-306.
- Chuang, W.Y., Young, T.H. and Chiu, W.Y. (2000). "The effect of acetic acid on the structure and filtration properties of poly (vinyl alcohol) membranes." *J. Membr. Sci.*, 172(1), 241-251.
- Coleman, J.N., Khan, U. and Gun'ko, Y.K. (2006). "Mechanical reinforcement of polymers using carbon nanotubes." *Adv. Mater.*, 18(6), 689-706.
- Crini, G. (2005). "Recent developments in polysaccharide-based materials used as adsorbents in wastewater treatment." *Prog. Polym. Sci.*, 30(1), 38-70.
- Cunha, A.G. and Gandini, A. (2010). "Turning polysaccharides into hydrophobic materials: a critical review. Part 2. Hemicelluloses, chitin/chitosan, starch, pectin and alginates." *Cellulose*, 17(6), 1045-1065.
- Déjardin, P. ed., (2006). *Proteins at solid-liquid interfaces*, Heidelberg: Springer.
- Deng, L., Su, Y., Su, H., Wang, X. and Zhu, X. (2006). "Biosorption of copper (II) and lead (II) from aqueous solutions by nonliving green algae *Cladophora*

fascicularis: equilibrium, kinetics and environmental effects.” *Adsorption*, 12 (4), 267-277.

Do D.D. (1998). *Adsorption Analysis: Equilibria and Kinetics*, Imperial College Press, London.

Dong, H.B., Xu, Y.Y., Yi, Z. and Shi, J.L. (2009). “Modification of polysulfone membranes via surface-initiated atom transfer radical polymerization.” *Appl. Surf. Sci.*, 255(21), 8860-8866.

Donia, A.M., Atia, A.A. and Elwakeel, K.Z. (2008). “Selective separation of mercury (II) using magnetic chitosan resin modified with Schiff's base derived from thiourea and glutaraldehyde.” *J. Hazard. Mater.*, 151(2), 372-379.

Duffus, J.H. (2002). “Heavy metals—a meaningless term?” *Pure. Appl. Chem.*, 74(5), 793–807.

El-Reash, Y.A. (2016). “Magnetic chitosan modified with cysteine-glutaraldehyde as adsorbent for removal of heavy metals from water.” *J. Environ. Chem. Eng.*, 4(4), 3835-3847.

Elwakeel, K.Z. (2010). “Environmental application of chitosan resins for the treatment of water and wastewater: a review.” *J. Dispersion Sci. Technol.*, 31(3), 273-288.

Ferrero, F., Tonetti, C. and Periolatto, M. (2014). “Adsorption of chromate and cupric ions onto chitosan-coated cotton gauze.” *Carbohydr. Polym.*, 110, 367-373.

Foo, .K.Y. and Hameed, B.H. (2010). “Insights into the modeling of adsorption isotherm systems.” *Chem. Eng. J.*, 156(1), 2-10.

Freundlich, H.M.F. (1906). “Über die adsorption in lasugen (Leipzig).” *Z. Phys. Chem. A*, 57, 385-470.

Fu, F. and Wang, Q. (2011). “Removal of heavy metal ions from wastewaters: a review.” *J. Environ. Manage.*, 92(3), 407-418.

Futalan, C. M., Kan, C.C., Lourdes M., Dalida P., Pascua, C., Hsien, K-J. and Wan, M-W. (2011a). "Nickel removal from aqueous solution in fixed bed using chitosan-coated bentonite." *Sustainable Environ. Res.*, 21(6), 391-401.

Futalan, C.M., Kan, C.C., Dalida, M.L., Hsien, K.J., Pascua, C. and Wan, M.W. (2011b). "Comparative and competitive adsorption of copper, lead, and nickel using chitosan immobilized on bentonite." *Carbohydr. Polym.*, 83(2), 528-536.

Gandhi, M.R., Kousalya, G.N., Viswanathan, N. and Meenakshi, S. (2011). "Sorption behaviour of copper on chemically modified chitosan beads from aqueous solution." *Carbohydr. Polym.*, 83(3), 1082-1087.

Ganesh, B.M., Isloor, A.M. and Ismail, A.F. (2013). "Enhanced hydrophilicity and salt rejection study of graphene oxide-polysulfone mixed matrix membrane." *Desalination*, 313, 199-207.

Ge, H., Hua, T. and Wang, J. (2017). "Preparation and characterization of poly (itaconic acid)-grafted crosslinked chitosan nanoadsorbent for high uptake of Hg 2+ and Pb 2+." *Int. J. Biol. Macromol.*, 95, 954-961.

Gerente, C; Lee, V. K. C; Cloirec, P. Le and McKay, G. (2007). "Application of chitosan for the removal of metals from wastewaters by adsorption — mechanisms and models review." *Critical Reviews Environ. Sci. Tech.* 37 (1), 41-127.

Gotoh, T., Matsushima, K. and Kikuchi, K.I. (2004). "Preparation of alginate–chitosan hybrid gel beads and adsorption of divalent metal ions." *Chemosphere*, 55(1), 135-140.

Guibal, E. (2004). "Interactions of metal ions with chitosan-based sorbents: a review." *Sep. Purif. Technol.*, 38(1), 43-74.

Guinesi, L.S. and Cavalheiro, E.T.G. (2006). "Influence of some reactional parameters on the substitution degree of biopolymeric Schiff bases prepared from chitosan and salicylaldehyde." *Carbohydr. Polym.*, 65(4), 557-561.

- Günay, A., Arslankaya, E. and Tosun, I. (2007). "Lead removal from aqueous solution by natural and pretreated clinoptilolite: adsorption equilibrium and kinetics." *J. Hazard. Mater.*, 146(1), 362-371.
- Haider, S. and Park, S.Y. (2009). "Preparation of the electrospun chitosan nanofibers and their applications to the adsorption of Cu (II) and Pb (II) ions from an aqueous solution." *J. Membr. Sci.*, 328(1), 90-96.
- Hall, K.R., Eagletow, L.C., Acrivers, A. and Vermenlem, T. (1966) "Pore and solid kinetics in fixed-bed adsorption under constant pattern condition." *Ind. Eng. Chem. Fundam.* 5, 212–218
- Hasan, S., Ghosh, T.K., Viswanath, D.S. and Boddu, V.M. (2008). "Dispersion of chitosan on perlite for enhancement of copper (II) adsorption capacity." *J. Hazard. Mater.*, 152(2), 826-837.
- Hebbar, R.S., Isloor, A.M. and Ismail, A.F. (2014). "Preparation of antifouling polyetherimide/hydrolysed PIAM blend nanofiltration membranes for salt rejection applications." *RSC Adv.*, 4(99), 55773-55780.
- Hebbar, R.S., Isloor, A.M., Ananda, K. and Ismail, A.F. (2016). "Fabrication of polydopamine functionalized halloysite nanotube/polyetherimide membranes for heavy metal removal." *J. Mater. Chem. A*, 4(3), 764-774.
- Hebbar, R.S., Isloor, A.M., Ismail, A.F., Shilton, S.J., Obaid, A. and Fun, H.K. (2015). "Probing the morphology and anti-organic fouling behaviour of a polyetherimide membrane modified with hydrophilic organic acids as additives." *New J. Chem.*, 39(8), 6141-6150.
- Hirano, S. and Ohe, Y. (1975). " Selective N-acylation of chitosan." *Agric. Biol. Chem.*, 39, 1337–1338.
- Ho, Y.S. and McKay, G. (1999). "Pseudo-second order model for sorption processes." *Process Biochem.*, 34(5), 451-465.

Hodgson, E. (2004). *A textbook of modern toxicology*, Third Ed., John Wiley and Sons, New York.

Hu, X.J., Wang, J.S., Liu, Y.G., Li, X., Zeng, G.M., Bao, Z.L., Zeng, X.X., Chen, A.W. and Long, F. (2011). "Adsorption of chromium (VI) by ethylenediamine-modified cross-linked magnetic chitosan resin: isotherms, kinetics and thermodynamics." *J. Hazard. Mater.*, 185(1), 306-314.

Huang, C., Chung, Y.C. and Liou, M.R. (1996). "Adsorption of Cu (II) and Ni (II) by pelletized biopolymer." *J. Hazard. Mater.*, 45(2), 265-277.

Huo, H., Su, H. and Tan, T. (2009). "Adsorption of Ag<sup>+</sup> by a surface molecular-imprinted biosorbent." *Chem. Eng. J.*, 150(1), 139-144.

Hussein, M.H., El-Hady, M.F., Sayed, W.M. and Hefni, H. (2012) "Preparation of some chitosan heavy metal complexes and study of its properties." *Polym. Sci., Ser. A*, 54(2), 113-124.

Janciauskaite, U., Rakutyte, V., Miskinis, J. and Makuska, R. (2008). "Synthesis and properties of chitosan-N-dextran graft copolymers." *React. Funct. Polym.*, 68(3), 787-796.

Janssen, R. and Ruyschaert, H. (1958). "The Infrared Spectra and the Structure of Some Pyrazol-5-Ones." *Bull. Soc. Chim. Belg.*, 67(5-6), 270-275.

Jiang, W., Su, H., Huo, H. and Tan, T. (2010). "Synthesis and properties of surface molecular imprinting adsorbent for removal of Pb<sup>2+</sup>." *Appl. Biochem. Biotechnol.*, 160(2), 467-476.

Jing, Y., Yin, N. and Yu, X. (2016). "Pb (II)-imprinted chitosan beads to enhance the adsorption property and selectivity: characterization, kinetics, and thermodynamics." *Desalination and Water Treat.*, 57(32), 15073-15082.

Justi, K.C., Favere, V.T., Laranjeira, M., Neves, A. and Casellato, A. (2005b). "Synthesis and characterization of modified chitosan through immobilization of complexing agents." *Macromol. Symp.*, Wiley-VCH Verlag, 229 (1), 203-207.

Justi, K.C., Fávere, V.T., Laranjeira, M.C., Neves, A. and Peralta, R.A. (2005a). “Kinetics and equilibrium adsorption of Cu (II), Cd (II), and Ni (II) ions by chitosan functionalized with 2 [-bis-(pyridylmethyl) aminomethyl]-4-methyl-6-formylphenol.” *J. Colloid Interface Sci.*, 291(2), 369-374.

Kabata-Pendias, A. and Pendias, H. (2000). *Trace elements in soils and plants*, CRC Press.

Kahu, S., Saravanan, D. and Jugade, R. (2014). “Effective detoxification of hexavalent chromium using sulfate-crosslinked chitosan.” *Water Sci. Technol.*, 70(12), 2047-2055.

Kamari, A., Pulford, I.D. and Hargreaves, J.S.J. (2011). “Chitosan as a potential amendment to remediate metal contaminated soil—a characterisation study.” *Colloids Surf., B*, 82(1), 71-80.

Kanagaraj, P., Nagendran, A., Rana, D., Matsuura, T., Neelakandan, S., Karthikkumar, T. and Muthumeenal, A. (2015). “Influence of N-phthaloyl chitosan on poly (ether imide) ultrafiltration membranes and its application in biomolecules and toxic heavy metal ion separation and their antifouling properties.” *Appl. Surf. Sci.*, 329, 165-173.

Kanamadi, R.D., Ahalya, N. and Ramachandra, T.V. (2006). “Biosorption of Heavy Metals by Low cost Adsorbents.” *CES Technical Report 112*, Centre for Ecological Sciences, I.I.Sc., Bangalore.

Kandile, N.G. and Nasr, A.S. (2014). “New hydrogels based on modified chitosan as metal biosorbent agents.” *Int. J. Biol. Macromol.*, 64, 328-333.

Kandile, N.G., Mohamed, H.M. and Mohamed, M.I. (2015). “New heterocycle modified chitosan adsorbent for metal ions (II) removal from aqueous systems.” *Int. J. Biol. Macromol.*, 72, 110-116.

Kang, S.Y., Lee, J.U., Moon, S.H. and Kim, K.W. (2004). “Competitive adsorption characteristics of Co<sup>2+</sup>, Ni<sup>2+</sup>, and Cr<sup>3+</sup> by IRN-77 cation exchange resin in synthesized wastewater.” *Chemosphere*, 56(2), 141-147.



- Karthik, R. and Meenakshi, S. (2015). "Removal of Pb (II) and Cd (II) ions from aqueous solution using polyaniline grafted chitosan." *Chem. Eng. J.*, 263, 168-177.
- Khan, A., Badshah, S. and Airoidi, C. (2011). "Biosorption of some toxic metal ions by chitosan modified with glycidylmethacrylate and diethylenetriamine." *Chem. Eng. J.*, 171(1), 159-166.
- Khan, A.A. and Singh, R.P. (1987). "Adsorption thermodynamics of carbofuran on Sn (IV) arsenosilicate in H<sup>+</sup>, Na<sup>+</sup> and Ca<sup>2+</sup> forms." *Colloids Surf., A*, 24(1), 33-42.
- Khor, E. (2001). "*Chitin: fulfilling a biomaterials promise.*" Elsevier Sci. Tech.: Maryland Heights, MO, USA.
- Kocak, N., Sahin, M., Arslan, G. and Ucan, H.I. (2012). "Synthesis of crosslinked chitosan possessing schiff base and its use in metal removal." *J. Inorg. Organomet. Polym. Mater.*, 22(1), 166-177.
- Kołodzyńska, D. (2011). "Chitosan as an effective low-cost sorbent of heavy metal complexes with the polyaspartic acid." *Chem. Eng. J.*, 173(2), 520-529.
- Kołodzyńska, D. (2012). "Adsorption characteristics of chitosan modified by chelating agents of a new generation." *Chem. Eng. J.*, 179, 33-43.
- Kousalya, G.N., Gandhi, M.R. and Meenakshi, S. (2010). "Sorption of chromium (VI) using modified forms of chitosan beads." *Int. J. Biol. Macromol.*, 47(2), 308-315.
- Krishnapriya, K. R.; Kandaswamy, M. (2009). "Synthesis and characterization of a crosslinked chitosan derivative with a complexing agent and its adsorption studies toward metal ( II ) ions." *Carbohydr. Res.* 344 (13), 1632-1638.
- Krishnapriya, K.R. and Kandaswamy, M.A. (2010). "New chitosan biopolymer derivative as metal-complexing agent: synthesis, characterization, and metal (II) ion adsorption studies." *Carbohydr. Res.*, 345 (14), 2013-2022.
- Kumar, R., Isloor, A.M. and Ismail, A.F. (2014). "Preparation and evaluation of heavy metal rejection properties of polysulfone/chitosan, polysulfone/N-succinyl

chitosan and polysulfone/N-propylphosphonyl chitosan blend ultrafiltration membranes.” *Desalination*, 350, 102-108.

Kumar, R., Isloor, A.M., Ismail, A.F. and Matsuura, T. (2013b). “Performance improvement of polysulfone ultrafiltration membrane using N-succinyl chitosan as additive.” *Desalination*, 318, 1-8.

Kumar, R., Isloor, A.M., Ismail, A.F. and Matsuura, T. (2013c). “Synthesis and characterization of novel water soluble derivative of chitosan as an additive for polysulfone ultrafiltration membrane.” *J. Membr. Sci.*, 440, 140-147.

Kumar, R., Isloor, A.M., Ismail, A.F., Rashid, S.A. and Al Ahmed, A. (2013a). “Permeation, antifouling and desalination performance of TiO<sub>2</sub> nanotube incorporated PSf/CS blend membranes.” *Desalination*, 316, 76-84.

Kumar, R., Isloor, A.M., Ismail, A.F., Rashid, S.A. and Matsuura, T. (2013d). “Polysulfone–Chitosan blend ultrafiltration membranes: preparation, characterization, permeation and antifouling properties.” *RSC Adv.*, 3(21), 7855-7861.

Kumar, R., Ismail, A.F., Kassim, M.A. and Isloor, A.M. (2013e). “Modification of PSf/PIAM membrane for improved desalination applications using Chitosan coagulation media.” *Desalination*, 317, 108-115.

Kurita, K. (2006). “Chitin and chitosan: functional biopolymers from marine crustaceans.” *Mar. Biotechnol.*, 8(3), 203-226.

Kurita, K., Hirakawa, M., Kikuchi, S., Yamanaka, H. and Yang, J. (2004). “Trimethyl silylation of chitosan and some properties of the product”. *Carbohydr. Polym.*, 56, 333–337.

Kurita, K., Ikeda, H., Yoshida, Y., Shimojoh, M. and Harata, M. (2002a). “Chemoselective protection of the amino groups of chitosan by controlled phthaloylation: facile preparation of a precursor useful for chemical modifications.” *Biomacromolecules* 3, 1–4.

Kurita, K., Mori, S., Nishiyama, Y. and Harata, M. (2002b) "N- Alkylation of chitin and some characteristics of the novel derivatives." *Polym. Bull.*, 48, 159–166.

Kurita, K., Uno, M., Saito, Y. and Nishiyama, Y. (2000). "Regioselectivity in protection of chitosan with the phthaloyl group." *Chitin Chitosan Res.* 6, 43–50.

Kyzas, G.Z. and Bikiaris, D.N. (2015). "Recent modifications of chitosan for adsorption applications: A critical and systematic review." *Mar. Drugs*, 13(1), 312-337.

Kyzas, G.Z. and Deliyanni, E.A. (2013). "Mercury (II) removal with modified magnetic chitosan adsorbents." *Molecules*, 18(6), 6193-6214.

Kyzas, G.Z. and Kostoglou, M. (2015). "Swelling–adsorption interactions during mercury and nickel ions removal by chitosan derivatives." *Sep. Purif. Technol.*, 149, 92-102.

Kyzas, G.Z., Bikiaris, D.N. and Lazaridis, N.K. (2008). "Low-swelling chitosan derivatives as biosorbents for basic dyes." *Langmuir*, 24(9), 4791-4799.

Kyzas, G.Z., Kostoglou, M. and Lazaridis, N.K. (2009). "Copper and chromium (VI) removal by chitosan derivatives—Equilibrium and kinetic studies." *Chem. Eng. J.*, 152(2), 440-448.

Kyzas, G.Z., Kostoglou, M., Lazaridis, N.K. and Bikiaris, D.N. (2013). "N-(2-Carboxybenzyl) grafted chitosan as adsorptive agent for simultaneous removal of positively and negatively charged toxic metal ions." *J. Hazard. Mater.*, 244, 29-38.

Lai, J.Y., Lin, F.C., Wang, C.C. and Wang, D.M. (1996). "Effect of nonsolvent additives on the porosity and morphology of asymmetric TPX membranes." *J. Membr. Sci.*, 118(1), 49-61.

Lang, G., Wendel, H. and Birkel, S. (1997). "Quaternary chitosan salts", *Chitin Handbook*, Muzzarelli R.A.A., Peter M.G., eds. Grottammare: Atec Edizioni, 67–70

Langmuir, I. (1916). "The constitution of solids and liquids part I. solids." *J. Am. Chem. Soc.*, 38, 2221-2295.

Lau, W.J., Ismail, A.F., Misdan, N. and Kassim, M.A. (2012). "A recent progress in thin film composite membrane: a review." *Desalination*, 287, 190-199.

Lebedev, A.V., Lebedeva, A.B., Sheludyakov, V.D., Kovaleva, E.A., Ustinova, O. L. and Kozhevnikov, I. B. (2005). "Synthesis of 3-substituted arylpyrazole-4-carboxylic acids." *Russ. J. Gen. Chem.*, 75 (5), 782-789.

Li, A., Lin, R., Lin, C., He, B., Zheng, T., Lu, L. and Cao, Y. (2016). "An environment-friendly and multi-functional absorbent from chitosan for organic pollutants and heavy metal ion." *Carbohydr. Polym.*, 148, 272-280.

Li, N. and Bai, R. (2005). "A novel amine-shielded surface cross-linking of chitosan hydrogel beads for enhanced metal adsorption performance." *Ind. Eng. Chem. Res.*, 44 (17), 6692-6700.

Li, N.N., Fane, A.G., Ho, W.W. and Matsuura, T. eds., (2011). *Advanced membrane technology and applications*, John Wiley & Sons.

Li, R., Guo, Z. and Jiang, P. (2010). "Synthesis, characterization, and antifungal activity of novel quaternary chitosan derivatives." *Carbohydr. Res.*, 345(13), 1896-1900.

Li, X., Zhou, H., Wu, W., Wei, S., Xu, Y. and Kuang, Y. (2015). "Studies of heavy metal ion adsorption on Chitosan/Sulfhydryl-functionalized graphene oxide composites." *J. Colloid Interface Sci.*, 448, 389-397.

Liu, J., Wu, H.T., Lu, J.F., Wen, X.Y., Kan, J. and Jin, C.H. (2015). "Preparation and characterization of novel phenolic acid (hydroxybenzoic and hydroxycinnamic acid derivatives) grafted chitosan microspheres with enhanced adsorption properties for Fe (II)." *Chem. Eng. J.*, 262, 803-812.

Liu, T., Wang, Z.L., Zhao, L. and Yang, X. (2012). "Enhanced chitosan/Fe 0-nanoparticles beads for hexavalent chromium removal from wastewater." *Chem. Eng. J.*, 189, 196-202.

Lu, Y., He, J. and Luo, G. (2013). "An improved synthesis of chitosan bead for Pb (II) adsorption." *Chem. Eng. J.*, 226, 271-278.

Lv, L., Chen, N., Feng, C., Zhang, J. and Li, M. (2017). "Heavy metal ions removal from aqueous solution by xanthate-modified cross-linked magnetic chitosan/poly (vinyl alcohol) particles." *RSC Adv.*, 7(45), 27992-28000.

Maczulak, A. (2010). *Pollution-Treating Environmental Toxins*, First ed., Infobase Pub., 74-75.

Malladi, S., Isloor, A.M., Isloor, S., Akhila, D.S. and Fun, H.K. (2013). "Synthesis, characterization and antibacterial activity of some new pyrazole based Schiff bases." *Arabian J. Chem.*, 6 (3), 335-340.

Martina, K., Leonhardt, S.E., Ondruschka, B., Curini, M., Binello, A. and Cravotto, G. (2011). "In situ cross-linked chitosan Cu (I) or Pd (II) complexes as a versatile, eco-friendly recyclable solid catalyst." *J. Mol. Catal. A: Chem.*, 334(1), 60-64.

Mende, M., Schwarz, D., Steinbach, C., Boldt, R. and Schwarz, S. (2016). "Simultaneous adsorption of heavy metal ions and anions from aqueous solutions on chitosan—Investigated by spectrophotometry and SEM-EDX analysis." *Colloids Surf., A*, 510, 275-282.

Miao, J., Chen, G., Gao, C. and Dong, S. (2008). "Preparation and characterization of N, O-carboxymethyl chitosan/Polysulfone composite nanofiltration membrane crosslinked with epichlorohydrin." *Desalination*, 233(1), 147-156.

Miao, J., Chen, G., Gao, C., Lin, C., Wang, D. and Sun, M. (2006). "Preparation and characterization of N, O-carboxymethyl chitosan (NOCC)/polysulfone (PS) composite nanofiltration membranes." *J. Membr. Sci.*, 280(1), 478-484.

Mohan, D. and Pittman, C.U. (2006). "Activated carbons and low cost adsorbents for remediation of tri- and hexavalent chromium from water." *J. Hazard. Mater.*, 137(2), 762-811.

Molinari, R., Gallo, S. and Argurio, P. (2004). "Metal ions removal from wastewater or washing water from contaminated soil by ultrafiltration–complexation." *Water Res.*, 38(3), 593-600.

Monier, M., Ayad, D.M. and Abdel-Latif, D.A. (2012). "Adsorption of Cu (II), Cd (II) and Ni (II) ions by cross-linked magnetic chitosan-2-aminopyridine glyoxal Schiff's base." *Colloids Surf., B*, 94, 250-258.

Monier, M., Ayad, D.M., Wei, Y. and Sarhan, A.A. (2010). "Adsorption of Cu (II), Co (II), and Ni (II) ions by modified magnetic chitosan chelating resin." *J. Hazard. Mater.*, 177(1), 962-970.

Nadavala, S.K., Swayampakula, K., Boddu, V.M. and Abburi, K. (2009). "Biosorption of phenol and o-chlorophenol from aqueous solutions on to chitosan–calcium alginate blended beads." *J. Hazard. Mater.*, 162(1), 482-489.

Nagireddi, S., Katiyar, V. and Uppaluri, R. (2017). "Pd (II) adsorption characteristics of glutaraldehyde cross-linked chitosan copolymer resin." *Int. J. Biol. Macromol.*, 94, 72-84.

Naimo, T.J. (1995). "A review of the effects of heavy metals on freshwater mussels." *Ecotoxicology*, 4(6), 341–362.

Negm, N.A. and Ali, H.E. (2010). "Modification of heavy metal uptake efficiency by modified chitosan/anionic surfactant systems." *Eng. Life Sci.*, 10(3), 218-224.

Nethaji, S., Sivasamy, A., Thennarasu, G. and Saravanan S. (2010). "Adsorption of Malachite Green dye onto activated carbon derived from *Borassus aethiopicum* flower biomass." *J. Hazard. Mater.*, 181(1), 271-280.

Ng, J.C.Y., Cheung, W.H. and McKay, G. (2002). "Equilibrium studies of the sorption of Cu (II) ions onto chitosan." *J. Colloid Interface Sci.*, 255(1), 64-74.

Ng, J.C.Y., Cheung, W.H. and McKay, G. (2003). "Equilibrium studies for the sorption of lead from effluents using chitosan." *Chemosphere*, 52(6), 1021-1030.

- Ngah, W.S. and Isa, I.M. (1998). "Comparison study of copper ion adsorption on chitosan, Dowex A-1, and Zerolit 225." *J. Appl. Polym. Sci.*, 67(6), 1067-1070.
- Ngah, W.W. and Fatinathan, S. (2006). "Chitosan flakes and chitosan–GLA beads for adsorption of p-nitrophenol in aqueous solution." *Colloids Surf., A*, 277(1), 214-222.
- Ngah, W.W. and Fatinathan, S. (2010). "Adsorption characterization of Pb (II) and Cu (II) ions onto chitosan-tripolyphosphate beads: kinetic, equilibrium and thermodynamic studies." *J. Environ. Manage.*, 91(4), 958-969.
- Ngah, W.W. and Hanafiah, M.A.K.M. (2008). "Removal of heavy metal ions from wastewater by chemically modified plant wastes as adsorbents: a review." *Bioresour. Technol.*, 99(10), 3935-3948.
- Ngah, W.W., Ab Ghani, S. and Kamari, A. (2005). "Adsorption behaviour of Fe (II) and Fe (III) ions in aqueous solution on chitosan and cross-linked chitosan beads." *Bioresour. Technol.*, 96(4), 443-450.
- Ngah, W.W., Endud, C.S. and Mayanar, R. (2002). "Removal of copper (II) ions from aqueous solution onto chitosan and cross-linked chitosan beads." *React. Funct. Polym.*, 50(2), 181-190.
- Ngah, W.W., Kamari, A. and Koay, Y.J. (2004). "Equilibrium and kinetics studies of adsorption of copper (II) on chitosan and chitosan/PVA beads." *Int. J. Biol. Macromol.*, 34(3), 155-161.
- Ngah, W.W., Kamari, A., Fatinathan, S. and Ng, P.W. (2006). "Adsorption of chromium from aqueous solution using chitosan beads." *Adsorption*, 12(4), 249-257.
- Ngah, W.W., Teong, L.C. and Hanafiah, M.A.K.M. (2011). "Adsorption of dyes and heavy metal ions by chitosan composites: A review." *Carbohydr. Polym.*, 83(4), 1446-1456.
- Nishimura, S., Kai, H., Shinada, K., Yoshida, T., Tokura, S., Kurita, K., Nakashima, H., Yamamoto, N. and Uryu, T. (1998). "Regioselective syntheses of sulfated

polysaccharides: specific anti-HIV-1 activity of novel chitin sulfates.” *Carbohydr Res.*, 306, 427–433.

No, H.K., Lee, K.S. and Meyers, S.P. (2000). “Correlation between physicochemical characteristics and binding capacities of chitosan products.” *J. Food Sci.*, 65(7), 1134-1137.

Osifo, P.O., Neomagus, H.W., Everson, R.C., Webster, A. and vd Gun, M.A. (2009). “The adsorption of copper in a packed-bed of chitosan beads: Modeling, multiple adsorption and regeneration.” *J. Hazard. Mater.*, 167(1), 1242-1245.

Özverdi, A. and Erdem, M. (2006). “Cu <sup>2+</sup>, Cd <sup>2+</sup> and Pb <sup>2+</sup> adsorption from aqueous solutions by pyrite and synthetic iron sulphide.” *J. Hazard. Mater.*, 137(1), 626-632.

Padaki, M., Isloor, A.M. and Wanichapichart, P. (2011a). “Polysulfone/N-phthaloylchitosan novel composite membranes for salt rejection application.” *Desalination*, 279(1), 409-414.

Padaki, M., Isloor, A.M., Fernandes, J. and Prabhu, K.N. (2011b). “New polypropylene supported chitosan NF-membrane for desalination application.” *Desalination*, 280(1), 419-423.

Padaki, M., Isloor, A.M., Wanichapichart, P. and Ismail, A.F. (2012). “Preparation and characterization of sulfonated polysulfone and N-phthaloyl chitosan blend composite cation-exchange membrane for desalination.” *Desalination*, 298, 42-48.

Paulino, A.T., Guilherme, M.R., Reis, A.V., Tambourgi, E.B., Nozaki, J. and Muniz, E.C. (2007). “Capacity of adsorption of Pb <sup>2+</sup> and Ni <sup>2+</sup> from aqueous solutions by chitosan produced from silkworm chrysalides in different degrees of deacetylation.” *J. Hazard. Mater.*, 147(1), 139-147.

Peeters, J.M.M., Boom, J.P., Mulder, M.H.V. and Strathmann, H. (1998). “Retention measurements of nanofiltration membranes with electrolyte solutions.” *J. Membr. Sci.*, 145(2), 199-209.



- Perez-Gonzalez, A., Urriaga, A.M., Ibáñez, R. and Ortiz, I. (2012). "State of the art and review on the treatment technologies of water reverse osmosis concentrates." *Water res.*, 46(2), 267-283.
- Pontalier, P.Y., Ismail, A. and Ghoul, M. (1997). "Mechanisms for the selective rejection of solutes in nanofiltration membranes." *Sep. Purif. Technol.*, 12(2), 175-181.
- Popuri, S.R., Vijaya, Y., Boddu, V.M. and Abburi, K. (2009). "Adsorptive removal of copper and nickel ions from water using chitosan coated PVC beads." *Bioresour. Technol.*, 100(1), 194-199.
- Prashanth, K.H. and Tharanathan, R.N. (2007). "Chitin/chitosan: modifications and their unlimited application potential—an overview." *Trends Food Sci. Technol.*, 18(3), 117-131.
- Qin, C., Du, Y., Zhang, Z., Liu, Y., Xiao, L. and Shi, X. (2003). "Adsorption of chromium (VI) on a novel quaternized chitosan resin." *J. Appl. Polym. Sci.*, 90(2), 505-510.
- Qiu, H., Lv, L., Pan, B.C., Zhang, Q.J., Zhang, W.M. and Zhang, Q.X. (2009). "Critical review in adsorption kinetic models." *J. Zhejiang Univ. Sci. A*, 10(5), 716-724.
- Redlich, O.J.D.L. and Peterson, D.L. (1959). "A useful adsorption isotherm." *J. Phys. Chem.*, 63(6), 1024-1024.
- Repo, E., Warchoń, J.K., Bhatnagar, A. and Sillanpää, M. (2011). "Heavy metals adsorption by novel EDTA-modified chitosan–silica hybrid materials." *J. Colloid Interface Sci.*, 358(1), 261-267.
- Rodda, D.P., Johnson, B.B. and Wells, J.D. (1993). "The effect of temperature and pH on the adsorption of copper (II), lead (II), and zinc (II) onto goethite." *J. Colloid Interface Sci.*, 161(1), 57-62.

Rojas, G., Silva, J., Flores, J.A., Rodriguez, A., Ly, M. and Maldonado, H. (2005). "Adsorption of chromium onto cross-linked chitosan." *Sep. Purif. Technol.*, 44(1), 31-36.

Rudie, B.J., Ross, G.S., Harrold, S.J. and Paulson, D.J. (1993). "Effects of surface force interactions on an NF/UF membrane." *Desalination*, 90(1-3), 107-118.

Salehi, E., Daraei, P. and Shamsabadi, A.A. (2016). "A review on chitosan-based adsorptive membranes." *Carbohydr. Polym.*, 152, 419-432.

Sankararamkrishnan, N., Dixit, A., Iyengar, L. and Sanghi, R. (2006). "Removal of hexavalent chromium using a novel cross linked xanthated chitosan." *Bioresour. Technol.*, 97(18), 2377-2382.

Santos, J.E., Dockal, E.R. and Cavalheiro, E.T. (2005). "Synthesis and characterization of Schiff bases from chitosan and salicylaldehyde derivatives." *Carbohydr. Polym.*, 60(3), 277-282.

Sargin, İ., Kaya, M., Arslan, G., Baran, T. and Ceter, T. (2015). "Preparation and characterisation of biodegradable pollen–chitosan microcapsules and its application in heavy metal removal." *Bioresour. Technol.*, 177, 1-7.

Sarkar, M. and Majumdar, P. (2011). "Application of response surface methodology for optimization of heavy metal biosorption using surfactant modified chitosan bead." *Chem. Eng. J.*, 175, 376-387.

Sayler, G.S., Nelson, J.D. and Colwell, R. R. (1975). "Role of Bacteria in bioaccumulation of mercury in the Oyster *Crassostrea virginica*." *Appl. Microbiol.*, 30(1), 91-96.

Shankar, P., Gomathi, T., Vijayalakshmi, K. and Sudha, P.N. (2014). "Comparative studies on the removal of heavy metals ions onto cross linked chitosan-g-acrylonitrile copolymer." *Int. J. Biol. Macromol.*, 67, 180-188.

Shariful, M.I., Sharif, S.B., Lee, J.J.L., Habiba, U., Ang, B.C. and Amalina, M.A. (2017). "Adsorption of divalent heavy metal ion by mesoporous-high surface area

chitosan/poly (ethylene oxide) nanofibrous membrane.” *Carbohydr. Polym.*, 157, 57-64.

Shen, C., Wang, Y., Xu, J. and Luo, G. (2013). “Chitosan supported on porous glass beads as a new green adsorbent for heavy metal recovery.” *Chem. Eng. J.*, 229, 217-224.

Shenvi, S., Ismail, A.F. and Isloor, A.M. (2014). “Enhanced Permeation Performance of Cellulose Acetate Ultrafiltration Membranes by Incorporation of Sulfonated Poly (1, 4-phenylene ether ether sulfone) and Poly (styrene-co-maleic anhydride).” *Ind. Eng. Chem. Res.*, 53(35), 13820-13827.

Shenvi, S.S., Isloor, A.M., Ismail, A.F., Shilton, S.J. and Al Ahmed, A. (2015). “Humic acid based biopolymeric membrane for effective removal of methylene blue and rhodamine B.” *Ind. Eng. Chem. Res.*, 54(18), 4965-4975.

Shimei, X., Jingli, W., Ronglan, W. and Jide, W. (2006). “Effect of degree of substitution on adsorption behavior of Basic Green 4 by highly crosslinked amphoteric starch with quaternary ammonium and carboxyl groups.” *Carbohydr. Polym.*, 66(1), 55-59.

Sikder, J., Pereira, C., Palchoudhury, S., Vohra, K., Basumatary, D. and Pal, P. (2009). “Synthesis and characterization of cellulose acetate-polysulfone blend microfiltration membrane for separation of microbial cells from lactic acid fermentation broth.” *Desalination*, 249(2), 802-808.

Sinha, V.R., Singla, A.K., Wadhawan, S., Kaushik, R., Kumria, R., Bansal, K. and Dhawan, S. (2004). “Chitosan microspheres as a potential carrier for drugs.” *Int. J. Pharm.*, 274(1), 1-33.

Smolders C.A., Reuvers, A. J., Boom, R.M. and Wienk, I.M. (1992). “Microstructures in phase-inversion membranes. Part 1. Formation of macrovoids.” *J. Membrane Sci.*, 73, 259-275.

Spinelli, V.A., Laranjeira, M.C. and Fávere, V.T. (2004). "Preparation and characterization of quaternary chitosan salt: adsorption equilibrium of chromium (VI) ion." *React. Funct. Polym.*, 61(3), 347-352.

Srivastava, S. and Goyal, P. (2010). *Novel Biomaterials: Decontamination of Toxic Metals from Wastewater*, Springer Science and Business Media.

Stuart, B. (2004). *Infrared spectroscopy*. John Wiley and Sons, Inc..UK.

Sud, D., Mahajan, G. and Kaur, M.P. (2008). "Agricultural waste material as potential adsorbent for sequestering heavy metal ions from aqueous solutions—A review." *Bioresour. Technol.*, 99(14), 6017-6027.

Suguna, M., Siva Kumar, N., Subba Reddy, A., Boddu, V.M. and Krishnaiah, A. (2011). "Biosorption of lead (II) from aqueous solution on glutaraldehyde cross-linked chitosan beads." *Can. J. Chem. Eng.*, 89(4), 833-843.

Tan, S., Wang, Y., Peng, C. and Tang, Y. (1999). "Synthesis and adsorption properties for metal ions of crosslinked chitosan acetate crown ethers." *J. Appl. Polym. Sci.*, 71(12), 2069-2074.

Tayel, A.A., Gharieb, M.M., Zaki, H.R. and Elguindy, N.M. (2016). "Bio-clarification of water from heavy metals and microbial effluence using fungal chitosan." *Int. J. Biol. Macromol.*, 83, 277-281.

Tirkistani, F.A. (1998). "Thermal analysis of some chitosan Schiff bases." *Polym. Degrad. Stab.*, 60(1), 67-70.

Trimukhe, K.D. and Varma, A.J. (2008). "Complexation of heavy metals by crosslinked chitin and its deacetylated derivatives." *Carbohydrate polymers*, 71(1), 66-73.

Udaybaskar, P., Iyengar, L. and Rao, A.V.S. (1990). "Hexavalent chromium interaction with chitosan." *J. Appl. Polym. Sci.*, 39(3), 739-747.

Uddin, M.K. (2017). "A review on the adsorption of heavy metals by clay minerals, with special focus on the past decade." *Chem. Eng. J.*, 308, 438-462.

Van't Hoff J. H. a) *Etudes de dynamique chimique, 1884*; b) *Studies in chemical dynamics*, (translation by T. Ewan and revised by E. Cohen), 1896; London: Williams and Norgate.

Varma, A.J., Deshpande, S.V. and Kennedy, J.F. (2004). "Metal complexation by chitosan and its derivatives: a review." *Carbohydr. Polym.*, 55(1), 77-93.

Vasconcelos, H.L., Camargo, T.P., Gonçalves, N.S., Neves, A., Laranjeira, M.C. and Fávere, V.T. (2008). "Chitosan crosslinked with a metal complexing agent: Synthesis, characterization and copper (II) ions adsorption." *React. Funct. Polym.*, 68(2), 572-579.

Vasconcelos, H.L., Fávere, V.T., Gonçalves, N.S. and Laranjeira, M.C. (2007). "Chitosan modified with Reactive Blue 2 dye on adsorption equilibrium of Cu (II) and Ni (II) ions." *React. Funct. Polym.*, 67(10), 1052-1060.

Vatanpour, V., Madaeni, S.S., Moradian, R., Zinadini, S. and Astinchap, B. (2011). "Fabrication and characterization of novel antifouling nanofiltration membrane prepared from oxidized multiwalled carbon nanotube/polyethersulfone nanocomposite." *J. Membr. Sci.*, 375(1), 284-294.

Vigato, P.A. and Tamburini, S. (2004). "The challenge of cyclic and acyclic Schiff bases and related derivatives." *Coord. Chem. Rev.*, 248(17), 1717-2128.

Vijaya, Y., Popuri, S.R., Boddu, V.M. and Krishnaiah, A. (2008). "Modified chitosan and calcium alginate biopolymer sorbents for removal of nickel (II) through adsorption." *Carbohydr. Polym.*, 72(2), 261-271.

Volesky, B. and Naja, G. (2005). "Biosorption: application strategies." *Proc. 16<sup>th</sup> Int. Biohydrometall. Symp.*, Cape Town, South Africa.

Waheed, S., Ahmad, A., Khan, S.M., Jamil, T., Islam, A. and Hussain, T. (2014). "Synthesis, characterization, permeation and antibacterial properties of cellulose acetate/polyethylene glycol membranes modified with chitosan." *Desalination*, 351, 59-69.

- Wan, M.W., Kan, C.C., Rogel, B.D. and Dalida, M.L.P. (2010). "Adsorption of copper (II) and lead (II) ions from aqueous solution on chitosan-coated sand." *Carbohydr. Polym.*, 80(3), 891-899.
- Wan, Y., Creber, K.A., Peppley, B. and Bui, V.T. (2006). "Chitosan-based electrolyte composite membranes: II. Mechanical properties and ionic conductivity." *J. Membr. Sci.*, 284(1), 331-338.
- Wang, J. and Chen, C. (2014). "Chitosan-based biosorbents: modification and application for biosorption of heavy metals and radionuclides." *Bioresour. Technol.*, 160, 129-141.
- Wang, J., and Chen, C. (2009). "Biosorbents for heavy metals removal and their future." *Biotechnol. Adv.*, 27, 195-226.
- Wang, L.K., Chen, J.P., Hung, Y.T. and Shammas, N.K. eds. (2009a). *Heavy metals in the environment*. CRC Press.
- Wang, L.K., Hung, Y.T. and Shammas, N.K. eds. (2007). *Advanced physicochemical treatment technologies*. Humana Press.
- Wang, R.M., He, N.P., Song, P.F., He, Y.F., Ding, L. and Lei, Z.Q. (2009b). "Preparation of nano-chitosan Schiff-base copper complexes and their anticancer activity." *Polym. Adv. Technol.*, 20(12), 959-964.
- Wang, S.F., Shen, L., Zhang, W.D. and Tong, Y.J. (2005). "Preparation and mechanical properties of chitosan/carbon nanotubes composites." *Biomacromolecules*, 6(6), 3067-3072.
- Wang, X. and Wang, C. (2016). "Chitosan-poly (vinyl alcohol)/attapulgitite nanocomposites for copper (II) ions removal: pH dependence and adsorption mechanisms." *Colloids Surf., A*, 500, 186-194.
- Webster, A., Halling, M.D. and Grant, D.M. (2007). "Metal complexation of chitosan and its glutaraldehyde cross-linked derivative." *Carbohydr. Res.*, 342(9), 1189-1201.

- Wu, F.C., Tseng, R.L. and Juang, R.S. (2010). "A review and experimental verification of using chitosan and its derivatives as adsorbents for selected heavy metals." *J. Environ. Manage.*, 91(4), 798-806.
- Xiao, Y. and Zhou, X. (2008). "Synthesis and properties of a novel crosslinked chitosan resin modified by L-lysine." *React. Funct. Polym.*, 68, 1281-1289.
- Xu, T. and Huang, C. (2008). "Electrodialysis-based separation technologies: A critical review." *AIChE J.*, 54(12), 3147-3159.
- Yan, Z., Haijia, S. and Tianwei, T. (2007). "Adsorption behaviors of the aminated chitosan adsorbent." *Korean J. Chem. Eng.*, 24(6), 1047-1052.
- Yuan, N.Y., Tsai, R.Y., Ho, M.H., Wang, D.M., Lai, J.Y. and Hsieh, H.J. (2008). "Fabrication and characterization of chondroitin sulfate-modified chitosan membranes for biomedical applications." *Desalination*, 234(1), 166-174.
- Yuvaraja, G., Yaping, Z., Weijiang, Z. and Jiao, X. (2017). "Magnetic-epichlorohydrin crosslinked chitosan schiff's base (m-ECCSB) as a novel adsorbent for the removal of Cu (II) ions from aqueous environment." *Int. J. Biol. Macromol.*, 97, 85-98.
- Zarghami, Z., Akbari, A., Latifi, A.M. and Amani, M.A. (2016). "Design of a new integrated chitosan-PAMAM dendrimer biosorbent for heavy metals removing and study of its adsorption kinetics and thermodynamics." *Bioresour. Technol.*, 205, 230-238.
- Zhang, L., Zeng, Y. and Cheng, Z. (2016). "Removal of heavy metal ions using chitosan and modified chitosan: A review." *J. Mol. Liq.*, 214, 175-191.
- Zhao, F., Yu, B., Yue, Z., Wang, T., Wen, X., Liu, Z. and Zhao, C. (2007). "Preparation of porous chitosan gel beads for copper (II) ion adsorption." *J. Hazard. Mater.*, 147(1), 67-73.

Zhou, L., Wang, Y., Liu, Z. and Huang, Q. (2009). "Characteristics of equilibrium, kinetics studies for adsorption of Hg (II), Cu (II), and Ni (II) ions by thiourea-modified magnetic chitosan microspheres." *J. Hazard. Mater.*, 161(2), 995-1002.

Zou, Y. and Khor, E. (2005). "Preparation of C-6 substituted chitin derivatives under homogeneous conditions." *Biomacromolecules*, 6, 80–87.



## **LIST OF RESEARCH PUBLICATIONS**

1. Balakrishna Prabhu K, Saidutta M.B., Arun M. Isloor, Girish Kamath. “A new chitosan biopolymer derivative for the removal of Cu (II) and Pb (II) from aqueous solutions: Synthesis, characterization and adsorption studies” (This article has been published in the September 2017 issue of *Jurnal Teknologi (Sciences & Engineering)* 79:6 (2017) 1–9).

2. K. Balakrishna Prabhua, M.B. Saidutta, Arun M. Isloor and Raghavendra Hebbar. “Improvement In Performance Of Polysulfone Membranes Through the Incorporation of Chitosan-(3-phenyl-1H-pyrazole-4-carbaldehyde)”  
(Revised manuscript is under review in the journal *Cogent Engineering*)

3. Balakrishna Prabhu K, Saidutta M.B., Arun M. Isloor. “Interactions of hexavalent chromium from aqueous medium with a new Schiff base chitosan derivative.”  
(This article has been published in *International Journal of Applied Engineering Research*, Volume 12, Number 14 (2017) pp. 4072-4082)



## **BIODATA**

**Mr. Balakrishna Prabhu K**

**Email:** [balakrishnaprabhu@yahoo.com](mailto:balakrishnaprabhu@yahoo.com)  
[balakrishna.prabhu@manipal.edu](mailto:balakrishna.prabhu@manipal.edu)

**Contact No:** +91 9880530636

**Date of Birth:** 3<sup>rd</sup> April, 1964

**Nationality:** Indian

**Presently employed at:** Manipal Institute of Technology, Manipal, India.

**Present Designation:** Associate Professor (Sr.)

**Official Address:** Dept. of Chemical Engineering,  
Manipal Institute of Technology,  
Manipal, Karnataka State,  
India. 576104

### **Work Experience**

Total of 29 years at Manipal Institute of Technology, Manipal, as a teaching faculty at various levels.

### **Educational Qualifications**

M.Tech. from the Department of Chemical Engineering, IIT Bombay (1988).

B.E. from the Department of Chemical Engineering, NITK Surathkal (1985) (then affiliated to Mangalore University).

### **Areas of Interest**

Mass Transfer, Environmental Engineering, Process control

